



The
University
Of
Sheffield.

**A comparison between *C9ORF72*-derived poly-GA
DPRs at different stages of protein aggregation
in neurons and glia**

Paolo Michelangelo Marchi

Thesis submitted for the degree of Doctor of Philosophy (PhD)

Sheffield Institute for Translational Neuroscience

Department of Neuroscience

March 2022

Statement

The work I did in Professor Azzouz's laboratory between 2018 and 2022 is the basis for the following PhD thesis. As a result of my PhD research, I wrote an entire manuscript to be considered for publication, with feedback and minor edits from other authors. This manuscript is available as a bioRxiv pre-print article with the following DOI: <https://doi.org/10.1101/2021.10.11.463891> and is currently (as of March 30th, 2022) under revision in the Life Science Alliance journal, EMBO press.

The abstract (p.3); the methods' chapter 2.2 (p.67-80); chapter 3.1 (p.82); chapter 3.3 (p.90); chapter 3.6 (p.104); chapter 4.2 (p.111-112); chapter 4.3 (p.116-122); chapter 5.2 (p.130); chapter 5.4 (p.137-139); chapter 5.5 (p.143 and 145) and movie legends (p.178-179) of my PhD dissertation are all identical to the bioRxiv article.

All authors of the bioRxiv article gave permission for the material to be included in this PhD thesis.

Abstract

The polymorphic hexanucleotide repeat expansion (HRE) in the *C9orf72* gene is the major cause of both familial and sporadic amyotrophic lateral sclerosis/frontotemporal dementia (ALS/FTD). The pathogenic HRE consists of hundreds to thousands of GGGGCC (G_4C_2) repeats, located in the first intron of the *C9orf72* gene.

A crucial driver of *C9orf72*-mediated ALS/FTD pathology is the unconventional repeat-associated non-AUG (RAN) translation of the HRE into five toxic dipeptide repeat (DPR) species. Among the five different DPRs generated by RAN translation, poly-GA appears to be the most abundantly detected as well as one of the most toxic DPR species.

This thesis focuses on the role of poly-GA DPRs in disease spread. We first illustrate the process of poly-GA oligomer coalescence into solid-like species. Importantly, poly-GA oligomers show a distinct ability to form fibrillar species of amyloid nature with characteristic β -sheets *in vitro*.

To dissect the process of cell-to-cell DPR transmission, we closely follow the fate of poly-GA DPRs in either their oligomeric or fibrillized form after administration in the cell culture medium. We observe that poly-GA DPRs are taken up via dynamin-dependent and -independent endocytosis, eventually converging at the lysosomal compartment and leading to spherical axonal structures in neurons. We then use a co-culture system to demonstrate astrocyte-to-motor neuron DPR propagation, showing that astrocytes may internalise and release aberrant peptides in disease pathogenesis.

Overall, our results shed light on the mechanisms of poly-GA cellular uptake and cell-to-cell propagation, suggesting lysosomal impairment as a possible feature underlying the cellular pathogenicity of these DPR species.

This thesis is entirely dedicated to my father Lorenzo. For his example, support, and unconditional love.

Acknowledgements

I'd like to start by thanking my primary supervisor, Professor Mimoun Azzouz, for the wonderful opportunity to work on this project in his laboratory. Throughout the project, Professor Azzouz provided me with ongoing support and mentoring, as well as the incredible opportunity to constantly improve my scientific skills in his laboratory over the course of four years. I'd also like to thank Dr Guillaume Hautbergue and Professor Laura Ferraiuolo, my second and third supervisors, for their ongoing encouragement, valuable advice, and support.

Dr Lara Marrone, Dr João Alves Cruzeiro, Dr Joseph Scarrott, Dr Christopher Webster, Dr Evangelia Karyka, Dr Matteo Cortese deserve special thanks for their insightful discussions, training, mentoring, and assistance with laboratory experiments and protocols. Thanks to Dr Colin Gray, Dr Christa Walther and Dr Darren Robinson for their support and mentoring with microscopy experiments. Thanks to Dr Jouni Tatalo for his support on statistics and Dr Stephen Ebbens for help with mathematical modelling on some of my experiments. Thanks to Dr Emma Smith and Professor Kurt De Vos for providing essential reagents. Thanks to Prof Laura Ferraiuolo and her team for providing iAstrocytes and Hb9-GFP motor neurons. Thanks to Dr Ronald Melki, Dr Luc Bousset and Dr Laurent Brasseur for providing recombinant proteins for my experiments.

A warm thank you also to Dr Michela Pulix, Dr Emily Graves, Mr Zih-Liang Yang, Mr Raffaele Marroccella, Dr Victor Alfred, Mr Allan Shaw, Dr Iliaria Giovannelli, Mr Andre Varcianna, Ms Lai Mei Wan, Mr Ian Coldicott, Dr Adrian Higginbottom, for actively helping with my PhD. Thank you to the This Week in Virology (TWIV) team for teaching me so much about the fascinating world of viruses, especially to Prof. Racaniello for his inspiring work in science communication and dissemination.

I'd also like to thank my parents, Ornella and Lorenzo, for their unconditional love and unwavering support throughout my life and studies. You are the driving force behind this accomplishment, and I could not have completed this PhD dissertation without you. Thank you also to my grandparents Agostino, Dina, and Fedora. Your love and example taught me so much, and I miss you every day. A special thanks to my dear brother Giacomo and his wife Alice (and I am very excited to be uncle Paolo!). Thank you also to all of my friends back home, especially Marco Buzzacchi and his genuine friendship. Thanks to John Giannetti for believing in me and being a true friend. Thank you to the new friends I met here in Sheffield on rather fortuitous occasions, especially Erik, Tania, and Enes; life can be generous and full of surprises at times. Finally, a special thanks to Hubashia, whose love and support throughout these years were the key to this achievement.

Table of Contents

<i>Statement</i>	2
<i>Abstract</i>	3
<i>Acknowledgements</i>	5
<i>Table of Contents</i>	6
<i>List of Figures</i>	9
<i>List of Tables</i>	11
<i>List of Abbreviations</i>	12
1. Introduction	18
1.1 Proteostasis imbalance in proteinopathies	19
1.1.1 Protein misfolding in neurodegenerative diseases.....	19
1.1.2 Aggregation as a complex phenomenon.....	21
1.1.3 Prion-like proteins and cell-to-cell propagation	24
1.1.4 The role of lysosomes in aggregate clearance	28
1.2 ALS and FTD as a unique spectrum of disease	32
1.2.1 Amyotrophic Lateral Sclerosis.....	32
1.2.2 Frontotemporal Dementia	36
1.2.3 Overlapping between ALS and FTD.....	39
1.2.4 Non-cell autonomous players in ALS/FTD.....	41
1.3 <i>C9ORF72</i> -linked ALS/FTD	44
1.3.1 <i>C9ORF72</i> gene and protein.....	44
1.3.2 C9-HRE disease mechanisms.....	47
1.3.2.1 <i>C9ORF72</i> haploinsufficiency	48
1.3.2.2 RNA foci-mediated toxicity.....	49
1.3.2.3 Non-AUG translation of dipeptide repeat proteins	51
1.3.3 Poly-GA dipeptide repeat proteins	55
1.4 Introduction to PhD project: aims and objectives.....	57

2. Materials and methods	58
2.1 Materials	59
2.1.1 Plasmid DNA	59
2.1.2 Antibodies	60
2.1.3 Reagents	61
2.1.4 Scientific devices and plates.....	64
2.1.5 Image analysis: softwares, algorithms, macros	65
2.1.6 Experimental <i>in vitro</i> models	66
2.1.7 DNA oligonucleotides.....	66
2.2 Methods	67
2.2.1 Cell culture	67
2.2.2 Conversion of skin fibroblasts to induced neural progenitor cells	67
2.2.3 iAstrocyte differentiation and co-culture system.....	68
2.2.4 Primary mouse cortical neurons	68
2.2.5 Dipeptide Repeat Proteins cloning	69
2.2.6 Transmission electron microscopy	70
2.2.7 Coalescence measurements	71
2.2.8 Immunocytochemistry.....	71
2.2.9 Flow cytometry	72
2.2.10 Immunoblotting.....	72
2.2.11 Perturbation of endocytosis	73
2.2.12 Lysosomal assays	73
2.2.13 Release of DPRs in the conditioned medium	74
2.2.14 APOJ enzyme-linked immunosorbent assay (APOJ ELISA).....	74
2.2.15 Mean-Square Displacement(Δt) analysis	75
2.2.16 Colour deconvolution for detecting two lysosomal populations	76
2.2.17 mRNA isolation and RT-qPCR.....	76
2.2.18 dSTORM imaging.....	78
2.2.18.1 Sample preparation	78
2.2.18.2 Immunocytochemistry and staining for dSTORM imaging	78
2.2.18.3 Colocalization analysis in dual colour dSTORM	79
2.2.18.4 3D dSTORM	80

2.2.19	Quantification and Statistical analysis.....	80
3.	<i>Recombinant poly-GA DPRs assemble into oligomers and β-sheet fibrils</i>	81
3.1	Introduction.....	82
3.2	Cloning, purification and labelling of recombinant DPRs.....	85
3.2.1	Protein purification, characterisation and fluorescent labelling	86
3.2.2	Analysis of GA/PA immunoreactivity and fluorescence labelling.....	88
3.3	Poly-GA oligomers coalesce into solid-like structures <i>in vitro</i>	90
3.4	Poly-GA oligomers form high-molecular weight species	93
3.5	Recombinant DPRs bind to cells in culture	96
3.6	Discussion.....	101
4.	<i>Uptake and endocytosis of poly-GA in glia and neurons.....</i>	106
4.1	Introduction.....	107
4.2	Uptake of poly-GA in glial cells.....	111
4.3	Endocytosis perturbs DPR uptake	116
4.4	DPR uptake in cortical neurons and lysosomal colocalization	119
4.5	Discussion.....	123
5.	<i>Lysosomal damage and cell-to-cell propagation of DPRs</i>	126
5.1	Introduction on lysosomal damage	127
5.2	Poly-GA DPRs produce partial lysosomal dysfunction.....	129
5.3	Introduction on cell-to-cell spreading.....	136
5.4	Poly-GA DPRs spread from astrocytes to motor neurons	137
5.5	Discussion.....	143
6.	<i>Final discussion and future perspectives</i>	146
6.1	Summary and project highlights	146
6.2	Future directions and main challenges.....	151
7.	<i>References.....</i>	154
8.	<i>Appendix</i>	177
	<i>Legends for supplementary Movies</i>	178
	<i>Research outputs from PhD.....</i>	180

List of Figures

Figure 1.1 Proteostasis defenses against misfolded proteins.....	20
Figure 1.2 Protein aggregation pathways	22
Figure 1.3 Prion-like model and cell-to-cell transmission	26
Figure 1.4 Lysosome homeostasis and protein aggregation.....	31
Figure 1.5 Neuroanatomical illustration of ALS pathology	33
Figure 1.6 Overview of FTD clinical syndromes.....	37
Figure 1.7 Mutations in ALS/FTD genes are linked to proteostasis pathways	40
Figure 1.8 Glial cells' proteostasis imbalance in ALS and FTD.....	43
Figure 1.9 <i>C9ORF72</i> gene, transcript variants and protein isoforms	45
Figure 1.10 C9 HRE-mediated pathological mechanisms.....	54
Figure 2.1 Cloning of Gly/Ala repeat constructs.....	69
Figure 3.1 Schematic diagram of recombinant proteins' production	83
Figure 3.2 Anti-GA or anti-PA immunoreactivity and fluorophore labelling for DPRs	89
Figure 3.3 <i>In vitro</i> coalescence of poly-GA and poly-PA recombinant DPRs.....	91
Figure 3.4 <i>In vitro</i> coalescence of poly-GA and poly-PA in 3D-rendering	92
Figure 3.5 Poly-GA oligomers form characteristic fibrils after 15 days <i>in vitro</i>	94
Figure 3.6 Deconvoluted FT-IR spectrum of GA fibrils	95
Figure 3.7 Binding of poly-GA assemblies to cells in culture	97
Figure 3.8 SMLM-TIRF clustering analysis of poly-GA fibrils on the surface of iAstrocytes	99
Figure 3.9 3D-STORM clustering analysis of poly-GA fibrils on the surface of iAstrocytes	100
Figure 4.1 Endocytic pathways and uptake of misfolded protein aggregates	109
Figure 4.2 DPR uptake in various cell lines and in healthy iAstrocytes	111
Figure 4.3 DPR uptake in healthy iAstrocytes shown by orthogonal views and 3D-rendering....	112
Figure 4.4 Trypan blue quenching effect on ATTO488 poly-GA fibrils	113
Figure 4.5 DPR motion after uptake in healthy iAstrocytes.....	115
Figure 4.6 Oligomeric vs fibrillar poly-GA DPRs entry-routes in glia.....	117
Figure 4.7 Oligomeric vs fibrillar poly-GA DPRs colocalization with lysosomes	118
Figure 4.8 DPR motion after uptake in primary cortical neurons	120
Figure 4.9 Poly-GA DPRs colocalize with endolysosomal organelles after uptake and accumulate in spherical axonal structures enriched with lysosomes.....	121

Figure 5.1 Endolysosomal organelles that colocalize with poly-GA DPRs present aberrant characteristics.....	129
Figure 5.2 ATP6V0E1 mRNA levels in cortical neurons are altered by poly-GA fibrils.....	130
Figure 5.3 DPR exposure does not change cathepsin levels in primary cortical neurons	131
Figure 5.4 DPR exposure does not change <i>in situ</i> lysosomal enzyme activities	132
Figure 5.5 Proteasome impairment and DPR exposure do not increase cleaved caspase-3 levels in primary cortical neurons.....	133
Figure 5.6 Galectin-3 levels do not increase in DPR-exposed HeLa cells.....	134
Figure 5.7 HeLa cells decrease their lysosomal pH after exposure to poly-GA	135
Figure 5.8 Alanine-rich DPRs undergo astrocyte-to-motor neuron propagation	138
Figure 5.9 Propagated DPRs do not show toxicity in receiving motor neurons.....	139
Figure 5.10 APOJ enzyme-linked immunosorbent assay.....	140
Figure 5.11 Alanine-rich DPRs undergo astrocyte-to-motor neuron propagation	142
Figure 6.1 Project outcomes and highlights	150
Figure 8.1 STORM-TIRF control images	177

List of Tables

Table 1.1 Prion-like properties of common misfolded aggregates.....	27
Table 1.2 Definitive ALS genes (ALSoD).....	35
Table 1.3 FTD genes	38
Table 2.1 Plasmid DNA. List of plasmid DNAs used in this project.....	59
Table 2.2 List of antibodies used in this study	60
Table 2.3 List of Chemicals, media, and compounds used in this study	61
Table 2.4 List of scientific devices used in this study	64
Table 2.5 List of softwares, algorithms and FIJI macros used in this study.....	65
Table 2.6 List of experimental <i>In vitro</i> models	66
Table 2.7 List of DNA oligonucleotides.	66
Table 2.8 List and characteristics of iAstrocytes used in this study.....	67

List of Abbreviations

aa	Amino acids
AAV	Adeno-associated virus
AAV9	AAV serotype 9
ACTB	Actin Beta gene
AD	Alzheimer's disease
ALS	Amyotrophic lateral sclerosis
ALSoD	ALS Online Genetics Database
ANOVA	Analysis of variance
APOJ	Apolipoprotein J
AR	Autosomal recessive
ATG5	autophagy related 5 gene
ATG7	autophagy related 7 gene
ATG9A	Autophagy related 9A gene
ATM	Ataxia telangiectasia mutated gene
ATPv0E1	ATPase H ⁺ Transporting V0 Subunit E1 gene
ATXN8	Ataxin 8 gene
Aβ	Amyloid beta
BAC	Bacterial artificial chromosome
BCA	Bicinchoninic acid
BDNF	Brain Derived Neurotrophic Factor
bp	Base pair
BSA	Bovine serum albumin
bvFTD	behavioral variant of FTD
C57BL/6	C57 black 6
C9ORF72	Chromosome 9 open reading frame 72 gene
C9orf72-L	C9orf72 long isoform
C9orf72-S	C9orf72 short isoform
Cas9	CRISPR associated protein 9
CCD	Charge-coupled device
CD44	CD44 antigen
Cdc48	Cell division control protein 48

cDNA	Complementary DNA
CHCHD10	coiled-coil-helix-coiled-coil-helix domain containing 10 gene
CHMP2B	Charged Multivesicular Body Protein 2B gene
CHMP6	Charged Multivesicular Body Protein 6 gene
CLs	Colocalizing Lysosomes
CM	Conditioned medium
CMLE	Classic Maximum Likelihood Estimation
CNS	Central Nervous System
CO₂	Carbon dioxide
CRISPR	Clustered regularly interspaced short palindromic repeats
CTSB	Cathepsin B gene
CTSD	Cathepsin D gene
CTSL	Cathepsin L gene
DAPI	4',6-diamidino-2-phenylindole
DBSCAN	Density-based spatial clustering of applications with noise
DENN	differentially expressed in normal and neoplastic cells
DIV	Days <i>in vitro</i>
DM1	Myotonic dystrophy type 1
DMEM	Dulbecco's Modified Eagle's Medium
DMSO	Dimethyl sulfoxide
DNA	Deoxyribonucleic acid
DNAse	Deoxyribonuclease
DPR	Dipeptide repeat protein
dSTORM	Direct stochastic optical reconstruction microscopy
ECL	Enhanced chemiluminescence
EDTA	Ethylenediaminetetraacetic acid
EGF	Epidermal growth factor
ELISA	Enzyme-linked immunosorbent assay
ENCALS	The European Network for the Cure of ALS
ER	Endoplasmic reticulum
ERAD	Endoplasmic-reticulum-associated protein degradation
ESCRT-III	Endosomal sorting complex required for transport-III
FACS	Fluorescence-activated cell sorting

fALS	familial Amyotrophic Lateral Sclerosis
FBS	Fetal bovine serum
FDA	Food and Drug Administration
FGF2	Fibroblast growth factor 2 precursor
FIG4	FIG4 Phosphoinositide 5-Phosphatase gene
FIJI	Fiji Is Just ImageJ
FIP200	Focal adhesion kinase-family Interacting Protein of 200 kDa
FRAP	Fluorescence recovery after photobleaching
FRC	Fourier ring correlation
FTD	Frontotemporal dementia
FTIR	Fourier transform infrared spectroscopy
FTLD	Frontotemporal lobar degeneration
FUS	Fused in sarcoma gene
GA	Glycine-alanine
GAPDH	Glyceraldehyde 3-phosphate dehydrogenase gene
GBA	Glucosylceramidase Beta gene
GDNF	Glial-derived neurotrophic factor
GDP	Guanosine diphosphate
GEF	Guanine nucleotide exchange factor
GFP	Green fluorescent protein
GP	Glycine-proline
GR	Glycine-arginine
GRN	Granulin Precursor gene
GTP	Guanosine-5'-triphosphate
GTPase	GTP-binding protein
Hb9	Homeodomain protein
HBSS	Hanks' Balanced Salt Solution
HCl	Hydrochloric acid
HD	Huntington's disease
HEK293T	Human embryonic kidney
HeLa	Henrietta Lacks
HFIP	Hexafluoroisopropanol

hnRNPs	Intracerebroventricular
HR23A	UV excision repair protein RAD23 homolog A
HR23B	UV excision repair protein RAD23
HRE	Hexanucleotide repeat expansion
HRP	Horseradish peroxidase
iMNs	Induced motor neurons
iNPC	Induced neural progenitor cell
iPSC	Induced pluripotent stem cell
KD	Knockdown
KO	Knockout
LAMP1	Lysosomal Associated Membrane Protein 1
LC3	Microtubule Associated Protein 1 Light Chain 3 Alpha
LCD	Low-complexity domain
LLoMe	L-leucyl-L-leucine methyl ester
LMNs	Lower motor neurons
LMP	Lysosomal membrane permeabilization
LSM	Laser scanning microscope
<i>MAPT</i>	Microtubule-associated protein tau gene
MATLAB	MATrix LABoratory
<i>MCOLN1</i>	Mucolipin TRP Cation Channel 1 gene
MG132	carbobenzoxy-L-leucyl-L-leucyl-L-leucinal
MN	Motor neuron
MNs	Motor neurons
mRNA	Messenger RNA
MSD	Mean Square Displacement
MVBs	Multivesicular bodies
NA	Numerical aperture
NCLs	Non-Colocalizing Lysosomes
nfvPPA	nonfluent variant primary progressive aphasia
NGS	Next-Generation Sequencing
NPC	Neural progenitor cell
<i>OPTN1</i>	Optineurin gene
ORF	Open reading frame

p62	Sequestosome-1
PA	Proline-alanine
PBS	Phosphate-buffered saline
PD	Parkinson's Diseases
PFA	Paraformaldehyde
PG	Proline-glycine
<i>PGRN</i>	Progranulin gene
PMSF	Phenylmethylsulfonyl fluoride
PR	Proline-arginine
<i>PRNP</i>	Prion Protein gene
PrP^C	Cellular prion protein
PrP^{Sc}	Scrapie isoform of the prion protein
PSF	Point spread function
<i>PSMC4</i>	Proteasome 26S Subunit, ATPase 4 gene
<i>PSMD11</i>	Proteasome 26S Subunit, Non-ATPase 11
Rab	Ras-associated binding
RAN	Repeat Associated Non-AUG translation
<i>RB1CC1</i>	RB1 Inducible Coiled-Coil 1
RGB	Red Green Blue
RIPA	Radioimmunoprecipitation assay
RNA	Ribonucleic acid
RNAP-II	RNA polymerase II
RNase	Ribonuclease
ROI	Region of interest
RRID	Research Resource Identification
rRNA	Ribosomal ribonucleic acid
RT	Reverse transcriptase
RT-qPCR	Reverse transcription-quantitative polymerase chain reaction
SAG	Smoothed Agonist
sALS	Sporadic Amyotrophic Lateral Sclerosis
SCA8	Spinocerebellar ataxia type 8
SD	Standard deviation
SDS	Sodium dodecyl sulfate

SDS-PAGE	sodium dodecyl sulfate–polyacrylamide gel electrophoresis
SEC	Size-exclusion chromatography
SEM	Standard error of the mean
siRNA	Small interfering RNA
SMLM	Single-molecule localization microscopy
SMN	Survival of motor neuron gene
SMCR8	Smith-Magenis Syndrome Chromosome Region candidate 8
SNR	Signal To Noise Ratio
SOD1	Superoxide Dismutase 1 gene
SPG15	Zinc Finger FYVE-Type Containing 26 gene
SPG47	Adaptor Related Protein Complex 4 Subunit Beta 1 gene
SQSTM1	Sequestosome 1 gene
svPPA	semantic variant of primary progressive aphasia
TARDBP	TAR DNA Binding Protein gene
TBK1	TANK Binding Kinase 1 gene
TBS	Tris-buffered saline
TBST	Tris-buffered saline with 0.1% Tween® 20 Detergent
TEV	Tobacco Etch Virus nuclear-inclusion-a endopeptidase
TGF-1	Transforming growth factor beta 1
TIRFM	Total internal reflection fluorescence microscopy
TMEM106B	Transmembrane Protein 106B gene
TSEs	Transmissible spongiform encephalopathies
UBQLN1	Ubiquilin 1 gene
Ubx3	UBX domain-containing protein 3
ULK1	Unc-51 Like Autophagy Activating Kinase 1 gene
UMNs	Upper motor neurons
UPS	Ubiquitin-Proteasome system
v-ATPase	Vacuolar-type ATPase
VCP	Valosin Containing Protein gene
Wdr41	WD repeat-containing protein 41
WT	Wild-type
XLD	X-linked Dominant

1. Introduction

1.1 Proteostasis imbalance in proteinopathies

1.1.1 Protein misfolding in neurodegenerative diseases

To function properly, the cell must orchestrate its complex proteostasis network, which controls the biogenesis, folding, degradation, and trafficking of all its proteins. The proteostasis network is made up of integrated biological pathways that work together to keep the proteome functional and well-balanced both inside and outside the cell. Protein folding is the physical process that converts a protein chain into a well-defined three-dimensional structure known as the "native" (or "folded") state. The native state of a protein is typically a folded conformation that allows it to function biologically ¹. Many proteins begin their folding co-translationally on the ribosome. The endoplasmic reticulum (ER) folds at least one-third of the proteome, aided by a complex family of chaperones, foldases, cofactors, and enzymes that all mediate various post-translational modifications ². Thus, there are many cellular pathways that ensure precise folding of newly synthesized native proteins under physiological conditions.

In most cases, failure to fold into native structure results in inactive proteins; however, in some cases, misfolded proteins acquire modified or toxic functionality. When a protein undergoes misfolding, the cell uses a number of quality control mechanisms that detect the protein and help to degrade it. These mechanisms, which prevent abnormal protein aggregation, are critical to the maintenance of cellular health and function ³. The ubiquitin-proteasome system (UPS), for example, plays an important role in the proteolysis of persistently misfolded proteins through poly-ubiquitination and degradation via the 26S proteasome, as well as in the control of protein turnover in the cell ⁴. The autophagy pathway also contributes to the prevention of protein aggregation. Autophagy is a quality control system in which cytoplasmic components are engulfed within double-membrane vesicles known as "autophagosomes" before fusing with lysosomes, which degrade the autophagic cargoes using a variety of hydrolytic enzymes ⁵. The chaperone system is another cellular system that prevents protein misfolding and aggregation. Multidomain proteins known as "molecular chaperones" have evolved to help nascent proteins reach their native fold and avoid protein aggregation ⁶. These proteins (members of the heat-shock protein family, in particular) recognise hydrophobic amino acid sequences exposed by misfolded proteins and provide critical assistance in favouring the rearrangements required for the acquisition of the correct three-dimensional protein conformation during translation and after cytotoxic stress.

Another quality control mechanism that aids in degrading misfolded protein is known as the ER-associated degradation (ERAD) pathway⁷. In fact, when misfolded proteins accumulate in the ER, the ER stress response activates the ERAD pathway, which acts as an integrated intracellular signalling system by retrotranslocating misfolded proteins to the cytosol and poly-ubiquitinating them for proteasomal degradation.

Understanding the aetiology of diseases characterised by excessive protein misfolding, such as neurodegenerative diseases, necessitates knowledge of proteostasis pathways and the factors that cause them to fail. Long-term accumulation of misfolded proteins induces DNA double-strand breaks⁸, oxidative stress⁹, mitochondrial damage¹⁰, and interference with RNA metabolism via sequestration of RNA-binding proteins¹¹. Particularly in the central nervous system, misfolded proteins impair the axonal transport machinery of neuronal cells¹², and cause astrogliosis¹³ and activation of microglia¹⁴.

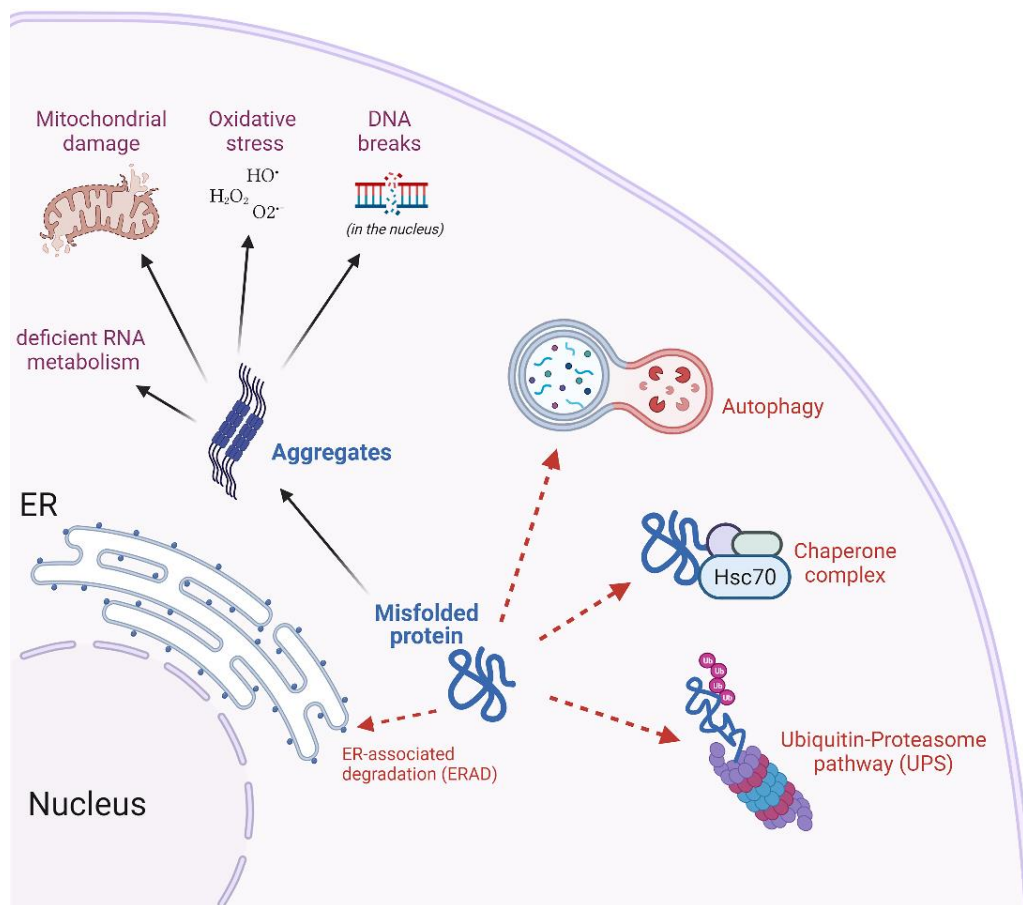


Figure 1.1 Proteostasis defenses against misfolded proteins

Misfolded proteins can aggregate and activate a variety of proteostasis mechanisms through which the cell attempts to control aggregation (i.e., autophagy, chaperones, UPS pathway, ERAD). If the proteostasis balance fails, misfolded proteins can coalesce into toxic protein aggregates that disrupt critical cellular functions. Figure created with BioRender.com under academic license.

Extensive evidence from genetic, pharmacological, and pathological studies supports the accumulation of pathological misfolded proteins as the cause of neuronal tissue damage and dysfunction in neurodegenerative diseases ¹⁵. As a result, imbalances in the proteostasis network are likely to play a role in disease aetiology ¹⁶.

1.1.2 Aggregation as a complex phenomenon

Misfolded proteins can form large "aggregates" (or "inclusions") in various tissues. These aggregates are not only found in neurodegenerative diseases, but also in systemic amyloidosis (in various organs), type 2 diabetes (in the pancreas), and dialysis-related amyloidosis (in joints and skeletal tissue) ¹⁷.

The misfolded protein that predominates in each aggregate is unique to each disease. What all of these illnesses have in common is that these aggregates are often made up of masses of non-branched filaments that are only a few nanometres in diameter but often microns in length.

These filaments, known as "amyloid fibrils", are made up of an ordered arrangement of thousands of copies of the misfolded protein ¹⁸⁻²¹. The name "fibril" derives from the aggregates' characteristic fibrillar morphology, which is visible under an electron microscope; and the name "amyloid" derives from the aggregate's underlying secondary structure, which has been shown to be a cross- β -motif via X-ray crystallography ²². This motif is created by laminating successive β -sheet layers, in which the individual strands of each β -sheet run perpendicular to the fibril axis (4.7 Å spacing) whereas the β -sheets (~10 Å spacing) are parallel to the fibril axis ²³. The cross- β -motif provides thermodynamic and kinetic stability to the aggregates, as well as resistance to proteolytic degradation ²⁴. These amyloid fibrils also bind the dye Congo red, which represents the classic histological definition of an amyloid material ²⁵. Congo red-stained amyloid fibrils, in particular, exhibit green birefringence under cross-polarized light ²⁶, and this is used as a diagnostic test for conditions in which misfolded proteins of various types are deposited in tissues as fibrils ²⁷.

In neurodegenerative diseases, the misfolded protein that predominantly constitutes each amyloid aggregate is specific to each disease: α -synuclein for Parkinson's disease (PD);

polyglutamine expansion of huntingtin for Huntington's disease (HD); A β and tau for Alzheimer's disease (AD); TDP-43 and C9ORF72 RAN proteins for amyotrophic lateral sclerosis and frontotemporal dementia (ALS/FTD).

The process of amyloid aggregation shares some underlying characteristics in all of these neurodegenerative diseases²⁵. It starts when a natively folded protein forms a monomeric protein precursor, which can be unfolded or partially folded²⁸. This monomeric precursor is prone to aggregation and becomes thermodynamically stable by incorporating additional monomers, a process known as '*nucleation*'. If the nucleation process is prolonged enough, it can result in the formation of cross- β amyloid-like fibrils. As fibrils grow, they go through a process known as '*elongation*', which involves the addition of new aggregation-prone species. This elongation results in an exponential increase in fibrillar material until nearly all free monomer has been converted into fibrils. The fibril yield reaches a plateau after this phase (the '*stationary phase*'). These steps are depicted in **Figure 1.2**.

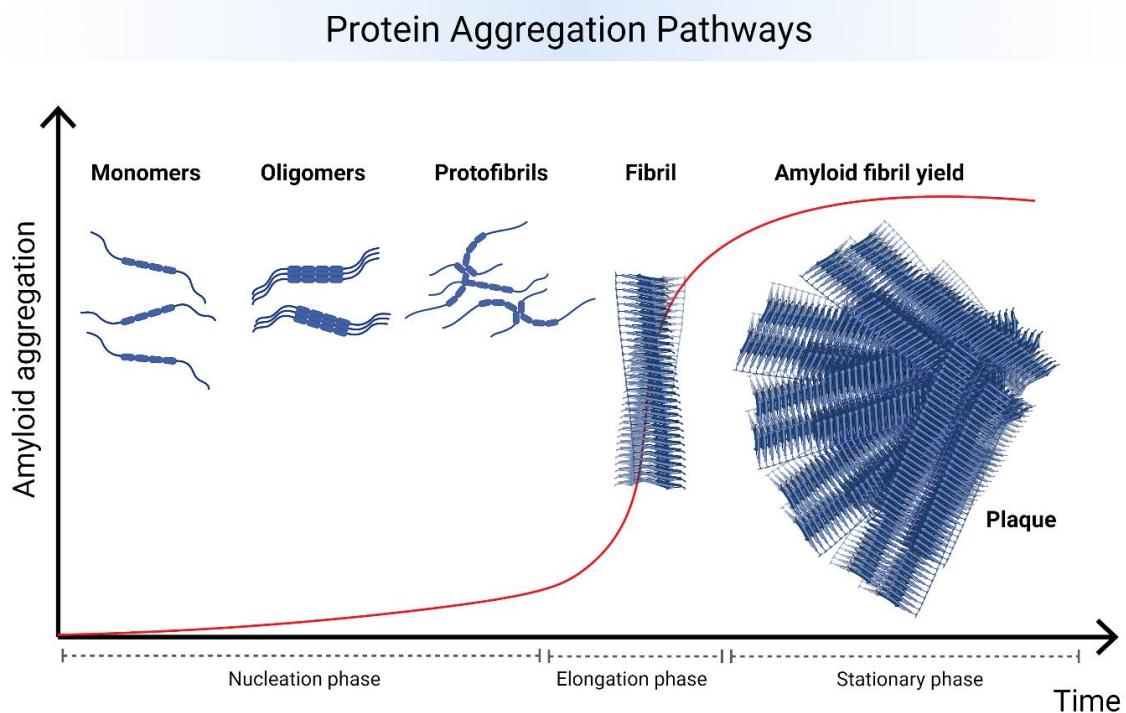


Figure 1.2 Protein aggregation pathways

Aggregation of a misfolded protein is a complex and heterogeneous process that involves different stages of structurally defined aggregate species over time. In general, the aggregation process can be divided into three chronological stages: a *nucleation phase* in which a few misfolded monomers begin to stabilise by incorporating more monomers; an *elongation phase* in which fibrillar structures form and continue to grow as a result of the addition of many monomeric species (these fibrils

usually have β -sheet secondary structure); and a final *stationary phase* in which the fibrils may coalesce into larger amyloid plaques but do not grow further because the monomer fraction has all been converted to fibrillar. Figure created with BioRender.com under academic license. Adapted and inspired from Iadanza et al. ²⁸

Protein aggregate formation is a highly dynamic and heterogeneous process, as illustrated by the presence of structurally diverse aggregates in **Figure 1.2**.

Neuropathological and genetic evidence strongly support the amyloid cascade hypothesis of AD, which proposes that A β peptide deposition in the brain is a central event in disease pathology ^{29–33}. According to the traditional interpretation of this hypothesis, the most relevant pathological A β species are late-stage amyloid plaques (composed of coalesced and aggregated fibrils). This classic amyloid view is also considered applicable in other neurodegenerative diseases such as PD or ALS/FTD. However, another school of thought contends that oligomers, which are smaller diffusible aggregates, are the primary pathogenic culprit, with late-stage plaques possibly serving as a reservoir for such species by disaggregating and releasing them ^{34,35}.

In the example of AD, the seeding activity of A β oligomers has been reported to be prominent in the early stages of pathogenesis of AD ^{36–39} and some A β deposits can be detected two decades before disease signs and symptoms appear (as early as 30–50 years of age in humans) ^{40–43}. Anti-A β monoclonal antibodies that primarily bind to monomeric A β (and, by extension, oligomeric forms of A β) do not, however, cause significant plaque clearance and are clinically ineffective ^{44,45}. One theory is that these antibodies are locked up by a huge pool of inactive oligomeric species and therefore miss the pool of bioactive A β oligomers ⁴⁶. To make matters worse, the lack of an uniform experimental description of which type of A β oligomeric species is harmful makes it impossible to understand and compare results amongst studies ⁴⁷. Indeed, the types and sizes of oligomers with disease-relevant action are still being contested, with some laboratories stating that extremely small A β dimers are toxic ⁴⁸, while others claim that bigger oligomers are toxic ⁴⁹.

Several monoclonal antibodies are capable of reducing the amyloid load by targeting late-stage A β plaques rather than monomeric/oligomeric species ⁵⁰. One of these, aducanumab, was recently granted accelerated approval by the FDA, with reduction of amyloid plaques

serving as a surrogate end point ⁵¹. With inconsistent data regarding clinical improvements⁵²⁻⁵⁴, the reason for authorisation and the amount of the therapeutic benefit from these antibodies are hotly debated. All these investigations demonstrate the problems that arise from a lack of understanding of Alzheimer's disease and whether lowering amyloid below a pathogenic threshold can stop already-started downstream processes. Overall, we know that the content and shape of a pathologically misfolded protein species varies in the early versus late phases of disease ^{55,56}. As a result, establishing the identities of aggregation species discovered at various disease stages will be crucial in neurodegenerative diseases such as AD, PD and ALS/FTD. The timing of drug administration during this process is also critical for developing new specific therapies for these diseases.

1.1.3 Prion-like proteins and cell-to-cell propagation

In practically all neurodegenerative diseases, the pathology is initially limited to a small location and then advances through defined anatomical routes in later stages, despite substantial variation in different individuals. In fact, the pathology usually reflects the progressive nature of the ongoing neurodegeneration which extends gradually in a spatiotemporal fashion in several areas of the central nervous system ⁵⁷⁻⁵⁹. This finding lends credence to the emerging theory of “prion-like” protein propagation in non-infectious neurodegenerative diseases.

The term “prion” was defined in 1982 by Stanley B Prusiner as the infectious agent that causes transmissible spongiform encephalopathies (TSEs), or prion diseases, a finding that earned Prusiner the 1997 Nobel Prize in Physiology or Medicine ^{60,61}. According to Prusiner, the prion (from *proteinaceous infectious only*) is devoid of nucleic acids and consists of an ‘infectious’ protein known as PrP^{Sc} that is capable of converting a normal host protein termed PrP^C (cellular prion protein) into a likeness of itself ⁶¹⁻⁶³. All prion diseases are essentially neurodegenerative diseases characterised by neuronal loss, vacuolation, and astrocyte and microglia activation ⁶⁴. Unfortunately, these illnesses go undetected until symptoms appear, and they are currently untreatable and fatal ⁶⁵. The most common human prion diseases (85–90% of all cases) are sporadic Creutzfeldt-Jakob disease and sporadic fatal familial insomnia,

both of which have an unclear aetiology ⁶⁶. The remaining percentage of human prion diseases consists of either *genetic* or *acquired* forms. Genetic forms are all caused by mutations in the *PRNP* gene, which encodes the cellular prion protein PrP^C. Acquired forms are instead caused by the transmission of pre-existing prions, for example orally or through inoculation of blood, cerebrospinal fluid, and transplanted tissue ⁶⁷; and also through the food chain, causing humans to develop Variant Creutzfeldt-Jacob disease (the "mad cow" disease) ⁶⁸.

According to the prion model, PrP^{Sc} aggregates are released from specific cells and then taken up by neighbouring cells, where they can seed the misfolding of the native conformer PrP^C and multiply and spread in different brain regions ⁶⁹. Importantly, mice lacking PrP^C are resistant to prion infection and disease ^{70,71} which strongly suggests that PrP^{Sc} infectivity is dependent on PrP^C.

Recent research has discovered a similar prion behaviour (namely 'prion-like') in misfolded proteins that are found to be accumulated in many common neurodegenerative diseases ^{72,73}. A β and tau in AD; α -synuclein in PD; TDP-43, SOD1, C9orf72-DPRs in ALS/FTD; and mutant huntingtin in Huntington's disease are just a few examples. These proteins, like prions, misfold, form aggregates, and spread along neuronal connectivity paths, seeding the misfolding of native conformers and thus contributing to disease progression. Unlike prions, these proteins are associated with non-infectious neurodegenerative diseases, and there is no evidence that surgical procedures or casual contact result in disease transmission between people, with the exception of A β (from contaminated growth hormone extracts) ^{74,75}.

Based on previous research, we selected some fundamental properties of prion-like proteins and depicted them in **Figure 1.3**. These include three important ones such as (i) ability to induce neurotoxicity in a cell, (ii) spreading from one cell to another, and (iii) seeding of native conformers in the naïve cell.

Table 1.1, on the other hand, describes the literature for AD, PD, and ALS/FTD in which these three properties for disease-specific pathological aggregates were observed.

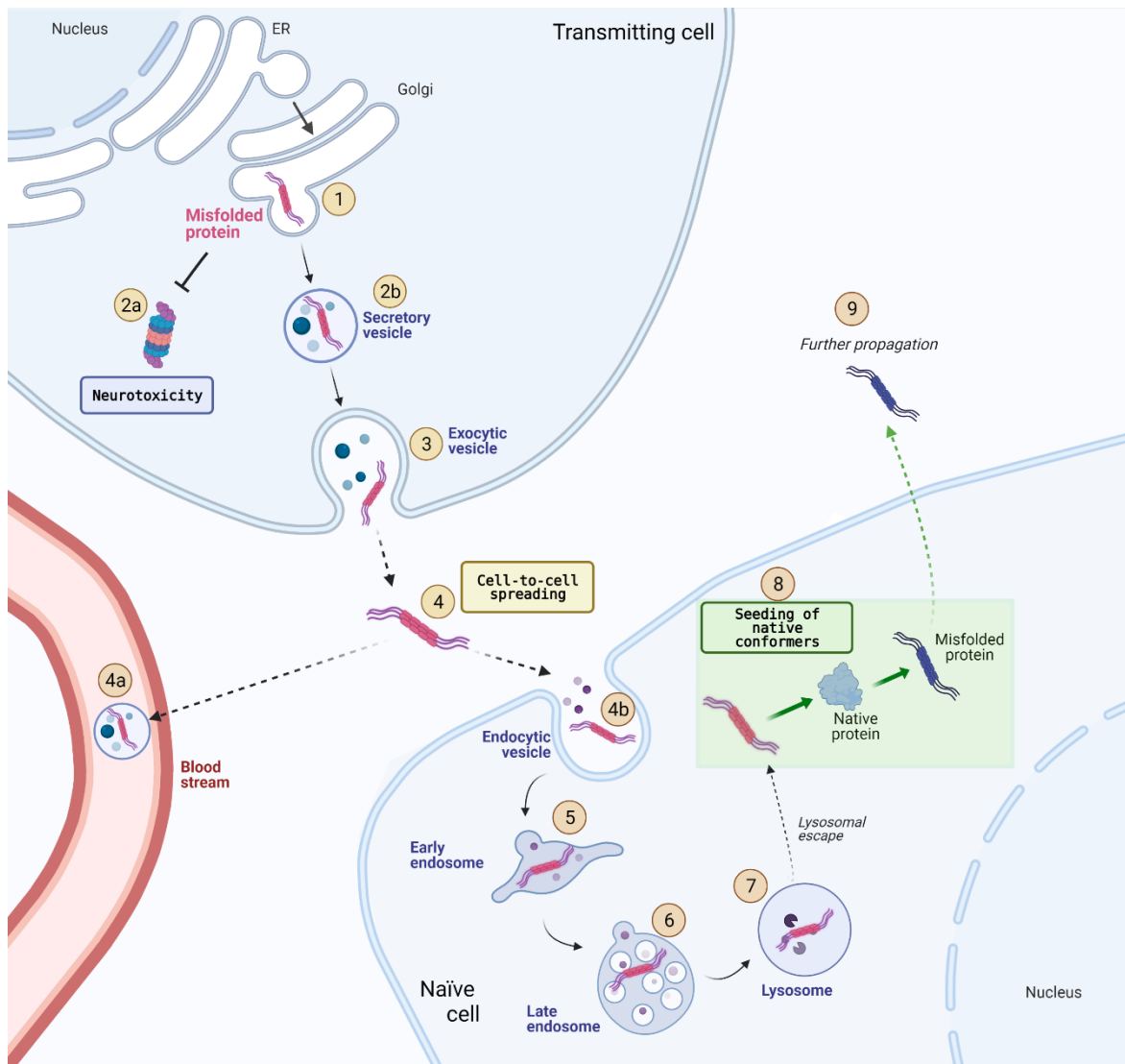


Figure 1.3 Prion-like model and cell-to-cell transmission

An overview of a model that describes some of the basic properties of prion-like proteins. The model's proposed events are highlighted in detail and numbered in chronological order in the figure (from 1 to 9). In brief, a misfolded protein forms in the ER and, via the Golgi (1), can either enter the cell cytoplasm and cause toxicity (2a) or be packaged into a secretory vesicle (2b). When a misfolded protein enters the secretory pathway, via exocytosis (3), it is released into the extracellular space and can either reach the bloodstream (4a) or spread to a neighbouring naïve cell, where it is endocytosed (4b, 5 and 6). Following endocytosis, the misfolded protein may undergo lysosomal escape, gaining access to the cell's cytoplasm (7), where it can seed its native conformer, which is already present in the cell, in a prion-like mechanism (8). Finally, these events can be repeated by introducing the newly misfolded conformer into another cell (9). Figure created with BioRender.com under academic license.

Associated disease(s)	Misfolded protein	Prion-like properties			
		Neurotoxicity	Cell-to-cell spreading	Seeding of native conformers	
Alzheimer's Disease	β -amyloid	<i>In cell culture</i>	<ul style="list-style-type: none"> Renner et al., 2010 Zhao et al., 2017 Cascella et al., 2017 	<ul style="list-style-type: none"> Nath et al., 2012 Domert et al., 2014 Song et al., 2014 	<ul style="list-style-type: none"> Olsson et al., 2018 Aoyagi et al., 2019
		<i>In vivo</i>	<ul style="list-style-type: none"> Eisele et al., 2009 Eisele et al., 2010 	<ul style="list-style-type: none"> Song et al., 2014 Roos et al., 2021 	<ul style="list-style-type: none"> Kane et al., 2000 Meyer-Luehmann et al., 2006 Roos et al., 2021
Frontotemporal Dementia	Tau	<i>In cell culture</i>	<ul style="list-style-type: none"> Nonaka et al., 2010 	<ul style="list-style-type: none"> Holmes et al., 2013 	<ul style="list-style-type: none"> Guo & Lee, 2011 Sanders et al., 2014
		<i>In vivo</i>	<ul style="list-style-type: none"> Clavaguera et al., 2013 	<ul style="list-style-type: none"> Clavaguera et al., 2013 	<ul style="list-style-type: none"> Boluda et al. 2015
Parkinson's Disease	α -synuclein	<i>In cell culture</i>	<ul style="list-style-type: none"> Desplats et al., 2009 	<ul style="list-style-type: none"> Danzer et al., 2009 Desplats et al., 2009 Loria et al., 2017 	<ul style="list-style-type: none"> Luk et al., 2009 Hansen et al., 2011 Volpicelli-Daley et al., 2011
		<i>In vivo</i>	<ul style="list-style-type: none"> Volpicelli-Daley et al., 2011 Luk et al., 2012 	<ul style="list-style-type: none"> Luk et al., 2012 	<ul style="list-style-type: none"> Kordower et al., 2008 Li et al., 2008 Rey et al., 2016
Huntington's Disease	Htt	<i>In cell culture</i>	<ul style="list-style-type: none"> Herrera et al., 2011 	<ul style="list-style-type: none"> Pecho-Vrieseling et al., 2014 	<ul style="list-style-type: none"> Ren et al., 2009
		<i>In vivo</i>	<ul style="list-style-type: none"> Babcock et al., 2015 	<ul style="list-style-type: none"> Babcock et al., 2015 Pecho-Vrieseling et al., 2014 	<ul style="list-style-type: none"> Pearce et al., 2015
Amyotrophic Lateral Sclerosis	SOD1	<i>In cell culture</i>	<ul style="list-style-type: none"> Benkler et al., 2018 	<ul style="list-style-type: none"> Münch et al., 2011 Grad et al., 2014 	<ul style="list-style-type: none"> Münch et al., 2011 Grad et al., 2011 Grad et al., 2014
		<i>In vivo</i>	<ul style="list-style-type: none"> Prudencio et al., 2010 	<ul style="list-style-type: none"> Ayers et al., 2016 Thomas et al., 2017 	<ul style="list-style-type: none"> Ayers et al., 2016 Thomas et al., 2017
Frontotemporal Dementia	TDP-43	<i>In cell culture</i>	<ul style="list-style-type: none"> Yamashita et al., 2014 	<ul style="list-style-type: none"> Nonaka et al., 2013 Feiler et al., 2015 Smethurst et al., 2020 	<ul style="list-style-type: none"> Nonaka et al., 2013 Shimonaka et al., 2016
		<i>In vivo</i>	<ul style="list-style-type: none"> Wils et al., 2010 	<ul style="list-style-type: none"> Ding et al., 2021 	<ul style="list-style-type: none"> Porta et al., 2018 Ding et al., 2021
	C9ORF72 DPRs	<i>In cell culture</i>	<ul style="list-style-type: none"> Chang et al., 2016 Zhou et al., 2017 Nihei et al., 2020 	<ul style="list-style-type: none"> Chang et al., 2016 Westergard et al., 2016 Zhou et al., 2017 	<ul style="list-style-type: none"> Khosravi et al., 2020
		<i>In vivo</i>	<ul style="list-style-type: none"> LaClair et al., 2020 Nguyen et al., 2020 	<ul style="list-style-type: none"> Morón-Oset et al., 2019 	<ul style="list-style-type: none"> Not shown yet

Table 1.1 Prion-like properties of common misfolded aggregates

The table depicts basic scientific studies that have described the occurrence of three important prion-like properties for common pathological aggregates in AD, PD, and ALS/FTD. The studies are classified according to whether they occurred in cell culture or *in vivo* settings. The three properties are as follows: (i) the ability to induce neurotoxicity in a cell, (ii) spreading from one cell to another, and (iii) seeding of native conformers in the naive cell. **References** ^{76 – 132}.

The cell-to-cell transmission of pathological protein aggregates is a potential unifying mechanism that underlies the progression of various neurodegenerative diseases. The propagated aggregates can interact with native conformers and change them into a misfolding state, thus promoting more aggregation and further spreading. The discovery that degenerating neuronal cells accumulate prion-like insoluble aggregates with a precise spatiotemporal distribution along the central nervous system has led to the hypothesis that protein aggregation and disease progression are two related phenomena^{133,134}. Many factors influence these two phenomena, including ageing¹³⁵, oxidative stress and mitochondrial dysfunction¹³⁶, membrane damage¹³⁷, disrupted phase-separation¹³⁸, impaired clearance¹³⁹, stress-granules disassembly¹⁴⁰, inflammation¹⁴¹ and the genetics of the individual¹⁴². Notably, protein aggregation can be especially harmful in postmitotic cells such as neurons, which cannot dilute out proteotoxins through cell division¹⁴³. Future research is required to better understand the spatiotemporal and cause-effect relationships of aggregate spreading, neurodegeneration and disease progression.

1.1.4 The role of lysosomes in aggregate clearance

Autophagy is a cellular process that uses lysosome-mediated degradation to remove cellular constituents such as nucleic acids, proteins, lipids, and organelles in order to support homeostasis, differentiation, development, and survival¹⁴⁴. The process of autophagy was first described in the 1960s¹⁴⁵, but it was the discovery of autophagy-related genes (*ATG* genes) in the 1990s that accelerated major advances at a molecular level in understanding this pathway^{146–149}.

Currently three forms of autophagy are described: macroautophagy, microautophagy, and chaperone-mediated autophagy. Briefly, macroautophagy involves the formation of double-membraned vesicles known as “autophagosomes” which engulf cargoes that are subsequently degraded after fusion with lysosomes¹⁵⁰; microautophagy involves invaginations or protrusions of the lysosomal membrane to capture cargoes directly into the

lysosome¹⁵¹; and chaperone-mediated autophagy uses chaperones, and not autophagosomes, to selectively identify and translocate cargoes directly across the lysosomal membrane¹⁵².

While three different forms of autophagy exist, all three result in the cargo being delivered to the lysosome for degradation and recycling. Lysosomal organelles degrade autophagic cargoes using acidic hydrolytic enzymes, whose optimal pH (4.5-5.0) is maintained by the lysosomal membrane proton pump v-ATPase¹⁵³. Lysosomes contain over 50 different degradative enzymes capable of hydrolysing proteins, DNA, RNA, polysaccharides, and lipids¹⁵⁴. Among these enzymes, cathepsin proteases have a major role in lysosomal functionality and particularly in the clearance of protein aggregates¹⁵⁵. For example, cathepsin L, B and D have been linked to the degradation of protein aggregates in common neurodegenerative diseases such as AD¹⁵⁶, PD¹⁵⁷, and polyglutamine (polyQ) diseases¹⁵⁸. Because cathepsins are proteases that catalyse irreversible cleavage of peptide bonds, their activities must be strictly regulated by the cell¹⁵⁹. However, altered expression of cathepsins (both at the RNA and protein levels) has been found in neurodegenerative diseases, particularly in ALS¹⁶⁰⁻¹⁶². In ALS *post-mortem* spinal cord tissue, cathepsin B protein levels are increased in the degenerative neurons of the lumbar region¹⁶⁰ and cathepsin B and D mRNAs are higher in spinal cord specimens of sporadic ALS cases¹⁶¹. Furthermore, cathepsin L protein levels have been found to be elevated in dopamine neurons of PD patients' *post-mortem* tissue¹⁶².

Along with molecular chaperones and the ubiquitin–proteasome system (UPS), lysosome-mediated degradation during autophagy is a key regulator of cellular proteostasis, working to (i) degrade misfolded protein aggregates via selective mechanisms (i.e. chaperone-mediated autophagy)¹⁵² and (ii) remove bulk protein aggregates via macroautophagy¹⁶³. Autophagic degradation is particularly crucial in neurons since they are postmitotic cells, unable to dilute out proteotoxins by cell division¹⁴³. Neuron-specific knockout of fundamental autophagy genes like *ATG5* and *ATG7* results in accumulation of protein aggregates, axonal degeneration and cell death in mice¹⁶⁴⁻¹⁶⁶. Conversely, boosting autophagy with pharmacological or genetic applications results in the diminishment of protein aggregation along with the promotion of health and longevity in various animal models¹⁶⁷⁻¹⁶⁹. For example, autophagy inducers improve the clearance of ALS-specific TDP-43 aggregates and promote survival of human stem cell-derived neurons¹⁷⁰.

Protein aggregates can accumulate in lysosomal organelles, causing the loss of lysosomal membrane integrity, mitochondrial dysfunction, and production of reactive oxygen species^{171–173}. These lysosomal disturbances can lead to excessive lysosomal exocytosis and therefore increase the extracellular release of aggregates¹⁷⁴, which might contribute to the progression of pathology via prion-like spreading^{175–178}. An overview of the relations between lysosomal homeostasis and protein aggregation is depicted in **Figure 1.4**.

The fact that lysosomal homeostasis is intimately linked to the control of aggregation-prone proteins is also demonstrated by genetic data. Mutations in the *PGRN* gene (progranulin), which controls lysosome biogenesis and function, have been linked to frontotemporal dementia (FTD) cases with the presence of ubiquitinated TDP-43-aggregates in cortical neurons^{179–181}; and mutations in the *TMEM106B* gene, which controls lysosome size and number, have been linked to FTD cases with *C9ORF72* expansion¹⁸². Furthermore, *TBK1* loss-of-function mutations have been linked to ALS and FTD^{183,184}, and *TBK1* activity loss in human motor neurons causes impaired endosomal maturation and lysosomal acidification, as well as increased cytoplasmic TDP-43 aggregation¹⁸⁵. A small fraction of sporadic and familial ALS cases has also been reported to have loss-of-function mutations in the optineurin gene (*OPTN*)¹⁸⁶; some of these mutations block important autophagy processes in cell culture, such as autophagosome-lysosome fusion¹⁸⁷. Notably, the optineurin protein promotes autophagosome formation¹⁸⁸ and protein aggregate clearance^{189,190}, emphasising the link between lysosomal dysfunction and protein aggregation once more.

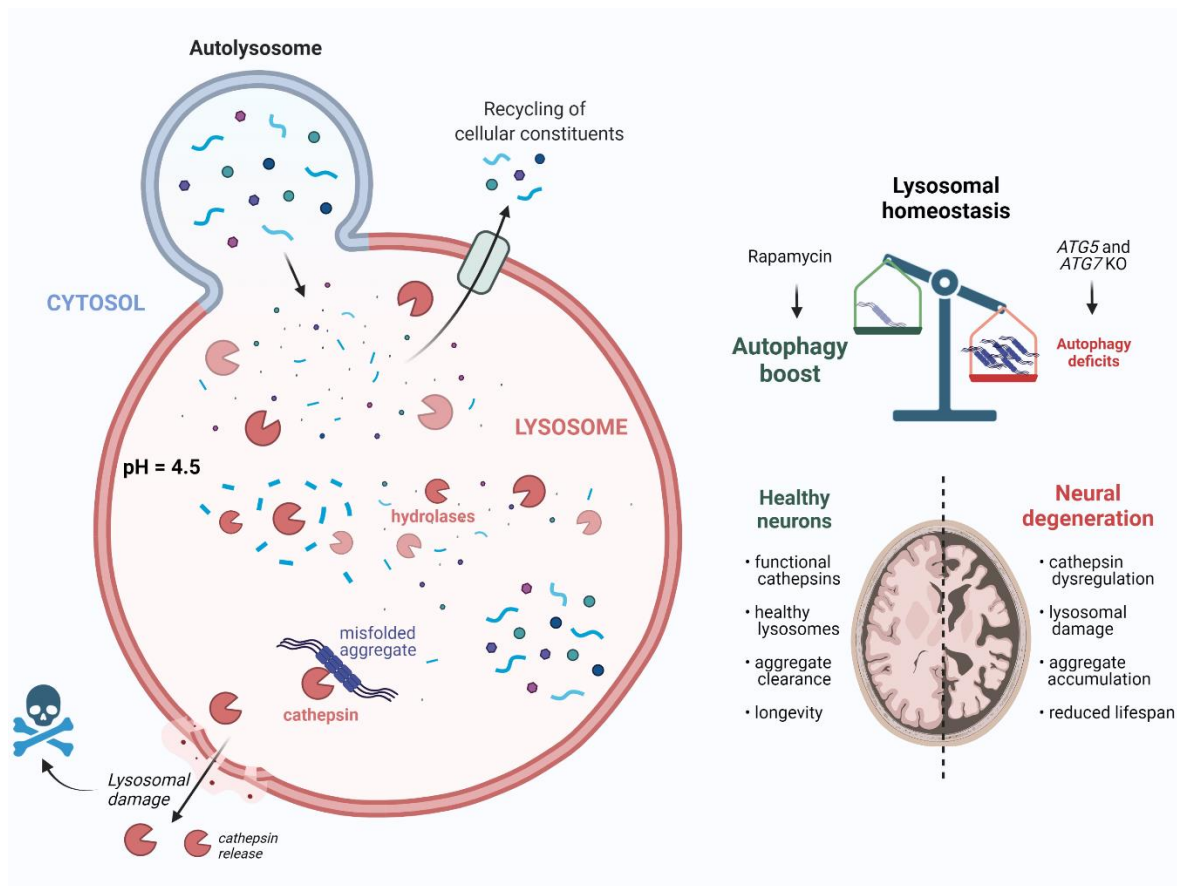


Figure 1.4 Lysosome homeostasis and protein aggregation

Evidence from mice and cell culture studies suggests that impaired lysosomal-mediated degradation is one of the most common factors contributing to the breakdown of proteostasis and the induction of tissue degeneration. Maintaining lysosomal homeostasis with functional cathepsin enzymes is critical for the cell's ability to clear misfolded aggregates and recycle cellular constituents. If these aggregates are not cleared properly, they can cause lysosomal damage and the subsequent release of cathepsins in the cytosol, ultimately leading to cell death activation. Increasing lysosome-mediated degradation by increasing autophagy (via rapamycin, for example) has been shown to reduce protein aggregation and promote health and longevity. Figure created with BioRender.com under academic license.

1.2 ALS and FTD as a unique spectrum of disease

1.2.1 Amyotrophic Lateral Sclerosis

Despite early case reports from the 1820s, the first systematic description of ALS dates from the 1860s, when French neurologist Jean-Martin Charcot linked the disease to its distinct neuropathology¹⁹¹. In a cervical cross-section of a spinal cord from an ALS patient, Charcot discovered debris in the anterior horn, as well as sclerosis (tissue stiffening) of the lateral columns and a general lack of cells¹⁹². The term *a-myo-trophic* is derived from the Greek language and stands for *no-muscle-nourishment*; whereas *lateral sclerosis* refers to the stiffening of the spinal cord's lateral columns as they degenerate¹⁹³. ALS only gained public recognition in the 1930s, when baseball player Lou Gehrig, the stoic New York Yankee who was the greatest first baseman in history, was forced to retire due to progressive muscle weakness¹⁹⁴.

ALS is the most common motor neuron (MN) disorder, characterised by the progressive degeneration of upper and lower motor neurons¹⁹⁵. Upper populations of motor neurons are found in the motor cortex; while lower populations reside in the brain stem and spinal cord and innervate the muscles (**Figure 1.5**). Muscular stiffness and spasticity happen when upper motor neurons fail; whereas when lower motor neurons are affected, they first cause spontaneous muscle twitching (fasciculations) and then muscle atrophy (thinning of muscle mass) as they degenerate and lose connectivity with muscles¹⁹⁶. These classic motor symptoms are frequently accompanied by cognitive deficiencies and emotional vulnerability¹⁹⁷, and approximately 14% of ALS patients meet the diagnostic criteria for frontotemporal dementia (FTD)¹⁹⁸. Most people with ALS die from respiratory failure within 3 to 5 years after diagnosis^{199,200} as late clinical manifestations involve the paralysis of skeletal muscles, including the diaphragm¹⁹⁶. Only a small percentage of ALS patients (~10%) can survive for 5 or more years^{201,202}.

There is currently no therapy that provides a significant clinical benefit to ALS patients. The FDA-approved drugs for the treatment of ALS, riluzole²⁰³ and edaravone²⁰⁴, provide a limited improvement in survival. Currently, the mainstay of care for individuals with ALS is timely symptom management, which includes nasogastric feeding and ventilatory support.

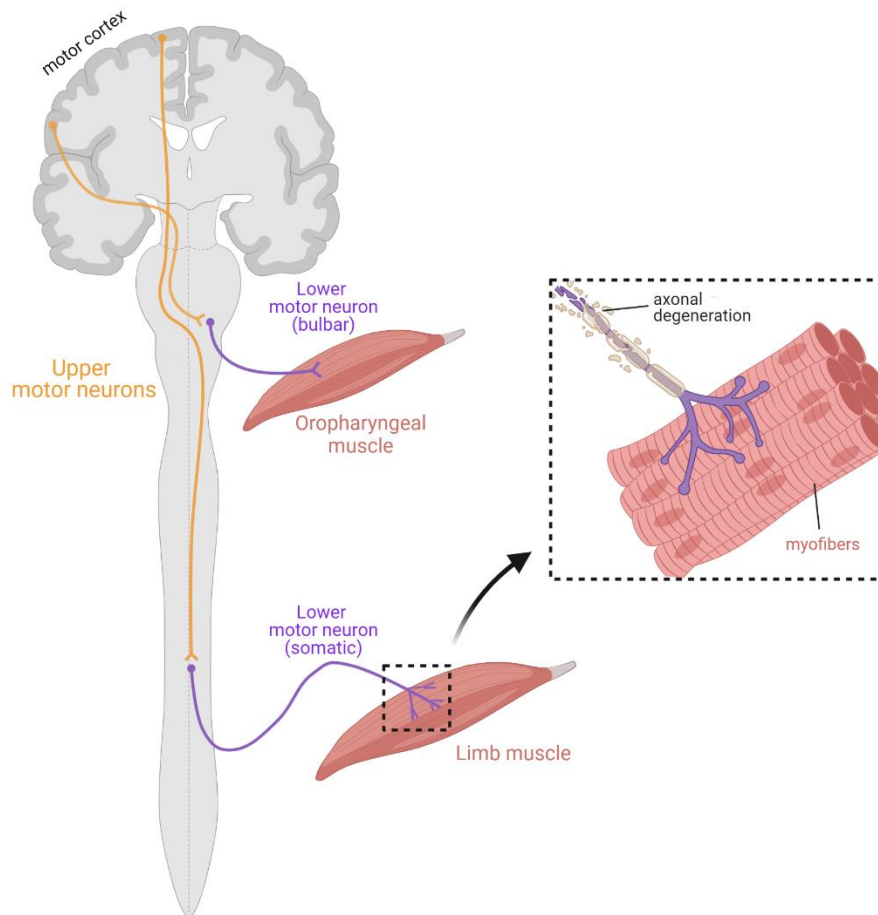


Figure 1.5 Neuroanatomical illustration of ALS pathology

Upper motor neurons (UMNs) of the motor cortex generate motor signals by integrating excitatory and inhibitory stimuli from surrounding cortical areas and translating them into signals that promote or inhibit voluntary movement. Following decussation, UMN axons connect to lower motor neurons (LMNs) in the brain stem (corticobulbar tract) and the spinal cord (corticospinal tract). To control contraction, LMNs make contact with skeletal muscles. Because of peripheral axonal degeneration, the neuromuscular junction of ALS patients is disrupted. Figure created with BioRender.com under academic license.

Age is the most important risk factor for ALS ^{205,206}. The mean or median age of disease onset is between 51 and 66 years ^{207–209}, with European patients typically experiencing ALS at a later age than patients from China, Cuba, and Uruguay ^{210,211}. By the age of 85, the risk of developing ALS is about 1 in 300 individuals ^{212,213}. However, ALS can also affect younger people in a small number of cases, giving rise to "juvenile" ALS (jALS) ²¹⁴. The global incidence of ALS ranges between 0.6 and 3.8 cases per 100,000 people per year (in Europe, 2.1–3.8) ^{211,212}. Men are affected 1.5 times more than women, and ethnicity may

influence ALS incidence (higher in non-Hispanic Caucasians compared to other populations)^{215,216}, though healthcare disparities are confounding factors²¹⁷.

Approximately 90-95% of cases do not have an associated family history and are referred to as sporadic ALS (sALS). These cases are thought to result from a complex interplay between environmental risk factors with susceptibility genes; however, other mechanisms such as *de novo* mutations²¹⁸ and environmental modifications to the epigenome remain a possibility²¹⁹. Studies have suggested links between increased ALS disease susceptibility and smoking²²⁰, military service²²¹, heavy metals exposure²²², frequent and strenuous leisure-time exercise²²³, head trauma^{224,225} and many others; however, the majority of these reports have been challenged by contradictory findings, and more unbiased population-based studies are needed²²⁶.

The remaining 10% of ALS cases have a known family history (familial ALS or fALS), in which a pathogenic mutation in one ALS gene is, in most cases, inherited in an autosomal-dominant manner with age-dependent penetrance^{227,228}. However, a pathogenic mutation in more than one ALS gene can be found in 5% of families with fALS, indicating oligogenic inheritance in ALS²²⁹.

The discovery of disease-associated loci was a game-changer in the field of ALS research, paving the way for the discovery of a number of pathogenic mechanisms at the disease's root. A database of ALS genes (ALSoD)²³⁰ with their associated phenotypes and a measure of their credibility is available at the World Federation of Neurology and ENCALS project website <http://alsod.iop.kcl.ac.uk>. In **Table 1.2**, we present the list of ALSoD "definitive ALS genes", which are defined in the database as "genes whose variants have been shown to increase the risk of ALS based on a statistical test." Despite this intricate and complex network of genes, pathogenic variants in only four of these genes contribute to more than 50% of familial cases and more than 10% of sALS, with variants in other genes found in only a small proportion of cases²³¹. These four major variants affect *SOD1*²³², the first gene linked to ALS, as well as *TARDBP*^{233,234}, *FUS*^{235,236}, and, more recently, *C9ORF72*^{237,238}, which will be the focus of this PhD research project.

Chromosome	Gene symbol	Protein	Inheritance
10q22.3	ANXA11	Annexin A11	AD
9p21.2	C9ORF72	Guanine nucleotide exchange factor C9orf72	AD
22q11.23	CHCHD10	Coiled-coil-helix-coiled-coil-helix domain-containing protein 10	AD
2q36.1	EPHA4	Ephrin type-A receptor 4	not known
16p11.2	FUS	Fused in Sarcoma	AD or AR
12q13.13	HNRNPA1	Heterogeneous nuclear ribonucleoprotein A1	AD
12q13.3	KIF5A	Kinesin heavy chain isoform 5A	AD
4q33	NEK1	Serine/threonine-protein kinase Nek1	AD
10p13	OPTN	Optineurin	AD or AR
17p13.2	PFN1	Profilin-1	AD
21q22.11	SOD1	Superoxide Dismutase 1	AD or AR
1p36.22	TARDBP	TAR DNA-binding protein 43	AD
12q14.2	TBK1	Serine/threonine-protein kinase TBK1	AD
Xp11.21	UBQLN2	Ubiquilin-2	XLD
19p13.11	UNC13A	Protein unc-13 homolog A	not known
20q13.21	VAPB	Vesicle-associated membrane protein-associated protein B/C	AD
9p13.3	VCP	Transitional endoplasmic reticulum ATPase	AD

Table 1.2 Definitive ALS genes (ALSoD)

List of ALSoD "definitive ALS genes", which are defined in the ALSoD database as "*genes whose variants have been shown to increase the risk of ALS based on a statistical test*". Abbreviations: AD = autosomal dominant; AR = autosomal recessive; XLD = X-linked dominant. The four major ALS variants are highlighted in purple.

1.2.2 Frontotemporal Dementia

Frontotemporal dementia (FTD) was first described in 1892 by the Czech neurologist Arnold Pick ²³⁹ and now refers to a wide range of clinical disorders characterised by progressive deterioration of personality, behaviour, language, cognition and motor function ²⁴⁰. These disorders are distinguished by the progressive degeneration of neurons in the superficial frontal cortex and the anterior temporal lobes ²⁴¹. In some cases (~30%), FTD patients are also diagnosed with ALS, and develop motor symptoms accompanied by corticospinal tract degeneration ^{242,243}.

FTD is also known as Frontotemporal Lobar Degeneration (FTLD) because it refers to the common atrophy of the frontal and anterior temporal lobes. Aside from this common neuropathological trait, FTLD is a clinically, genetically, and pathologically diverse group of disorders ²⁴⁴.

Nowadays, most clinicians recognise FTLD as falling into three major variants. There is one behavioural variant called *behavioural variant FTD* (bvFTD); and two language variants called *semantic variant primary progressive aphasia* (svPPA) and *nonfluent variant primary progressive aphasia* (nfvPPA) ²⁴⁵, as shown in **Figure 1.6**. BvFTD is the most common of these variants, and it is characterised by progressive changes in behaviour, personality, emotional reactivity and executive skills ²⁴⁶. SvPPA is characterized by difficulties with semantic understanding and naming, whereas nfvPPA is characterized by impaired speech and grammar ²⁴⁷. Despite their distinct early manifestations, the clinical phenotypes of these variants may overlap in later stages as the disease affects larger areas of the frontal and temporal lobes ^{248,249}. Furthermore, the core FTD disorders frequently overlap with other FTD-related traits like ALS, progressive supranuclear palsy, and corticobasal syndrome ²⁵⁰. Most FTD patients have global cognitive deficits and difficulties eating, moving, and swallowing by the end stage of disease progression ²⁵¹. Death is usually caused by infection-associated pneumonia and occurs 4–8 years after the onset of symptoms ^{251–253}.

There is currently no FDA-approved disease-modifying treatment for FTD ²⁵⁴; however, symptomatic treatments such as selective serotonin reuptake inhibitors and atypical antipsychotic agents are frequently used to manage behavioural abnormalities ²⁵⁵. No effective therapies are available for cognitive complaints in FTD, which frequently involve executive function, memory, and language ²⁵⁶. Non-pharmacological interventions, such as caregiver training, physical exercise, and speech therapy, can be beneficial in some cases ²⁵⁷.

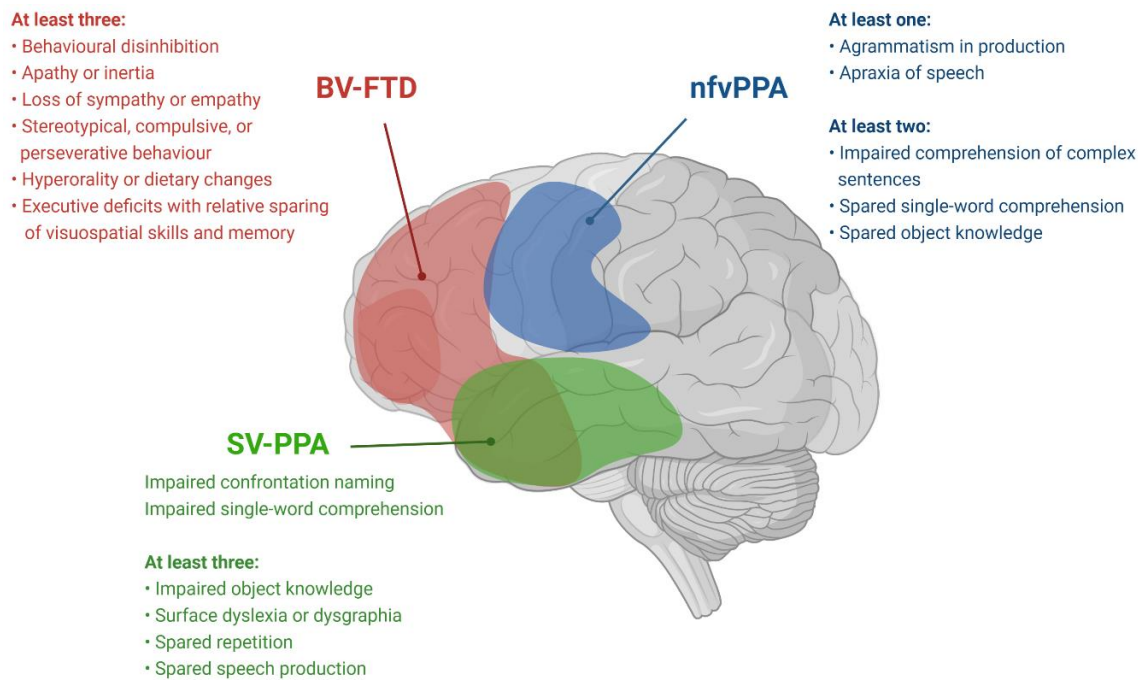


Figure 1.6 Overview of FTD clinical syndromes

Patterns of brain atrophy associated with FTD clinical syndromes are depicted, according to imaging findings reported in Peet et al., 2021²⁵⁸. In the later stages of the disease, atrophy becomes more pronounced, widely affecting the frontal and temporal lobes. Diagnostic criteria for clinical diagnosis of FTD are also reported, based on the classification presented in the seminal review of Bang et al., 2015²⁵¹. Figure created with BioRender.com under academic license.

Ageing is the primary risk factor for FTD²⁵⁹. The mean age at diagnosis is estimated to be 69 years²⁶⁰, but in the majority of cases the first symptoms manifest earlier, between the ages of 45 and 64 years^{261,262}. Because symptoms appear relatively early, FTD is sometimes defined as a “young-onset dementia”, and constitutes the most common type of dementia in people under the age of 60²⁶³. Global-scale studies to monitor FTD incidence are still lacking, but as an indication, in the United States, the incidence of FTD for 45–64 years-old people ranges from 2.7 to 4.1 per 100,000 person-years²⁶⁴. No gender-associated differences were observed in the vast majority of epidemiological studies²⁶⁵.

About 60-70% of patients with FTD have no apparent family history of dementia and are considered to be sporadic cases²⁶⁶. These cases might arise from a combination of genetic and environmental risk factors, but this has not been thoroughly investigated. However, head trauma and thyroid disease have been linked to an increased risk of sporadic FTD, while other factors (such as smoking, alcohol, and chemical exposure) have not²⁶⁷.

In the remaining 30-40% of FTD cases, the disease is familial and most often inherited in an autosomal dominant manner²⁶⁸. Pathogenic variants in three major genes, *MAPT*, *GRN*, and *C9ORF72*, have been found in 60% of familial FTD cases²⁴⁴. *C9ORF72* mutations are typically the most common, accounting for 25% of these cases. Other mutations, which are rarer, occur in several genes and are estimated to be present in ~5% of familial FTD cases²⁶⁹. Table 1.3 shows a comprehensive list of genes with variants directly implicated in FTD.

Chromosome	Gene symbol	Protein	Inheritance
9p21.2	<i>C9ORF72</i>	Guanine nucleotide exchange factor C9orf72	AD
16p13.3	CCNF	Cyclin F	not known
22q11.23	CHCHD10	Coiled-coil-helix-coiled-coil-helix domain-containing protein 10	AD
3p11.2	CHMP2B	Charged multivesicular body protein 2b	AD
16p11.2	FUS	Fused in Sarcoma	AD or AR
17q21.31	<i>GRN</i>	Progranulin	AD
17q21.31	<i>MAPT</i>	Microtubule-associated protein tau	AD
14q24.2	PSEN1	Presenilin-1	AD
5q35.5	SQSTM1	Sequestosome-1/ Ubiquitinbinding protein p62	AD
1p36.22	TARDBP	TAR DNA-binding protein 43	AD
12q14.2	TBK1	Serine/threonine-protein kinase TBK1	AD
2p13.3	TIA1	Cytotoxic granule associated RNA binding protein TIA1	AD or AR
2q35	TUBA4A	Tubulin alpha-4A chain	AD
Xp11.21	UBQLN2	Ubiquilin-2	XLD
9p13.3	VCP	Transitional endoplasmic reticulum ATPase	AD

Table 1.3 FTD genes

List of genes with variants directly implicated in the aetiology of FTD.

Abbreviations: AD = autosomal dominant; AR = autosomal recessive; XLD = X-linked dominant. The three major FTD variants are highlighted in purple.

1.2.3 Overlapping between ALS and FTD

As previously mentioned, we currently know that approximately 14% of ALS patients meet the diagnostic criteria for FTD¹⁹⁸ and, conversely, 30% of FTD patients are also diagnosed with ALS^{242,243}. Clinical studies in the 1980s began to report loss of cognitive-behavioural function and dementia in a subset of ALS patients²⁷⁰ (although these were actually noted more than a century ago²⁷¹). A decade later, these clinical reports grew in number and drew attention to the cognitive deficits observed in ALS²⁷². During that time, neuroimaging studies on ALS patients began to show evidence of cerebral abnormalities in areas involved in language and executive functions, similar to those found in FTD cases^{273–275}.

In 2006, a breakthrough study by Neumann and co-workers revealed the presence of ubiquitin- and TDP-43-positive inclusions in several regions of *post-mortem* central nervous system (CNS) tissue from ALS and FTD patients¹⁸¹. These aggregates were found to be unusually common in these two diseases²⁷⁶, but not in other neurodegenerative illnesses, so they were proposed as the first common neuropathological hallmark of both ALS and FTD. Importantly, the overlap of such ubiquitin- and TDP-43-pathology suggested that these disorders shared a common pathological process.

In addition to the clinical and neuropathological overlap, reports of families with relatives suffering from ALS, FTD, or both suggested evidence of shared genetic susceptibility to these two diseases^{277,278}. The pattern of heredity observed in these studies was consistent with dominant autosomal inheritance²⁷⁸. Efforts to identify the underlying genetic defect were launched quickly, with a series of genetic linkage studies in large ALS and FTD families. These efforts were aided by the extraordinary progress made in genome sequencing technologies during the first decade of the twenty-first century, with the introduction of next-generation sequencing (NGS)²⁷⁹. The first series of genetic studies identified various genetic loci linked to ALS and FTD, with one locus on chromosome 9p standing out, though the exact gene and nature of the mutation remained unknown^{280–283}. Finally, in 2011, two independent research teams published ground-breaking findings that revealed a hexanucleotide GGGGCC repeat expansion in the *C9ORF72* gene as the most common genetic cause of both ALS and FTD in Europe and North America^{237,284}. Interestingly, this genetic cause is extremely infrequent in Asia and the Middle East^{285,286}; implying potential founder effects or the presence of different environmental and genetic

risk factors^{286,287}. The hexanucleotide repeat expansion in the *C9ORF72* gene (hereafter referred to as C9-HRE) has provided the unmistakable genetic signature for considering ALS and FTD as part of the same disease spectrum, which is now known as C9 ALS/FTD²⁸⁸. The C9-HRE is found in roughly 40% of familial ALS cases in Europe and the United States, and 25% of familial FTD cases in Europe²⁸⁶. This mutation was also discovered in 7% of sporadic ALS cases and 6% of sporadic FTD cases²⁸⁶.

The pathogenic C9-HRE is not the only genetic marker shared by ALS and FTD. Despite the fact that *SOD1* is unique to familial ALS and *MAPT* and *GRN* are unique to familial FTD, several other pathological variants in shared genes have been observed in both fALS and fFTD, including *C9ORF72*, *TARDBP*, *VCP*, *SQSTM1*, *FUS*, *TBK1*, and *CHCHD10*²⁸⁹. Interestingly, many of these genes are involved in proteostasis pathways. Indeed, as illustrated in **Figure 1.7**, nearly all the shared genetic markers between ALS and FTD are involved in protein production (*TARDBP*, *FUS*), trafficking (*C9ORF72*, *MAPT*, *CHMP2B*), and protein degradation (*C9ORF72*, *GRN*, *VCP*, *SQSTM1*, *TBK1*, *UBQLN1*).

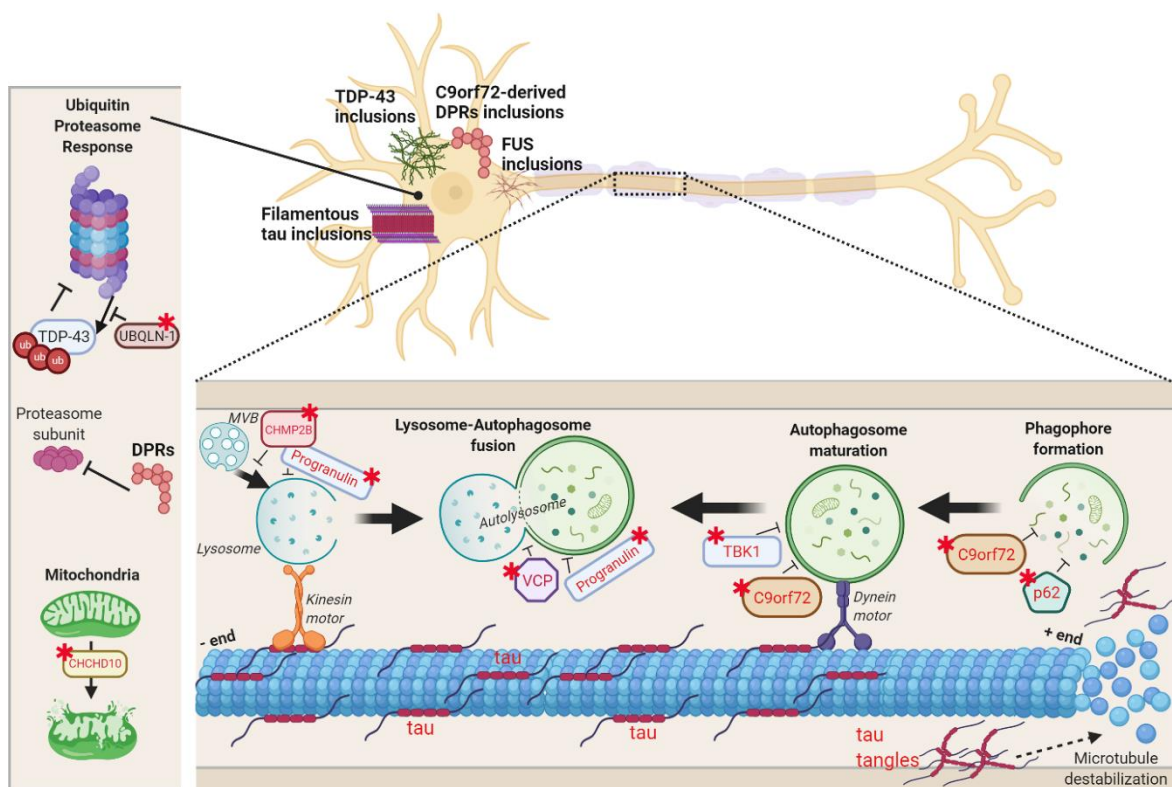


Figure 1.7 Mutations in ALS/FTD genes are linked to proteostasis pathways

Mutations in ALS/FTD are linked to pathways of protein production (*TARDBP*, *FUS*), trafficking (*C9ORF72*, *MAPT*, *CHMP2B*) and protein degradation (*C9ORF72*, *GRN*, *VCP*, *SQSTM1*, *TBK1*, *UBQLN1*). The red stars represent proteins encoded by mutated genes. Mutations of these genes will

encode for altered proteins resulting in impairment of the Ubiquitin-Proteasome Response and autophagy. *CHCHD10* mutations disrupt mitochondrial cristae and have a profound effect on the mitochondrial structure. Proteins accumulated in ubiquitin-positive inclusions in post-mortem brain tissue of ALS/FTD cases are shown in the neuron cytoplasm (TDP-43, FUS, DPRs and Tau). Figure created with BioRender.com under academic license.

Protein nomenclature: TDP-43 (*TARDBP* gene), p62 (*SQSTM1* gene), progranulin (*GRN* gene), tau (*MAPT* gene). Abbreviations: DPRs, dipeptide repeat proteins; Ub, ubiquitin; MVB, Multivesicular body.

1.2.4 Non-cell autonomous players in ALS/FTD

Given the importance of glial cells in modulating neuronal synaptic activity, neurodegenerative diseases cannot be viewed solely as 'neuron-centric'²⁹⁰. Multiple studies over the last two decades have shown that non-neuronal cells contribute to the pathological mechanism in these diseases and are thought to have a particular influence on disease progression^{291–293}. It is becoming clear, particularly in the context of ALS and FTD, that non-cell autonomous processes contribute to neuronal unit damage and death; however, the extent of this contribution is not fully understood^{294,295}. Several studies have begun to suggest that less-defined contributions from glia^{296,297}, blood vessels²⁹⁸ and perivascular fibroblast cells²⁹⁹ may play a role in ALS disease progression and may explain the variability of disease progression seen in sporadic ALS. These findings called into question the neuron-centric theory and prompted a rethinking of our understanding of disease variability.

In this section, we discuss how glia dysfunction (e.g., microglia and astrocytes) contributes to ALS and FTD neuropathology, and in particular how aberrant changes in glial proteostasis interfere with neuronal homeostasis.

Genes with pathological variants common in ALS and FTD (*C9ORF72*, *TBK1*, *OPTN1*, *SQST1*, *VCP*) have been shown to encode proteins that are important for proteostasis balance, specifically for the autophagy pathway³⁰⁰. Many of these genes are particularly important in microglial cells, where they regulate fundamental biological processes such as phagocytosis and inflammation^{301–303}. Because microglial phagocytosis and inflammation have striking morphological, mechanistic and functional similarities with autophagy^{304–308}, it is possible that these microglial processes rely on a balanced autophagy to function properly. Indeed, recent findings suggest that microglial cells with autophagy dysfunction may be abnormally activated and toxic, whereas microglia with functional autophagy may be required for disease protection. This hypothesis could explain why *null* mice for the *C9ORF72* gene, which is involved in autophagy induction and regulation^{309–312}, develop age-related neuroinflammation with specific changes in microglial inflammatory function³¹³. Progranulin deficiency also impairs microglial phagocytosis^{179,314}, and progranulin is an important autophagy protein³¹⁵ (its gene, *GRN*, is also linked to familial FTD). Furthermore, in *SOD1*-mutant rat microglia cultures, trehalose-mediated autophagy reduces microglial activation³¹⁶, possibly by blocking microglial inflammatory cytokines³¹⁷.

Similar to microglia, astrocytes can phagocytose and release inflammatory chemicals and are involved in immune-related processes³¹⁸. Because astrocytes share these functions with microglia, they may also be involved in phagocytic or inflammatory responses via autophagy. Although we know very little about proteostasis imbalance in astrocytes, some studies suggest that astrocytes from ALS and FTD models have dysfunctional proteostasis. Astrocytes in *SOD1*-ALS mouse models are immunopositive for ubiquitinated-*SOD1* inclusions³¹⁹ and exhibit glutamate-mediated excitotoxicity³²⁰. Deficits in specific autophagy or proteasome regulators may exacerbate vulnerability not only in neurons but also in astrocytes, making these glial cells less effective in supporting neuronal homeostasis. Mutations in essential autophagy ALS genes, such as *FIG4*, are likely to have synergistic effects in both neurons and glia; astrocytes carrying *FIG4* mutations do accumulate p62-positive inclusions and are thus less capable of providing protective support to neurons^{321–323}. In a lysosomal storage disease study³²⁴, astrocytes with autophagic-lysosomal dysfunction were unable to metabolically support neurons and thus contributed directly to neurodegeneration.

The autophagy pathway (and, more broadly, proteostasis) in the CNS has been studied primarily in neurons, leaving other cell types largely unexplored. Unless we improve our

understanding of non-neuronal cell contributions and mechanisms preceding disease onset, clinical variability in disease progression will continue to confound the design and evaluation of ALS and FTD treatments. The impact of glial cell proteostasis deficits on neuronal homeostasis needs to be better understood, both in terms of disease progression and in terms of how ALS/FTD mutations in autophagy genes can eventually act synergistically in non-neuronal and neuronal cells.

In **Figure 1.8**, we show how proteostasis imbalances observed in glial cells (microglia and astrocytes) can increase the differential susceptibility of motor neurons to degenerate.

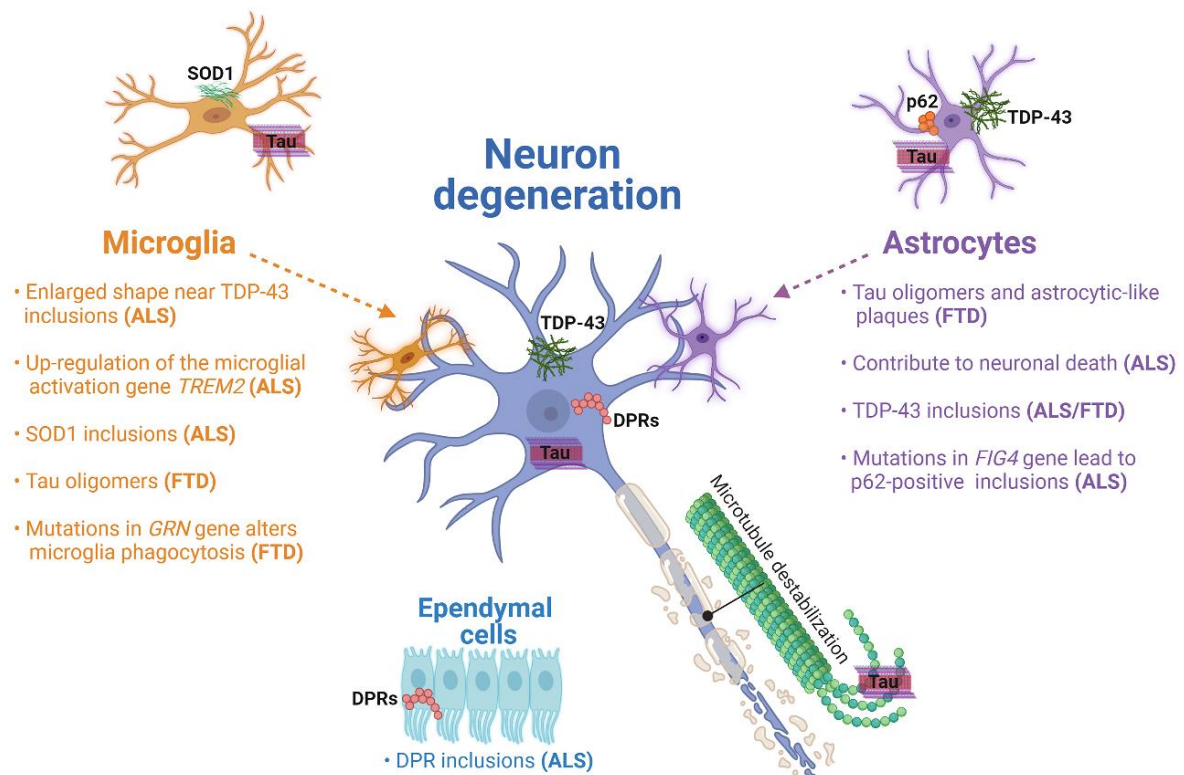


Figure 1.8 Glial cells' proteostasis imbalance in ALS and FTD

Visual representation of various pathological processes and alterations in glial cells contributing to proteostasis imbalance in ALS and FTD; according to published research findings. The presence of protein inclusions is also shown in neuronal and glial cells. Changes in microglia that are relevant to the diseases are highlighted in orange text, while changes in astrocytes are highlighted in purple text. Figure created with BioRender.com under academic license.

1.3 *C9ORF72*-linked ALS/FTD

1.3.1 *C9ORF72* gene and protein

The age of disease onset among carriers of the *C9ORF72* repeat expansion is usually between 50 and 64 years (range: 27-83 years), regardless of the presenting manifestations, which can be pure ALS, pure FTD, or a combination of the two phenotypes^{288,325}. Disease duration ranges from 1 to 22 years^{285,286}. The C9-HRE mutation is known to have an incomplete and age-dependent penetrance: it is generally non-penetrant in individuals younger than 35 years old, 50% penetrant by 58 years old, and nearly fully penetrant by 80 years old²⁸⁶. However, the penetrance pattern may also be influenced by environmental, genetic, lifestyle, or hormonal factors^{287,326}; and there are some rare cases of patients developing disease in their twenties or other patients surviving into their ninth decade without symptoms³²⁶. C9 ALS/FTD is inherited in an autosomal dominant manner. Almost all individuals diagnosed with the disease inherited the C9-HRE from a heterozygous parent, who is affected in most cases but may not have clinical manifestations of the disorder due to age-dependent reduced penetrance³²⁵.

The human *C9ORF72* gene (ENSG00000147894) on the ENSEMBL database³²⁷ is reported to be approximately 38 kilobases-long and spans a total of 11 exons, 10 of which are protein coding. Importantly, the C9-HRE is located between the non-coding exons 1a and 1b.

Alternative splicing and the use of different transcription sites result in 3 main annotated human *C9ORF72* mRNA variants: V1 (ENST00000379997.7), V2 (ENST00000380003.8) and V3 (ENST00000619707.5). These 3 transcript variants encode for 2 different protein isoforms: C9orf72-S (NP 659442.2), a short protein isoform with 222 amino acids, and C9orf72-L (NP 060795.1), a long protein isoform with 481 amino acids. Transcripts V2 and V3 encode for C9orf72-L, while transcript V1 encodes for C9orf72-S²³⁷, as shown in **Figure 1.9**.

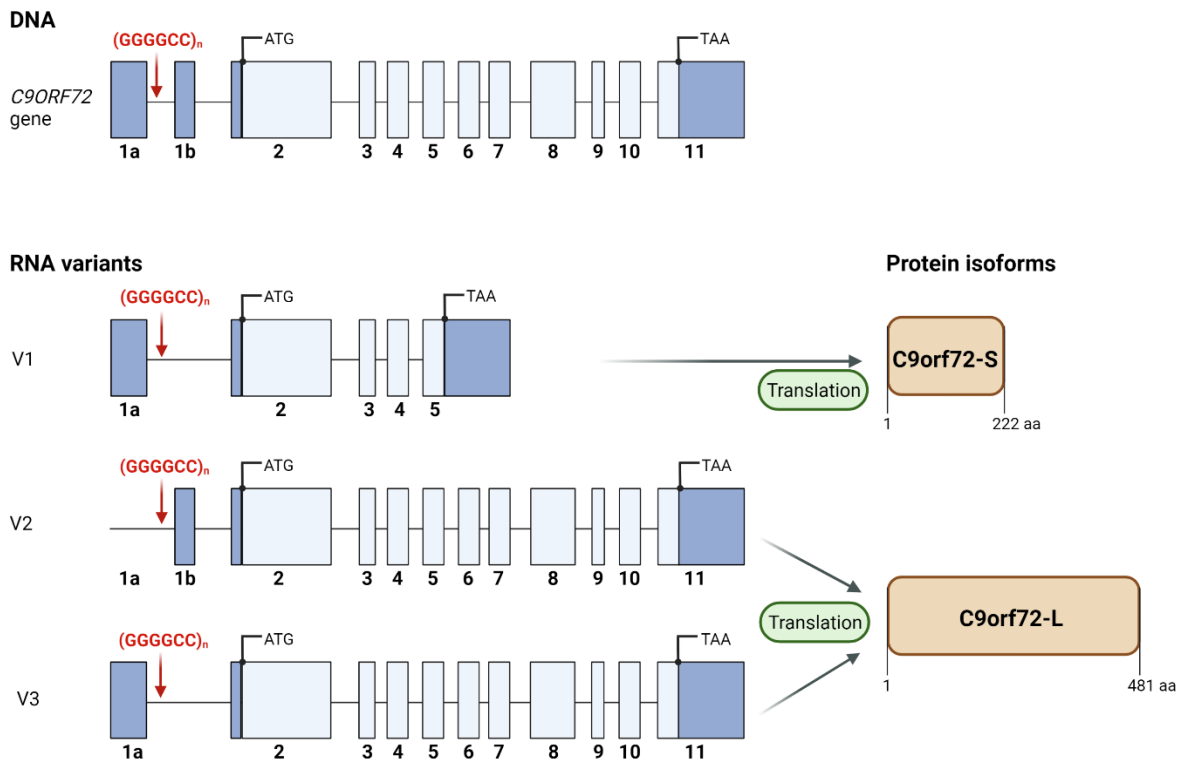


Figure 1.9 *C9ORF72* gene, transcript variants and protein isoforms

Schematic representation of the *C9ORF72* gene and the 3 main annotated transcript variants (V1, V2, V3). Coding and non-coding exons are depicted as blue and light-blue boxes, respectively. The C9 HRE is highlighted in red; it can be found either in the promoter region (in V2) or in the first intron between non-coding exons 1a and 1b (in V1 and V3). V1 encodes C9orf72-S (short), a 222-amino acid protein with a molecular weight of 24 kDa, while V2 and V3 encode C9orf72-L (long), a 481-amino acid protein with a molecular weight of 54 kDa. Figure created with BioRender.com under academic license. Adapted and inspired from Balendra & Isaacs, 2018²⁸⁸.

Even after the discovery of the pathogenic C9 HRE in 2011, the biological role of the C9orf72 protein remained largely unknown for some time. The first clues about the role of the C9orf72 protein came from bioinformatics studies that identified multiple novel homologs of the DENN module (DENN: differentially expressed in Normal and Neoplastic cells) in several proteins, including C9orf72³²⁸. The DENN module is an ancient and conserved protein module that has been shown to act as a GDP-GTP exchange factor (GEF) for Rab GTPases, which are regulators of nearly all membrane trafficking events in eukaryotes³²⁹. Proteins with DENN domains are able to activate Rab GTPases by inducing

their dissociation of GDP and consequent binding to GTP. As a result of these bioinformatic studies, it was predicted that C9orf72 could have Rab-GEF activity and be involved in membrane trafficking. Later studies revealed that C9orf72 colocalized with Rab proteins involved in autophagy and endocytic transport, such as Rab1, Rab5, Rab7, Rab11; and that C9orf72 depletion dysregulated autophagy in neuronal cell cultures³³⁰. Webster and colleagues discovered that the C9orf72 protein is a Rab1a effector that regulates the translocation of the ULK1 autophagy initiation complex to the phagophore, and that disrupting C9orf72 function in neurons inhibits autophagy³³¹. C9orf72 was discovered to form a large multiprotein complex along with Smith-Magenis chromosome region 8 (Smcr8) and WD repeat-containing protein 41 (Wdr41)^{309,332}. This tripartite complex has been shown to function as a Rab-GEF, activating two small Rab GTPases, Rab8a and Rab39b, which are involved in autophagy and membrane trafficking^{332,333}. However, the GEF activity of C9orf72-Smcr8-Wdr41 is still being debated and is not universally accepted. New research suggests that the complex may actually function as a GTPase activating protein (GAP) for Rabs, specifically for Rab8a and Rab11a³³⁴⁻³³⁷, thus stimulating the GTPase activity of these proteins and terminating their signalling event. *In vivo* studies have added to our understanding of the C9orf72 protein's function. Several studies began to produce C9ORF72-knockout (C9-KO) mice, which demonstrated that these animals have autoimmune and inflammation phenotypes such as splenomegaly, autoantibody production, glomerulonephropathy, neutrophilia, thrombocytopenia, increased inflammatory cytokines, and a high mortality rate³³⁸⁻³⁴⁰. These findings suggested that the C9orf72 protein might play an important role in suppressing inflammation and the development of autoimmunity, even in the context of gut bacteria-induced inflammation³⁴¹. C9-KO mice, interestingly, had higher levels of autophagy proteins (p62 and LC3) in the spleen, confirming C9orf72's role in autophagy regulation^{313,339}.

Future research will be needed to better identify the physiological functions of the C9orf72 protein, particularly by investigating its isoform-specific functions (C9orf72-S vs C9orf72-L).

1.3.2 C9-HRE disease mechanisms

As previously discussed, the hexanucleotide repeat expansion (C9-HRE) in the *C9ORF72* gene is the major genetic cause of familial forms of ALS and FTD^{237,284}.

The C9-HRE is highly polymorphic and distinguishing between normal and pathogenic repeat number remains difficult. The number of repeats in healthy controls is typically less than 30 (7-8 repeats in most control individuals), whereas pathogenic C9-HRE can have hundreds to thousands of repeats^{342,343}. The size of the smallest expansion unit that confers disease risk is unknown, but recent research suggests that a threshold of 24-30 repeats could be used to distinguish pathogenic from neutral expansions^{342,344}. However, the number of repeats detected in a single individual should be interpreted with caution, as the C9-HRE expansion units have been shown to be highly heterogeneous in a single individual's brain regions and cell types, a phenomenon known as "somatic mosaicism"^{342,345}. Somatic mosaicism of the C9-HRE within the CNS may explain some of the clinical heterogeneity observed between patients, but it is currently poorly understood²⁸⁸. The C9-HRE's intrinsic structural variability may contribute to this phenomenon; in fact, the C9-HRE can fold into a variety of complex secondary structures, including "G-quadruplexes"³⁴⁶⁻³⁴⁸, which are stable four-stranded DNA helical structures that can form within G-rich DNA and RNA sequences³⁴⁹. Furthermore, Xi and colleagues reported epigenetic features of the C9-HRE by discovering that this region is methylated in every C9-ALS patient³⁵⁰; this finding was replicated in the C9-BAC mouse model of ALS³⁵¹. However, it is unclear how methylation of C9-HRE may participate in C9-HRE somatic mosaicism or in any C9 ALS/FTD pathological feature.

Despite the fact that the C9-HRE mutation was discovered relatively recently, progress in understanding its pathogenic effects has been rapid. There have been three competing but non-exclusive mechanisms proposed: (i) loss of function of the *C9orf72* protein due to *C9ORF72* haploinsufficiency, (ii) toxic gain of function from sense and antisense C9-HRE RNAs that form "RNA foci" and (iii) toxic gain of function from the translation of the C9-HRE RNAs into dipeptide repeat proteins³⁵².

These mechanisms are all likely to contribute to disease to some extent but determining their relative importance at various disease stages is critical for informing therapeutic strategies.

1.3.2.1 *C9ORF72* haploinsufficiency

In parallel with the discovery of the C9-HRE in ALS/FTD patients, several research groups have started to observe reduced levels of *C9ORF72* mRNA in C9 ALS/FTD *post-mortem* tissue, induced pluripotent stem cells (iPSCs), iPSC-derived motor neurons, lymphoblast cell lines and blood samples^{237,353–359}. Furthermore, reduced C9orf72 protein levels were found in *post-mortem* frontal cortex tissue from ALS and FTD patients^{360,361}.

This body of evidence led researchers to believe that *C9ORF72* "haploinsufficiency" may contribute to C9 ALS/FTD. Haploinsufficiency in genetics describes a model of dominant gene action in diploid organisms: when one allele is inactivated, the remaining functional allele is *insufficient* to maintain normal gene function³⁶².

The C9-HRE, as previously stated, is made up of repetitive GC-rich sequences and secondary structures (e.g., G-quadruplexes). These characteristics can, in theory, disrupt transcription by reducing RNA polymerase II (RNAPII) elongation and leading to the deposition of repressive chromatin marks, as shown in other contexts³⁶³. However, the nature of the mechanism by which C9-HRE leads to *C9ORF72* haploinsufficiency remains unknown. Nonetheless, it is thought that the inability of RNAPII to read through the C9-HRE mutation reduces the abundance of the endogenous *C9ORF72* mRNA product. This, in turn, may result in reduced translation of the C9orf72 protein, which plays important roles in endolysosomal pathways and inflammation responses^{313,331,340}.

Different research groups investigated the possibility that C9orf72 protein loss-of-function could be pathogenic, thus leading to ALS/FTD-specific disease phenotypes. A significant effort was made to create various *C9ORF72* gene knockout (C9-KO) or gene knockdown (C9-KD) animal models. Some of the first experiments were carried out in popular model organisms such as *C. elegans*³⁶⁴ and zebrafish³⁵⁴, in which C9-KO and C9-KD caused paralysis and degeneration of motor neurons, respectively.

However, whether *C9ORF72* haploinsufficiency can cause neurodegeneration and ALS/FTD phenotypes on its own has been the subject of extensive research and debate. Indeed, contradictory evidence has been presented demonstrating how loss of function alone is insufficient to explain many key pathological features of C9 ALS/FTD. Among the evidence is the finding that C9 homozygous human patients do not have more severe symptoms than heterozygous patients³⁶⁵. Furthermore, in human induced motor neurons

(iMNs), decreased *C9orf72* protein levels work in tandem with *C9ORF72* gain-of-function mechanisms to cause neurodegeneration³⁶⁶. Murine studies provide additional evidence that *C9ORF72* haploinsufficiency may not be capable of triggering ALS/FTD phenotypes on its own. *C9*-KO mice show no motor neuron degeneration or motor deficits^{309,367–370}. This indicates that the *C9orf72* protein may not be fully essential in mice or there may be redundancy of the *C9ORF72* gene in this species. As previously discussed, *C9*-KO mice showed inflammation and autoimmune phenotypes^{309,340,367–370}, with some having shorter survival³⁴⁰. Immune responses in macrophages and microglia were altered, implying that the *C9orf72* protein may regulate immune homeostasis. Because autophagy plays a role in the immune system^{371,372}, this regulation could be mediated by autophagy.

Clearly, more research is needed to determine the role of defective autophagy in neuronal loss in *C9* ALS/FTD, but it is well established that autophagy loss in neuronal cells can cause neurodegeneration and motor deficits. This evidence is based on neuron-specific knockouts of the essential autophagy genes *ATG7*, *ATG5*, and *RB1CC1* (*FIP200*) in mice, which resulted in neurodegeneration, progressive motor deficits, and protein aggregate accumulation^{164,165,373,374}. Interestingly, some of the motor deficits observed in these KO mice were similar to those seen in ALS-mouse models (e.g., abnormal limb-clasping reflexes)^{319,375,376}. However, neural-specific *C9*-KO in mice did not result in motor neuron degeneration or motor function defects³⁷⁷.

Considering all of this, loss-of-function is unlikely to be the primary pathogenic mechanism of *C9* ALS/FTD-linked neurodegeneration, and gain-of-function paradigms must also be considered.

1.3.2.2 RNA foci-mediated toxicity

In the very first reports of the *C9*-HRE^{237,284}, RNA-mediated toxicity was proposed as a possible pathogenic mechanism of *C9* ALS/FTD. In fact, the authors discovered intranuclear RNA inclusions with distinct morphology known as "RNA foci" in *post-mortem* CNS tissue from *C9* ALS/FTD patients^{237,284}. Since then, RNA foci in the frontal cortex, hippocampus, cerebellum, and spinal cord of *C9* ALS/FTD patients have been consistently observed^{378–380}. The presence of RNA foci in *C9* ALS/FTD disease models, including iPSC-derived

neurons^{355,359} and iPSC-derived motor neurons^{381,382} from affected individuals, has also been reported.

In C9 ALS/FTD, the mechanism of RNA foci formation involves bi-directional transcription of the C9-HRE, which generates sense and antisense RNA transcripts. As C9-HRE bi-directional transcription continues, these RNAs accumulate in the nucleus and, due to their complex secondary structures, may engage in specific or non-specific interactions with RNA-binding proteins³⁸³. Such interactions may result in robust protein sequestration and the formation of intranuclear RNA inclusions (referred to as *RNA foci*) that can be detected using *in situ* hybridization^{237,284}.

RNA foci were discovered in 1995 in myotonic dystrophy types 1 and 2, and their associated toxicity has been known ever since³⁸⁴. They are now also found in other neurological disorders, including fragile X-associated tremor ataxia syndrome, Huntington's disease-like 2, and spinocerebellar ataxias³⁸⁵.

It was quickly hypothesised in C9 ALS/FTD that sense and antisense RNA foci could sequester fundamental RNA-binding proteins (RBPs) and splicing factors, disrupting their normal function and causing cellular toxicity and pathogenicity. A number of RBPs have been identified as interacting with C9 RNAs *in vitro* and in patient tissue, and some of these proteins co-localized with RNA foci^{355,381,386–388}. Members of the protein family of heterogeneous nuclear ribonucleoproteins (hnRNPs) were found to be particularly enriched in RNA foci^{386,388–390}; these proteins play critical roles in mRNA splicing and gene expression³⁹¹, and their interaction with RNA foci began to suggest that RNA metabolism may be impaired as a gain-of-function mechanism in C9 ALS/FTD. Furthermore, it was discovered that the C9-HRE sense RNA interfered with translation in *Drosophila* and primary rodent neurons by binding ribonucleoprotein transport granules, which are a group of compartments (including stress granules) that are known to play a role in post-translational modifications³⁹².

Despite this mounting evidence, comparative studies in *Drosophila*^{393,394} and mouse models expressing the human *C9ORF72* gene with hundreds of hexanucleotide repeats – created with a bacterial artificial chromosome (BAC)^{395,396} – do not support a role for C9-HRE-derived RNA foci in toxicity. Indeed, these animal models consistently fail to induce motor phenotypes or neurodegeneration while reproducing the appearance of RNA foci^{395,396}. These findings are also consistent with the controversial mouse model expressing the human *C9ORF72* gene with 500 hexanucleotide repeats, namely “C9-500” model, from the Liu et

al. study³⁹⁷, which has recently gained criticism after two independent research teams found no abnormalities in survival, motor function, or neurodegeneration in two large C9-500 animal cohorts³⁹⁸; this mouse model displays RNA foci. One possible explanation for the discrepancy between these results is that the housing environment may contribute to phenotypic manifestations in C9-500 animals, as vivarium-dependent commensal microorganisms have been shown to modify the severity of phenotypes in other ALS mouse models^{341,399}. Another possibility is that the genetic background of the mice in the Liu et al. study³⁹⁷ hampered the analysis. Indeed, C9-500 mice were initially generated and studied on an FVB/N genetic background, which is a problematic background for modelling neurological diseases due to inherent seizure activity⁴⁰⁰, marked gait ataxia, as well as decreased locomotor and exploratory activity⁴⁰¹, and has also been linked to a syndrome of sudden death and variable CNS lesions known as “space cadet syndrome”^{402,403}. As a result, mis-assignment of effect to the C9-500 transgene may have occurred in the Liu et al. study, especially given the relatively small number of C9-500 mice and controls used³⁹⁷. Overall, more research is needed to determine whether the C9ORF72 transgene is sufficient to cause disease-associated phenotypes in mice, which is a critical step in understanding C9 ALS/FTD pathogenesis.

1.3.2.3 Non-AUG translation of dipeptide repeat proteins

Repeat-associated non-ATG translation (RAN translation) was first described as a new pathophysiological pathway in spinocerebellar ataxia type 8 (SCA8) and myotonic dystrophy type 1 (DM1)⁴⁰⁴. RAN translation is a non-canonical mechanism in which a nucleotide repeat expansion can be translated in the absence of an ATG start codon, and thus in more than one open reading frame (ORF). In the case of SCA8, the CAG trinucleotide expansion in the *ATXN8* gene is canonically translated in the +0 ORF, producing poly-glutamine peptides; however, RAN translation also occurs with initiation in the +1 ORF (AGC, poly-serine) and the +2 ORF (GCA, poly-alanine)⁴⁰⁴.

This mechanism was first discovered in C9 ALS/FTD by two independent groups who reported the presence of aggregated polypeptides in the *post-mortem* CNS tissue of ALS/FTD patients^{356,405}. The authors discovered three types of polypeptides: poly-GA,

poly-GP, and poly-GR, and it became clear that these were the products of RAN translation of the sense RNA strand (GGGGCC) in three ORFs. Later, several groups reported the presence of other polypeptides derived from the antisense RNA strand (CCCCGG) in *post-mortem* tissue from patients: poly-PR, poly-PG, and poly-PA ^{405–408}.

It is now clear that, following C9-HRE bi-directional transcription, sense and antisense C9-HRE RNAs can reach the cytoplasm and undergo RAN translation, resulting in 5 types of dipeptide repeat proteins (DPRs) ⁴⁰⁹ – poly-GP is produced from both RNAs. These DPR inclusions are most commonly found in the frontal cortex, basal ganglia, motor cortex, hippocampus, cerebellum, and spinal cord ^{410–413}, and are typically positive for p62 and ubiquitin while being TDP-43 negative ^{407,414–417} – less than 4% of DPR inclusions are TDP-43 positive.

These findings sparked a lot of interest in the possibility that DPRs are the primary cause of neurodegeneration in C9 ALS/FTD. This hypothesis was tested in several research models, including zebrafish ^{418,419}, *Saccharomyces cerevisiae* ⁴²⁰, *D. melanogaster* ^{393,421,422} and mice ^{423–426}, and it demonstrated that the expression of DPRs, specifically poly-GA, poly-GR, and poly-PR, could cause neurodegeneration as well as various behavioural and motor deficits. DPR expression was also found to be toxic in iPSC-derived cortical and motor neurons ^{427,428}.

These and other studies have revealed a complex network of pathogenic pathways elicited by the various DPRs. Poly-GA DPRs, for example, which are the most abundant DPR species, cause toxicity by interfering with the proteasome pathway ⁴²⁹. Furthermore, these DPR species have been shown to sequester the DNA repair-ubiquitin-associated HR23A and HR23B proteins, which are involved in proteasomal degradation ^{430,431} – an in-depth review of poly-GA will be discussed in the following chapter.

Other DPR species, such as poly-GR and poly-PR DPRs, have been shown to influence the formation of membrane-less organelles ^{427,432}, which are organelles that lack a proper membrane (i.e., nucleolus, stress granules, nuclear pore complex, Cajal bodies, and nuclear speckles) ⁴³³. In particular, these DPRs can bind proteins containing low complexity sequence domains, which are essentially domains involved in the dynamics of liquid-liquid phase separation for the formation of membrane-less organelles ⁴³². Poly-GR and poly-PR DPRs also associate with stress granules or TDP-43-positive RNA granules, causing the granules to become less dynamic, which may result in TDP-43 aggregation ⁴³⁴; they also interfere with nucleocytoplasmic trafficking ^{420,435}, mitochondrial ribosomal proteins ⁴³⁶ and rRNA biogenesis ⁴²⁷, thus indicating that there are several mechanisms by which they may

exert their toxicity. Proline-rich DPRs, such as poly-GP and poly-PA, are thought to be relatively inert. In many *Drosophila* models, these species did not turn out to be toxic^{393,437}. However, poly-GP DPRs localize to cytoplasmic and nuclear foci in a *Drosophila* line that expresses the C9-HRE and are able to induce cell death when proteasomes are inhibited⁴³⁸. Despite the substantial evidence that DPRs play a significant role in the pathophysiology of C9 ALS/FTD, one issue that should be considered is that the majority of these studies use overexpression paradigms, which are likely to result in higher DPR levels than would be found in patients. Additionally, DPRs are observed in C9-BAC transgenic mice without any consistent motor phenotype or neurodegeneration^{395,396,398}. Moreover, a few studies report a lack of correlation between the presence of DPRs and the anatomical patterns of neuronal atrophy^{439,440}, raising questions about the true severity of DPR toxicity in C9 ALS/FTD patients – although it could be argued that DPR detection in dying neurons would be challenging.

In summary, scientific research has made tremendous progress in understanding the pathogenicity of C9 ALS/FTD since the discovery of the C9-HRE in the year 2011. The data gathered over these years appears to indicate that a single C9 HRE-driven mechanism may not be sufficient to cause disease. Instead, in people who have more than 24-30 units of the C9-HRE, loss- and gain-of-function events are likely to synergize with ageing and possibly other factors (environment, hormone levels, other genetic risks, etc.). The synergistic hypothesis between loss- and gain-of-function mechanisms has recently received additional support from a number of intriguing studies. Boivin and colleagues, for example, demonstrated that reduced autophagy caused by *C9ORF72* haploinsufficiency synergizes with DPR toxicity to cause neuronal cell death⁴⁴¹; and this has been proposed in other studies in human induced motor neurons³⁶⁶ and mice⁴⁴².

Figure 1.10 depicts the three mechanisms of C9-HRE-mediated toxicity discussed in chapters 1.3.1, 1.3.2, and 1.3.3.

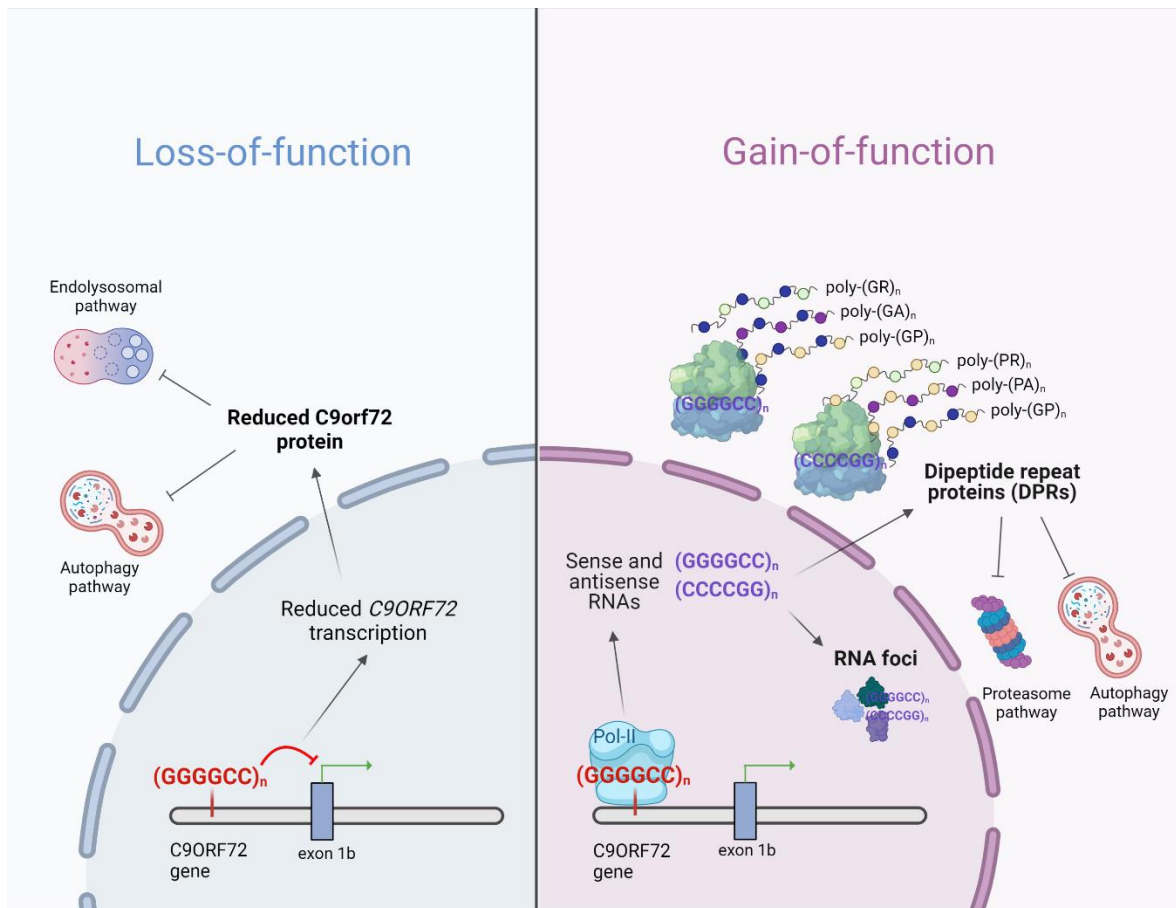


Figure 1. 10 C9 HRE-mediated pathological mechanisms

The figure shows the 3 main mechanisms by which C9-HRE can cause ALS/FTD. On the one hand, *C9ORF72* loss-of-function events result in lower *C9orf72* protein levels, impairing the protein's normal autophagy regulation function. *C9ORF72*-gain of function events, on the other hand, generate RNA foci that sequester RNA-binding proteins, altering RNA metabolism in the cell; additionally, neurotoxic dipeptide repeat proteins (DPRs) can be produced from both sense and antisense C9-HRE, leading to neurodegeneration phenotypes and possibly spreading to neighbouring cells. Figure created with BioRender.com under academic license. Adapted and inspired from Gitler & Tsuiji, 2016⁴⁴³.

1.3.3 Poly-GA dipeptide repeat proteins

Poly-GA DPRs were found to be the most abundant DPR species in *post-mortem* tissue from C9 ALS/FTD patients ^{444,445}. *In vitro* assemblies of poly-GA form ribbon-type sheet fibrils containing cross- β -sheets, which are common structures formed by other pathological proteins (e.g., A β , tau) in amyloid diseases; according to transmission electron microscopy and atomic force microscopy ⁴⁴⁶. Poly-GA appears to mediate toxicity in cell cultures by directly impairing the ubiquitin-proteasome system (UPS) and inducing endoplasmic reticulum-related stress pathways ^{429,438,444}.

Poly-GA has been shown to sequester UPS components such as Unc119, ubiquilin-1 and -2 ^{416,429}; among these proteins, Unc119 is particularly important for controlling axonal protein trafficking and synaptic signal transduction, and its poly-GA-induced loss-of-function causes neurotoxicity ⁴²⁹. Several studies have shown that poly-GA can directly associate with the proteasome; in particular, Guo *et al.* used cryo-electron tomography to report that poly-GA specifically leads the 26S proteasome to stalled degradation ⁴⁴⁷. Another study reported poly-GA interaction with the proteasomal subunit PSMC4 ¹³². Proteasome activation via rolipram treatment or overexpression of the proteasome protein PSMD11 can reverse poly-GA aggregation and pathology ¹³². In addition to these proposed pathways, poly-GA can also induce R-loop formation and defects in ATM-mediated DNA repair signalling, precipitating C9 HRE-mediated DNA damage in cell culture and *in vivo* ⁴²⁶.

Poly-GA-overexpressing mice have been generated by various research teams. Interestingly, these mice exhibit motor and cognitive deficits, as well as cerebellar atrophy, astrogliosis, and TDP-43 pathology ^{132,431,448}. In some mice, the poly-GA overexpression resulted in selective neuron loss, inflammation, muscle denervation, and wasting; and poly-GA inclusions were found not only in the CNS but also in skeletal muscle ¹²⁸. Some of these phenotypes were attributed to poly-GA DPRs mediating the sequestration of proteins involved in the proteasome and nucleocytoplasmic transport pathways ⁴³⁰. Interestingly, the Edbauer group covalently coupled 10-GA repeats to maleimide-activated ovalbumin (as an adjuvant), resulting in an immunisation strategy for these poly-GA mouse models. After immunisation, the mice were protected from developing motor deficits and microglia activation, which were instead common in non-immunised controls ¹⁴. Nguyen *et al.* used another immunisation strategy, in which human antibodies recognising poly-GA were

produced and injected into C9-BAC transgenic mice; these antibodies resulted in a decrease of GA, GP, and GR levels in C9 models, as well as a reduction in neurodegeneration and an improvement in behaviour and survival¹²⁹; however, the mouse model used has recently led to controversial reports for some of these phenotypes³⁹⁸.

Emerging findings also show that poly-GA can propagate from cell-to-cell in cell culture and in *Drosophila*^{130,131,446}. Surprisingly, poly-GA was the only DPR species found to be capable of spreading in the nervous system of *Drosophila*¹³¹. This discovery may point to a unique propensity of poly-GA to spread throughout the brain, which may contribute to the higher abundance of poly-GA in patient tissue. Interestingly, Khosravi and colleagues discovered that poly-GA can spread and promote cytoplasmic mislocalization and aggregation of TDP-43 in naive cells in a non-cell-autonomous manner¹³². This suggests that poly-GA may act as prion-like proteins, capable of spreading pathology from a focal region to other areas of the brain and thus extending pathology in those regions. These properties are consistent with those observed for other major neuropathological proteins previously discussed in **Table 1.1** (page 27). However, *in vivo* evidence of poly-GA toxicity in naive cells (after spreading) in mammals is still lacking.

1.4 Introduction to PhD project: aims and objectives

The C9-HRE is the primary genetic cause of both ALS and FTD, and its non-AUG dependent translation into 5 types of dipeptide repeat proteins (DPRs) is thought to be a primary pathogenic mechanism. Poly-GA has been found more frequently in histopathological studies of C9 ALS/FTD CNS tissue than the other DPR types. As a result, there is a research interest to elucidate the mechanisms by which C9 DPR aggregates, particularly poly-GA, may cause toxicity and neurodegeneration in C9 ALS/FTD.

In my PhD project, I have investigated the role of poly-GA DPRs in disease spread. After producing recombinant poly-GA DPRs, I have shown that small oligomers of this protein can convert into solid-like aggregates and form characteristic β -sheet fibrils *in vitro* (test-tube). The amyloid nature of poly-GA DPRs is shared by other relevant pathological protein aggregates (A β - tau, α -synuclein), thus suggesting that this DPR species may play a role in C9 ALS/FTD neuropathology. Either oligomeric or fibrillar forms of poly-GA DPRs were then administered in various cell culture systems, and their uptake was closely monitored especially in glial cells such as astrocytes. I have also tested the potential role of endocytosis in poly-GA uptake by blocking broad endocytosis (incubating cells at 4°C) or blocking specific pathways, such as clathrin- and caveolin-mediated endocytosis, which rely on the GTPase dynamin. Interestingly, it was discovered that when the same poly-GA species is used at different amyloid stages (oligomers vs fibrils), the endocytic pathway for cell entry varies. Potential prion-like properties of poly-GA DPRs were then explored, in particular by looking into the possibility that poly-GA could propagate from astrocytes to motor neurons. I have subsequently shown that astrocytes play a role in the transmission of poly-GA to neighbouring motor neurons, which could be a non-cell autonomous contributor to C9 ALS/FTD neuropathology.

Overall, my findings shed light on the binding, uptake, and release pathways of poly-GA aggregates in glial cells; hence improving our understanding of non-neuronal cell contributions and mechanisms in C9 ALS/FTD. We believe that future therapies for C9 ALS/FTD could benefit from blocking DPR uptake and release routes not only in neuronal cells but also in glia.

2. Materials and methods

2.1 Materials

2.1.1 Plasmid DNA

Table 2.1 Plasmid DNA. List of plasmid DNAs used in this project.

Plasmid	Obtained from:
pAG416-Gal-PA50	<p>pAG416-Gal-PA50 was a gift from Aaron Gitler (Addgene plasmid # 84902 ; http://n2t.net/addgene:84902 ; RRID:Addgene_84902)</p> <p>Sequence available in Addgene: https://www.addgene.org/browse/sequence/166529/</p> <p>This plasmid contains the DNA sequence encoding the poly-PA₅₀ repeat protein, followed by sequences encoding Myc and FLAG epitope tags.</p> <p>⁴²⁰ Jovicic et al. <i>Nat Neurosci.</i> 2015 Sep;18(9):1226-9.</p>
pCI-neo	<p>The pCI-neo mammalian expression vector was a gift from Professor Kurt De Vos (Promega plasmid # E1841, accession number GenBank: U47120.2)</p> <p>Sequence available in GenBank: https://www.ncbi.nlm.nih.gov/nuccore/U47120</p> <p>This plasmid contains <i>XhoI</i> and <i>NotI</i> restriction sites, which are then used for the subcloning of the DNA sequence encoding poly-GA₃₄ repeat protein.</p> <p>⁴⁴⁹ Brinster et al. <i>PNAS</i> 1988 85,836–40.</p>
pETM11-ACS	<p>pETM11-ACS was a gift from Frank Schulz (Addgene plasmid # 108943 ; http://n2t.net/addgene:108943 ; RRID:Addgene_108943)</p> <p>Sequence available in Addgene: https://www.addgene.org/108943/</p> <p>This plasmid contains the Tobacco Etch Virus (TEV) cleavage site and the DNA encoding for 6 Histidine amino acid residues. These DNA sequences are fundamental for the purification of the final recombinant proteins (either poly-PA₅₀ or poly-GA₃₄)</p> <p>⁴⁵⁰ Dirkmann et al. <i>ChemBiochem.</i> 19(20), 2146-2151.</p>

2.1.2 Antibodies

Table 2.2 List of antibodies used in this study

REAGENT	DILUTION	SOURCE	IDENTIFIER
Antibodies			
Chicken polyclonal anti-vimentin	ICC (1:4000)	Sigma-Aldrich	Cat#AB5733
Goat anti-chicken IgG (H+L) secondary antibody, Alexa Fluor 488	ICC (1:1000)	Thermo Fisher Scientific	Cat# A-11039
Goat anti-mouse IgG (H+L) Cross-adsorbed secondary antibody, Alexa Fluor 488	ICC (1:1000)	Thermo Fisher Scientific	Cat# A-11001
Goat anti-mouse IgG F(ab), Atto488	ICC (1:1000)	Hypermol	Cat# 2112-250UG
Goat anti-Mouse IgG(H+L)-HRP Conjugate antibody	WB (1:5000)	Bio-rad	Cat# 172-1011
Goat anti-rabbit IgG (H+L) Cross-adsorbed secondary antibody, Alexa Fluor 488	ICC (1:1000)	Thermo Fisher Scientific	Cat# A-11008
Goat anti-rabbit IgG (H+L) secondary antibody, Alexa Fluor 647	ICC (1:1000)	Thermo Fisher Scientific	Cat# A-21244
Goat anti-Rabbit IgG(H+L)-HRP Conjugate antibody	WB (1:5000)	Millipore	Cat# 12-348
Mouse monoclonal anti-Cathepsin B	ICC (1:500)	Santa Cruz	Cat# sc-365558
Mouse monoclonal anti-Cathepsin D	ICC (1:1000)	Santa Cruz	Cat# sc-377299
Mouse monoclonal anti-Cathepsin L	ICC (1:1000)	Santa Cruz	Cat# sc-390367
Mouse monoclonal anti-Galectin 3	ICC (1:100)	Santa Cruz	Cat# sc-374253
Mouse monoclonal anti-LAMP1 Clone H4A3	ICC (1:50)	Abcam	Cat# ab25630
Mouse monoclonal anti-V5	WB (1:1000)	Thermo Fisher Scientific	Cat# R960-25
Mouse monoclonal anti- α -Tubulin Clone DM1A	WB (1:3000)	Sigma-Aldrich	Cat# T9026
Rabbit monoclonal anti-V5 Clone D3H8Q	WB (1:1000) ICC (1:1000)	Cell Signaling	Cat# 13202S
Rabbit polyclonal anti-AP repeat	WB (1:1000)	Proteintech	Cat# 24493-1-AP
Rabbit polyclonal anti-Caspase 3, active (cleaved)	ICC (1:400)	Cell signaling	Cat# 96615
Rabbit polyclonal anti-CD44	ICC (1:1000)	Abcam	Cat# ab157107
Rabbit polyclonal anti-GA repeat	WB (1:1000)	Proteintech	Cat# 24492-1-AP

Abbreviations: ICC= immunocytochemistry; WB = western blotting

2.1.3 Reagents

Table 2.3 List of Chemicals, media, and compounds used in this study

REAGENT	SOURCE	IDENTIFIER
Chemicals, media, and compounds		
(±)Blebbistatin	Abcam	Cat# ab120425
2-mercaptoethanol	Thermo Fisher Scientific	Cat# 21985023
Animal-Free Recombinant Human EGF	Peprotech	Cat# AF-100-15
Bafilomycin A1 from <i>Streptomyces griseus</i>	Millipore	Cat# 88899-55-2
Bovine Serum Albumin (BSA)	Sigma-Aldrich	Cas# 9048-46-8
Brain-derived neurotrophic factor (BDNF) human	Sigma-Aldrich	Cat# B3795
BrightCell MEMO Photostable Media	Sigma-Aldrich	Cat# SCM144
Bromophenol blue, Tracking dye	Abcam	Cat# ab146339
Catalase from bovine liver	Sigma-Aldrich	Cat# C9322-1G
Cysteamine	Sigma-Aldrich	Cat# M9768-5G
Defined Trypsin Inhibitor	Thermo Fisher Scientific	Cat# R007100
Dimethyl sulfoxide (DMSO)	Merck	Cat# PHR1309
DMEM, high glucose, HEPES, no phenol red	Thermo Fisher Scientific	Cat# 21063029
Dulbecco's Modified Eagle's Medium/Nutrient Mixture F-12 Ham	Sigma-Aldrich	Cat# D6421
Dulbecco's Modified Eagle Medium (DMEM)	Sigma-Aldrich	Cat# D7777
Dynasore, dynamin inhibitor	Abcam	Cat# ab120192
Enhanced ChemiLuminescence (ECL) substrate	Thermo Fisher Scientific	Cat# 32106
Ethylenediaminetetraacetic acid (EDTA)	Sigma-Aldrich	Cat# E9884
Everspark buffer	Idylle	https://www.idylle-labs.com/everspark-by-eternity
Fetal Bovine Serum (FBS)	Sigma-Aldrich	Cat# F6178
Fibronectin bovine plasma	Sigma-Aldrich	Cat# F1141
Fluoromount aqueous mounting medium	Sigma-Aldrich	Cat# F4680
GDNF from mouse	Sigma-Aldrich	Cat# SRP3200

Gibco™ AlbuMAX™ I Lipid-Rich BSA	Gibco	Cat# 11020021
Gibco™ B-27™ Supplement (50X), serum free	Gibco	Cat# 17504044
Gibco™ GlutaMAX™ Supplement	Gibco	Cat# 35050061
Gibco™ N-2 Supplement (100X)	Gibco	Cat# 17502001
Glucose oxidase	Serva	Cat# 22778.01
Glutaraldehyde solution	Sigma-Aldrich	Cat# 340855
Glycerol	Sigma-Aldrich	Cat# G5516
Glyoxal, 40 wt. % solution in water	Sigma-Aldrich	Cat# 107-22-2
Hanks' Balanced Salt solution (HBSS)	Sigma-Aldrich	Cat# H9269
Heparin sodium salt from porcine intestinal mucosa	Sigma-Aldrich	Cat# H5515
Hoechst Stain solution	Sigma-Aldrich	Cat# H6024
Human Clusterin (APOJ) ELISA Kit	Proteintech	Cat# KE00110
Leu-Leu methyl ester hydrobromide (LLOMe)	Sigma-Aldrich	Cat# L7393
L-Glutamine for cell culture, 200 mM	Lonza	Cat# BE17-605E
LysoSensor Green DND-189	Thermo Fisher Scientific	Cat# L7535
Lysosome-Specific Self-Quenched Substrate	Abcam	Cat# ab234622
LysoTracker™ Green DND-26	Thermo Fisher Scientific	Cat# L7526
MG-132, proteasome inhibitor	Abcam	Cat# ab141003
Neurobasal™ Medium	Thermo Fisher Scientific	Cat# 21103049
Nocodazole	Sigma-Aldrich	Cat# M1404
Nuclease-free water	Qiagen	Cat# 129117
Paraformaldehyde powder, 95% (PFA)	Sigma-Aldrich	Cat# 158127
Penicillin-Streptomycin Mixture	Lonza	Cat# 09-757F
Pierce BCA Protein Assay Kit	Thermo Fisher Scientific	Cat# 23225
Poly-D-Lysine solution, 1.0 mg/mL	Sigma-Aldrich	Cat# A-003-M
Protease Inhibitor Cocktail	Promega	Cat# G6521
QuantiFast SYBR® Green RT-PCR Kit	Qiagen	Cat# ID: 204156
Recombinant Human FGF-basic (154 a.a.)	Peprtech	Cat# 100-18B

Retinoic acid	Sigma-Aldrich	Cat# R2625
RNase-Free DNase Set	Qiagen	Cat# ID: 79254
RNeasy Mini Kit	Qiagen	Cat# 74104
Smoothened Agonist (SAG)	Sigma-Aldrich	Cat# 566660
Sodium Deoxycholate Detergent	Thermo Fisher Scientific	Cat# 89904
Sodium Dodecyl Sulfate (SDS)	Sigma-Aldrich	Cat# 11667289001
TetraSpeck™ Microspheres, 0.1 μm, fluorescent blue/green/orange/dark red	Thermo Fisher Scientific	Cat# T7279
Transferrin from Human Serum, Alexa Fluor 647 conjugate	Thermo Fisher Scientific	Cat# T23366
Tris base	Sigma-Aldrich	Cat# TRIS-RO
Triton™ X-100	Sigma-Aldrich	Cat# X100
Trypan Blue solution	Sigma-Aldrich	Cat# T8154
Trypsin	Sigma-Aldrich	Cat# 1.08444
Tween® 20	Promega	Cat# H5152
Vacuolin-1, lysosomal exocytosis inhibitor	Santa Cruz Biotechnology	Cat# 351986-85-1

2.1.4 Scientific devices and plates

Table 2.4 List of scientific devices used in this study

NAME	BRAND	IDENTIFIER
Devices, microscopes, plate formats		
Bio-Rad C1000 Touch™ Thermal Cycler	Bio-Rad Laboratories	https://www.bio-rad.com/
HTS microplate reader PHERAstar FSX	BMG Labtech	https://www.bmglabtech.com/
Ibidi μ -Slide 8 Well	Ibidi	Cat# 80826
JEOL JEM-1400 series 120kV Transmission Electron Microscope	JEOL	https://www.jeolusa.com/
Leica TCS SP5 Confocal	Leica	https://www.leica-microsystems.com/
LSRII flow cytometer	BD Bioscience	https://www.bdbiosciences.com/
MSE Soniprep 150	MSE Centrifuges	N/A
Nikon Eclipse Ti microscope	Nikon	N/A
Nitrocellulose Transfer Membrane- 0.22 μ m	Abcam	Cat# ab133413
Nunc MicroWell 96-Well Optical-Bottom Plates with Polymer Base	Thermo Fisher Scientific	Cat#165305
Opera Phenix® high-throughput system	PerkinElmer	https://www.perkinelmer.com
Precision Cover Glasses, #1.5H Thickness, 22 x 22 mm (for dSTORM)	ThorLabs	Cat# CG15CH2
Syngene G:BOX EF	Syngene	https://www.syngene.com/
Ultrasonic processor UIS250v	Hielscher Ultrasonic	https://www.hielscher.com/s250l_vial_sonication_01.htm
XonaChips® Standard Neuron Device 450 μ m barrier 5PK (SND450)	Xona microfluidics	Cat# SND450
Zeiss LSM 880 with Airyscan	Zeiss	https://www.zeiss.com/

2.1.5 Image analysis: softwares, algorithms, macros

Table 2.5 List of softwares, algorithms and FIJI macros used in this study

NAME	BRAND	WEBSITE / PUBLICATION
Softwares, algorithms, macros		
Arivis Vision 4D	Arivis AG	arivis.com
BD FACSDiva software (version 8.0.1)	BD Bioscience	N/A
Bio-Rad CFX Manager software	Bio-Rad Laboratories	https://www.bio-rad.com/
Clus-DoC package for clustering analysis	Matlab 2014b or later	Pageon et al., 2016
Columbus Image Data Storage and Analysis System	PerkinElmer	perkinelmer.com
FIJI Macro: Quantification of cell fluorescent intensity – by Paolo M Marchi	Fiji	https://github.com/paoloM1990/Quantification-of-cell-fluorescent-intensity
FIJI NanoJ-SQUIRREL plug-in	Fiji	Culley et al., 2018
FIJI software	Fiji	Schindelin et al, 2012
FIJI ThunderSTORM plug-in	Fiji	Ovesný et al, 2014
FIJI TrackMate plug-in	Fiji	Tinevez et al., 2017
FIJI Trainable Weka Segmentation plug-in	Fiji	Arganda-Carreras et al, 2017
GeneSys software for G:BOX EF	Syngene	https://www.syngene.com/
Graphpad Prism v8.4.1	GraphPad	https://www.graphpad.com/scientific-software/prism
Huygens Professional version 19.10	Scientific Volume Imaging	http://svi.nl
Imaris v7.7.2	Bitplane AG	Imaris.oxinst.com
MATLAB analysis: Guide to TrackMate Matlab MSD – by Paolo M Marchi	Matlab 2014b or later	https://github.com/paoloM1990/Guide-to-TrackMate-Matlab-MSD
MATLAB class @msdanalyzer – by Jean-Yves Tinevez	Matlab 2014b or later	https://github.com/tinevez/msdanalyzer
NIS-Elements Microscope Imaging Software	Nikon	N/A

2.1.6 Experimental *in vitro* models

Table 2.6 List of experimental *In vitro* models

REAGENT or RESOURCE	SOURCE	IDENTIFIER
Experimental Models: Cell Lines		
1321N1 astrocytoma cell line	Sigma-Aldrich	Cat#86030402
E15.5 embryos of wild-type C57BL/6 mice	N/A	University of Sheffield
Hb9-GFP mouse embryonic stem cells	N/A	Gift from Thomas Jessel, Columbia University, New York
Human skin fibroblasts sample	N/A	University of Sheffield Ethical approval to use human skin fibroblasts is in place for this project (REC approval 12/YH/0330)

2.1.7 DNA oligonucleotides

Table 2.7 List of DNA oligonucleotides.

The sequences of RT-qPCR primers (for *Mus musculus*) as they were ordered from Sigma.

Gene Symbol	Primer forward (5'-3')	Primer reverse (5'-3')
ACTB	GCTCCTCCTGAGCGCAAGTA	AGCTCAGTAACAGTCCGCCTA
ATP6V0E1	GGGTCCTAACCGGGGAGTTA	ACAGAGGATTGAGCTGTGCC
CTSB	GCTCTTGTGGGCATTGGG	ACTCGGCCATTGGTGTGAAT
CTSD	CTTGGGCATGGGCTACCCTC	TTGCCCTTCTGGGTCCTGTT
CTSL	CGCCTTCGGTGACATGACCA	TCTTGTGCTTCTGGTGGCGG
GAPDH	GGTCATGAGCCCTCCACAA	TGAAGGGTGGAGCCAAAAG
GBA	GGGCAGCAAACCTCCCTAGCAG	GGATGCAGGGTTGGGCACCATA
MCOLN1	TGCTGTGGACCAGTACCTGA	GTAGTACCGCTGGCAGAGAG

2.2 Methods

2.2.1 Cell culture

1321N1 astrocytoma cells ⁴⁵¹ were cultured in DMEM supplemented with 10% FBS and 5 U ml⁻¹ Penstrep.

Hb9-GFP mouse stem cells were cultured as described ⁴⁵² and differentiated into motor neurons with 2 μM retinoic acid and 1 μM Smoothed Agonist (SAG) for 5 days. Embryoid bodies were then dissociated with papain. All cells were maintained in a 37 °C incubator with 5% CO₂.

2.2.2 Conversion of skin fibroblasts to induced neural progenitor cells

Skin fibroblasts from one healthy control and two C9 ALS patients (Table 2.6) were reprogrammed as previously described ⁴⁵³. Briefly, 10⁴ fibroblasts were grown in one well of a six-well plate. Day one post-seeding the cells were transduced with retroviral vectors containing Oct 3/4, Sox 2, Klf 4 and c-Myc. Following one day of recovery in fibroblast medium (DMEM and 10% FBS), the cells were washed 1× with PBS and the culture medium was changed to Neural Progenitor Cell (NPC) conversion medium comprised of DMEM/F12 (1:1) GlutaMax, 1% N2 supplement, 1% B27, 20 ng/ml FGF2, 20 ng/ml EGF and 5 ng/ml heparin. As the cell morphology changes and cells develop a sphere-like form, they can be expanded into individual wells of a six-well plate. Once an induced neural progenitor cell (iNPC) culture is established, the media is switched to NPC proliferation media consisting of DMEM/F12 (1:1) GlutaMax, 1% N2, 1% B27, and 40 ng/ml FGF2.

Patient sample	Cell type	Gender	Ethnicity	Age at biopsy collection (years)
155v2	Healthy control	Male	Caucasian	40
161	Healthy control	Male	Caucasian	31
183	C9orf72 ALS	Male	Caucasian	50
78	C9orf72 ALS	Male	Caucasian	66
CS14	Healthy control	Female	Caucasian	52

Table 2.8 List and characteristics of iAstrocytes used in this study.

2.2.3 iAstrocyte differentiation and co-culture system

iNPC-derived human astrocytes (herein referred to as iAstrocytes) were yielded as previously described^{453,454}. Briefly, iNPCs were switched to astrocyte proliferation media, which includes DMEM, 10% FBS and 0.2% N2 supplement. Cells were grown in 10 cm dishes coated with fibronectin for 7 days unless otherwise stated. For the co-culture system, we treated iAstrocytes with 1 μ M DPRs for 24h, then plated Hb9-GFP mouse motor neurons on top of the astrocyte layer and kept this co-culture system for 48h before fixation and confocal imaging.

2.2.4 Primary mouse cortical neurons

Primary cortical neurons were produced from E15.5 embryos of wild-type C57BL/6 mice. Brains were harvested and hemispheres were divided. In HBSS^{-/-} medium, meninges and midbrain were removed in order to isolate the cortical tissue, which was then incubated with trypsin for cell dissociation. Single-cell suspension was obtained by mechanical pipetting in appropriate trituration solution (HBSS^{+/+} with 1% albumax, 25mg Trypsin inhibitor, 10mg/ml DNase stock). Finally, cortical neurons were resuspended in Neurobasal medium with B27, 1% Pen/Strep and 1% Glutamine, and seeded on Xona silicon device (#RD450) coupled with a 35mm dish previously coated with poly-D-lysine. Cells were maintained in a 37 °C incubator with 5% CO₂, changing medium every two days. Neurotrophic factors (2 ng/ml BDNF, 2ng/ml GDNF) were added into the medium to favour the correct directionality of axonal growth through the microgrooves. After 12 days in culture, cells were stained with Lysotracker Green and live imaging was performed with Airyscan microscopy (Zeiss LSM 880) at 1.5Hz for 2 minutes (561 nm and 488 nm channels; 63x 1.4NA oil immersion lens).

2.2.5 Dipeptide Repeat Proteins cloning

V5-tagged 34x GA repeat

The following method for the production of V5-tagged 34x GA repeat was performed by the group of Prof. Kurt De Vos (Department of Neuroscience, University of Sheffield, UK).

The V5-tagged 34x GA repeat was obtained using an expandable cloning strategy with AgeI and MreI as compatible enzymes ⁴⁵⁵.

A “start acceptor” pCI-Neo vector (Promega) was first constructed by cloning a V5-3xGly/Ala insert into the XhoI/NotI sites (ctc gag gcc acc atg ggc aaa ccg att ccg aac ccg ctg ctg ggc ctg ctg gat agc acc ggt gca ggt gct ggc gcc ggc gga tcc gaa ttc tag ccg cgg ccg c) and a “start donor” vector with a 14xGly/Ala insert (ctc gag acc ggt gca ggt gct gga gct ggt gca ggt gct gga gca ggt gct gga gca ggt gct ggc gcc ggc gga tcc gaa ttc ccg cgg ccg c) in the XhoI/NotI sites. These vectors (“start acceptor” and “start donor”) were then used to propagate the GA repeats to construct 34 GA repeats, as shown in the following figure:

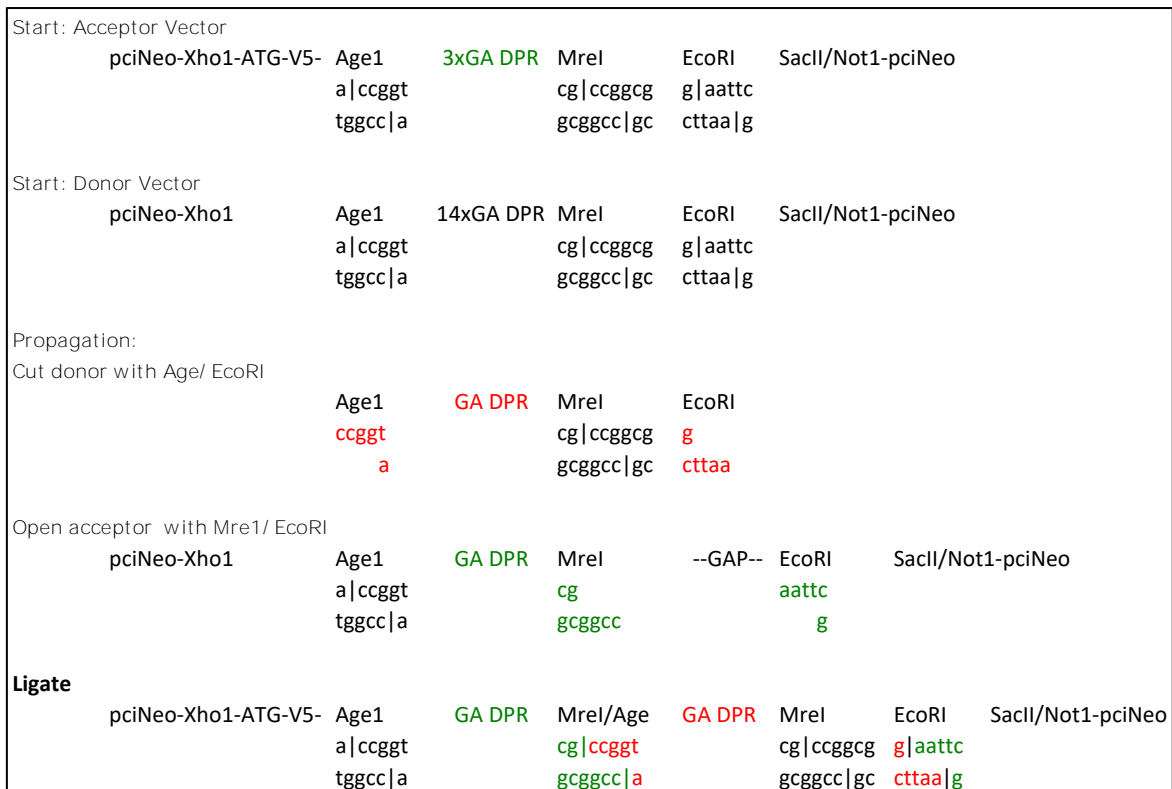


Figure 2.1 Cloning of Gly/Ala repeat constructs

FLAG-tagged 50x PA repeat

The plasmid pAG416-Gal, which encodes for the PAx50 dipeptide repeats, was obtained from Addgene as described in the thesis section 2.1.1 (Addgene plasmid # 84902).

Subcloning into pETM-11 vector

DNA sequences encoding V5 tag followed by 34 repeats of GA or 50 repeats of PA were subcloned in a bacterial expression vector containing an N-terminal 6xHis-Tag and a TEV protease cleavage site (pETM-11 vector, EMBL).

In particular, the V5-tagged 34x GA construct was subcloned in the pETM-11 vector using *NcoI* and *NotI* restriction sites; whereas the FLAG-tagged 50x PA repeat construct was subcloned in the pETM-11 vector using *NcoI* and *XhoI* restriction sites.

Transformation of bacterial cells (*E. coli* BL21) with plasmids containing these repeat constructs was performed; and protein purification steps are described in Chapter 3.2.1.

2.2.6 Transmission electron microscopy

The morphology of poly-GA fibrils was assessed by Transmission Electron Microscopy in a Jeol 1400 microscope before and after fragmentation following adsorption onto carbon-coated 200 mesh grids and negative staining with 1% uranyl acetate. The images were recorded with a Gatan Orius CCD camera (Gatan). The β -sheet amyloid component of fibrillar poly-GA assemblies was also assessed and confirmed by Fourier-transform infrared (FTIR) spectroscopy as described in a previous study from Dr Melki's team ²¹. Importantly, before the addition to the medium, fibrillar DPRs were sonicated for 5 min at 80% amplitude with a pulse cycle of 5 seconds on and 2 seconds off (MSE Soniprep 150); this procedure is required to disperse the aggregated β -sheet assemblies.

2.2.7 Coalescence measurements

For phase-separation experiments, soluble GA and PA DPRs (stock concentration = 100 μM) were diluted in ddH₂O to either 20 μM , 10 μM or 1 μM . After vortexing, the mixture was pipetted onto glass-bottom slides (Ibidi), and assembly formation was monitored over time. Images were acquired immediately, as well as after 2 and 24 hours using a Leica SP5 confocal microscope with a 63x 1.4NA oil immersion objective, 561 nm channel. To capture fine details for 3D rendering, assemblies were imaged with a z-stack following Nyquist sampling for optimized pixel density⁴⁵⁶. Huygens Professional software (version 19.10) was used to deconvolve z-stack data using the CMLE algorithm (with SNR:10 and 40 iterations) and subsequently for 3D-volume and –surface rendering thus generating **Movies S1 and S2**. The 3D rendering for **Movies S3 and S4** was performed using the software Imaris v7.7.2; no deconvolution was applied here. Number, circularity and size of DPR assemblies were quantified with Fiji⁴⁵⁷ and plotted using GraphpadPrism 8. The Fiji plug-in Trainable Weka Segmentation⁴⁵⁸ was used to finely measure the circularity of liquid-like droplets in heterogeneous PA assemblies (20 μM , 24h) (**Figure 3.4D**).

2.2.8 Immunocytochemistry

After the addition of the DPRs, all the single-cell cultures were washed five to six times with PBS and fixed with 4% PFA for 30 min at room temperature. After fixation, cells were washed two times with PBS, permeabilized for 10 minutes with 0.1% Triton-X 100:PBS and additionally washed twice with PBS. Subsequently, cells were incubated with the blocking agent 3% BSA for 30 min and then incubated overnight at 4°C with primary antibodies (in 3% BSA). Cells were then washed 3× with PBS and incubated for 1h with the corresponding Alexa Fluor secondary antibodies at 1:1000 dilution (in 3% BSA) and with Hoechst when needed. Cells were washed 3x with PBS, and coverslips were mounted onto glass slides using Fluoromount aqueous mounting medium. In the case of imaging with Opera Phenix® high-throughput system, coverslipping of 96-well plate is not required, and cells were imaged in PBS solution. Primary antibodies used were: Anti-Vimentin (1:4000), anti- α Tubulin (1:1000), anti-CD44 (1:1000), anti-Cathepsin B (1:500), anti-Cathepsin D (1:1000), anti-Cathepsin L (1:1000), anti-Galectin 3 (1:100), and anti-LAMP1 (1:50) (**Table 2.2**).

2.2.9 Flow cytometry

1321N1 human astrocytoma cells (1.2×10^6 /sample) were washed six times in PBS (to eliminate any remaining DPRs in the media), trypsinized and then resuspended in 500 μ l of PBS. Suspended cells were then analysed by using an LSRII flow cytometer (BD Bioscience) with excitation at 488 nm and BD FACSDiva software (version 8.0.1; BD Bioscience) to excite the ATTO550 fluorophore. Detection of ATTO550+ signal was set at 610/20 voltage. Cells not treated with DPRs acted as control producing the gating to discriminate between the ATTO550+ and the ATTO550- cells.

2.2.10 Immunoblotting

In order to collect protein extracts, iAstrocytes were washed six times in PBS (to eliminate any remaining DPRs in the media) and lysed in RIPA buffer (20 mM Tris-HCl pH 7.5, 137 mM NaCl, 10% glycerol, 1% Tryton X-100, 0.5% sodium deoxycholate, 2mM EDTA, 0.1% SDS, supplemented with protease inhibitor cocktail) on ice for 20 minutes. The protein extracts were then collected in the supernatant and the concentration of each protein extract was estimated using a BCA assay. Equal quantities of protein were mixed with 4 \times loading “Laemmli” buffer (0.4 M sodium phosphate pH 7.5, 8% SDS, 40% glycerol, 10% 2-mercaptoethanol, 0.05% bromophenol blue), heated to 95 °C for 5 min, and processed for either dot-blot or western blot. Nitrocellulose membranes (0.22 μ m pores) were blocked in 1x TBS with 0.05% Tween (1x TBST) with 5% w/v non-fat dry milk for 1h, and then incubated with primary antibodies in 1x TBST 5% w/v non-fat dry milk at either room temperature for 2h or 4 °C overnight.

Primary antibodies used were: anti-V5 (1:1000; CellSignaling), anti- α -tubulin (1:3000), anti-GA repeat (1:1000), anti-AP repeat (1:1000) (**Table 2.2**).

Membranes were then washed three times for 5 min with 1x TBST and incubated with either an anti-mouse IgG-HRP-conjugate (1:5000) or an anti-rabbit IgG-HRP-conjugate (1:5000). Enhanced ChemiLuminescence (ECL) substrate was then added to the membrane to enable detection, and nonsaturated images were acquired using a G:BOX EF machine and GeneSys software.

2.2.11 Perturbation of endocytosis

Exposure of cells to low-temperature conditions is a commonly used method for nonspecific inhibition of endocytosis. Healthy control iAstrocytes were primed with 30 min of exposure to 4°C, and then the DPR assemblies (diluted in ice-cold DMEM) were delivered to the cells and incubated at 4°C for an additional time of 1 hour. The same procedure was applied for Alexa647-labelled transferrin, an established marker of clathrin-coated pits⁴⁵⁹. In parallel conditions, cells exposed to DPR assemblies or transferrin were incubated with DMEM at 37°C for 1 hour. For the dynamin inhibition experiment, following the established protocol⁴⁶⁰, cells were primed for 30 min with Dynasore (or 0.2% DMSO) and incubated at 37°C in serum-free medium before addition of transferrin or poly-GA fibrils for 1 hour. Cells were subsequently fixed in Glyoxal solution (pH=5) for 30 minutes⁴⁶¹ and imaged with confocal microscopy (Zeiss LSM 880, Airyscan mode) from the plane of sharp focus. From the images, using FIJI and creating a macro (<https://github.com/paoloM1990/Quantification-of-cell-fluorescent-intensity>), the Mean grey values of Atto550 or Alexa647 whole-cell signals were calculated. In the case of the 37-4°C endocytosis experiment, mean grey values were log-transformed (log10) only for better graph visualization.

2.2.12 Lysosomal assays

Lysosomal *in situ* Enzyme Activity was measured by using Lysosome-Specific Self-Quenched Substrate (Abcam Cat No. ab234622) at manufacturers recommended dosage. In brief, primary mouse cortical neurons were exposed to poly-GA DPRs for 24 hours (or were left untreated), and Lysosome-Specific Self-Quenched Substrate was added during the final 1 hour of the 24-hour period. Cells were then fixed with 4% PFA at room temperature for 15 minutes before being imaged with a Zeiss LSM 880 confocal microscope on glass-bottom slides (Ibidi). FIJI was used to analyse the images, and the mean fluorescence intensity of the substrate was quantified per neuronal cell.

Lysosomal staining with the fluorescent acidotropic probe, LysoSensor Green DND-189, was performed according to the manufacturer's recommendations (ThermoFisher Scientific, #L7535). Briefly, HeLa cells on a 96-Well Optical-Bottom Plate were exposed to poly-GA DPRs for 24 hours (or were left untreated), and LysoSensor Green was added during the final 1 hour of the 24-hour period (1 µM final concentration). After incubation, live cells

were transferred to the PerkinElmer Opera Phenix® high-throughput system for imaging (40x 1.1NA lens). Using the Columbus Image Analysis System, the mean fluorescence intensity of LysoSensor Green was quantified per cell.

2.2.13 Release of DPRs in the conditioned medium

To detect the cell release of ATTO550 DPRs into the conditioned medium, we initially added 1µM of DPRs to the culture medium for 24h. After DPR uptake, cells were washed at least five times with PBS to remove remaining assemblies in the medium and then incubated for 24h with PhenolRed-free FBS-free DMEM. This conditioned medium (CM) was harvested in tubes which were subsequently centrifuged at 200g for 4 minutes to remove any remaining debris and dead cells. Finally, the HTS microplate reader PHERAstar FSX was used to measure ATTO550 fluorescence intensity (thus relative DPR concentration) in the CM on a 96-well plate. The optical module used for the fluorescence intensity measurement of each well was set to 540-20 nm (excitation light) and 590-20 nm (emission light), covering the whole area of the well. Importantly, we tested for linear dependence of fluorescence on concentration to evaluate potential inner filter effect⁴⁶² by using nine known dilutions of purified DPRs in PhenolRed-free FBS-free DMEM; the plotted fluorescence values originated a standard curve with $R^2 > 0.95$.

2.2.14 APOJ enzyme-linked immunosorbent assay (APOJ ELISA)

Apolipoprotein J (APOJ) (also known as clusterin) was measured in conditioned medium from either untreated or treated iAstrocytes for 24 hours with various recombinant DPRs (poly-GA fibrils, poly-GA oligomers, poly-PA oligomers). The conditioned medium was collected in tubes and centrifuged at 500g for 4 minutes to remove any remaining debris and dead cells. After that, samples were diluted 1:10 and analysed within the range of the standard curve. APOJ protein levels were measured using a human APOJ ELISA kit (Proteintech, #KE00110) following the manufacturer's instructions. The HTS microplate reader PHERAstar FSX was used to measure the absorbance of APOJ standards at 450 nm with the correction wavelength set to 630 nm. Regression analysis using the Four-parameter logistic curve-fit (4-PL) method was used to determine the best-fit standard curve.

2.2.15 Mean-Squared Displacement(Δt) analysis

Human iAstrocytes were exposed to 1 μ M ATTO550-labeled Poly-GA DPR fibrils for 24h. Cells were then washed several times with PBS and, while keeping them in 5% CO₂ and 37°C, z-stack live-imaging was performed by taking 60 frames at ~1frame/s rate (1 frame = 1 full z-stack) at ~190nm lateral resolution (Zeiss LSM880, airyscan mode).

Single DPR aggregates were then detected as single particles and analysed by the open-source FIJI-plugin TrackMate⁴⁶³ using difference of Gaussians (DoG) detection (estimated blob diameter = 0.8 μ m; threshold = 100) and Simple LAP tracker (linking max distance = 1 μ m; gap-closing = 1 μ m; max frame gap = 5). **Movie S5** was produced in 3D-volume rendering mode using Arivis Vision 4D software after complete image stack deconvolution was performed for each frame with Huygens Professional version 19.10 (CMLE algorithm, SNR:20, 40 iterations).

The *xy* data for each tracked object was analysed to determine Mean-Squared Displacements (MSD) as a function of time-step, Δt . For untethered non-interacting objects moving freely within the media, MSD(Δt) is expected to evolve linearly with a gradient equal to 4D, where D is the Brownian translational Diffusion coefficient. If the object also experiences ballistic motion (i.e. constant translational velocity magnitude and direction), which could approximately describe microtubule transport⁴⁶⁴, the MSD(Δt) becomes quadratic and is represented by the equation: $MSD = 4D\Delta t + v^2\Delta t^2$, where *v* is the average ballistic velocity⁴⁶⁵. Consequently, MSD(Δt) data was fitted to this expression to identify any trajectories that showed non-zero values for *v*, and so possibly reflect microtubule directed motion. For this analysis, the time range fitted was 20 seconds, and only trajectories greater than 30 seconds in length were analysed (380 separate trajectories met this criterion).

For the MSD(Δt) analysis on DPR trajectories in primary mouse cortical neurons, we firstly used TrackMate for producing DPR tracks and then we implemented the MATLAB class @msdanalyzer written by Jean-Yves Tinevez (<https://github.com/tinevez/msdanalyzer> GitHub), already used in a previous study⁴⁶⁶ and explained in its details⁴⁶⁷. MSD plots and Log-Log fit plots were produced with MATLAB R2018b using the aforementioned class. A detailed explanation of how the analysis was performed (from the generation of Trackmate DPR tracks to the production of graphs after MSD analysis) can be found on Github at the following link: <https://github.com/paoloM1990/Guide-to-TrackMate-Matlab-MSD>

2.2.16 Colour deconvolution for detecting two lysosomal populations

We developed custom scripts in MATLAB to produce colour deconvolution algorithms that separated “Non-Colocalized Lysosomes” (NCLs) and “Colocalized Lysosomes” (CLs). NCLs corresponded to the signal of LysoTracker Green devoid of any overlapping with ATTO550-DPRs signal. CLs, instead, corresponded to the merged signal generated by LysoTracker Green – ATTO550-DPR colocalization.

Briefly, 8-bit RGB time-lapse images were split into individual frames and a fuzzy colour detection algorithm was applied to identify and isolate regions of interest. Resulting images were binarised by applying a global Otsu threshold, and then de-noised using a median filter.

2.2.17 mRNA isolation and RT-qPCR

Primary cortical neurons were produced from E15.5 embryos of wild-type C57BL/6 mice. Total RNA from primary mouse cortical neurons (after 10 days *in vitro*) exposed to poly-GA oligomers or poly-GA fibrils (or untreated) for 24h was isolated using RNeasy Mini Kit, according to the manufacturer’s manual. During RNA extraction, treatment with DNase I was applied to get rid of contaminating DNA.

RT-qPCR was carried out using the QuantiFast SYBR Green RT-PCR Kit. Briefly, a 10 μ l volume reaction was set up by using 2 μ l total RNA (diluted to a concentration of 10 ng/ μ l in nuclease-free H₂O), 5 μ l 2x QuantiFast SYBR Green RT-PCR Master Mix, 1 μ M forward primer, 1 μ M reverse primer, 0.1 μ l QuantiFast RT mix and nuclease-free water.

Following an initial reverse transcription step at 50°C for 10 min and a 5 min denaturation step at 95°C, the cDNA was amplified by 39 cycles of 95°C for 10 sec followed by a combined annealing/extension step at 60°C for 30 sec. This was followed by subsequent melt curve analysis (to ensure primer specificity), with data collected over a temperature range of 65–95°C in 0.5°C increments. The described thermocycler program is shown here:

Reverse transcription:

50°C 10 minutes

Activation of Taq DNA polymerase (and inactivation of Reverse transcriptase):

95°C 5 minutes

Cycle 39x: Denaturation and combined annealing/extension:

95°C 10 seconds

60°C 30 seconds

Final elongation:

65°C to 95°C with 0.5°C increments

Hold:

10°C

RT-qPCR was performed on a Bio-Rad C1000 Touch™ Thermal Cycler. Bio-Rad CFX Manager software was used to analyse signal intensity and relative gene expression values were determined using the $\Delta\Delta C_t$ method, with GAPDH RNA used as a reference gene.

The RT-qPCR product was then visualized on a 2% agarose gel, after loading 10 μ l of product along with 2 μ l of 6x gel loading dye. After electrophoresis (at 120V for 40 minutes), the gel visualization showed RT-qPCR products matching the expected bp size.

2.2.18 dSTORM imaging

2.2.18.1 *Sample preparation*

High-precision (#1.5H Thickness) glass coverslips were thoroughly rinsed in deionized water and dried. The glass coverslips were coated for 5 minutes at room temperature with fibronectin diluted in PBS (1:400) before iAstrocytes were plated.

2.2.18.2 *Immunocytochemistry and staining for dSTORM imaging*

Healthy control iAstrocytes were exposed to 0.5 μ M ATTO-647N-labeled DPR fibrils and oligomers for 24h. Cells were then washed 6 times with PBS to remove the remaining DPRs in the medium and then fixed for 60 minutes in 4% PFA (+0.2% glutaraldehyde) diluted in PBS. This long fixation period was used to minimize molecule motility⁴⁶⁸.

For dual-colour dSTORM imaging, PFA-fixed cells were quenched in 50 mM NH₄Cl in PBS for 5 min at room temperature, followed by permeabilization with 0.1% Triton-X 100 in PBS and blocking of non-specific binding sites with 2% BSA.

Staining with anti-LAMP1 Mouse primary mAb (1:50) was performed overnight at 4°C. Cells were washed with 3 x PBS for 5 minutes and incubated for 2h with Anti-Mouse IgG F(ab) ATTO488 (H+L) (1:1000; HyperMOL) to yield minimal linkage error⁴⁶⁹. Post-fixation in 4% PFA (+0.2% glutaraldehyde) for 30 minutes was applied to further reduce molecule motility when needed.

Coordinates were tracked with Nikon NIS-Element software for computational drift correction and, in a separate sample, tetraspeck beads (100 nm diameter) were imaged as fiduciary landmarks for chromatic realignment. Dual-colour dSTORM imaging was performed under reducing condition preparing a 1 ml solution of 39.5 mM Tris buffer with 7.9 mM NaCl (pH 8), 10% glucose (=100 mg), 100 mM cysteamine, 500 μ g/ml glucose oxidase, and 40 μ g/ml catalase. Approximately 8'000-10'000 frames per channel were acquired. Diffraction limited images of each channel were also acquired, providing the reference for subsequent NanoJ-SQUIRREL analysis⁴⁷⁰ of image artefacts (**Figure 4.7C**).

All imaging was carried out on an inverted Nikon Eclipse Ti microscope equipped with a 100× oil immersion objective (N.A. 1.49) using an Andor iXon EMCCD camera (image pixel size, 151.57 nm). ATTO-647N and ATTO-488 were imaged using 639 nm and 488 nm lasers for a 10-ms or 20-ms exposure time. We used Nikon NIS-Elements software for both image acquisition and reconstruction. After image reconstruction, the package ChriSTORM⁴⁷¹ was used for translating NIS-Elements localization files into compatible files for image rendering by the open-source FIJI plugin ThunderSTORM⁴⁷². Thus, ThunderSTORM enabled the ultimate visualization of data acquired by STORM imaging (**Figure 4.7A**). Using the Nikon NIS-Elements software, single molecules were localised with a lateral localization accuracy of ~20 nm for 647 channel and of ~45 nm for 488 nm channel based on the Thompson equation⁴⁷³ (**Figure 4.7B**). In addition, by using NanoJ-SQUIRREL FIJI plug-in, we have implemented block-wise FRC resolution mapping to provide local resolution measurements of our dSTORM dataset⁴⁷⁰ (**Figure 4.7B**).

2.2.18.3 *Colocalization analysis in dual colour dSTORM*

For colocalization analysis, graphs are indicative of ~5-6 healthy iAstrocytes with 5 ROIs taken in regions juxtaposed to the nucleus of each cell (n = 3 biological experiments). The choice of ROIs was based by excluding artefact-rich areas with the FIJI plug-in NanoJ-Squirrel⁴⁷⁰. For colocalization analysis, we used the open-source software Clus-DoC⁴⁷⁴ to generate colocalization maps (Co-Loc maps) which highlighted areas of molecular interaction between the two channels with the following parameters: L(r)-r radius = 20nm; Rmax = 500nm; Step= 10nm; Colocalization threshold = 0.4; Min colocalized points/cluster = 10. These parameters were also chosen in accordance with a previously published study that used LAMP1 staining (as in our case)⁴⁷⁵.

2.2.18.4 3D dSTORM

Nikon NIS-Element software and a Nikon Eclipse Ti microscope were used for 3D STORM imaging. We used an astigmatic lens in the light path - directly in front of the camera. To summarise, the NIS-Element calibration algorithm was first applied to tetraspeck beads in z-stack mode (600-800 nm of z-stack). Because of the astigmatism, the point spread function (PSF) of the beads changes along the z-axis; this PSF change is used by the calibration algorithm to estimate the position along the z-axis. For each imaged channel, a new calibration was applied (although in our case we only imaged ATTO647N dye, thus one channel).

2.2.19 Quantification and Statistical analysis

All data are presented as means \pm SEM or means \pm SD, where indicated. On normally distributed data, statistical differences were analysed using Unpaired two-tailed Student's t-test (with Welch's correction, when SDs were not equal) for pairwise comparisons or one-way ANOVA (with Tukey's correction) for comparing groups of more than two. On non-normally distributed data, the non-parametric Kolmogorov-Smirnov test or Kruskal-Wallis test (with Dunn's multiple comparisons) were used for pairwise comparisons or for comparing multiple groups, respectively. Normal distribution was tested with Shapiro-Wilk test and Q-Q plot. $P < 0.05$ was considered statistically significant. All graphs and tests were generated using GraphpadPrism 8.

3. Recombinant poly-GA DPRs assemble into oligomers and β -sheet fibrils

3.1 Introduction

A crucial driver of C9orf72-mediated ALS/FTD pathology is the unconventional repeat-associated non-AUG (RAN) translation of the GGGGCC repeat expansion into five toxic dipeptide repeat proteins (DPRs). *Post-mortem* tissue of ALS/FTD patients contains ubiquitin- and p62-positive DPR inclusions predominantly in the frontal cortex, hippocampus and cerebellum of neuronal cells^{356,414,416,417}, with rare occurrence in glia⁴⁷⁶. There is a near absence of DPR inclusions in spinal cord motor neurons from ALS cases (0.1% of cells)⁴¹⁵; however, it could be argued that these DPRs could have resided in motor neurons that had already died prior to histological examination.

Among the five different DPR species generated by RAN translation (-GA, -GP, -PA, -PR, -GR), poly-GA appears to be the most abundantly detected in ALS/FTD patients' CNS *post-mortem* tissues, and thus the longest lasting in the CNS^{445,477}. Poly-GA toxicity has been documented both in cell culture and *in vivo*^{127,418,478} and correlates with motor deficits, cognitive defects and inflammatory response in mice^{128,424,427}. Initial efforts to identify molecular mechanisms of poly-GA toxicity revealed that these DPRs interact with components of the ubiquitin-proteasome system, such as p62, ubiquilin-1, ubiquilin-2, and UV excision repair protein RAD23 homologs A and B (HR23A and HR23B)^{416,429,430}; and specifically lead the 26S proteasome to stalled degradation⁴⁴⁷. Emerging evidence shows that poly-GAs can also rapidly spread throughout the *Drosophila* brain in a repeat length- and age-dependent manner¹³¹, in agreement with their ability to spread and drive cytoplasmic mislocalization and aggregation of TDP-43 in cell cultures^{126,130,132,448}.

This chapter describes the first steps we took to produce recombinant poly-GA proteins. By using an *Escherichia coli*-based expression system, we successfully produced and purified poly-GA proteins consisting of 34-GA dipeptide repeats.

These 34-GA DPRs were subsequently labelled with a specific fluorescent dye to allow their rapid visualization in cell culture settings via fluorescence microscopy. Furthermore, the DNA sequence encoding the short V5 epitope tag (derived from the P and V proteins of the paramyxovirus simian virus 5) was cloned into our constructs for producing the recombinant proteins. Besides recombinant poly-GA, another recombinant protein such as poly-PA was produced by the same techniques to serve as an experimental control in later studies.

Briefly, the following scheme illustrates the various steps taken in the production of recombinant proteins.

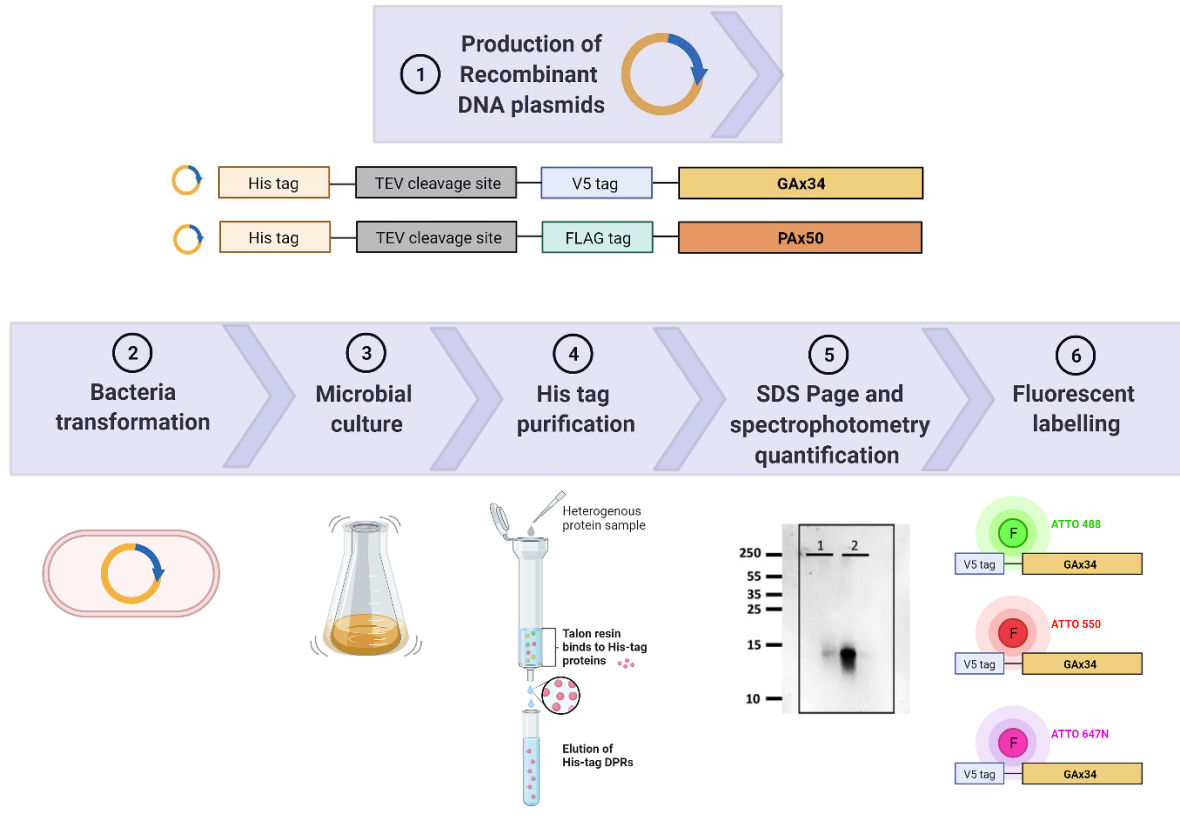


Figure 3.1 Schematic diagram of recombinant proteins' production

DNA sequences encoding V5-tag followed by 34 repeats of GA or FLAG-tag followed by 50 repeats of PA were subcloned in a bacterial expression vector containing an N-terminal 6xHis-Tag and a TEV protease cleavage site. The *E. coli* BL21 strain was transformed with these recombinant plasmids. His-tagged proteins were purified on Talon columns. Eluted fractions were analysed by SDS-PAGE, and proteins were quantified spectrophotometrically and labelled with fluorescent dyes. Figure created with BioRender.com under academic license.

Each step of this experimental scheme will be discussed in detail during the course of this Results' chapter.

There are several advantages of having our recombinant proteins linked to a fluorescent dye and, at the same time, being tagged with the V5 epitope. Fluorescent microscopy can be used to rapidly detect the recombinant proteins via the fluorescent dye (both fixed- and live-

imaging modalities can be used), and the dye's fluorescent signal can be confirmed down the line with anti-V5 immunoassays on fixed cells or blotted membranes (i.e., immunostaining, immunoblotting).

The construction of this easy-to-use system offers the exciting ability to monitor the presence of 34-GA dipeptide repeats upon their administration to the cell culture medium. This experimental setting mimics a situation in which an exogenous protein is potentially circulating in the extracellular space (or cell culture medium) and can come into contact with a cell or more than one cell.

Numerous biological processes such as plasma membrane binding, endocytosis, phagocytosis, lysosomal degradation and cell-to-cell transmission can be studied in cell culture to follow the fate of an exogenous recombinant protein after its addition to the cell culture medium. Recombinant proteins are crucial instruments for investigating biological processes, and their manufacture for research purposes is primarily motivated by the process's cost-effectiveness, simplicity, and speed, as well as appropriate product yields.

This chapter will also describe the *in vitro* assembly of the generated recombinant proteins. By “in vitro assembly”, we define the process underlying the coalescence of purified proteins in the test tube, thus *in vitro*.

No research has yet looked into the potential for poly-GA recombinant proteins to undergo liquid-liquid phase separation *in vitro*, contrarily to other DPR species such as poly-GR and poly-PR for which this process has been extensively investigated⁴⁷⁹.

Along the line of *in vitro* experiments, we will also investigate whether our recombinant poly-GA has the ability to form high-molecular weight species with characteristic and distinct morphological features, for example, by forming fibrillar assemblies.

The investigation of poly-GA DPRs at various aggregation stages (oligomers vs fibrils) represents an important opportunity for cell culture research. Because the repeat length is the same (34-GA), potential differences in biological processes (e.g., membrane binding, endocytic routes of uptake, cell-to-cell transmission) would be solely attributable to the stage of aggregation. This area of research is largely unexplored in C9 ALS/FTD, as to the best of our knowledge no study has yet provided a comparative assessment of the properties of the same DPR species at different aggregation stages.

In the final section of this chapter, we will address the potential of our recombinant proteins to bind to the cell surface upon administration into cell culture medium.

3.2 Cloning, purification and labelling of recombinant DPRs

Some results had already been generated as part of this thesis project, which began in April 2018, by the groups of Professor Kurt De Vos (Department of Neuroscience, University of Sheffield, UK) and Dr Ronald Melki (Institute Francois Jacob MIRCen, CEA and Laboratory of Neurodegenerative Diseases, CNRS, France). These laboratories' work consisted in the production of recombinant poly-GA and poly-PA proteins. In particular:

- Professor De Vos' team cloned the V5-tagged 34-GA repeat construct
- Dr Melki's team produced the FLAG-tagged 50-PA repeat construct and produced all recombinant proteins

V5-tagged 34-GA repeat

Briefly, V5-tagged 34x GA repeat was obtained using an expandable cloning strategy with *AgeI* and *MreI* as compatible enzymes⁴⁵⁵, as explained in detail in Section 2.2.5. The V5-tagged 34-GA construct was then subcloned in the pETM-11 vector (Addgene plasmid #108943), using *NcoI* and *NotI* restriction sites. The pETM-11 vector contains an N-terminal 6xHis-Tag and a TEV protease cleavage site, which are useful sites for later purification. Transformations of plasmids containing the 34-GA repeat were performed using *E. coli* BL21 and purification steps are described in Chapter 3.2.1.

FLAG-tagged 50-PA repeat

Briefly, the plasmid pAG416-Gal, which contains the DNA encoding for 50-PA repeats, was obtained from Addgene (Addgene plasmid #84902). The FLAG-tagged 50-PA repeat construct was then subcloned in the pETM-11 vector, using *NcoI* and *XhoI* restriction sites. Transformations of plasmids containing the 50-PA repeat construct were performed using *E. coli* BL21 and purification steps are described in Chapter 3.2.1.

This collaboration among different groups enabled me to begin my PhD project in 2018, when I could readily test these recombinant proteins for GA/PA immunoreactivity (Chapter 3.2.2) and for various cell culture experiments (3.3 onward Chapters).

3.2.1 Protein purification, characterisation and fluorescent labelling

Poly-GA and poly-PA proteins were expressed in *E. coli* BL21 and purified on 5 mL Talon column (Clontech®) loaded with Cobalt. The proteins were eluted with a linear gradient of 12 ml from buffer A (20mM Tris pH 7.5, 250mM NaCl, 5mM Imidazole, 1mM β Mercaptoethanol, Glycerol 10% PMSF 0.1mM) to buffer B (20mM Tris pH 7.5, 250mM NaCl, 250 mM Imidazole, 1mM β Mercaptoethanol, Glycerol 10% PMSF 0.1 mM).

Eluted fractions were analysed by SDS-PAGE, and proteins were quantified spectrophotometrically using a molar extinction coefficient of $\epsilon_{GA} = 2980 \text{ M}^{-1} \text{ cm}^{-1}$ and $\epsilon_{PA} = 4470 \text{ M}^{-1} \text{ cm}^{-1}$.

It is important to mention that the eluted fractions of poly-GA and poly-PA proteins are composed of what we defined as “oligomers”, which essentially indicates that these recombinant proteins are composed of a small number of identical monomers with defined dipeptide repeat length (-34 for GA and -50 for PA). As demonstrated by our collaborator Dr Melki ²¹, the oligomeric state of poly-GA and poly-PA proteins was determined by assessing their apparent molecular weights using size-exclusion chromatography (SEC). In brief, proteins freshly solubilized in hexafluoroisopropanol (HFIP) were dried and the resulting film was resuspended in PBS buffer. Following this treatment, all DPRs were found to be soluble. In PBS, poly-GA protein showed two species with apparent molecular weights of 21 and 6.4 kDa; and poly-PA protein showed two species with apparent molecular weights of 105 and 32 kDa, as well as a third species corresponding to aggregated PA protein. The weights were calculated using the SEC elution volume/void volume (V_e/V_o) ratio. Poly-GA and poly-PA proteins were thus classified as “oligomers” because they were mostly monomeric in nature but contained varying amounts of low and high molecular weight species, corresponding to small and larger multimeric species. Furthermore, our collaborator Dr Melki investigated the secondary structure of these oligomers using circular dichroism spectroscopy and discovered that poly-GA is 10% α -helix, 1% β -sheet, and 89% random coil; whereas poly-PA is 20% α -helix, 2% β -sheet, and 78% random coil ²¹.

Prior to labelling these poly-GA and poly-PA oligomers with fluorescent dyes, we wanted to see if these oligomers could assemble into high-molecular-weight species during various assembly conditions (e.g., buffers, temperature and agitation). Poly-PA oligomers remained mostly soluble in all conditions tested, with a fraction ranging from 10 to 20% of the proteins

forming amorphous aggregates ²¹. Poly-GA oligomers, on the other hand, successfully assembled into fibrillar aggregates that bundled together in purification buffer or PBS at 4°C for 15 days without shaking. This result was observed using transmission electron microscopy and will be explained in greater detail later in Chapter 3.4. The assembly of poly-GA fibrils was followed using a sedimentation assay and SDS-PAGE analysis to provide biochemical characterisation; in brief, poly-GA fibrils were spun at 100 000g for 30 minutes to remove unassembled polypeptides, and the disappearance of monomeric poly-GA from the SDS-PAGE gel over time was measured and followed by Coomassie Blue staining, as reported ²¹.

In the following chapters, we will further discuss the distinction between poly-GA oligomers and poly-GA fibrils (i.e., Section 3.4 of Chapter 3).

Nonetheless, all recombinant proteins produced were labelled with one of the following dyes:

- **ATTO-488** → Atto-Tec #AD488-35; labelling ratio is Atto:DPR 1:2
- **ATTO-550** → Atto-Tec #AD550-35; labelling ratio is Atto:DPR 5:1
- **ATTO-647N** → Atto-Tec #AD647-35; labelling ratio is Atto:DPR 2:1

Unreacted N-Hydroxysuccinimide-dye was removed by centrifugation (100'000g, 30 minutes, 4°C). Labelled assemblies were flash-frozen in liquid nitrogen and stored at -80°C.

3.2.2 Analysis of GA/PA immunoreactivity and fluorescence labelling

Immunoreactivity and fluorescent labelling of the generated GA/PA-repeat recombinant proteins were confirmed by resolving the samples with dot-blotting or protein gel electrophoresis.

Recombinant poly-GA fibrils, poly-GA oligomers or poly-PA oligomers were blotted in a 2-fold serial dilution onto a nitrocellulose membrane. Vacuum filtration was used to transfer proteins onto the membrane (dot-blotting), which was then stained with respective anti-repeat antibodies (anti-GA=Proteintech 24492-1-AP; anti-PA=Proteintech 24493-1-AP). Quantification of blots from anti-GA or anti-PA staining revealed a decreasing signal with increasing serial dilutions (**Figure 3.2A**), indicating that our sample contains DPR-specific sequences that are recognised and bound by anti-DPR antibodies.

Fluorescence labelling of poly-GA oligomers and poly-GA fibrils with ATTO-647N dyes was also investigated. Recombinant proteins were loaded onto an acrylamide gel for SDS-PAGE and then scanned with a gel fluorescent scanner. After SDS-PAGE, the ATTO-647N fluorescence signal was detected on the gel, and Coomassie blue staining was used as a loading control (**Figure 3.2B**). A similar procedure was used to detect a 647N fluorescence signal from a dot-blotted membrane (**Figure 3.2B**). Furthermore, the fluorescence labelling of poly-GA fibrils with ATTO-550 dyes was confirmed in similar blots by detecting the ATTO550 signal with a gel fluorescence scanner (**Figure 3.2C**).

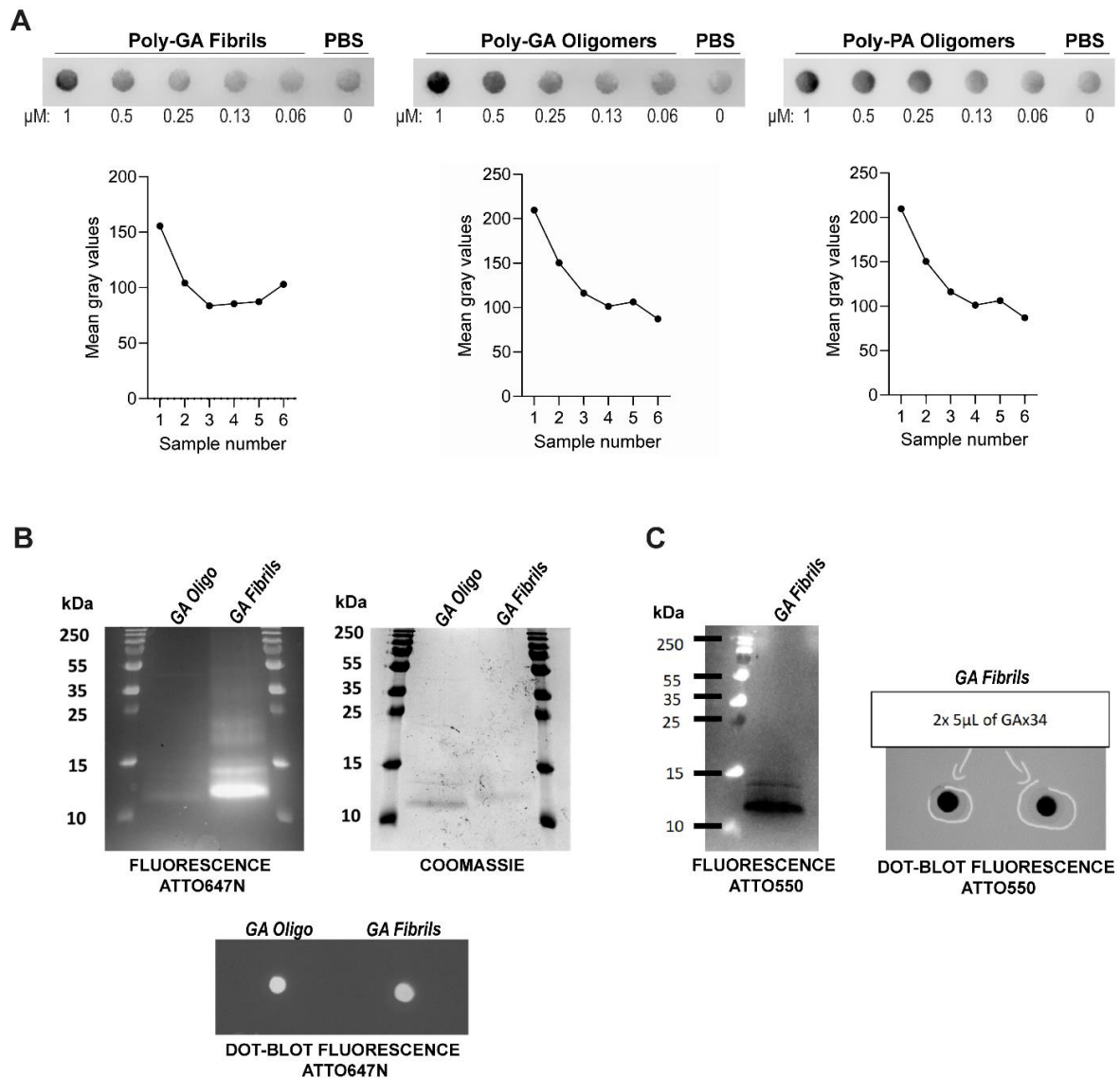


Figure 3.2 Anti-GA or anti-PA immunoreactivity and fluorophore labelling for DPRs

A) Dot-blotted membrane of purified poly-GA fibrils, poly-GA oligomers or poly-PA oligomers in serial dilution after staining with the respective anti-repeat antibodies (anti-GA=Proteintech 24492-1-AP; anti-PA=Proteintech 24493-1-AP). PBS indicates a control condition with no purified proteins. Graphs show quantification of Mean grey values for each corresponding condition. Data information, sample numbers: n^o1 = 1 μM ; n^o2 = 0.5 μM ; n^o3 = 0.25 μM ; n^o4 = 0.13 μM ; n^o5 = 0.06 μM ; n^o6 = PBS only. **B)** Poly-GA oligomers and fibrils labelled by ATTO-647N (molar ratio Atto:GA = 2:1) exhibit fluorescent signal and Coomassie staining after protein gel electrophoresis and fluorescent signal after dot-blot. While both oligomers and fibrils exhibit fluorescence signal, the fibrils' signal is three times higher (left). On the Coomassie gel, the quantity of monomers and fibrils is comparable (centre). **C)** 5 μL at 100 μM (4,5 μg) of fibrillar poly-GA labelled by ATTO-550 (molar ratio Atto:GA = 5:1) were resolved on an acrylamide gel, and the fluorescence of Atto-550 (black signal) was recorded (*left*). Two samples were also analysed by dot blot on nitrocellulose membrane, and the fluorescence of Atto-550 is displayed (black signal) (*right*).

3.3 Poly-GA oligomers coalesce into solid-like structures *in vitro*

Recently, it was discovered that arginine-rich DPRs, such as poly-GR and poly-PR, undergo *in vitro* phase separation⁴⁷⁹ and alter the liquid-like properties of stress granules and nucleoli^{427,480}. However, it is unclear whether and how DPR phase-separation events contribute to ALS/FTD pathogenesis.

In this section, we aimed to investigate the aggregation propensity of our recombinant poly-GA and poly-PA DPRs in the test-tube, namely *in vitro*, which has yet to be described in the literature.

Using confocal fluorescence microscopy, we first investigated the aggregation of poly-GA and -PA at various concentrations. In brief, we diluted our recombinant poly-GA and poly-PA DPRs (stock concentration = 100 μ M) in ddH₂O to either 20 μ M, 10 μ M or 1 μ M. Following vortexing, the mixture was pipetted onto glass-bottom slides, and assembly formation was tracked over time using ATTO550 fluorescence detection. Images were acquired immediately, as well as after 2 and 24 hours. To capture fine details for 3D rendering, the DPR assemblies were imaged with a z-stack following Nyquist sampling⁴⁵⁶ for optimized pixel density (63x 1.4NA, oil objective).

We discovered that both ATTO550-labeled DPRs coalesced into microscopic protein clusters in the absence of any molecular crowders and at low salt concentrations (**Figure 3.3A** and **3.3B**). Cluster formation was much faster for poly-PA than poly-GA, and it increased with increasing protein concentration (1 μ M, 10 μ M, 20 μ M) (**Figure 3.3C**) and incubation length (0h, 2h, 24h) for both DPR species (**Figure 3.3D**).

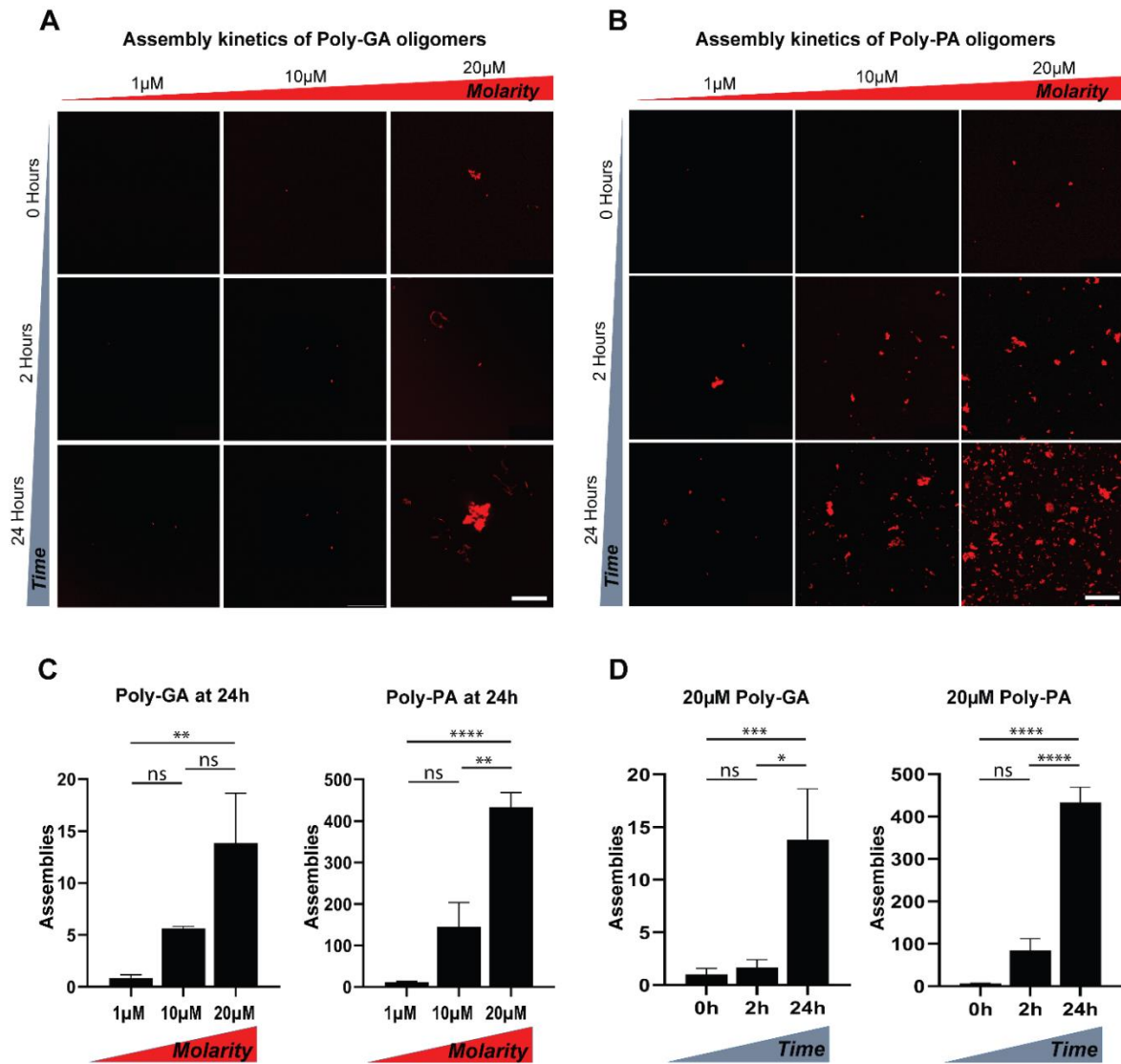


Figure 3.3 *In vitro* coalescence of poly-GA and poly-PA recombinant DPRs

Aggregation of **A)** poly-GA and **B)** poly-PA oligomers *in vitro*, with relative quantification of the number of assemblies formed upon **C)** increasing molarity or **D)** time. Scale bar = 50 μm. Bar graphs of mean ± SEM. One-way ANOVA with Tukey's multiple comparisons test. * $P \leq 0.05$, ** $P \leq 0.01$, and **** $P \leq 0.0001$. The data were collected from 2 independent biological replicates.

The shape and size of the generated poly-GA and -PA clusters differed significantly. As a result, we examined their 3D-volume rendering using Z-stack confocal microscopy and CMLE deconvolution (**Figure 3.4A and 3.4B**). The irregular and compact solid-like structure of the 3D-reconstructed poly-GAs was revealed (**Movie S1**). The 3D-reconstructed poly-PAs, on the other hand, were made of very small spherical particles (circularity = 0.95; **Figure 3.4C-E**) that resembled liquid-like droplets (**Movie S2**).

Importantly, additional methods should be used to determine the material state of these assemblies; based on our data, we cannot conclude that poly-GA assemblies are solid and that poly-PA assemblies are liquid, so we defined them as "solid-like" or "liquid-like." Methods such as fluorescence recovery after photobleaching (FRAP) and measurement of 'inverse capillary velocity' should be used to provide more information on the material state of these assemblies, and these will be briefly discussed later in chapter 3.6.

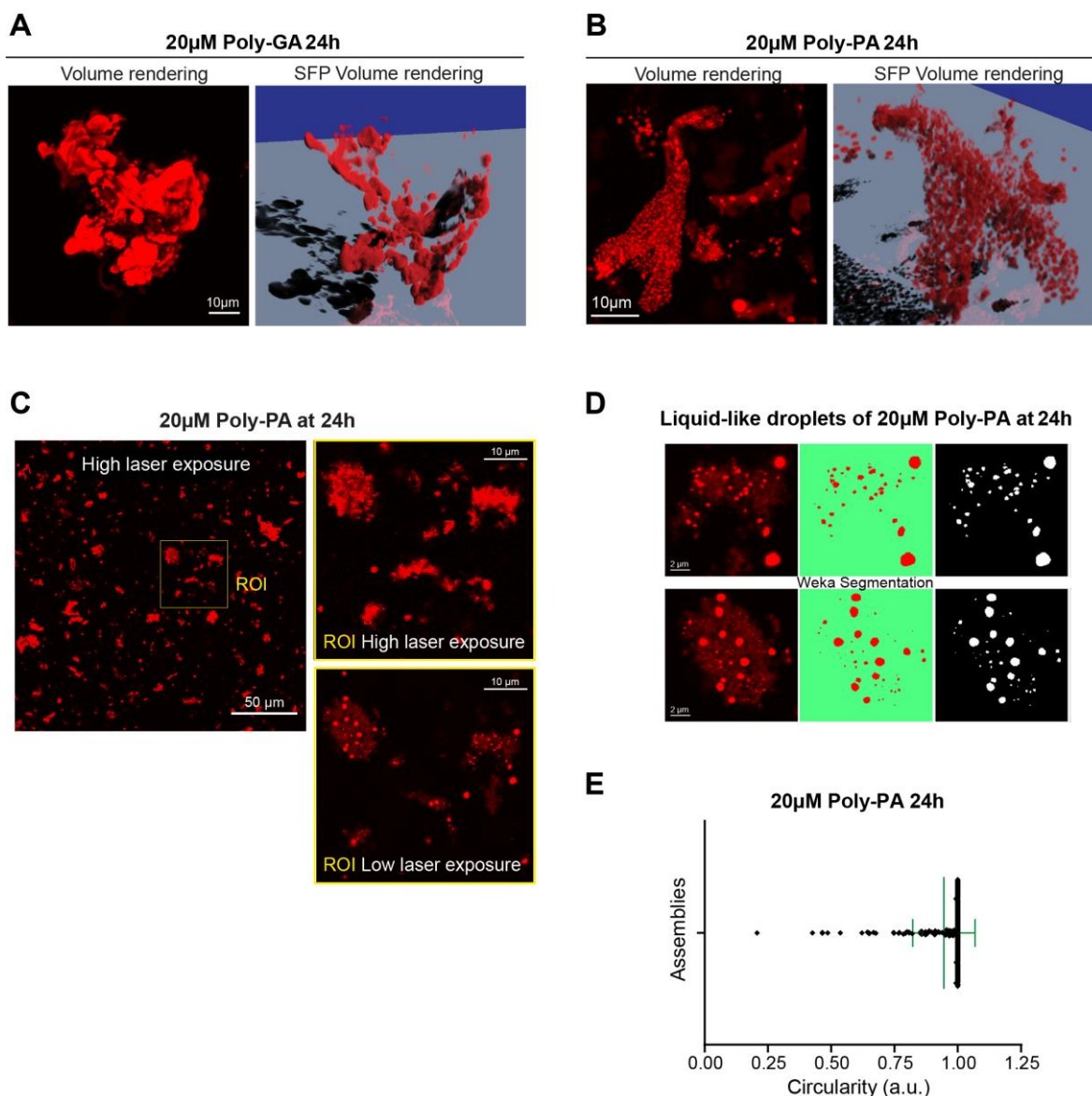


Figure 3.4 *In vitro* coalescence of poly-GA and poly-PA in 3D-rendering

A) The largest poly-GA structures formed at 20µM 24h are shown in 3D rendered images; the corresponding movie is shown in **Movie S1**. **B)** The largest poly-PA structures formed at 20µM 24h are shown in 3D rendered images; the corresponding movie is shown in **Movie S2**.

C) Confocal image showing the *in vitro* coalescence of poly-PA assemblies at 20 μ M, 24h. The image was first acquired with high laser intensity and then with low laser intensity and Nyquist sampling, so the liquid-like droplets became distinguishable. D) After segmenting the poly-PA liquid-like droplets with the Trainable Weka Segmentation FIJI plug-in⁴⁵⁸, E) the liquid-like droplets' average circularity was calculated to be 0.95 (\pm SD).

Overall, the events observed in our test-tube experiments highlight the propensity of poly-GA and poly-PA oligomers to aggregate *in vitro*. When poly-GA and poly-PA oligomers are incubated in the presence of low salt concentrations, they coalesce into heterogeneous assemblies.

3.4 Poly-GA oligomers form high-molecular weight species

During amyloid formation, partially folded and/or unfolded proteins assemble into oligomeric species, which can then recruit monomers and thus nucleate the assembly into amyloid fibrils. The fibrils are then elongated until nearly all of the free monomer has been converted to a fibrillar form²⁸.

As previously stated, we wanted to explore the ability of poly-GA oligomers to assemble into higher molecular weight species when compared to poly-PA oligomers.

As a result, we used longer incubation times than in Figure 3.3 to investigate the ability of poly-GA and poly-PA oligomers to assemble *in vitro*. We experimented with different assembly conditions such as buffers, temperature, and agitation.

It is worth noting that only poly-GA oligomers formed fibrillar aggregates. Within 15 days of incubation, poly-GAs were bundled together as fibrils in purification buffer or PBS at 4°C without shaking, as observed by transmission electron microscopy after negative staining with Uranyl acetate (**Figure 3.5A**). Poly-PA proteins, on the other hand, remained mostly soluble in all conditions tested, with only a small percentage forming amorphous aggregates (**Figure 3.5B**).

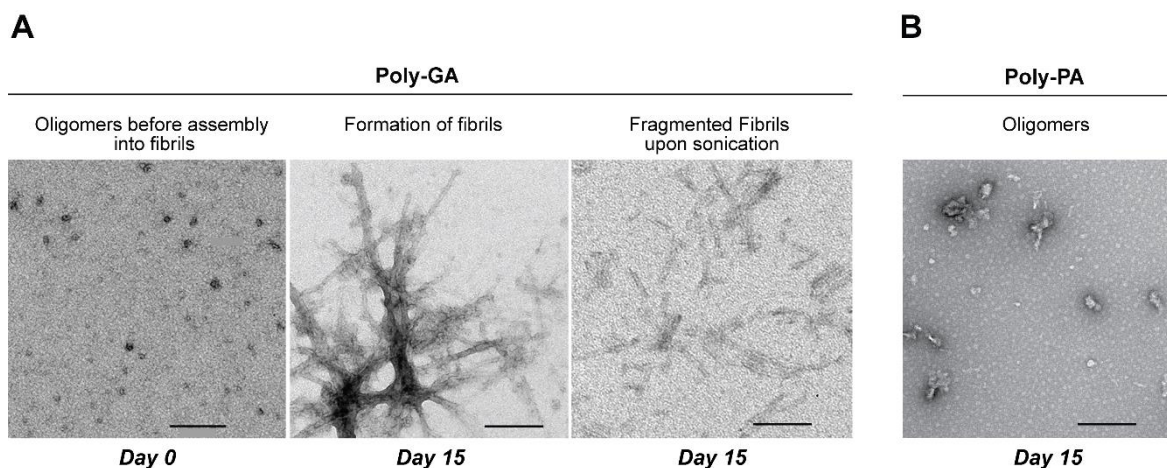
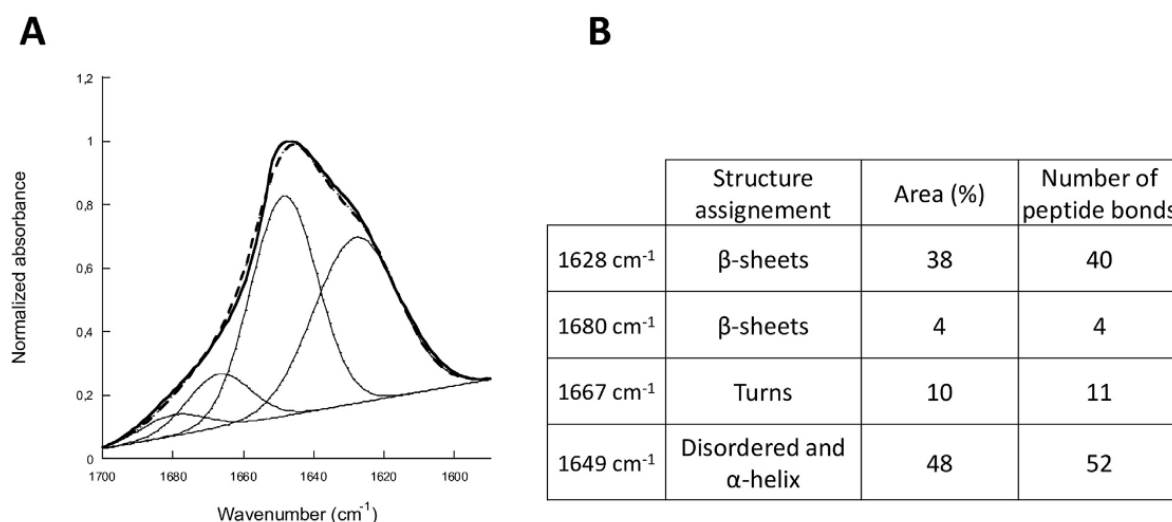


Figure 3.5 Poly-GA oligomers form characteristic fibrils after 15 days *in vitro*

Electron micrographs show that poly-GA oligomers form characteristic fibrils after 15 days *in vitro* (A), unlike poly-PA oligomers (B). Poly-GA fibrils are shown before and after sonication, which drives the production of fragmented fibrils. Scale bars = 200 nm.

Fourier-transform infrared (FTIR) spectroscopy confirmed the β -sheet amyloid component of the poly-GA fibrils. This result was obtained from our collaborator Dr Ronald Melki²¹. His team showed that the FTIR spectrum of fibrillar GA-34 proteins clearly shows a shoulder at 1620 cm^{-1} and a peak centred at 1628 cm^{-1} , indicating that GA-34 fibrils contain cross β -sheets and are thus amyloid in nature (Figure 3.6A). Fourier deconvolution of the spectra reveals that 42% of the GA-34 amino acid residues are involved in β -sheet structures within the protein's fibrillar form, while the remaining 58% of amino acid residues are disordered (Figure 3.6B).



From L. Brasseur et al. / *Biochemical and Biophysical Research Communications* 526 (2020) 410-416. With permission from the authors.

Figure 3.6 Deconvoluted FT-IR spectrum of GA fibrils

(A) GAx34 fibrils deconvoluted FT-IR spectrum. GAx34 fibrils were washed 3 times in D₂O with repeated cycles of spinning/resuspension. FTIR spectra (*thick line*), Fourier deconvolution (*thin lines*) and curve fit (*dashed line*) data are presented. FT-IR spectrum was fitted using a Gaussian species model centred at 1628, 1680 (β-sheets), 1649 (disordered and α-helix) and 1667 (loops) cm⁻¹. (B) Secondary structure estimation of GAx34 fibrils obtained by deconvolution of FTIR spectrum. The percent of the area and the associated number of peptide bonds are listed for each structure assignment.

In summary, our poly-GA oligomers produced distinctive solid-like assemblies, nucleation growth and 3D-architecture and uniquely assembled into characteristic β-sheet fibrils.

3.5 Recombinant DPRs bind to cells in culture

Because poly-GA oligomers formed fibrillar assemblies *in vitro*, we raised several intriguing questions about the possibility of comparing these two forms of the same protein not only *in vitro* but also in cell culture by administering these assemblies directly into the cell culture medium.

We initially began to investigate whether there would be differences in the ability of poly-GA oligomers vs poly-GA fibrils to bind to cells in culture. We used an immortalised human astrocyte cell line, 1321N1 human astrocytoma⁴⁵¹, to investigate this question because increasing evidence implicates astrocytes as significant non-cell-autonomous contributors of *C9ORF72*-associated ALS/FTD pathogenesis⁴⁸¹ and DPR aggregation in glial cells is understudied.

Cultured 1321N1 human astrocytoma cells were first exposed to 1 μ M of poly-GA oligomers or poly-GA fibrils (and poly-PA oligomers as a control) for 24 hours. This time period was selected as a safe window during which recombinant proteins could potentially bind cells and even undergo cell uptake. Importantly, before the addition to the medium, poly-GA fibrils were sonicated to disperse the aggregated β -sheet assemblies and to generate fibrillar particles that are suitable for endocytosis (with an average size of 45-55 nm). We then eliminated any remaining DPRs in the media after 24 hours by performing six washes in PBS. The cells were then trypsinized to remove them from the plate and resuspended in 500 μ l of PBS. Suspended cells were then analysed by flow cytometry with excitation light at 488 nm. Cells that had not been treated with DPRs served as controls, producing gating to distinguish between ATTO550+ and ATTO550- cells. We detected that 6.2%, 3.3% and 12.8% cells were positive for the ATTO550-labelled poly-GA fibrils, poly-GA oligomers and poly-PA oligomers, respectively (**Figure 3.7A**).

Dot blotting was then used to validate the flow cytometry results. In brief, we extracted proteins from 1321N1 astrocytoma and human iNPC-derived astrocytes (iAstrocytes) that had been exposed for 24 hours to poly-GA oligomers or poly-GA fibrils. After that, vacuum filtration was used to transfer proteins onto a nitrocellulose membrane, which was then stained with an anti-V5 tag antibody, which recognises the V5 antigen covalently linked to our poly-GA assemblies. We were able to confirm that the V5-tag DPR signal was present in all protein extracts derived from DPR-exposed 1321N1 astrocytoma and iAstrocytes

(**Figure 3.7B**). Notably, these iAstrocytes were derived from a healthy individual (155v2 line: Caucasian male, age 60).

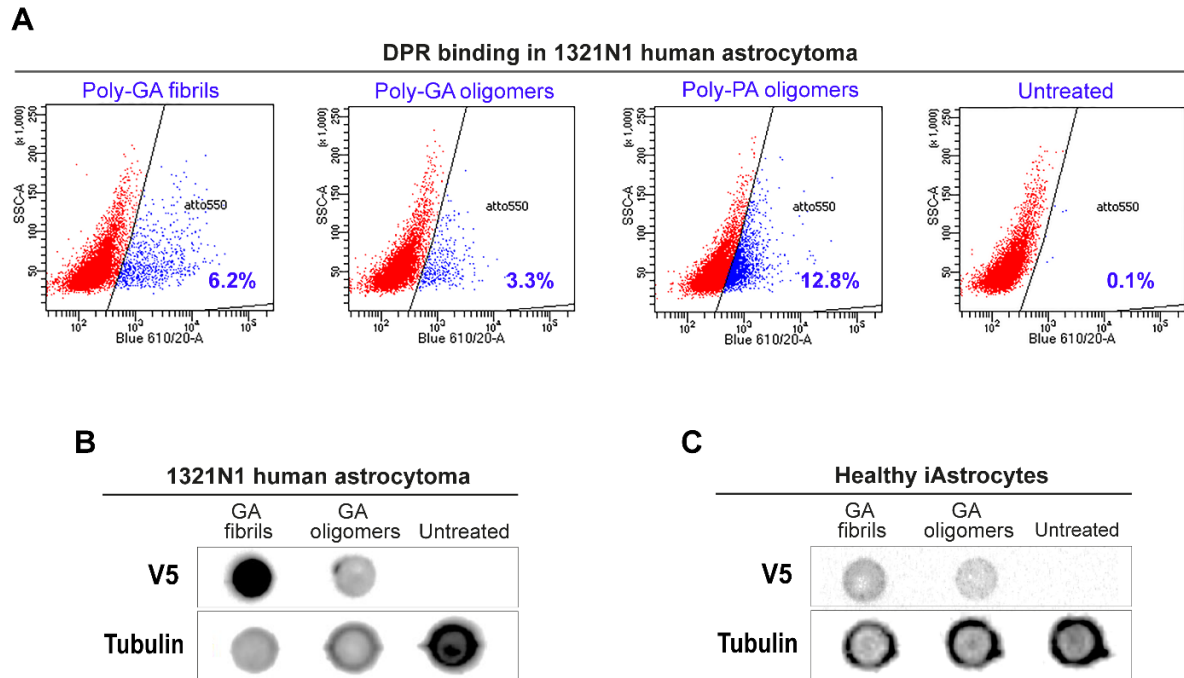


Figure 3.7 Binding of poly-GA assemblies to cells in culture

A) Scatter density plots showing ATTO550+ (blue) and ATTO550- (red) light scattering events detected by flow cytometry in 1321N1 human astrocytoma cells from a total of 10'000 events. Detection of ATTO550+ signal was set at 610/20 voltage. Cells not treated with DPRs acted as control producing the gating to discriminate between the ATTO550+ and the ATTO550- cells. The data were collected from 3 independent biological replicates. After 24h DPR exposure, total protein of 1321N1 human astrocytoma cells (**B**) or healthy iAstrocytes (**C**) was extracted into lysis buffer and then dot blotted onto a nitrocellulose membrane using a microfiltration apparatus. The membranes were then sliced into strips and analysed by anti-V5 immunostaining to show sub-populations of cells positive for V5-tagged DPRs. The data were collected from 3 independent biological replicates.

Protein aggregates may organize as clusters at the recipient plasma membrane and establish aberrant interactions that trigger increased cellular vulnerability⁴⁸². To quantitatively assess the clustering of DPRs at the surface of glial cells, we took advantage of single-molecule localization microscopy (SMLM)⁴⁸³ and total internal reflection fluorescence microscopy (TIRFM)^{484,485}.

We exposed healthy control-derived iAstrocytes to 1 μ M ATTO647N labelled poly-GA fibrils over time and evaluated whether sub-diffractive assemblies could be detected on the surface of the cell membrane via SMLM-TIRF. Only fibrils labelled with ATTO647N dye were chosen for this experiment as this photoswitchable dye is highly suitable for single-molecule detection applications and high-resolution microscopy⁴⁸⁶. We decided against using poly-GA oligomers in this experiment because early time points, such as 6h, might not be long enough for the oligomers to assemble into visible aggregates (few oligomers at 6h might be below the resolution limit even using SMLM). Cells were extensively washed with PBS (6x times) before fixation and imaging. Importantly, we imaged an iAstrocyte cell that had previously not been exposed to poly GA DPRs to rule out potential imaging artefacts caused by autofluorescent molecules illuminated by the 647nm laser source and confirmed the absence of autofluorescence artefacts (Appendix - **Figure 8.1**, page 173).

After exposing iAstrocytes to ATTO647N poly-GA fibrils, we observed multiple sub-diffractive assemblies that could not be visible and identifiable via conventional wide-field microscopy (**Figure 3.8A; Movie S9**). These sub-diffractive assemblies of poly-GA fibrils immediately clustered on the cell surface of iAstrocytes and were detected as clustered molecules via a density-based clustering algorithm, namely DBSCAN (**Figure 3.8B and 3.8C**). From our SMLM-TIRF imaging we noticed that, in general, less than 30% of the total fraction of the detected poly-GA molecules appears to be in clusters. This suggests that the remaining fraction of poly-GA molecules (70%) is sparsely distributed along the membrane surface and thus remains undetectable using a density-based clustering algorithm. Notably, when exposure to poly-GA fibrils was conducted over 3 different experimental time-points, such as 6h, 24h and 48h, these clusters did not present any significant rearrangement in the 2D membrane space over time. For example, we observed no change at 6h, 24h or 48h in the percentage of clustered molecules or in the average number of molecules per cluster, as well as in the average cluster area. Only the cluster circularity significantly decreased with time (**Figure 3.8D**).

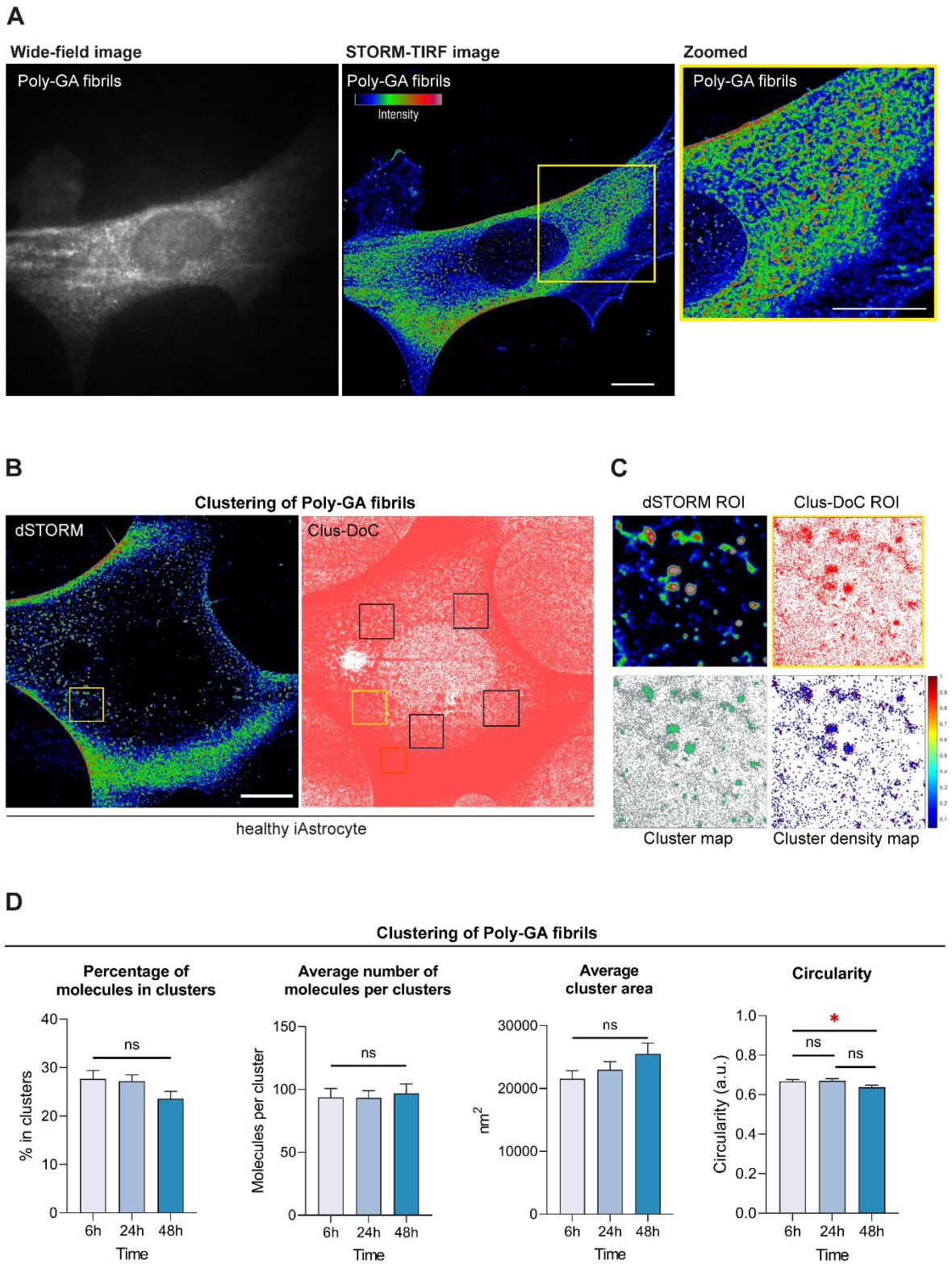


Figure 3.8 SMLM-TIRF clustering analysis of poly-GA fibrils on the surface of iAstrocytes

A) Wide-field diffraction-limited image shows the diffuse presence of ATTO647N poly-GA fibrils across the cell with no distinguishable aggregate structures. SMLM-TIRF super-resolved image (8'000 frames, dSTORM) shows sub-diffractive clusters of poly-GA fibrils with colour-coded

intensity (red=maximum, blue=minimum) wherein major aggregate structures can now be discerned, as shown in the zoomed ROI. **B)** After dSTORM acquisition (left), clustering of ATTO647N poly-GA fibrils was analysed by Clus-DoC DBSCAN algorithm (right) on 5 regions of interest (ROI) per cell. Number of cells = 6 per biological replicate. The analysed ROIs are represented as black squares (*right*), with the yellow square representing the panel B example. **C)** In the cluster density maps of the ROI, the colour scale of the Cluster density map (bottom right) represents the normalized relative density of clustered DPR molecules from 0 (min value) to 1 (max value). **D)** Quantification of the clustering of ATTO647N poly-GA fibrils at the plasma membrane of healthy control-derived (n.155) iAstrocytes 6h, 24h and 48h post-administration. Bar graphs of mean \pm SEM. Kruskal-Wallis non-parametric test with Dunn's multiple comparisons after testing normal distribution with the Shapiro-Wilk test. * $P \leq 0.05$. The data were collected from 3 independent biological replicates.

We finally performed 3D-STORM to observe the clustering of poly-GA fibrils on the 3D-membrane space of iAstrocytes after 24h. We found that a variety of clusters was present, ranging from densely packed molecules at the membrane interface to spherical clusters, probably indicative of potential compartmentalization into endo-lysosomal organelles (**Figure 3.9**).

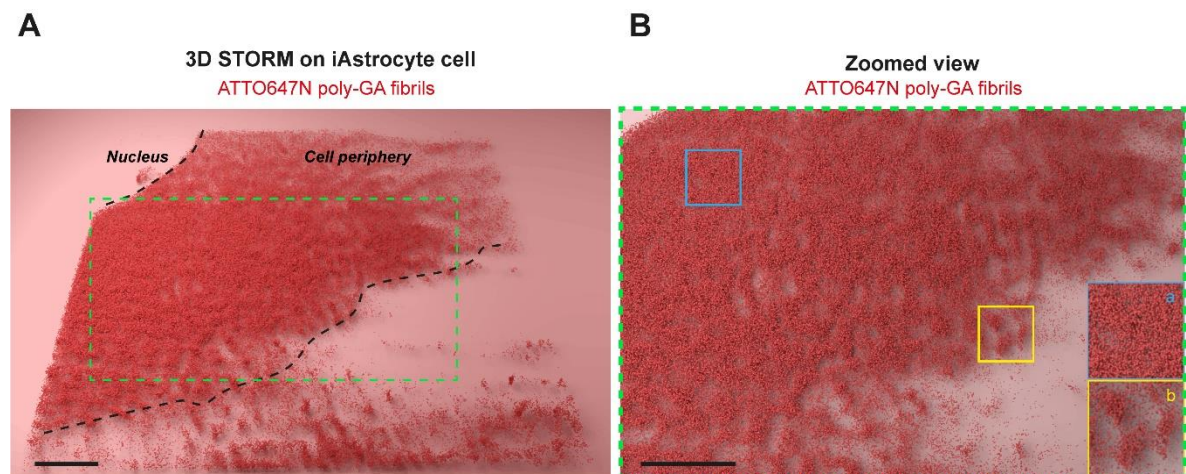


Figure 3.9 3D-STORM clustering analysis of poly-GA fibrils on the surface of iAstrocytes

A) 3D-STORM imaging was used to visualize ATTO647N labelled poly-GA fibrils in healthy iAstrocytes after 24h uptake. Scale bar = 5 μ m. B) The zoomed view shows how molecules of poly-GA fibrils can be densely clustered (inset a) but also compartmentalized in spherical structures (inset b). Scale bar = 5 μ m.

In conclusion, we demonstrated that poly-GA fibrils bind to the cell surface of iAstrocytes. Some of these fibrils form molecule clusters, but these clusters do not appear to change over the time periods we studied (6h, 24h, 48h). We also developed the first framework for studying *C9ORF72*-derived DPRs at the cell surface using 3D high-resolution SMLM-TIRFM.

3.6 Discussion

Recombinant proteins are extremely useful in the biological research. Their use offers advantages in terms of production speed, cost-effectiveness, and the ability to rapidly investigate cellular responses to stress and disease. Researchers can use this technology to clone the DNA encoding a specific protein into an expression vector and then express the protein in expression systems such as bacteria, yeast, insect cells, and mammalian cells ⁴⁸⁷. After these steps, the protein is ready for purification and characterization.

We decided to create recombinant poly-GA DPRs as part of our research. This choice was made because the most detectable ubiquitinated aggregates in the *post-mortem* brain tissue of C9 ALS/FTD patients are poly-GA DPRs. The accumulation of these ubiquitinated proteins observed in histopathological studies is most likely the result of the disease, rather than the cause. Proteostasis imbalance probably begins decades before the patients' deaths (pre-symptomatic stage), when cells go through a series of complex responses to counteract protein supersaturation ^{488,489}. In support of this hypothesis, the end-stage inclusions are mainly composed of fibrillar deposits; these are thought to be far less toxic than prefibrillar oligomeric species that are present at earlier disease stages ^{47,490–492}. For most ALS/FTD aggregation proteins, the question of which aggregation stage (monomers, oligomers, fibrils) of the same misfolded protein contributes the most to disease pathogenesis remains unresolved. To the best of our knowledge, only one study in the context of *C9ORF72*-derived DPRs has shown a clear morphological aggregate via electron microscopy corresponding to fibrillar end-stage inclusion of poly-GA in the *post-mortem* brain of a patient with C9 ALS/FTD ⁴⁴⁴. This suggests that fibrillar aggregates of poly-GA DPRs are

most likely aggregated inclusions that have accumulated at the end-stage of the disease after an initial disease phase (of unknown duration) dominated by monomeric and oligomeric species.

Poly-GA toxicity has been documented both in cell culture and *in vivo* by several studies. For example, poly-GA DPRs produce toxicity in *Zebrafish*⁴¹⁸ and mice^{14,128}. These DPRs are capable of recapitulating ALS/FTD pathological hallmarks in mice such as neuron loss, TDP-43 abnormalities and muscle wasting¹²⁸, and some of these phenotypes are reduced or prevented via active poly-GA vaccination¹⁴.

For all of these reasons, we believed that studying poly-GA aggregation *in vitro* and in cell culture settings by comparing oligomers *vs* fibrils would aid in our understanding of C9 ALS/FTD pathogenesis. In this chapter, we have described the production of recombinant poly-GA and poly-PA DPRs. Poly-PA was used as an experimental control, as discussed previously.

After showing how the recombinant proteins were produced, we wanted to investigate the *in vitro* coalescence of poly-GA and poly-PA oligomers. We firstly showed that the *in vitro* coalescence of poly-GA and poly-PA oligomers increased in correlation with protein concentration and incubation time. However, while poly-GAs formed large and solid-like assemblies, poly-PAs produced small spherical liquid-like droplets. This result is in agreement with the reported reduced toxicity of poly-PA DPR species^{393,493} since maintenance of liquid-phase homeostasis was proposed to be non-pathogenic in protein aggregation^{138,494,495}. However, *in vitro* features alone cannot predict cellular pathogenicity, hence we caution against taking our *in vitro* findings as a meaningful association for poly-PA lower toxicity described in the literature. Some of the concentrations used in our *in vitro* assays (10 μ M, 20 μ M) are much higher than what we would expect to see in a cell. In fact, in general, there is no conclusive evidence that the same principles demonstrated in *in vitro* coalescence (or phase-separation) assays apply in the physiological environment inside living cells in their crowded milieu⁴⁹⁶. In this context, despite the excitement in the cell biology community for phase separation studies *in vitro*, some researchers emphasise the need of quantitative measurements on proteins in their endogenous state and physiological abundance⁴⁹⁶. Nonetheless, our coalescence study is intriguing because it demonstrates that poly-GA aggregation is much slower than poly-PA aggregation and that these DPR species form very distinct three-dimensional aggregates that resemble solid-like structures for poly-

GA and liquid-like droplets for poly-PA. More experiments will be required to investigate the relevance of this *in vitro* observation in the context of living cells, and a more intense scientific effort is needed to provide better quantitative measurements on the endogenous state and physiological abundance of DPR proteins in different cell models. On a different note, as previously stated in chapter 3.3, we specifically refrain from drawing any conclusions about the exact material state of poly-GA and poly-PA assemblies and instead use the terms "solid-like" and "liquid-like" to demonstrate that these results are in fact not conclusive. To determine whether poly-GA assemblies are solid or poly-PA assemblies are liquid, more precise and detailed methods should be used. Fluorescence recovery after photobleaching (FRAP), for example, is frequently used to assess sample liquidity. A defined region of the protein assembly is irreversibly bleached in a typical FRAP experiment, and the kinetics of fluorescent signal recovery in the bleached area (due to the exchange of bleached and nonbleached protein) can be used to extract diffusion coefficients by fitting the data to a diffusion model⁴⁹⁷. These coefficients can provide some information about the sample's liquid or solid material state, but they must be interpreted with caution and supported by other complementary assays⁴⁹⁸. Measurement of 'inverse capillary velocity', which is a ratio of viscosity to surface tension, is another method for determining the material state of a protein assembly. This ratio can be estimated by using live-imaging microscopy to follow the fusion of protein droplets and measuring the time it takes for two droplets to completely fuse into one⁴⁹⁷; an example of this method can be found in the context of germline P granules in *Caenorhabditis elegans* embryo experiments⁴⁹⁹. For more information on some of these strategies and other techniques for determining the material state of a protein assembly in the test-tube, we refer to two well-written reviews on the subject^{500,501}. One of the limitations of the results presented in chapter 3.3 is the absence of some of the assays just described, which could have provided us with more information about the material state of the poly-GA and poly-PA assemblies.

Next, we aimed to investigate whether poly-GA oligomers could form β -sheet fibrils *in vitro*. Our results showed that poly-GA readily assembled into fibrillar structures within 15 days of incubation, as opposed to poly-PA DPRs. Since the transition to β -sheet fibrils exposes hydrophobic amino acid residues⁵⁰², we speculate that poly-GA could lead to significant problems of insolubility as previously described in cell culture studies^{127,128,418,477}. GA DPRs have been previously described to have a strong propensity to aggregate and form fibrils

positive for Congo red or thioflavin T⁴⁴⁶. These fibrils would form a parallel β -sheet structure speculated to display similar aggregation properties as the A β peptide in Alzheimer's disease⁴⁴⁶. The ability of poly-GA oligomers to form distinct fibrillar aggregates is consistent with a previous study that found short synthetic GA peptides to have the highest propensity to aggregate⁵⁰³. This is especially interesting given that the majority of DPR inclusions in patient brains are poly-GA positive^{445,477}.

We next wanted to perform comparative experiments featuring poly-GA oligomers *vs* poly-GA fibrils to explore whether differences in the aggregation stage could produce biological differences in cell culture. Because the repeat length is the same (34-GA), any changes in features like membrane binding would be due only to the aggregation stage. The comparison of aggregation-prone proteins at different stages of amyloid assembly (i.e. early-stage oligomers *vs* late-stage fibrils) is being extensively studied in the field of Alzheimer's and Parkinson's diseases for proteins such as A β , tau, and α -synuclein³⁶⁻³⁹ but has never been explored in the context of dipeptide repeat proteins in C9-linked ALS/FTD.

The physiological concentration of DPRs in affected cells is likely to be far lower than 20 μ M⁵⁰⁴. Because we observed *in vitro* coalescence events with as little as 1 μ M of DPRs, we decided to perform our cell-based experiments using this concentration, which presumably recapitulates more physiologically relevant conditions. We used a combination of flow cytometry and dot-blotting methods to determine whether poly-GA binds to cells after 24 hours in cell culture. We used flow cytometry to detect the fluorescent dye covalently linked to the DPRs after exposing 1321N1 human astrocytoma cells or iAstrocytes to poly-GA assemblies (or poly-PA). Dot-blot and anti-V5 staining were also performed on protein extracts from 1321N1 astrocytoma or iAstrocytes treated with V5-tagged poly-GAs.

To further confirm that poly-GA binds to cells in culture we took advantage of SMLM and TIRF microscopy. Single-molecule localization microscopy (SMLM) is a relatively new imaging modality that won the Nobel Prize in Chemistry in 2014 and is regarded as one of the most important super-resolution techniques⁵⁰⁵. SMLM resolution exceeds the diffraction limit of light microscopy, with resolutions of 10-20 nm. SMLM allows for the imaging of single molecules as well as the study of low-level molecular interactions at the subcellular level. Similarly to tau⁵⁰⁶, A β ⁷⁶ and α -Syn aggregates⁵⁰⁷, our results showed that poly-GA fibrils accumulated at the plasma membrane and formed detectable clusters. However, the

percentage of molecules in clusters did not change over the course of 48 hours. These findings imply that the clustering of poly-GA fibrils is kinetically slow, and that molecules may re-cluster over time without any detectable change in molecule density (per cluster), at least as far as our system can tell. Surprisingly, less than 30% of poly-GA SMLM molecules appeared in clusters, implying that DPR molecules at the plasma membrane may continuously diffuse and detach or undergo processing within the cell ^{91,110,508}. These findings show that fibril clustering is kinetically slower in a cellular setting, and that assemblies may form persistent connections with their plasma membrane partners. Importantly, the clustered fraction may represent the population of packaged molecules that will be internalized and further processed ^{91,110,508}.

Cross-talk of protein aggregates with plasma membrane components may be responsible for pathogenic protein uptake and the initiation of harmful signalling pathways, as previously demonstrated for mutant Superoxide Dismutase 1 (SOD1) in the context of ALS ^{110,112}.

In the following Chapter, we will look more closely at the cellular uptake of poly-GA DPRs, as well as the potential role of endocytosis in DPR uptake.

4. Uptake and endocytosis of poly-GA in glia and neurons

4.1 Introduction

Over the last few decades, our understanding of neurodegenerative diseases has primarily focused on neurons and their networks. However, the “neuron-centric” paradigm for these ailments is a gross simplification of what happens in the central nervous system (CNS) of people who are suffering from neurodegeneration⁴⁸⁸. It is becoming increasingly clear that glial cells play a significant role in neurodegenerative diseases^{453,509-512}, but the degree to which these cells contribute to pathogenesis and disease symptoms is not fully understood.

Glia, or more specifically neuroglia, are a highly heterogeneous population of cells that includes astrocytes, oligodendrocytes and microglia. Astrocytes, in particular, are star-shaped glia that can be found in all parts of the brain, and are almost equal in number to neurons in some regions (i.e. human cortex)⁵¹³. Astrocytes, in particular, play an important role in the brain as they are involved in CNS homeostasis and repair⁵¹⁴, but they also nourish neurons and regulate ion and neurotransmitter concentrations in the extracellular environment, all of which are important factors in influencing synaptic signalling⁵¹⁵. Remarkably, it is estimated that a single astrocyte can enter in contact with several hundred dendrites and envelope up to 100,000 synapses in hippocampal or cortical regions of the mammalian brain^{516,517}.

Interestingly, some studies suggest that astrocytes, derived for example from reprogrammed fibroblasts from an ALS patient, are characterized by dysfunctional or unbalanced proteostasis. For example, in SOD1-ALS mouse models, astrocytes are immunopositive for ubiquitinated-SOD1 inclusions³¹⁹ and are specifically located in proximity to motor neurons⁵¹⁸. The hypothesis that proteostasis imbalance in astrocytes could directly synergize with proteostasis imbalance in neurons merits further investigation. One of the first hints at this potential mechanism came from a cell culture study in which abnormally reactive SOD1-astrocytes were capable of directly inducing ubiquitin- and p62-positive inclusions in co-cultured motor neurons. This phenotype was linked to the secretion of the multifunctional cytokine TGF-1 from astrocytes⁵¹⁹.

In *post-mortem* C9 ALS/FTD brains, DPR inclusions are substantially more common in neurons than glia⁴⁷⁶. Several studies failed to detect DPR inclusions in glial cells at autopsy^{405,414,520}, even in the glia-enriched subcortical and spinal cord white matter⁴¹⁷. Only ependymal cells in the central canal of the spinal cord and the lateral ventricle wall had DPR

glial inclusions⁴¹⁶. Ependymal cells are a type of glial cell that is in direct contact with the cerebrospinal fluid (CSF) and helps maintain fluid balance⁵²¹. Interestingly, poly-GP DPRs were detected in the CSF of C9 ALS/FTD patients^{504,522}.

These findings suggest that DPRs can be released from cells. It is unclear why DPR inclusions are so common in ependymal cells and what the significance of DPR accumulation in the CSF is. However, based on these few studies, it appears reasonable to conclude that DPR aggregation and propagation in glial cells has non-cell autonomous effects that may influence neuronal viability.

Compartments of the endolysosomal system have been implicated in both seeding and cell–cell propagation of misfolded protein aggregates. In Alzheimer's disease, for example, intraneuronal A β accumulation has been observed to precede extracellular plaque formation in the affected brain^{523,524}, and a population of toxic peptides may be released and then taken up by different cells, thus initiating the aggregation cascade. Endocytic uptake of several misfolded proteins, including A β ^{508,525}, tau^{526,527}, α -synuclein^{96,528} and SOD1⁵²⁹ has been extensively demonstrated to occur in cell culture settings through various mechanisms (i.e. clathrin-dependent or -independent endocytosis, macropynocytosis), as shown in **Figure 4.1**.

It has also been suggested that endolysosomal organelles might be critical cellular compartments for aggregate seeding. For example, knockdown of the *CHMP6* gene results in strong enhancement of tau aggregation in cell culture⁵³⁰. The CHMP6 protein is part of the endosomal sorting required for transport complex III (ESCRT-III) which is involved in multivesicular bodies (MVBs) formation and sorting of endosomal cargo proteins into MVBs⁵³¹. Similar mechanisms may be at work in the context of ALS-FTD because impairing endocytosis increases TDP-43 toxicity, aggregation, and protein levels, all of which correlate with exacerbation of locomotor dysfunction in a TDP-43 ALS fly model⁵³². According to a study in *Saccharomyces cerevisiae*, proteins involved in endocytic functions, such as Cdc48/VCP and Ubx3, appear to be critical in regulating the turnover and toxicity of TDP-43⁵³³.

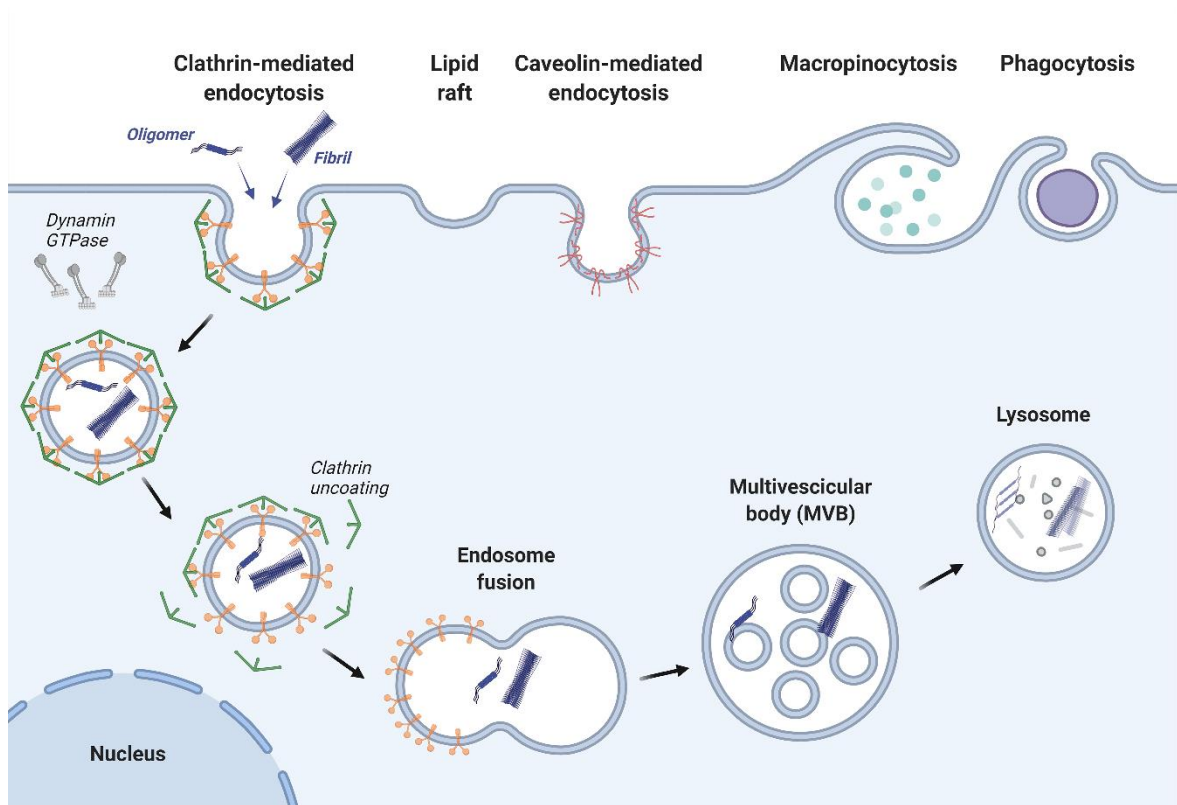


Figure 4.1 Endocytic pathways and uptake of misfolded protein aggregates

There are several endocytosis pathways, including clathrin-dependent, caveolin-dependent, and clathrin- and caveolin-independent. Macropinocytosis is an actin-driven process of engulfment and uptake of fluids and membranes. The figure also depicts phagocytosis, which is a cellular process for ingesting and eliminating particles larger than 0.5 μm in diameter, such as microorganisms, foreign substances, and apoptotic cells. Lipid rafts are also shown, and they are lipid-enriched microdomains in the plasma membrane that have been proposed as a site for A β aggregation and uptake⁵³⁴.

Endocytosis, such as the clathrin-mediated pathway, can transport oligomeric or fibrillar aggregates into cells. Internalized aggregates can then be sorted back to the cell's surface or into other compartments (multivesicular bodies (MVBs) and lysosomes) for degradation. These aggregates can seed and disrupt endosomal and lysosomal function within endosomes and lysosomes. Figure created with BioRender.com under academic license.

Almost all of the aforementioned cell culture studies have been made possible by the widespread use of recombinant proteins. The use of recombinant proteins, combined with the ease of access to continuous cell lines on a plastic dish, allows researchers to study detailed mechanisms of cellular uptake. Indeed, uptake routes can be modulated using new pharmacological tools or genetic manipulations. Small-molecule inhibitors, in particular, are useful for studying rapid cellular effects because they can stop endocytosis in minutes and are usually reversible. Small interfering RNA (siRNA)-mediated knockdown or other genetic manipulations (for example, CRISPR-Cas9) can also be used to modulate gene expression in genes that control various endocytic pathways.

A comprehensive understanding of the mechanisms that control aggregate uptake and dissemination is critical for the development of therapeutics as well as understanding why specific neuronal subtypes and brain regions are more susceptible to specific diseases.

Despite many efforts over the last decade to identify *C9ORF72*-derived dipeptide repeat proteins^{406,407,535}, no equivalent effort has been put into understanding the underlying mechanisms that control DPR uptake and spreading. To the best of our knowledge, only two studies have provided some insight into the uptake⁵³⁶ and release¹³⁰ routes that DPRs may use to enter or exit cells and cause toxicity. However, the single study on DPR uptake only revealed some cell entry mechanisms for poly-GR DPRs and no other DPR species⁵³⁶.

In this Chapter, we looked in depth at the cellular uptake of poly-GA DPRs in glial cells and how it is influenced by endocytosis inhibition.

First, we looked into whether various cells could take DPRs from the medium and internalise them. Second, we examined the mobility of the DPRs once they were internalised in glia and neurons. Third, we conducted additional research on the movement of internalised DPRs from the endosome to the lysosome compartment of these cells.

Importantly, we decided to perform all of our cell-uptake experiments using the concentration range 0.5-1 μ M, which presumably recapitulates more physiologically relevant conditions in live cells⁵⁰⁴.

4.2 Uptake of poly-GA in glial cells

To evaluate DPR uptake, we exposed various cell types (HEK293T, HeLa, iNPC-derived human astrocytes, human fibroblasts) to our recombinant DPRs for 1h, 2h and 4h. Using high-throughput confocal microscopy, we quantified the number of largely visible DPR aggregates in these cell types. Our results on ~8,000 cells/culture showed that in all these cell lines poly-GA oligomers are taken up into large visible aggregates more readily than poly-GA fibrils and poly-PA oligomers. Additionally, for all DPR species and across all cell types, the uptake increases with time (**Figure 4.2**).

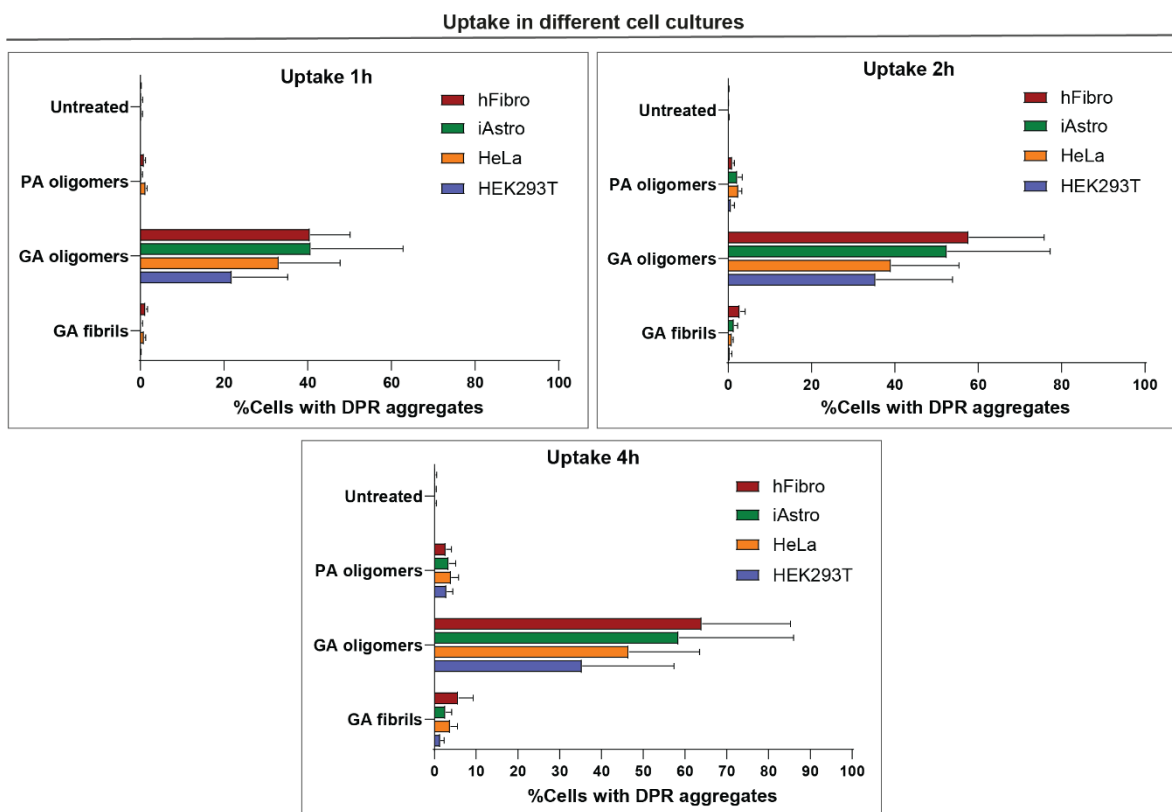


Figure 4.2 DPR uptake in various cell lines and in healthy iAstrocytes

Quantitative analysis of the %cells displaying large DPR aggregates overtime (1h, 2h, 4h). Different cell cultures were used in this experiment such as human fibroblasts (hFibro, red), iAstrocytes (iAstro, green), HeLa cells (orange), and HEK293T cells (blue). ~8'000 cells/culture were analysed. Bar graphs of mean \pm SEM. The data were collected from 3 independent biological replicates.

Because increasing evidence implicates astrocytes as significant non-cell autonomous contributors of C9 ALS/FTD pathogenesis⁴⁸¹, we aimed at investigating poly-GA DPR uptake in healthy iNPC-derived human astrocytes (herein referred to as iAstrocytes). We firstly confirmed DPR internalization in vimentin-stained iAstrocytes by using Z-stack airyscan confocal microscopy, orthogonal views (**Figure 4.3A**) and 3D-volume rendering (**Figure 4.3B**; **Movies S3 and S4**). Vimentin is a marker for intermediate filaments, which are cytoskeletal structural components that form an intricate network in most cells' cytoplasm.

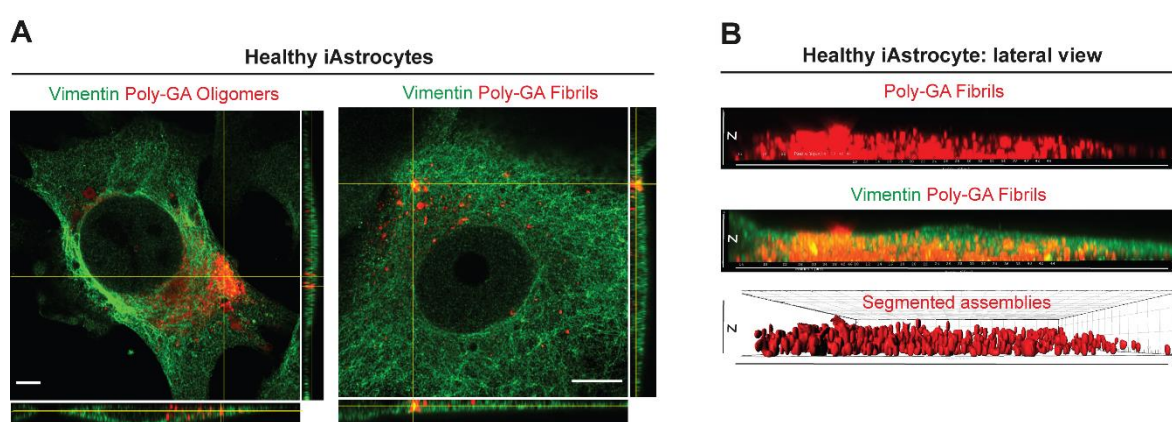


Figure 4.3 DPR uptake in healthy iAstrocytes shown by orthogonal views and 3D-rendering

A) Orthogonal views from airyscan microscopy show the uptake of poly-GA oligomers and poly-GA fibrils in vimentin-stained healthy iAstrocytes after 24h exposure. Scale bar = 10 μ m. **B**) 3D-rendered lateral view of a single vimentin-stained healthy iAstrocyte shows the uptake of poly-GA fibrils through the xz dimension. Corresponding movies are shown in **Movies S3 and S4**. The data were collected from 3 independent biological replicates.

We further showed DPR uptake in glial cells via a “trypan blue quenching” experiment. Trypan blue is a cell impermeable dye and is often used as a quenching agent for green fluorescence. Since the dye does not penetrate into live cells, it has the capacity to quench only the fluorescence signal on the cell membrane but not the signal located in the internal milieu of the cell^{537,538}. This experiment was carried out for both poly-GA fibrils and oligomers, but we will only show a proof-of-concept example for fibrils.

The 1321N1 astrocytoma cell line was exposed to ATTO488-labelled poly-GA fibrils for 24 hours (5 μ M). After several PBS washings, cells were stained with the nuclear marker Hoechst 33342 for 5 minutes and subjected to live imaging with confocal microscopy. Subsequently, 4 mg/ml trypan blue was applied in the cell culture medium for 2 minutes to quench the extracellular/membrane-bound ATTO488-fluorescence. Green fluorescence was analysed before and after the addition of trypan blue in live cells. We demonstrated that the majority of the green fluorescent signal of poly-GA fibrils is maintained after the addition of trypan blue (**Figure 4.4**), suggesting that these proteins are indeed taken up by the cells from the medium and subsequently internalised.

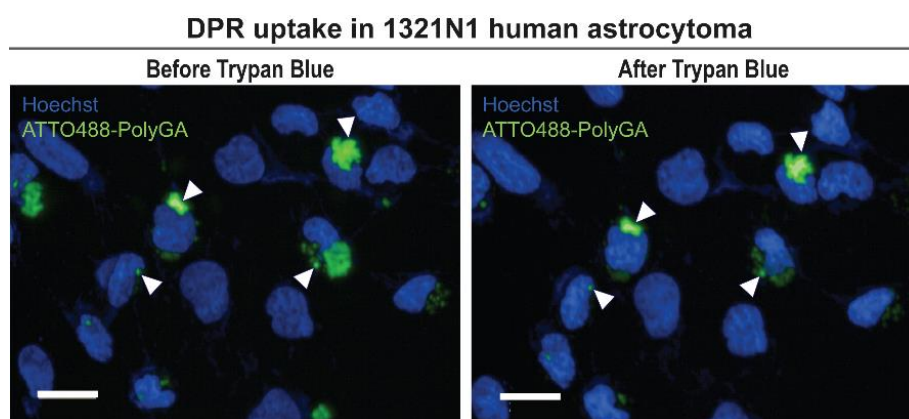


Figure 4.4 Trypan blue quenching effect on ATTO488 poly-GA fibrils

To confirm the uptake of Poly-GA fibrils in glia, trypan blue was used to quench any external or membrane-bound fluorescence coming from ATTO488-labelled poly-GA added to the medium of 1321N1 human astrocytoma cells for 24h. As shown in the figure, the majority of poly-GA fluorescent signal is conserved after the addition of trypan blue (*arrow heads*), suggesting that these aggregates are taken up by the cells and internalised. The data were collected from 2 independent biological replicates.

DPR uptake was further evidenced by live imaging of iAstrocytes and subsequent quantification of DPR average velocity (\mathbf{v}) with a *Mean Square Displacement* analysis. Extensive details on how this analysis was performed are reported in section 2.2.15 (Materials & Methods, page 73).

Briefly, the *Mean Square Displacement* (MSD) is a measure of the deviation of the position of a particle with respect to a reference position over time. The MSD is measured over time to determine if a particle is spreading solely due to random diffusion (also named Brownian diffusion), or if an active force is also contributing. The MSD was calculated for all the trajectories of ATTO550 positive DPRs during live imaging over time. Subsequently, a mathematical model was created to fit the MSD vs time data for an object undergoing Brownian diffusion, also with the possibility of a ballistic propulsion velocity.

Our analysis showed non-zero values for DPR average velocity (\mathbf{v}), which, according to our mathematical model, indicates that DPR motion is not solely due to random diffusion, but an active force is also contributing (**Figure 4.5A and 4.5B**). Interestingly, our model suggests that this active force could be descriptive of microtubule-mediated transport, as reported in a previous study⁴⁶⁴.

To obtain the experimental confirmation, we exposed healthy iAstrocytes to DPRs (24h) and subsequently subjected the cells to a 30 minute-treatment with the microtubule de-polymerising agent nocodazole (30 μM). Cells were fixed and stained with anti-tubulin antibody to confirm microtubule de-polymerization. Our results show that the microtubule de-polymerising agent nocodazole induces cellular relocation of these DPRs (**Figure 4.5C**), hence suggesting that a certain fraction of poly-GAs undergoes microtubule-mediated transport after cell entry.

DPR uptake and trajectories in healthy iAstrocytes

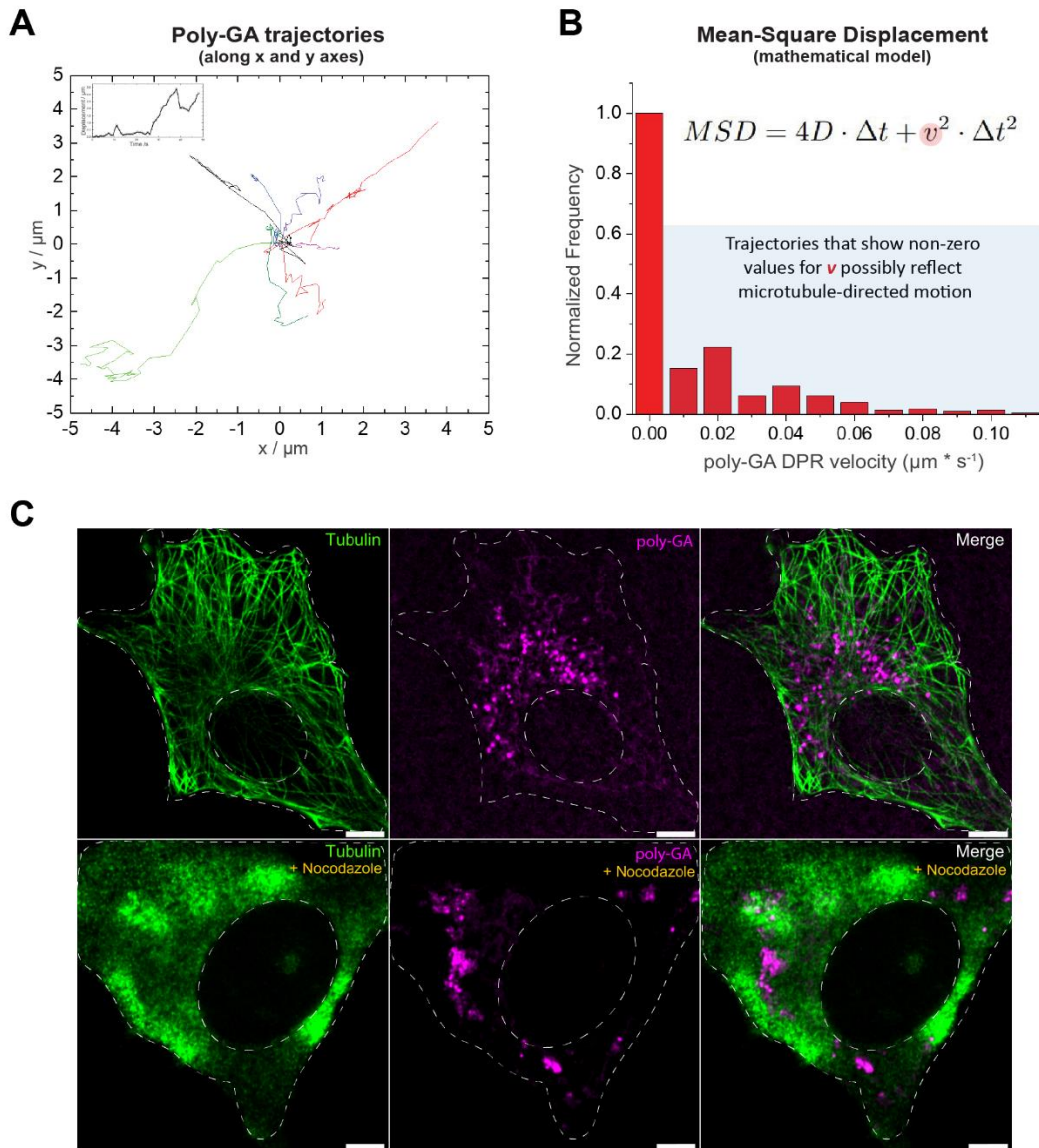


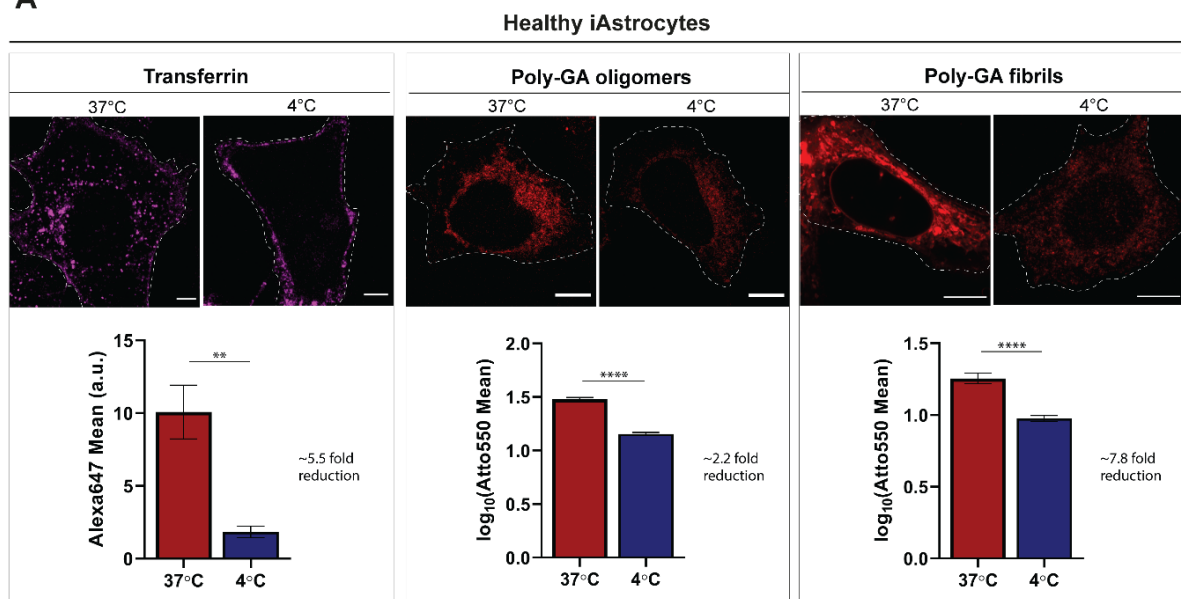
Figure 4.5 DPR motion after uptake in healthy iAstrocytes

After 24h exposure to DPRs, healthy iAstrocytes were prepared for confocal live-imaging and ATTO550 DPR trajectories were analysed via mean Square Displacement. **A)** Some tracks, analysed with TrackMate, are shown in the xy space. Corresponding movie shown in **Movie S5**. **B)** Quantification of DPR average velocity v is displayed in the corresponding graph, in which trajectories that show non-zero values for v are suggestive of microtubule-directed motion. **C)** After 24h exposure to DPRs, healthy iAstrocytes were subjected to a 30 minute pre-treatment with the microtubule de-polymerising agent nocodazole (30 μM) before fixation. Confocal images are shown, following anti-tubulin (green) immunostaining and ATTO550 fluorophore detection for DPRs (magenta). Nocodazole treatment induces cellular relocation of DPRs. Scale bar = 10 μm (upper panel), 5 μm (lower panel). The data were collected from 2 independent biological replicates.

4.3 Endocytosis perturbs DPR uptake

To test the potential involvement of endocytosis in DPR uptake, we performed a generalised block of all endocytic pathways by lowering the culture temperature to 4°C prior to fixation⁵³⁹. To confirm the successful inhibition of endocytosis we visually monitored the uptake of transferrin, a well-established marker of the coated pit pathway^{459,540}. Interestingly, low-temperatures reduced the uptake of poly-GA oligomers by 2.2-fold and of poly-GA fibrils by ~8-fold ($P^{****} \leq 0.0001$) in iAstrocytes (**Figure 4.6A**). We next inhibited dynamin-dependent endocytosis by the use of dynasore^{460,541}, and this resulted in a 2.4-fold uptake reduction of poly-GA fibrils ($P^{****} \leq 0.0001$) but no change in poly-GA oligomers uptake (**Figure 4.6B**). Upon comparison with other DPR oligomeric species (such as poly-PA), we observed that specifically poly-GA oligomers do not use dynamin-dependent endocytosis for cell entry.

A



B

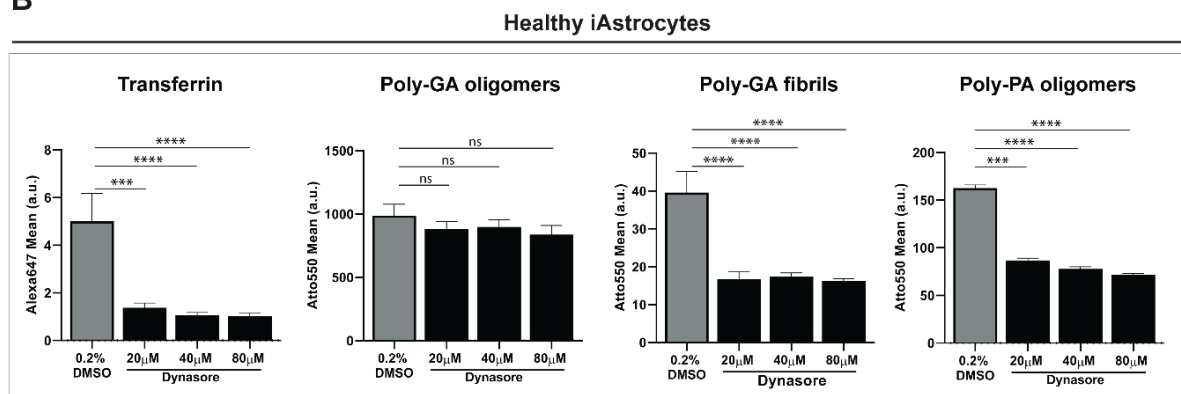


Figure 4.6 Oligomeric vs fibrillar poly-GA DPRs entry-routes in glia

A) Confocal images of Alexa647-Transferrin (control) and ATTO550-Poly-GA aggregates after 1h uptake at 37°C or at 4°C in healthy iAstrocytes. Quantification of the log₁₀ transformed-Mean grey values is reported in bar graphs of mean ± SEM. ≥300 cells/condition. Kolmogorov-Smirnov non-parametric test after testing normal distribution with the Shapiro-Wilk test. **P ≤ 0.01, and ****P ≤ 0.0001. The data were collected from 4 independent biological replicates. **B)** Quantification of the Mean grey values of Alexa647-Transferrin (control) and ATTO550-DPRs upon 1h treatment with Dynasore (or 0.2% DMSO). Bar graphs of mean ± SEM. ≥250 cells/condition. Kruskal-Wallis non-parametric test with Dunn's multiple comparisons after testing normal distribution with the Shapiro-Wilk test. ***P ≤ 0.001, and ****P ≤ 0.0001. The data were collected from 3 independent biological replicates.

To better investigate the differences in uptake between oligomeric vs fibrillar poly-GA DPRs, we evaluated the accumulation of these proteins in endolysosomal organelles following 24h from administration. We exposed healthy iAstrocytes to ATTO647N-labelled poly-GA fibrils or oligomers (0.5µM for 24h) and quantified the degree of colocalization with LAMP1-stained endolysosomes by dual-colour dSTORM. As mentioned in Chapter 3, the ATTO647N dye is highly suitable for single-molecule detection applications and high-resolution microscopy⁴⁸⁶.

Our dual-colour dSTORM analysis revealed that while ~17% of the input poly-GA fibrils co-localized with endolysosomes, only less than 5% poly-GA oligomers did (3.4-fold difference; P*** ≤ 0.001). Additionally, LAMP1 organelles showed higher enrichment for poly-GA fibrils than for poly-GA oligomers (1.6-fold difference; P*** ≤ 0.001) (**Figure 4.7A**). The achieved lateral resolution of dual colour dSTORM as well as the analysis of potential imaging artifacts is shown for both DPR and LAMP1 channels (**Figure 4.7B and 4.7C**).

Together, these findings suggest that DPR uptake is present in various cell culture systems and endocytosis plays a role in DPR uptake in iAstrocytes.

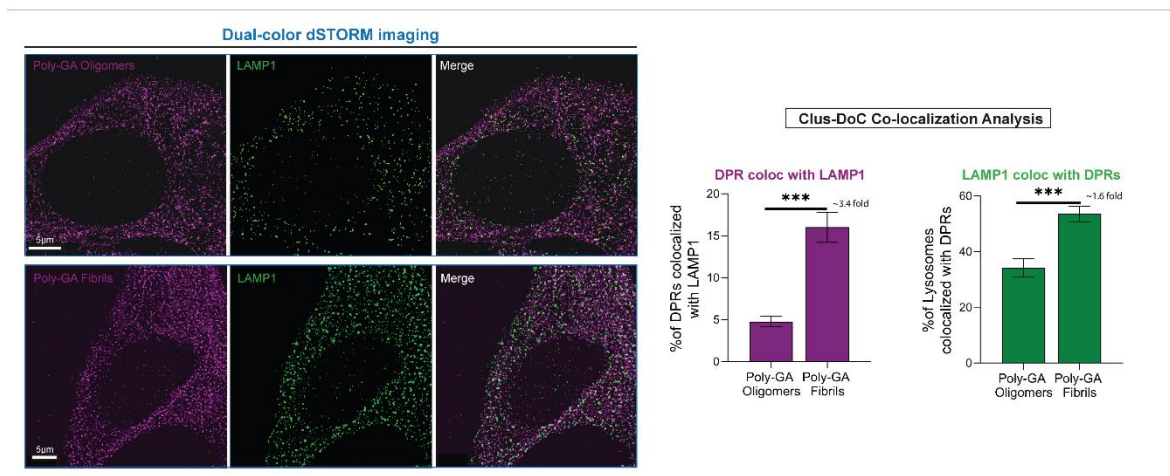
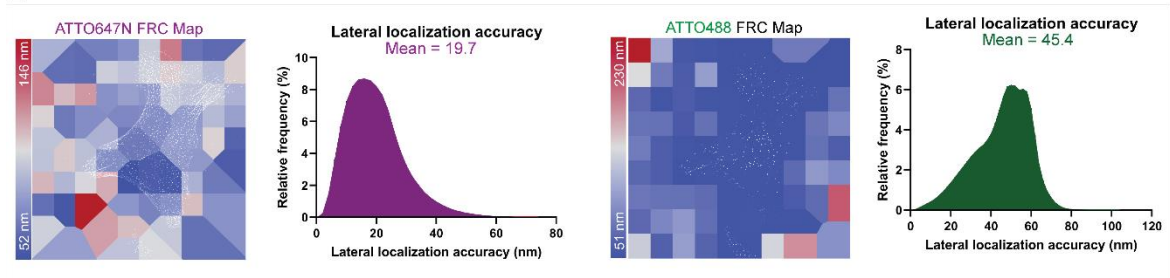
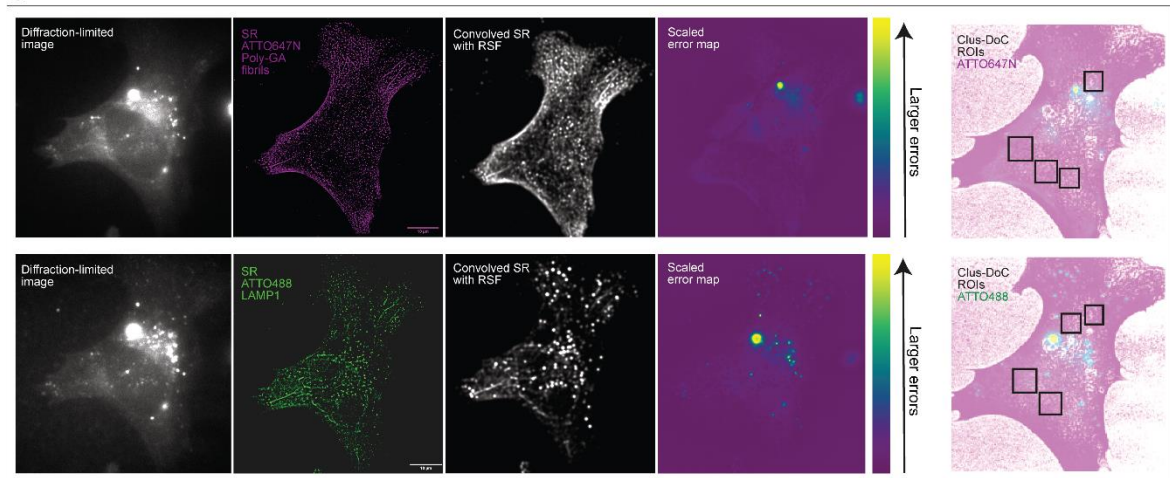
A**Healthy iAstrocytes****B****C**

Figure 4.7 Oligomeric vs fibrillar poly-GA DPRs colocalization with lysosomes

A) Healthy iAstrocytes were imaged by dual colour STORM after 24h incubation with ATTO647N-PolyGA oligomers or fibrils (magenta) and anti-LAMP1 staining (green). Clus-DoC co-localization analysis for Poly-GA relative to LAMP1 (magenta graph), and LAMP1 relative to Poly-GA (green graph) shows the respective %colocalized molecules (among total molecules detected). Scale bar = 5 μm . Bar graphs of mean \pm SEM; graphs are indicative of 30 ROIs (4 μm x 4 μm) per condition chosen only in artefact-free regions. Unpaired two-tailed t-test with Welch's correction. *** $P \leq 0.001$. The data were collected from 3 independent biological replicates. **B)** The lateral resolution of

dSTORM images was measured implementing block-wise Fourier Ring Correlation (FRC) resolution mapping in NanoJ-SQUIRREL⁴⁷⁰. As the resolution is anisotropic, the maps represent specific colour-coded regions of estimated resolution for each channel. The lateral resolution achieved, on average, is approximately 50-60 nm for both ATTO488 and ATTO647N channels. We also show the estimations of the lateral localization accuracy of both channels based on the Thompson equation⁴⁷³ (calculated with NIS-Elements software). **C)** For lysosomes-Poly-GA fibrils co-localization analysis, diffraction-limited images of each channel were acquired. These images were used as a reference for subsequent NanoJ-SQUIRREL analysis of image artefacts in super-resolution dSTORM images. Each panel (upper and bottom) shows (from left to right): single iAstrocyte cell imaged in TIRF (reference image), super-resolution reconstruction of dSTORM data set on that same cell ('SR'), super-resolution image convolved with appropriate Resolution Scale Function ('Convolved SR with RSF'), and a quantitative map of errors between reference and convolved SR images ('Scaled error map'; colour scale indicates the magnitude of the error). Based on NanoJSquirrel-analysis of artefacts, specific ROIs for all the co-localization analysis performed in our work were chosen in artefact-free regions of the cell.

4.4 DPR uptake in cortical neurons and lysosomal colocalization

Our DPR-endolysosomal colocalization finding led us to hypothesize that poly-GA oligomers might have the ability to escape endolysosomal routes and trigger cellular toxicity via lysosomal disruption. Therefore, we next sought to test whether poly-GAs could cause lysosomal impairment in cortical neurons, which are cells that undergo typical degeneration in ALS-FTD and display a large number of DPR inclusions in post-mortem tissue of ALS-FTD patients⁴⁴⁵.

Primary cortical neurons were produced from E15.5 embryos of wild-type C57BL/6 mice. After growing primary mouse cortical neurons into microfluidic culture chambers, we used live imaging and detected poly-GA uptake in the soma (point of DPR exposure) as well as in the proximal axon. We subsequently performed a *Mean Square Displacement* analysis of the trajectories of poly-GA oligomers and poly-GA fibrils during live imaging at the proximal axon compartment.

Our findings show that poly-GA DPRs shuttle along axons by a mixture of diffusive (Brownian), transported and constrained motion (**Figure 4.8**).

DPR motion along cortical neuron axons

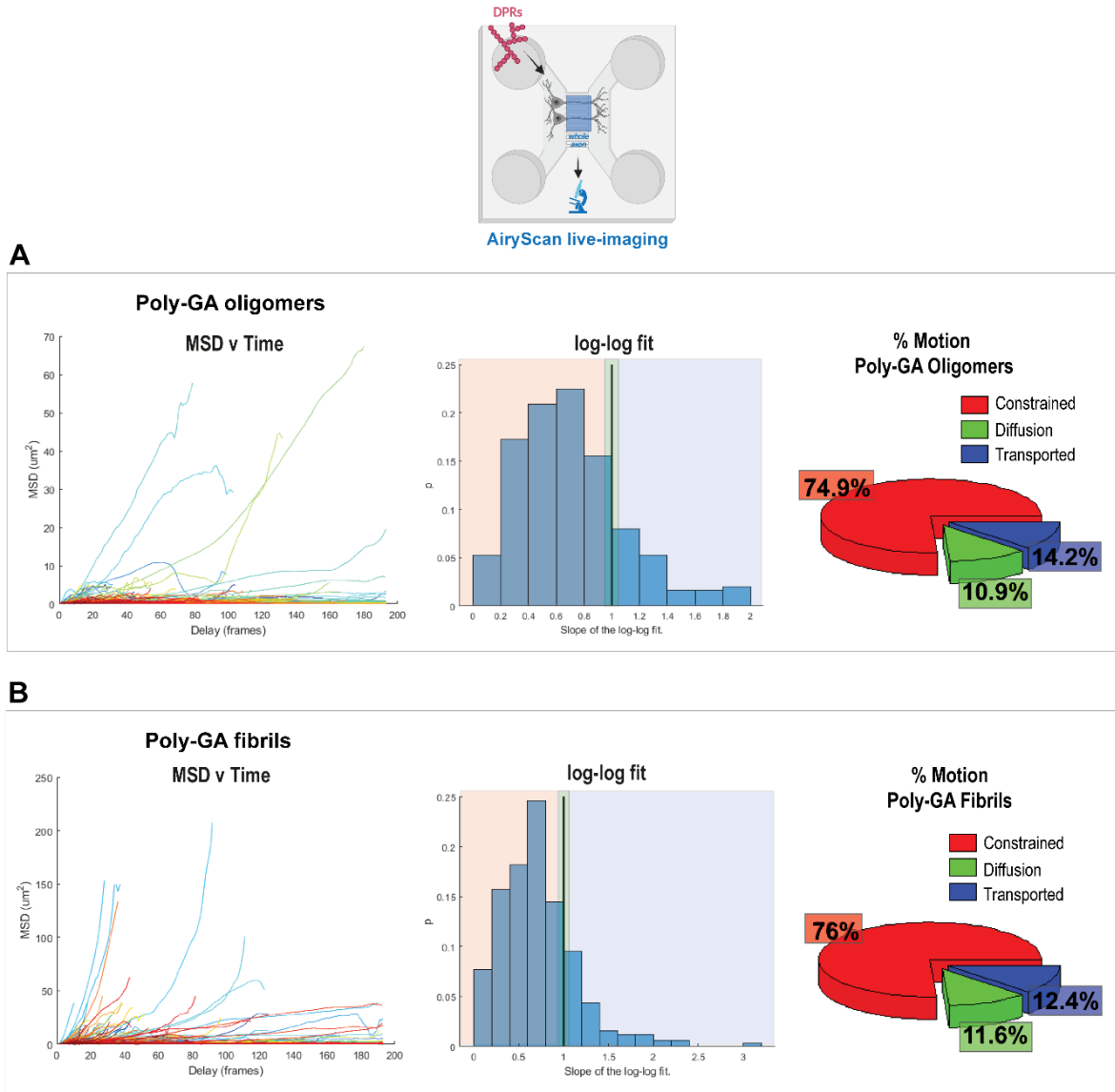


Figure 4.8 DPR motion after uptake in primary cortical neurons

Mean Square Displacement (MSD) analysis of the trajectories of poly-GA oligomers (**A**) or poly-GA fibrils (**B**) after AiryScan live-imaging in cortical neuron axons. The plots of MSD values vs time delay are shown; alongside with the plots showing the Log-Log Fit of the MSD. In a Log-Log Fit plot, the MSD curves can be approximated by straight lines of: slope 1 for diffusion motion, slope 2 for transported motion, and less than 1 for constrained motion; these are quantified and shown in the respective pie charts. ≥ 1000 tracks/condition. The data were collected from 3 independent replicates.

Constrained motion was the predominant DPR motion throughout the axons (**Figure 4.8**); suggesting that these proteins are mostly anchored to static axonal structures.

We indeed found that poly-GA DPRs accumulated in large spherical structures in the axon, implying a failure of their axonal transport (**Figure 4.9A**, middle panel). Interestingly, by zooming into few spherical axonal structures with higher resolution, we observed the presence of small poly-GA proteins erratically moving within each structure (**Figure 4.9A**, right panel; **Movie S6**). We then used the lysosomal dye LysoTracker Green and observed that some of these axonal structures contain poly-GA DPRs colocalizing with lysosomal organelles (**Figure 4.9B**), as also shown in **Movie S7**.

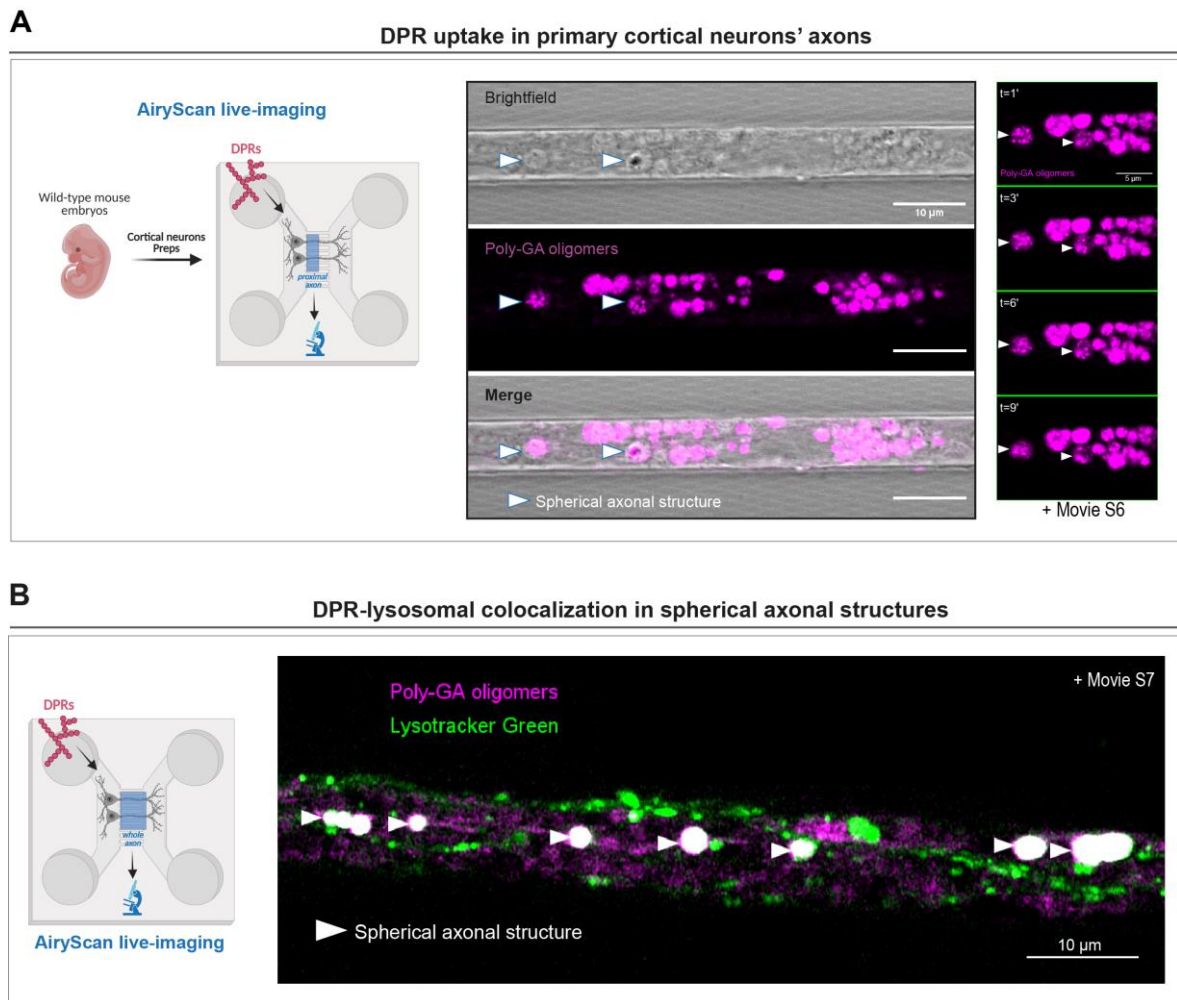


Figure 4.9 Poly-GA DPRs colocalize with endolysosomal organelles after uptake and accumulate in spherical axonal structures enriched with lysosomes

A) Confocal images showing accumulation of poly-GA assemblies in large spherical structures (arrow heads) along the axons of primary mouse cortical neurons. A combination of brightfield

imaging and fluorescence detection of the ATTO550-labeled poly-GAs was used to detect these swellings specifically in the axons residing in the microfluidic chamber microgrooves. By zooming into few spherical structures with higher resolution (airyscan mode), during live-imaging, we report the presence of small poly-GA assemblies' particles erratically moving within each structure overtime (*right panel*); corresponding movie is shown in **Movie S6. B**) Confocal images showing accumulation of poly-GA assemblies in large spherical structures along the axons of primary mouse cortical neurons. Upon the application of the lysosomal dye LysoTracker Green, we show that some of these structures contain poly-GA DPRs that colocalize with lysosomal organelles (*arrowheads*); corresponding movie is shown in **Movie S7**. The data were collected from 3 independent biological replicates.

In conclusion, we demonstrated that poly-GA DPRs can enter primary mouse cortical neurons after being added to the cell culture medium. Interestingly, some DPRs accumulate in the soma while others accumulate in the proximal axon compartment. We show that poly-GA DPRs are abundant in spherical axonal structures and co-localize with lysosomal organelles.

4.5 Discussion

When aggregate seeds are exposed to the extracellular milieu and then internalised by naive receiving cells, aggregate pathology spreads across brain regions. It has been proposed that cellular uptake of protein aggregates is a critical step in determining their seeding potential. In fact, vesicles and membranes have been proposed to be used by aggregate seeds to promote further seeding and propagation in the cell's internal environment.

The mechanisms governing the uptake of exogenous DPR aggregates are not well understood. However, this is likely a fundamental process driving DPR aggregation and pathogenicity, and we think that future therapies in the context of C9 ALS/FTD would benefit from understanding the specific routes of DPR-uptake- and -release that could be targeted pharmacologically.

This Chapter sheds new light on the uptake routes of DPR aggregates, particularly in glial cells but also, to a lesser extent, in neurons. We chose to focus on DPR uptake in astrocytes because increasing evidence implicates them as significant non-cell autonomous contributors of C9 ALS/FTD pathogenesis^{294,481}. We covered several aspects of DPR uptake in astrocytes, particularly using human iAstrocytes derived from a healthy donor.

One of the aspects we covered, which had never been seen before, was the DPR motion after 24 hours of exposure to the cell medium. We developed a mathematical model to which we fitted experimental data, specifically DPR trajectories in live astrocytes (measured by confocal live imaging), and as a result, we discovered that a subset of DPRs exhibits motion characteristics typical of microtubule-driven transport. We confirmed this finding by using the microtubule depolymerizing agent nocodazole, which caused uptaken DPRs to relocate within the cells. If we can disrupt poly-GA distribution in our data by depolymerizing microtubules, this could imply the presence of direct or indirect polyGA-microtubule interactions. This observation is in line with recent findings related to poly-PR DPRs, which have been shown to associate with multiple proteins involved in microtubule-based transport in spinal cord lysates, and to directly bind microtubules⁵⁴². More research is needed to determine whether poly-GA can bind with key partners of the microtubule-transport system, disrupting key components of this fundamental cell transport.

We then presented findings that included mechanistic details of DPR uptake in glial cells. We found that at least some poly-GA DPRs are internalised by endocytosis in iAstrocytes: low-temperature exposure (which inhibits all endocytic pathways) reduced poly-GA oligomer uptake by 2.2-fold and poly-GA fibril uptake by 8-fold. Another research group had previously demonstrated DPR uptake via endocytosis, but only for poly-PR; in that case the uptake of poly-PR peptides was significantly inhibited by clathrin knockdown or chlorpromazine, an inhibitor of clathrin-mediated endocytosis⁵³⁶.

When we used the drug dynasore to inhibit dynamin-dependent endocytic pathways, we only saw a decrease in poly-GA fibril uptake but no change in poly-GA oligomer uptake. This could rule out the possibility that poly-GA oligomers use dynamin-dependent pathways for cell entry, such as clathrin-mediated or caveolin-dependent endocytosis. The discovery that the same poly-GA aggregate species, but at different amyloid stages (oligomers vs fibrils), uses different cell entry routes remains intriguing. Our results indeed show that poly-GA fibrils are dynamin-dependent, whereas poly-GA oligomers are not.

One possible explanation is that small oligomers can directly translocate across the plasma membrane, avoiding cellular uptake and clearance⁵⁴³⁻⁵⁴⁶. This is a well-known phenomenon, and some scientists believe that oligomers (rather than fibrils) are responsible for pathology because they invade endolysosomal organelles, damage their membranes, and cause more aggregate seeding as well as cellular toxicity. To test the hypothesis that oligomers might escape lysosomal vesicles, we used super-resolution imaging to examine the degree of co-localization between poly-GA DPRs and LAMP1-stained endolysosomal organelles in iAstrocytes and found that poly-GA oligomers had lower lysosomal co-localization than poly-GA fibrils. Thus, our findings suggest that poly-GA DPRs may evade lysosomes.

We then decided to administer poly-GA DPRs to primary mouse cortical neurons to see if the neurons could uptake these assemblies. When poly-GAs were administered to the neuronal soma in microfluidic culture chambers, they were readily taken up and appeared in the soma and proximal axon after 24 hours. We demonstrated (via *Mean square displacement* analysis) that poly-GAs move with a combination of Brownian motion, diffusion, and microtubule-directed motion by monitoring their motion with live imaging. Furthermore, poly-GAs are transported along axons and accumulate in stalling lysosomes which are found in spherical axonal structures.

In this Chapter, we provided detailed mechanistic insights into DPR uptake in glia and, to a lesser extent, neurons. Overall, our findings emphasise the importance of endocytosis as a route of internalisation for *C9ORF72*-derived DPRs, expanding previous knowledge of DPR uptake⁵³⁶ to alanine-rich species.

Interestingly, Zhou and colleagues recently demonstrated that uptake of poly-GA DPRs, if it occurs in cells expressing the GGGGCC repeat expansion, can result in the formation of nuclear RNA foci¹²⁶. Although we haven't tested the uptake of DPRs in cells that express the repeat expansion in depth, it remains an intriguing observation because it demonstrates how exogenous DPRs, when taken up by naive receiving cells, cause subsequent toxicity with *C9ORF72*-specific pathological hallmarks.

We believe that future therapies for C9 ALS/FTD could benefit from blocking DPR uptake and release routes in glia as well as neuronal cells.

5. Lysosomal damage and cell-to-cell propagation of DPRs

5.1 Introduction on lysosomal damage

Numerous studies have suggested that amyloid-mediated neurodegenerative disorders are linked to abnormalities in the autophagic-lysosomal degradation pathway.

Lysosomes are membrane-enclosed cytoplasmic organelles that contain hydrolytic enzymes and regulate critical aspects of autophagy. Most of these enzymes work at low pH ($\text{pH} \leq 5$) in the lysosomal lumen, which is kept acidic by the vacuolar (H^+) ATPase (or V-ATPase). When the membrane of lysosomes is damaged or permeabilized, a process called Lysosomal Membrane Permeabilization (LMP), the luminal contents of these organelles can be released into the cytosol and cause indiscriminate degradation of cellular components⁵⁴⁷. As a result of LMP, lysosomal proteases such as cathepsins⁵⁴⁸ can accumulate in the cytosol and initiate a cascade of events culminating with the activation of cell death^{173,549}

Importantly, it was recently found that misfolded protein aggregates can induce or exacerbate LMP in cell culture studies. After cell-entry, exogenous misfolded aggregates accumulate in lysosomal organelles and damage their membranes via LMP^{172,177,530,550}. This mechanism has been proposed to either directly induce cell death or, perhaps more intriguingly, to promote further seeding of the aggregates within the cell. The latter hypothesis could be caused by damaged autophagic vesicles which are unable to degrade amyloid aggregates, thus providing fertile ground for further aggregation and spreading. Exogenous α -synuclein^{172,177}, tau⁵³⁰, and polyQ-expanded huntingtin⁵⁵⁰ trigger LMP after endocytic uptake and, in some cases, LMP is linked to an increase of their aggregate seeding^{177,530}. However, the mechanisms by which LMP may lead to further seeding are not well understood.

Nonetheless, the cell can repair or contain LMP in a variety of ways. For example, cytosolic proteins known as "galectins" can recognise a damaged lysosomal membrane by binding to β -galactosides on the luminal membrane leaflet⁵⁵¹. Following that, as in the cases of galectin-8 and galectin-3, these proteins target the damaged lysosome for autophagic degradation⁵⁵². This mechanism prevents LMP from causing lysosomal degradation and cell death in the long run. Galectins have already transitioned from a cytosolic "diffuse" distribution to a lysosomal "punctate" distribution when they bind to their carbohydrate ligands. This transition is easily detected by immunofluorescence and has evolved into a

powerful assay for determining when a cell experiences lysosomal damage/repair ⁵⁴⁹. Interestingly, Flavin *et al.* found that exogenous α -synuclein fibrils can induce a punctate distribution of galectin-3 after being added to cell culture medium ⁵⁵⁰. This study exemplifies the following proof-of-concept: exogenous protein aggregates (i) enter cells through endocytosis, (ii) invade lysosomal organelles, and (iii) activate LMP.

In this Chapter, we wanted to see if our recombinant poly-GA assemblies could cause lysosomal damage in neurons.

The levels of some cathepsin proteins in DPR-treated cells were determined using immunofluorescence assays. Likewise, we assessed the levels of apoptotic markers. In addition, we looked at the lysosomal profile of DPR-positive cells versus DPR-negative cells. We accomplished this by employing a variety of assays that measured lysosomal pH levels as well as lysosome capacity to degrade specific substrates.

Because previous research has shown that oligomers can cause lysosomal damage more frequently than fibrils ⁵⁵⁰, we perform systematic comparisons of poly-GA fibrils vs poly-GA oligomers in the majority of our experiments.

5.2 Poly-GA DPRs produce partial lysosomal dysfunction

Previously, in Chapter 4.4, we demonstrated the uptake of poly-GA in primary cortical neurons, particularly in the soma and proximal axon compartments. Moreover, we reported that poly-GA fibrils and oligomers strongly co-localize with lysosomal organelles in these neurons, especially in spherical axonal structures.

Here, we wanted to follow up on these findings by exploring whether lysosomes that co-localize with DPRs ("Colocalized Lysosomes", CLs) have different characteristics or functionality compared to those lysosomes that do not colocalize with DPRs ("Non-Colocalized Lysosomes", NCLs). We separated these lysosomal populations using colour deconvolution algorithms (**Movie S8**). In proximal axonal regions, CLs exhibited decreased displacement, decreased speed, and increased size compared to NCLs (**Figure 5.1**).

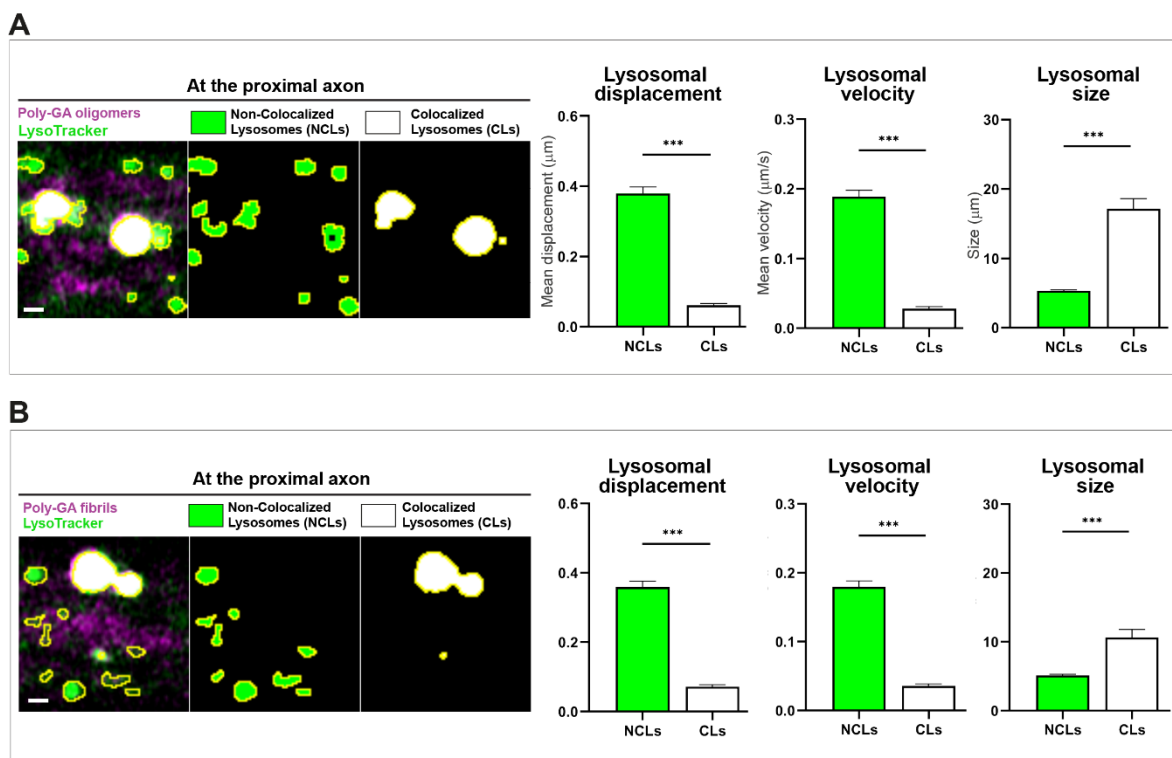


Figure 5.1 Endolysosomal organelles that colocalize with poly-GA DPRs present aberrant characteristics

Co-localization analysis between all the poly-GA oligomers (**A**) or the poly-GA fibrils (**B**) and the lysosomes contained in the cortical neurons' proximal axons. We separated "Non-Colocalized Lysosomes" (NCLs) and "Colocalized Lysosomes" (CLs) to analyse displacement, speed and size. Scale bars = 1 μm . Bar graphs of mean \pm SEM. Unpaired two-tailed t-test with Welch's correction. *** $P \leq 0.001$. The data were collected from 3 independent biological replicates.

Next, we exposed the cortical neurons to poly-GA fibrils and oligomers for 24 hours and examined the transcriptional profile of various lysosomal metabolism genes. In particular, RNA was extracted and RT-qPCR was performed for the following genes: CTSL, CTSB, CTSD, GBA, MCOLN1, and ATP6V0E1. The genes CTSL, CTSB, and CTSD encode cathepsin L, B and D, respectively. These genes were chosen because of the importance of cathepsins in the degradation of protein aggregates including α -synuclein and $A\beta$ ¹⁵⁵; conversely cathepsin deficiencies lead to increased aggregate burden^{156,553}. The gene GBA encodes for glucocerebrosidase and was chosen because its level negatively correlates with α -synuclein aggregation⁵⁵⁴. Finally, the genes MCOLN1 and ATP6V0E1, which encode mucolipin-1 and the subunit of the V-ATPase V0 complex, were chosen to assess whether poly-GA could lead to alterations of functional lysosomal channels which regulate important processes such as fission and fusion or acidic pH in the lysosome.

While transcripts encoding various cathepsins (CTSL, CTSB, CTSD), a lysosomal hydrolase (GBA), and a cation-permeable lysosomal channel (MCOLN1) did not change in response to DPRs, transcriptional levels of ATP6V0E1 (a component of the V-ATPase) increased in response to poly-GA fibrils (**Figure 5.2**). In conclusion, our findings suggest that poly-GA fibrils (rather than oligomers) disrupt the transcript levels of ATP6V0E1 in neurons.

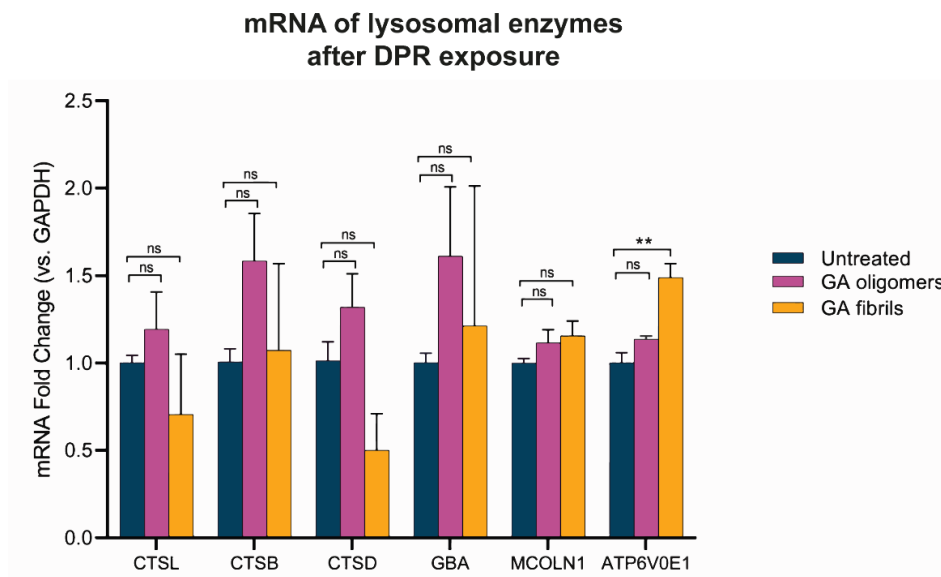


Figure 5.2 ATP6V0E1 mRNA levels in cortical neurons are altered by poly-GA fibrils

Quantification of relative expression levels after RT-qPCR for genes involved in lysosomal metabolism. RNA was isolated from primary mouse cortical neurons (10 days in culture) exposed or not to poly-GA oligomers or poly-GA fibrils for 24h, retrotranscribed and subjected to

quantitative real-time PCR. Only the transcriptional levels of ATP6V0E1 (a component of the V-ATPase) were increased upon treatment with poly-GA fibrils compared to control untreated neurons. One-way ANOVA with Tukey's multiple comparisons test. $**P \leq 0.01$. The data were collected from 3 independent biological replicates.

Next, we used immunofluorescence assays to determine the levels of some cathepsin proteins in neurons treated with poly-GA DPRs for 24 hours. We concentrated our research on cathepsins L, B, and D in particular because each of these enzymes has previously been linked to the degradation of misfolded protein aggregates^{157,553,555}.

In our results, the levels of cathepsins L, B, and D in neurons exposed to poly-GA (or poly-PA) DPRs for 24 hours showed no difference when compared to untreated neurons (**Figure 5.3**).

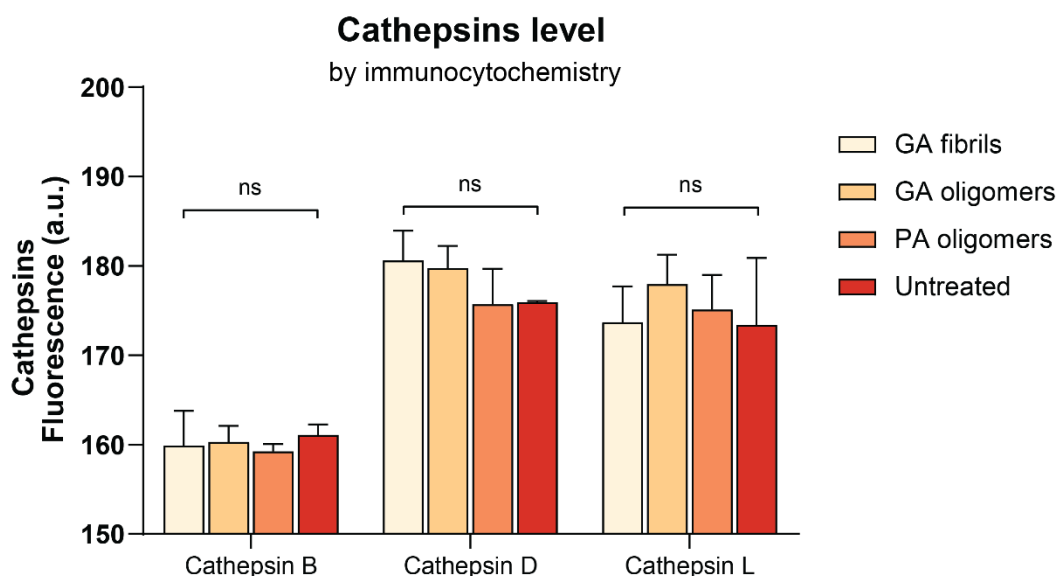


Figure 5.3 DPR exposure does not change cathepsin levels in primary cortical neurons

Immunofluorescence assays were used to compare the protein levels of cathepsins L, B, and D in neurons exposed to DPRs for 24 hours versus untreated neurons. Our study found no difference in cathepsin levels between DPR-treated and untreated cells. One-way ANOVA with Tukey's multiple comparisons test. $ns = P > 0.05$. The data were collected from 2 independent biological replicates.

Using self-quenched enzymatic substrates (LysoSubstrate) that are targeted to lysosomes⁵⁵⁶, we then quantified *in situ* lysosomal enzyme activities in primary mouse cortical neurons. Neuronal lysosomes showed no difference in LysoSubstrate levels after 24 hours of poly-GA exposure, indicating that poly-GA does not cause significant changes in lysosomal functionality (**Figure 5.4A** and **5.4B**).

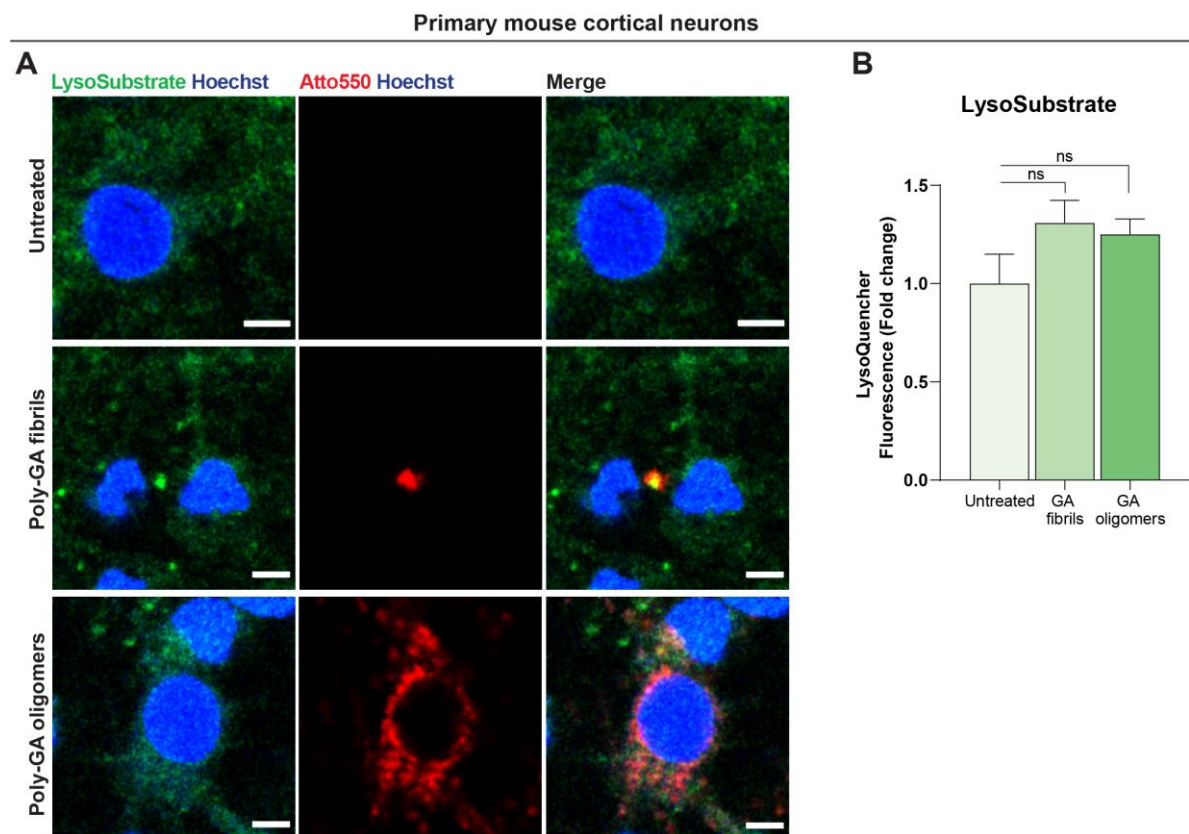


Figure 5.4 DPR exposure does not change *in situ* lysosomal enzyme activities

(A) Primary mouse cortical neurons were exposed to poly-GA DPRs for 24 hours (or were left untreated), and Lysosome-Specific Self-Quenched Substrate (Abcam, #ab234622) was added during the final 1 hour of the 24-hour period to measure lysosomal *in situ* enzyme activity. Scale bars = 5µm. (B) Mean fluorescence intensity of Lysosome-Specific Self-Quenched Substrate was quantified per neuronal cell. Bar graphs of mean ± SEM. One-way ANOVA with Tukey's multiple comparisons test. ns = P > 0.05. The data were collected from 3 independent biological replicates.

Next, we used immunofluorescence assays to see if the 24-hour DPR exposure caused an increase in apoptosis in neurons. The cleaved (thus active) form of caspase-3 is generally considered a universal marker of apoptosis because caspase-3 activity is required for most biochemical events associated with this pathway⁵⁵⁷. As a result, we used a specific antibody that recognises the fully active cleaved form of caspase-3 as an apoptosis marker. For this assay, we combined DPR exposure with the cell-permeable proteasome inhibitor MG132. We reasoned that by inhibiting the 26S proteasome with MG132, we could potentially increase the DPR aggregate burden and stimulate neurons to undergo apoptosis more quickly. Thus, we treated neurons with DPRs for 24 hours, and added 1mM of MG132 during the last 1 hour (or 3 hours, or 5 hours) of the 24-hour span.

The levels of cleaved caspase-3 in proteasome-impaired neurons exposed to poly-GA (or poly-PA) DPRs for 24 hours showed no difference when compared to proteasome-impaired neurons that did not receive DPRs (**Figure 5.5**).

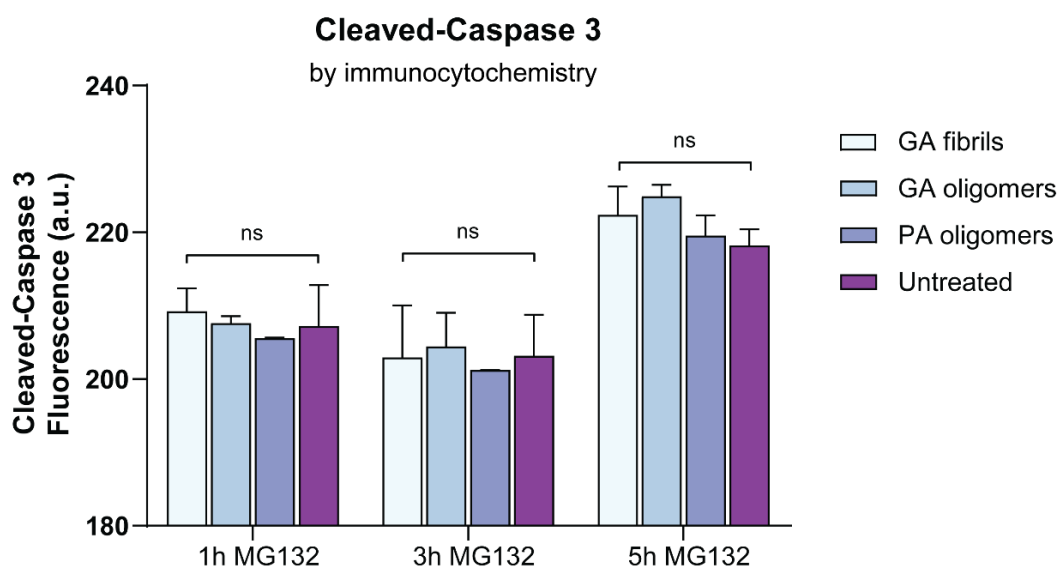


Figure 5.5 Proteasome impairment and DPR exposure do not increase cleaved caspase-3 levels in primary cortical neurons

Immunofluorescence assays were used to compare cleaved caspase-3 protein levels in proteasome-impaired neurons with or without DPR exposure for 24 hours. During the last 1 hour (or 3 hours, or 5 hours) of the 24-hour span, the cell-permeable proteasome inhibitor MG132 (at 1mM) was utilised to cause proteasome impairment. The levels of cleaved caspase-3 did not differ between the groups studied. One-way ANOVA with Tukey's multiple comparisons test. ns = $P > 0.05$. The data were collected from 2 independent biological replicates.

Finally, we used the galectin-3 puncta assay to look for lysosomal damage in DPR-exposed cells. We used the lysosomotropic drug L-leucyl-L-leucine Methyl Ester (LLOMe) as a positive control that causes lysosomal damage and thus the formation of galectin-3 puncta⁵⁵². Lysosomotropic drugs initially diffuse across lysosomal membranes and then accumulate in the lysosomes to disrupt its membrane integrity, resulting in the release of lysosomal proteases in the cytosol and, eventually, apoptosis^{558,559}.

Our primary mouse cortical neurons appeared to be extremely LLOMe resistant. Various LLOMe concentrations and time points were tested, but this experimental framework proved difficult because we needed to use large amounts of LLOMe for a long time to see galectin-3 puncta formation, which produced the desired phenotype but also killed most of the cells. Because we couldn't easily induce lysosomal damage in primary mouse cortical neurons, we chose HeLa cells for a proof-of-concept experiment. We exposed HeLa cells to poly-GA fibrils for 24 hours and then added 1mM LLOMe for the last hour. As expected, LLOMe treatment resulted in the formation of galectin-3 puncta (**Figure 5.6A**). However, galectin-3 immunofluorescence levels in DPR-exposed HeLa cells did not increase when compared to untreated cells, regardless of LLOMe treatment. (**Figure 5.6B**).

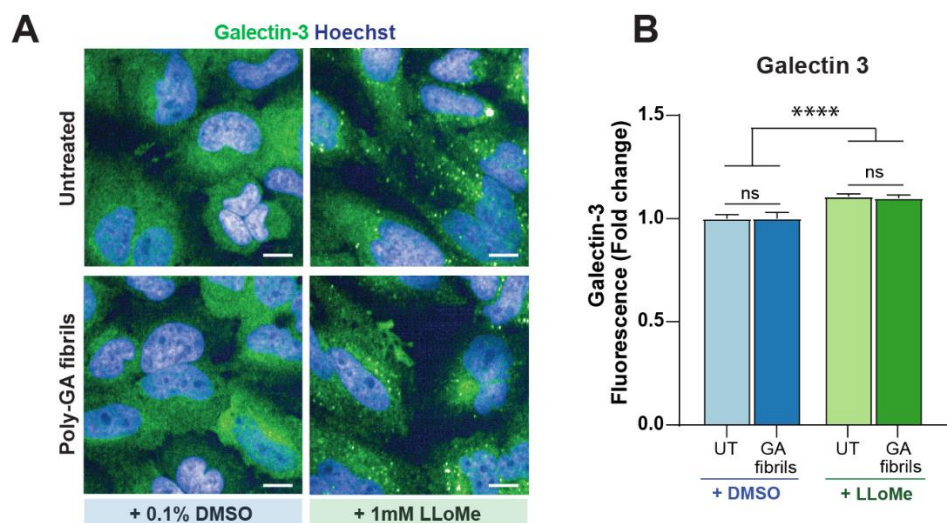


Figure 5.6 Galectin-3 levels do not increase in DPR-exposed HeLa cells

The galectin-3 immunofluorescence assay was used to compare galectin-3 protein levels in HeLa cells exposed or not exposed to poly-GA fibrils for 24 hours. During the last 1 hour of the 24-hour span, the lysosomotropic drug LLOMe (at 1mM) was used to induce lysosomal damage, which is visible by galectin-3 puncta formation (positive control) (**A**). Regardless of LLOMe treatment, the levels of galectin-3 did not differ between HeLa cells exposed or not exposed to poly-GA fibrils. Bar graphs of mean \pm SEM. Unpaired two-tailed t-test with Welch's correction (**B**). ns = $P > 0.05$ and **** $P \leq 0.0001$. The data were collected from 3 independent biological replicates.

Despite the lack of evident lysosomal malfunction in cells treated with poly-GA in these assays, we discovered that HeLa cells decreased their lysosomal pH after 24 hours of exposure to poly-GA fibrils or oligomers, which corresponded to an increase in LysoSensor fluorescence (**Figure 5.7A** and **5.7B**). This suggests that poly-GA may impair lysosomal acidification and stimulate cellular responses aimed at increasing lysosomal pH.

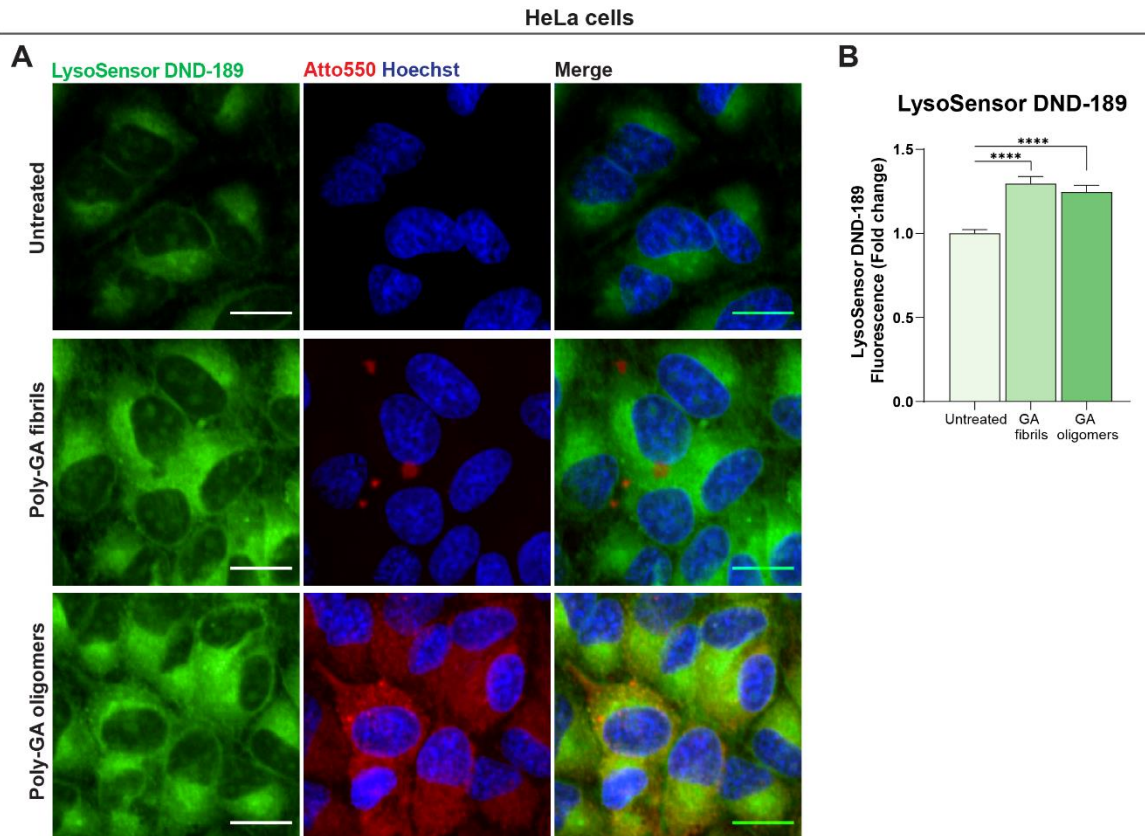


Figure 5.7 HeLa cells decrease their lysosomal pH after exposure to poly-GA

(A) HeLa cells were exposed to poly-GA DPRs for 24 hours (or were left untreated), and LysoSensor Green DND-189 was added during the final 1 hour of the 24-hour period to measure changes in lysosomal pH (this dye exhibits increasing fluorescence as pH decreases). (B) Mean fluorescence intensity of LysoSensor was quantified in live HeLa cells. Bar graphs of mean \pm SEM. One-way ANOVA with Tukey's multiple comparisons test. **** $P \leq 0.0001$. The data were collected from 3 independent biological replicates.

In summary, there was no obvious lysosomal damage in mouse cortical neurons or HeLa cells after 24 hours of poly-GA exposure, but cellular responses aimed at increasing or regulating lysosomal acidification were detected (increase of ATP6V0E1 mRNA, and LysoSensor signal).

5.3 Introduction on cell-to-cell spreading

A variety of harmful amyloid proteins move from cell-to-cell during neurodegenerative diseases, accelerating the development of cellular pathology and disease progression. Understanding how disease-associated amyloid proteins invade target cells and cause cellular dysfunction is critical to understanding how neurodegenerative disorders progress. The cell-to-cell transmission of pathological aggregates is a possible unifying mechanism underlying the progression of various neurodegenerative diseases, including ALS/FTD ⁷³.

Because of their ability to template further aggregation, SOD1 and TDP-43 assemblies have prion-like properties in cell culture and *in vivo*. In cultured cells, mutant SOD1-aggregates have been shown to spread ¹¹² and spinal cord homogenates from transgenic animals overexpressing mutant SOD1 can produce wild-type and mutant SOD1 aggregation in naïve cell cultures ⁵⁶⁰. When the same homogenates are injected into non-symptomatic transgenic mice with SOD1 mutations, they cause early-onset pathology in the spinal cord, midbrain, and brainstem ¹¹⁴. As for TDP-43, Nonaka and colleagues reported convincing evidence for its prion-like behaviour when they added human ALS TDP-43 pathological brain extracts into cultured cells and observed the formation of ubiquitinated, phosphorylated, and insoluble cytoplasmic TDP-43 inclusions ⁵⁶¹.

Because the GGGGCC pathogenic repeat expansion in the *C9ORF72* gene is the primary genetic cause of both ALS and FTD, it is necessary to investigate mechanisms by which *C9ORF72*-derived DPRs may cause toxicity and neurodegeneration, potentially causing the pathology to spread in different interconnected neuronal regions.

Recent evidence suggests that DPRs possess prion-like propagation features in cell culture settings. The cell-to-cell propagation of DPRs may be relevant to the disease process, which is an important question for future research. DPRs may affect important cellular processes and create a positive feedback loop of toxicity in the cells in which they propagate by altering *C9ORF72*-dependent cellular processes such as *C9ORF72* transcription levels, RNA foci formation, and further DPR production.

Studies have shown that DPRs can spread in neuroblastoma cells, iPSC-derived spinal motor neurons, and fibroblasts from ALS patients ^{125,126,130}, as well as in the *Drosophila* nervous system ¹³¹. This propagation can occur via both exosome-dependent and exosome-

independent pathways¹³⁰. Poly-GP DPRs have also been found in the cerebrospinal fluid of *C9ORF72* ALS/FTD patients, indicating that DPRs can be secreted by cells^{504,522}.

A number of cell culture and *in vivo* studies have shown that ALS astrocytes contribute to motor neuron death^{291,294,295,453,562–567} and it has been speculated that the release of pathological proteins may be at the heart of the observed neurotoxicity. Previous research has implicated astrocytes in the intercellular traffic of the scrapie isoform of the prion protein (PrP^{Sc}), α -synuclein and A β assemblies, and subsequent neuronal injury^{99,568,569}.

In this section of the Chapter, we wanted to look into the ability of poly-GA DPRs residing in glia to propagate in neighbouring neuronal cells, particularly cells that undergo classic degeneration in ALS-FTD such as motor neurons. In fact, neuron-to-astrocyte spreading for DPRs has previously been reported¹³⁰ but the opposite directionality has yet to be investigated. The spread of DPRs may cause pathology to spread in connected neuronal pathways, leading to disease progression.

5.4 Poly-GA DPRs spread from astrocytes to motor neurons

Although it has been shown that DPRs can transfer from neurons to astrocytes¹³⁰, nothing is known about the role of glial cells in the dissemination of DPRs. For example, no study to our best knowledge has yet unveiled whether DPRs can propagate from astrocytes to neurons. To test the possibility of this directionality, we established a co-culture system between iAstrocytes and Hb9-GFP mouse motor neurons. Briefly, we treated healthy iAstrocytes with 1 μ M DPRs for 24h, performed a number of PBS washes to remove remaining assemblies, and subsequently plated Hb9-GFP mouse motor neurons over the astrocyte layer. We kept this co-culture system for 48h before fixation and confocal imaging (**Figure 5.8A**). We observed that, after astrocytic uptake, DPR assemblies underwent astrocyte-to-neuron propagation as confirmed by orthogonal views (**Figure 5.8B**). Different DPRs showed different percentages of propagation to motor neurons, with poly-GA fibrils

being the most efficient at spreading (detected in 24% of motor neurons) when compared to oligomeric species (poly-GA: 4%; poly-PA: 7%) (**Figure 5.8C**).

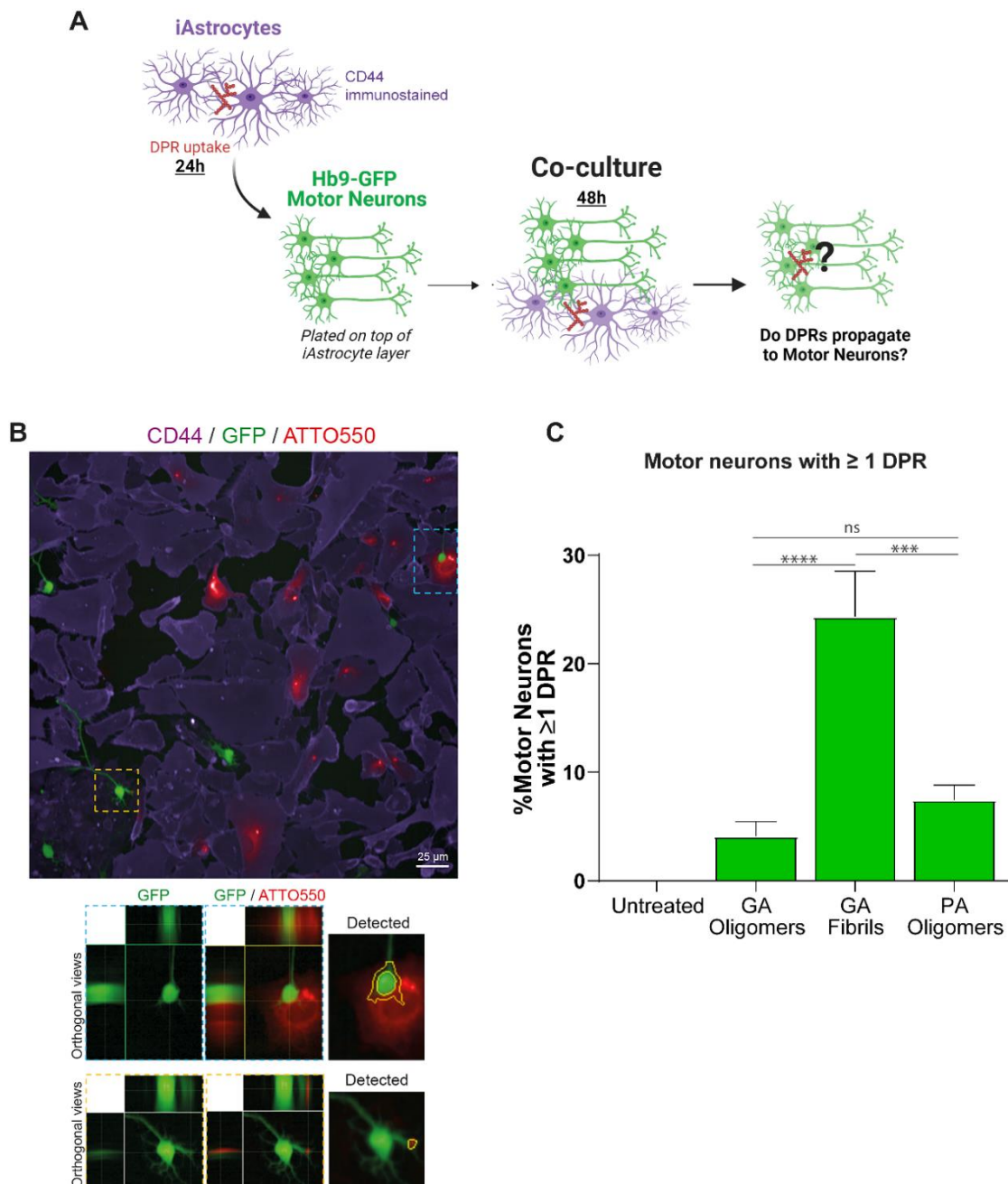


Figure 5.8 Alanine-rich DPRs undergo astrocyte-to-motor neuron propagation

A) Schematic representation of the iAstrocytes-MNs co-culture system. **B)** Orthogonal views from confocal images show the presence of ATTO550 DPRs (red) in the GFP-positive MNs (green); CD44 is shown in violet as the astrocytic marker. **C)** Quantification of the percentage of motor neurons containing at least one DPR aggregate in the various 48h co-culture systems. Bar graphs of mean \pm SEM. One-way ANOVA with Tukey's multiple comparisons test. \sim 120 neurons/condition. ns = $P > 0.05$. The data were collected from 3 independent biological replicates.

To make sure that iAstrocytes indeed release DPRs, we also ran an assay on single-cultured iAstrocytes in which we quantified the release of DPRs into the conditioned medium (CM). To do so, we have initially added 1 μ M of DPRs to the culture medium for 24h, washed in PBS and then incubated for 24h with CM. The CM was harvested in tubes, centrifuged and analysed at the spectrophotometer, which quantified ATTO550 fluorescence intensity (thus relative DPR concentration, after normalization with known DPR concentrations: $R^2 > 0.95$). Our findings show that all DPRs are indeed detected in the CM (**Figure 5.9A**).

We then investigated whether the astrocyte-to-neuron transmission of DPRs could contribute to motor neuron damage as a non-cell autonomous effect. However, no evident cytotoxicity was found in motor neurons upon co-cultures with iAstrocytes that contained and transmitted DPRs (**Figure 5.9B**).

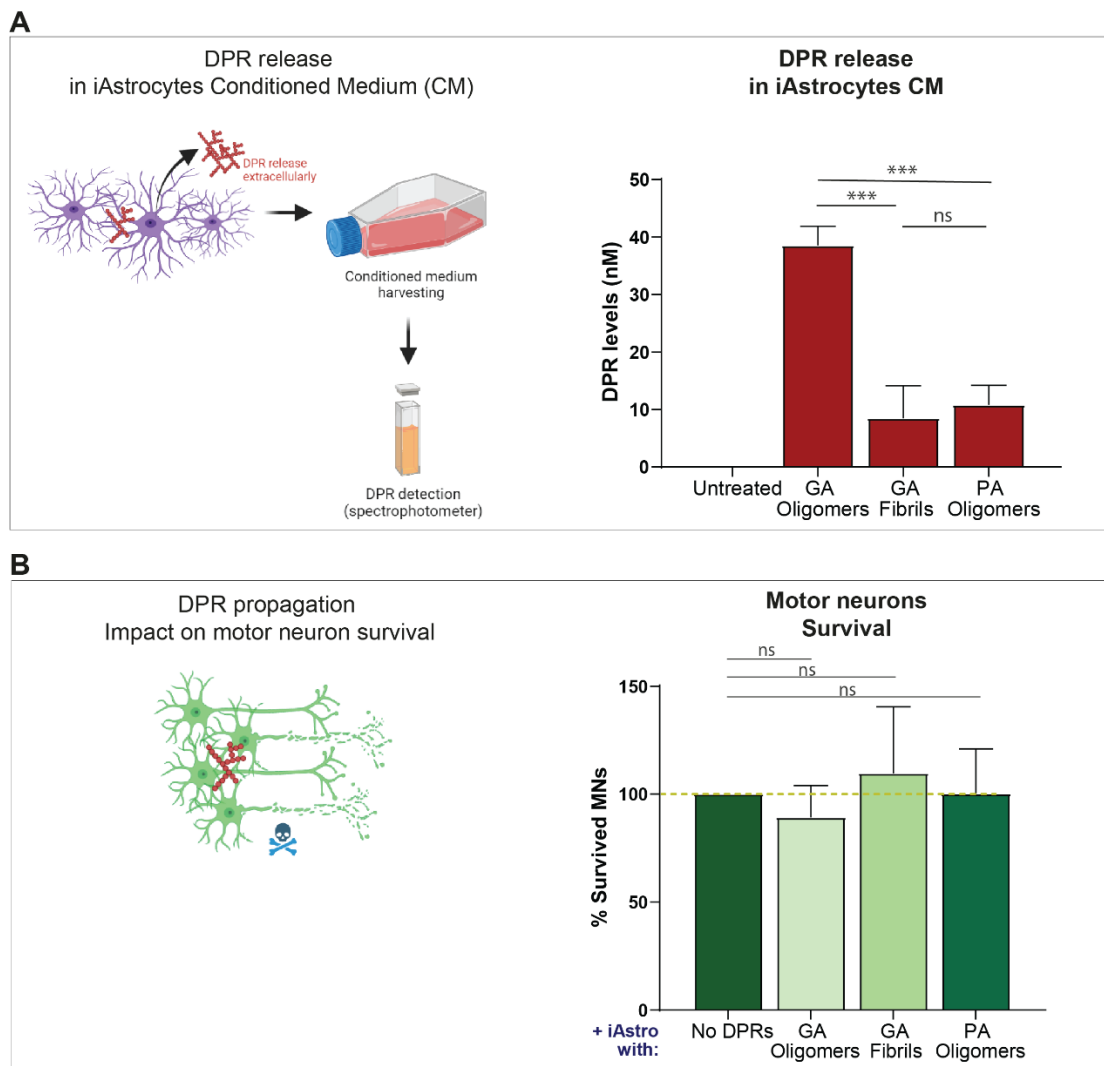


Figure 5.9 Propagated DPRs do not show toxicity in receiving motor neurons

A) Quantification of DPR levels present in the conditioned medium of healthy iAstrocytes, via spectrophotometric analysis. Bar graphs of mean \pm SEM. One-way ANOVA with Tukey's multiple

comparisons test. ns = $P > 0.05$, and $***P \leq 0.001$. The data were collected from 4 independent biological replicates. **B)** Quantification of motor neuron survival upon 48h co-culture with iAstrocytes containing and transmitting DPRs. Bar graphs of mean \pm SEM. One-way ANOVA with Tukey's multiple comparisons test. ~ 120 neurons/condition. ns = $P > 0.05$. The data were collected from 3 independent biological replicates.

Furthermore, no increase in APOJ, a lipoprotein secreted in lipoparticles that has been linked to astrocyte-induced toxicity⁵⁷⁰, was found in the CM of single-cultured iAstrocytes (three distinct control groups) exposed to different DPRs. APOJ levels, as measured by enzyme-linked immunosorbent assay (ELISA), were actually reduced after exposure to poly-GA oligomers (and partially to poly-PA), implying that DPRs may interfere with APOJ-mediated lipoparticle release (**Figure 5.10A** and **5.10B**).

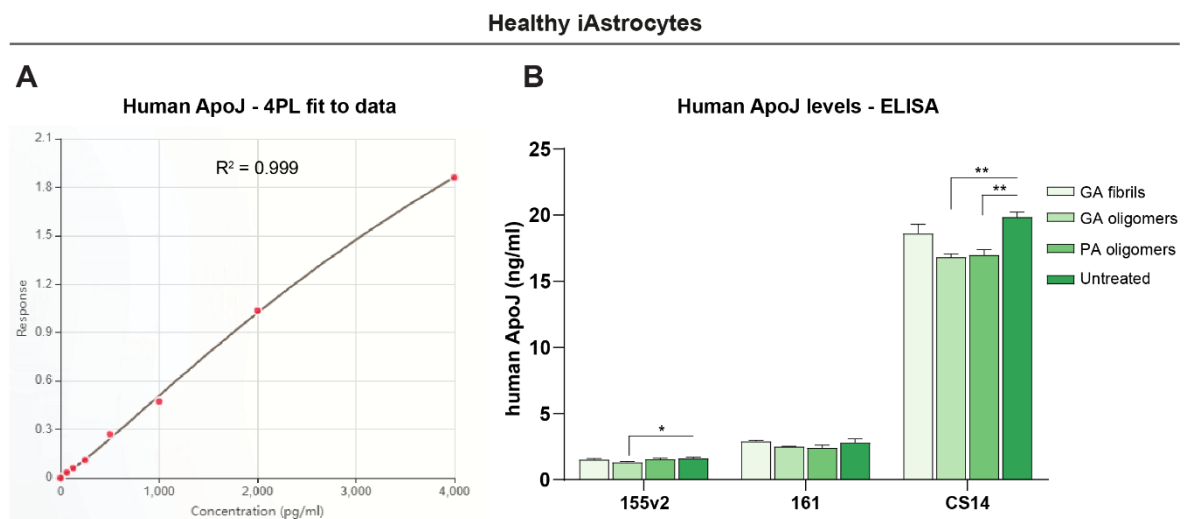


Figure 5.10 APOJ enzyme-linked immunosorbent assay

Apolipoprotein J (APOJ) protein levels were measured in three distinct healthy lines of iAstrocytes' conditioned medium. **(A)** Regression analysis with the Four-parameter logistic curve-fit (4-PL) method was used to determine the best-fit standard curve based on 2-fold serial dilutions of APOJ standards and absorbance at 450nm. **(B)** iAstrocytes were either left untreated or treated for 24 hours with various recombinant DPRs (poly-GA fibrils, poly-GA oligomers, poly-PA oligomers), and then APOJ protein levels in their conditioned medium were measured and calculated using the previously generated 4-PL standard curve. Bar graphs of mean \pm SEM. One-way ANOVA with Tukey's multiple comparisons test (control group is "untreated"). * $P \leq 0.05$, ** $P \leq 0.01$, *** $P \leq 0.001$, and **** $P \leq 0.0001$. The data were collected from 3 independent biological replicates.

We then wanted to create co-cultures of astrocytes and motor neurons using *C9ORF72*-patient derived iAstrocytes. We treated these astrocytes with our recombinant DPRs and then co-cultured them with motor neurons for 48 hours. We hypothesised that because *C9ORF72*-ALS-derived cells have been shown to have autophagy deficits³³¹, adding DPRs to them would further seed aggregation and potentially toxic effects on co-culture motor neurons. However, when motor neurons were co-cultured with *C9ORF72*-patient derived iAstrocytes containing uptaken DPRs, no obvious cytotoxicity was observed (**Figure 5.11A**).

We then investigated whether inducing pharmacological changes in biological pathways such as autophagy, lysosomal exocytosis, or apoptosis could affect the amount of DPR aggregates released by single-cultured healthy iAstrocytes. Indeed, lysosomes may participate in intercellular aggregate transfer, including lysosomal exocytosis of their contents, or they may travel through actin-based structures known as "tunnelling nanotubes" for direct cell–cell transfer^{174,571}. In a similar context, autophagic failure has been linked to the exocytosis and intercellular transfer of pathological protein aggregates such as α -synuclein⁵⁷². We found no difference in DPR release into the conditioned medium of iAstrocytes when Vacuolin-1 inhibited lysosomal exocytosis and Bafilomycin-A1 inhibited autophagic flux (**Figure 5.11B**). Also, blebbistatin-induced inhibition of membrane blebbing, which could improve astrocyte survival, had no effect on DPR release (**Figure 5.11B**).

Taken together, our results show that iAstrocytes can efficiently release poly-GA and poly-PA DPRs into the culture medium and, when co-cultured with motor neurons, they are able to transmit DPRs to neuronal cells. Although we did not observe any obvious cell death after transmission with our system, we hypothesise that astrocytes may serve as hubs for the internalisation and release of abnormal peptides in ALS.

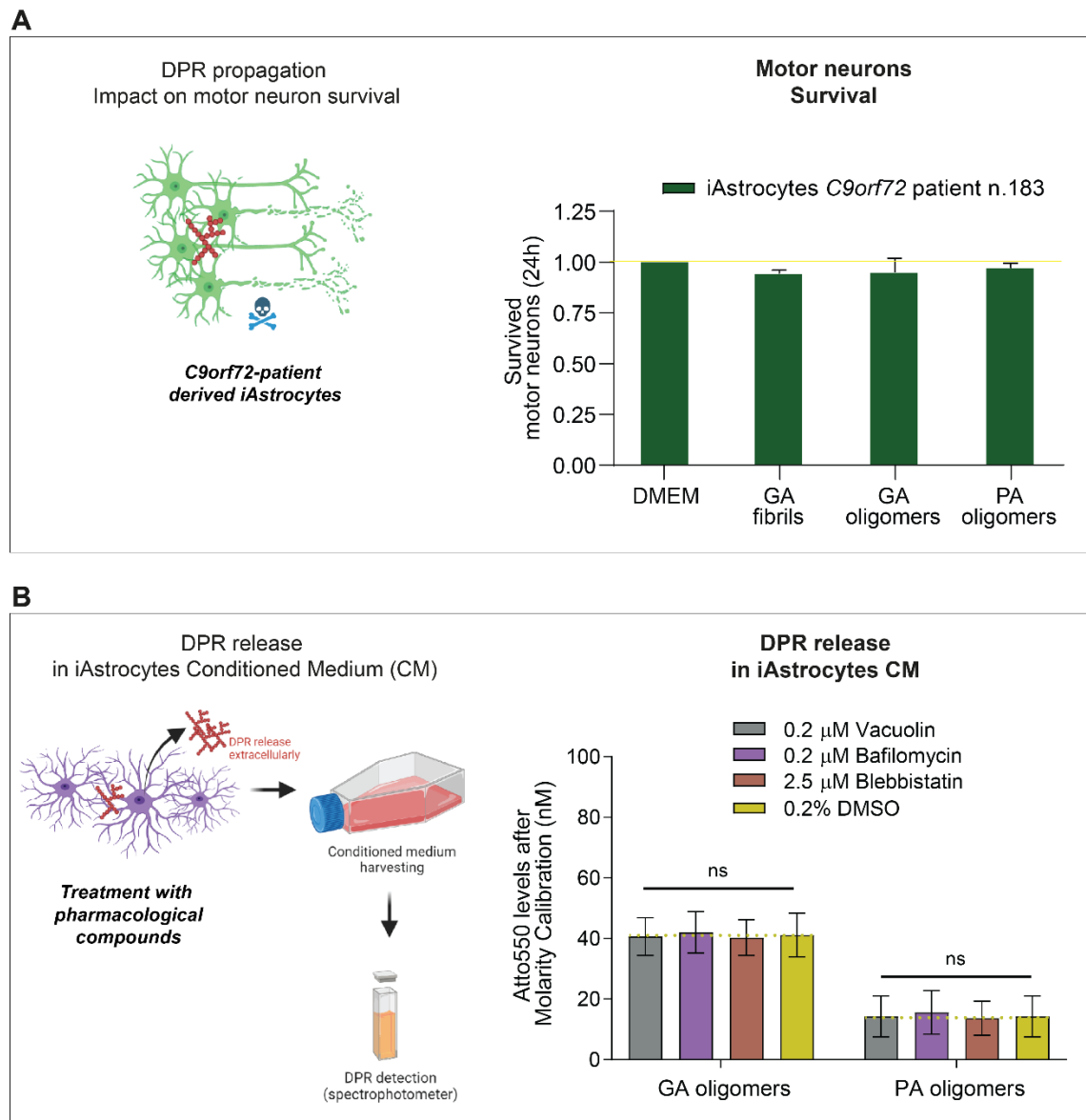


Figure 5.11 Alanine-rich DPRs undergo astrocyte-to-motor neuron propagation

A) Quantification of motor neuron survival upon 48h co-culture with *C9ORF72*-patient derived iAstrocytes containing and transmitting DPRs. Data were normalized to control condition (co-culture between motor neurons and DPR-free astrocytes). One-way ANOVA with Tukey's multiple comparisons test; ns = $P > 0.05$. The data were collected from 3 independent biological replicates.

B) Spectrophotometer quantification of DPR levels (ATTO550 fluorescence) present in the conditioned medium of healthy control-derived iAstrocytes treated with pharmacological compounds. Upon inhibition of lysosomal exocytosis (0.2μM Vacuolin-1), autophagic flux (0.2μM Bafilomycin A1) or membrane blebbing (2.5μM Blebbistatin), we did not observe any decrease of DPR release. Data were normalized to 0.2% DMSO control condition for ATTO550 background fluorescence. One-way ANOVA with Dunnett multiple comparisons test. ns = $P > 0.05$. The data were collected from 2 independent biological replicates.

5.5 Discussion

Pathological protein aggregates in neurons and glia are a hallmark of most neurodegenerative diseases ⁵⁷³. In the context of *C9ORF72*-ALS/FTD, aggregation of the RAN translation-derived poly-GA DPRs is one of the proposed mechanisms for inducing proteasome impairment, DNA damage, cognitive disability, motor deficits, pro-inflammatory responses and neurodegeneration, as demonstrated by numerous cell culture and *in vivo* studies ^{127,128,424,430,447,535}.

Our findings that poly-GA DPRs accumulate in abnormally immotile and enlarged lysosomes imply that these proteins may impair the function of these organelles in neurons. Because of the polarity of neurons, the regulation of lysosomal motility and size is especially important: lysosomes need to access specific cytoplasmic locations to perform their various functions, and lysosomal size is critical for fission and fusion events. Mutations in genes that encode for components regulating lysosomal motility cause a variety of neurological disorders ⁵⁷⁴, and lysosome size is altered in a number of human diseases ⁵⁷⁵.

It should be noted that lysosome positioning and movement are dependent on a complex interplay of interactions with microtubule motors, the actin cytoskeleton, and other organelles ⁵⁷⁴. Our recombinant DPRs could also disrupt key lysosomal partners, such as microtubules or microtubule motors. Indeed, it was recently shown that arginine-rich DPRs impede translocation of dynein and kinesin-1 motor complexes and bind microtubules promoting their pausing and detachment ⁵⁴². We speculate that similar mechanisms could be behind the behaviour observed following poly-GA DPR internalization, as our data showed that poly-GAs are cellularly relocated upon nocodazole treatment, thus suggesting the presence of poly GA-microtubule interactions.

Our data on lysosomal functionality also revealed that 24h exposure to poly-GA fibrils increased ATP6V0E1 transcript levels when compared to untreated or poly-GA oligomers exposure. ATP6V0E1 is a component of the multi-subunit ATPase enzyme, which is essential in eukaryotes for the acidification of intracellular organelles. As demonstrated in HeLa cells with a drop in lysosomal pH (LysoSensor) after poly-GA exposure, upregulation of ATP6V0E1 mRNA may represent a biological response to poly-GA clearance, presumably by maintaining or enhancing lysosomal pH acidic gradients via V-ATPase activity.

We also looked into whether recombinant DPRs could affect the levels of lysosomal enzymes. Cathepsins are the most abundant lysosomal proteases, found primarily in acidic endo/lysosomal compartments where they play important roles in intracellular protein degradation, energy metabolism, and immune responses¹⁵⁵. In our study, we looked at the protein levels of three important cathepsins: cathepsin L, B, and D. These three cathepsin proteins have been associated with ALS-FTD neuropathology, especially cathepsin B and D. Indeed, cathepsin B protein and mRNA levels are increased in post-mortem spinal cords from ALS patients^{160,161}, as well as cathepsin D mRNA¹⁶¹. In our results, the levels of cathepsins L, B, and D in neurons exposed to poly-GA (or poly-PA) DPRs for 24 hours showed no difference when compared to untreated neurons. Because some cells in DPR-treated cells do not internalise these assemblies, the cathepsin results may be skewed by this cell population. Alternatively, cathepsins could rise immediately after poly-GA exposure or at other times that were not included in our study (24h exposure only).

We then wanted to see if poly-GA oligomers and poly-GA fibrils could cause apoptosis or lysosomal damage after being internalised in primary mouse cortical neurons. DPR-treated cells showed no signs of increased apoptosis when compared to DPR-free neurons. We also evaluated *in situ* lysosomal activity and found no clear lysosomal damage mechanism produced by exposure to poly-GA. Furthermore, we were unable to detect increased damage in HeLa cells after 24 hours of exposure to poly-GA fibrils using galectin-3 as a sensitive reporter for endo-lysosomal damage. These findings could imply that DPRs are not toxic at these early time points. New experiments with more time points and different DPR molarities are required to determine whether and when DPRs may cause cellular damage. Despite the lack of evident lysosomal malfunction in cells treated with poly-GA in these assays, we discovered that HeLa cells decreased their lysosomal pH after 24 hours exposure to poly-GA fibrils or oligomers, which corresponded to an increase in LysoSensor fluorescence. This suggests that poly-GA may enhance lysosomal acidification.

We finally sought to investigate whether poly-GA oligomers and poly-GA fibrils could show differences in the ability to undergo cell-to-cell propagation, a process previously observed for various DPR species in neuronal cell cultures^{125,126,130,132} as well as in the *Drosophila* nervous system¹³¹. We proceeded to explore these questions by establishing a co-culture system between iAstrocytes and Hb9-GFP mouse motor neurons; this system was used because of two main reasons: (i) the largely unexplored role of glia in DPR propagation with relation to neurons, (ii) and the previously described role of astrocytes as “hubs” for

intercellular propagation of protein aggregates^{99,568,569}. Our co-culture experiments showed that poly-GA DPRs undergo astrocyte-to-motor neuron propagation, with the fibrils being 6-times more efficient in transferring to motor neurons compared to oligomers. Thus, DPRs at later stages of aggregation might be more prone to transfer from affected to naïve cells, which is in agreement with previous findings related to other amyloid proteins⁵⁷⁶. The release of DPRs into the conditioned medium of a monolayer of cultured iAstrocytes did not decline when lysosomal exocytosis or membrane blebbing were inhibited. Therefore, we speculate that DPRs may passively reach the extracellular space by leakage through damaged cell membranes, as already shown for α -synuclein and tau^{577–579}, or via other routes, possibly involving secretion via exosomes¹³⁰.

Somewhat surprisingly, we were not able to detect any cytotoxicity in co-cultured motor neurons associated to poly-GA DPRs, nor any increase in APOJ lipoprotein in iAstrocyte conditioned medium, which has previously been linked to astrocyte-induced toxicity and astrocyte activation⁵⁷⁰. Because multiple DPR species were not present in our experiments at the same time, it is possible that cytotoxicity of motor neurons is dependent on the synergistic presence of several DPR species in iAstrocytes. Additional DPRs may cause higher levels of astrocyte activation that may negatively affect motor neurons.

Activation of astrocytes or microglia in transgenic mice expressing poly-GA has been demonstrated in a number of studies. For example, at six months of age, GFP-GA₅₀ mice have higher transcript and protein levels of the astrogliosis marker *Gfap* in the brain⁴³⁰, whereas CFP-GA₁₄₉ mice have upregulation of phagocytic microglia markers such as CD68 and *Iba1* in the spinal cord⁴²⁴. Furthermore, GFP-GA₁₇₅ mice, but not GFP-PR₁₇₅ mice, exhibit disease-associated microglial pro-inflammatory responses as well as an interferon-response microglial signature consistent with *C9ORF72* ALS patients¹²⁸. It is intriguing to speculate that extracellular poly-GA aggregates released from glial cells (as observed in our study) may be present in mice and play a role in the activation of pro-inflammatory responses that promote the damage of motor neurons. Microglia activation correlates with disease progression in ALS patients, and *C9ORF72* carriers have higher microglia activation than non-carriers⁵⁸⁰; however, the role of poly-GA aggregation in this response remains unknown.

Overall, our findings suggest that astrocytes (and, more broadly, glial cells) play an important role in the transmission of *C9ORF72*-derived DPRs to neighbouring motor neurons. Whether this mechanism could constitute a “non-cell autonomous” contributor in *C9ORF72*-ALS/FTD neuropathology remains to be fully elucidated.

6. Final discussion and future perspectives

6.1 Summary and project highlights

It is now understood that ALS and FTD are closely related conditions with clinical, pathological, and genetic similarities. ALS is known as the most common adult-onset motor neuron disorder and one of the most common adult-onset neurodegenerative disease ⁵⁸¹. FTD is the second leading cause of dementia in people under the age of 65, after Alzheimer's disease ²⁶⁴; and, according to the World Health Organization, the number of people with dementia worldwide is expected to rise significantly between 2030 and 2050 ⁵⁸².

Overall, ALS and FTD are two fatal diseases that relentlessly progress to death within 3-5 years of diagnosis for ALS patients ^{199,200} or 4–8 years after the onset of symptoms for FTD patients ^{251–253}. Currently, the Food and Drug Administration (FDA) has approved two drugs for the treatment of ALS: riluzole and edaravone, both of which provide modest improvements in mortality and/or function ⁵⁸³. There are currently no FDA-approved disease-modifying drugs for FTD, but symptomatic treatments are frequently used ²⁵⁵. Recent advances in our understanding of the underlying pathophysiologic processes that contribute to ALS and FTD have resulted in the development of numerous investigational therapies. Despite extensive research, the vast majority of human clinical trials have failed to demonstrate clinical efficacy. Recently, Biogen and Ionis' tofersen failed to meet the primary endpoint in a phase III trial of an antisense candidate for SOD1-linked fALS ⁵⁸⁴ in late 2021. These findings were yet another setback for ALS patients and their families.

The impact of these devastating diseases on working-age people with young families represents a significant health and economic burden on society. The national economic burden of ALS in the United States is estimated to be between US\$ 279-472 million ⁵⁸⁵, with some estimates reaching US\$ 1.3 billion ⁵⁸⁶. Despite the lack of aggregated national data, the economic burden of FTD has been estimated to be as high as US\$119,654 per patient, which is nearly double the patient costs reported for Alzheimer's disease ⁵⁸⁷. Aside from the financial burden, research has revealed significant psychological distress in both ALS/FTD patients and caregivers, revealing the truly devastating nature of this disorder. For example, studies have revealed that ALS patients suffer from hopelessness, end-of-life

anxiety, and depression⁵⁸⁸. Furthermore, families affected may require assistance in coping with such an overwhelming disease, as it has been reported that children with an ALS parent are at a higher risk of internalising behaviour, depressive symptoms, and reactive problems than children with healthy parents⁵⁸⁹. Feelings of depression, anxiety and distress also increase in ALS caregivers as the patient's disease progresses^{590,591}. Patients with ALS require increasing assistance with all activities of daily living, their ability to speak or write deteriorates and the physical demands of their care become more onerous. ALS caregivers are estimated to spend 11 hours per day with the patient⁵⁹² and feel a strong sense of responsibility for their care and survival, especially when mechanical ventilation is used. Similarly, assistance of FTD patients²⁵¹ is linked to caregiver distress, depressive symptoms, and poor quality of life^{593,594}. This reality emphasises the critical need for progress in the treatment of these disorders, which can only be accomplished by developing fundamental research on the underlying pathophysiology and using this knowledge to pursue new therapeutic avenues.

Over the last 25 years, our understanding of the genetics of ALS and FTD has evolved, with the discovery of an increasing number of genes linked to both familial and sporadic cases; for example, more than 120 genetic variants have been associated with an increased risk of ALS (<http://alsod.iop.kcl.ac.uk>)¹⁹⁶. Because it is the most common genetic cause of both ALS and FTD, the hexanucleotide expansion of the *C9ORF72* gene (C9-HRE) is an appealing therapeutic target for which an effective treatment would benefit a large number of patients and have a significant impact on affected families. However, the pathological mechanisms of C9-HRE are not completely understood, particularly the role of dipeptide repeat proteins (DPRs). Misfolding and aggregation of disease-specific proteins, which results in the formation of filamentous cellular inclusions, is a feature of neurodegenerative diseases. These aggregated proteins usually form fibrillar shapes that are enriched in β -sheet secondary structures and accumulate in neurons and glia progressively spreading in different CNS regions via 'prion-like propagation'.

In this thesis, we have explored a role for poly-GA DPRs in disease spread. We created recombinant poly-GA and poly-PA DPRs with the help of collaborators Prof De Vos and Dr Melki. We described the characterization of these recombinant proteins in Chapter 3 and demonstrated that poly-GA oligomers can directly convert into solid-like aggregated states *in vitro* (test-tube) without the formation of any liquid-like intermediaries. Previous research has shown that other DPR species have similar *in vitro* properties. In particular, poly-PR and

poly-GR have been shown to coalesce *in vitro* and undergo liquid-liquid demixing^{427,432,479}, a process thought to be involved with the transition from a soluble protein to a solid and aggregated species, that could potentially alter stress granules and nucleoli^{427,480,595,596}. However, as discussed in Chapter 3 (page 97), these *in vitro* features alone cannot predict cellular pathogenicity, and these studies should be interpreted with caution.

In the same Chapter, we demonstrated that poly-GA can form characteristic β -sheet amyloid fibrils *in vitro*. The fibrillization of poly-GA (but not poly-PA) into fibrillar structures similar to those found in pathological proteins of sporadic or genetic TDP-43 proteinopathies⁵⁹⁷, tauopathies⁵⁹⁸, and synucleinopathies⁵⁹⁹ suggests a link between these diverse neurodegenerative diseases. This finding is especially intriguing given that the majority of DPR inclusions in patient brains are poly-GA positive⁴⁷⁸. According to FTIR measurements, the fibrillar poly-GA we generated are amyloid in nature, which is consistent with previous observations made with poly-GA with a low number of repeats⁴⁴⁶. As previously stated, our study was unable to generate fibrillar poly-PA, and our collaborator Dr Melki was also unable to successfully generate fibrils from poly-GP²¹. These findings suggest that the formation of poly-GA amyloid fibrils could contribute to pathogenicity as a C9-HRE-mediated gain-of-function mechanism.

In Chapter 4, we wanted to closely monitor the fate of poly-GA DPRs in either their oligomeric or fibrillized forms after administration in cell culture medium. In particular, we wanted to compare cellular uptake of recombinant poly-GA oligomers and fibrils to see if differences in the aggregation stage could lead to differences in cell entry. In a variety of cell culture systems (HeLa, HEK, human fibroblasts, iAstrocytes), we discovered that poly-GA oligomers are more easily taken up into large visible aggregates than poly-GA fibrils or other oligomeric species such as poly-PA. We then chose glial cells as our primary cellular system, specifically iAstrocytes. *C9ORF72*-derived DPR inclusions are much more abundant in neurons than glia in post-mortem ALS/FTD brains⁴⁷⁶. As a result, the non-cell autonomous role of glial pathological aggregates in the neuropathology of ALS/FTD is currently unknown. We went on to show that poly-GA DPRs are taken up by iAstrocytes via dynamin-dependent and -independent endocytosis, eventually converging at the lysosomal compartment. Interestingly, while a dynamin-specific inhibitor strongly inhibits the cellular entry of poly-GA fibrils, it has no effect on the entry of oligomeric poly-GA. Thus, fibrils seem highly susceptible to cell-mediated uptake, which is consistent with the behaviour of other fibrillar aggregates such as α -synuclein and tau^{545,600}. Despite a clear

endocytic contribution to fibrillary species uptake, other cell entry mechanisms cannot be ruled out. For example, because DPR fibrils were densely clustered at the plasma membrane at all times (6h, 24h, 48h), these species could puncture the plasma membrane thus accessing the cell; as shown for other pathological proteins ⁶⁰¹.

Overall, our findings in Chapter 4 emphasise the importance of endocytosis as a route of internalisation for DPRs, expanding on previous knowledge of DPR uptake, which was previously demonstrated only for poly-GR ⁵³⁶. Many extracellular or cell-surface macromolecules that are taken up by the endocytic pathway end up in lysosomes ⁶⁰². Because we discovered that cell-mediated uptake of poly-GA is mostly dependent on endocytosis, we wanted to see if these species would be degraded by astrocyte proteolytic systems. According to our findings, 20% of GA fibrils but only 5% of GA oligomers co-localized with lysosomes. As a result, we hypothesise that oligomeric poly-GA assemblies may evade the endolysosomal system, avoiding internalisation and lysosomal surveillance; a feature that has been linked to toxicity of certain oligomers ¹⁷⁷.

Inducing lysosomal membrane damage is one of the proposed mechanisms for avoiding lysosomal degradation, and this is a topic covered in Chapter 5. There has been little research into the ability of exogenous DPR to cause lysosomal damage after cell entry. The only study that shows the effects of DPR uptake on cell functionality is the work of Zhou and colleagues which revealed that exposure to recombinant poly-GA increases repeat RNA levels and seeds aggregation of all DPR proteins in cells expressing a C9-HRE ⁶⁰³. Our findings do not indicate any obvious lysosomal damage mechanism triggered by poly-GA DPR exposure; however, we show that poly-GA may impair lysosomal acidification.

In the final section of Chapter 5, we looked into whether poly-GA DPRs could undergo cell-to-cell transfer. We used a co-culture system to show astrocyte-to-motor neuron DPR propagation, implying that astrocytes may serve as hubs for the internalisation and release of abnormal peptides during disease pathogenesis.

The key results of this PhD research project are highlighted in **Figure 6.1**.

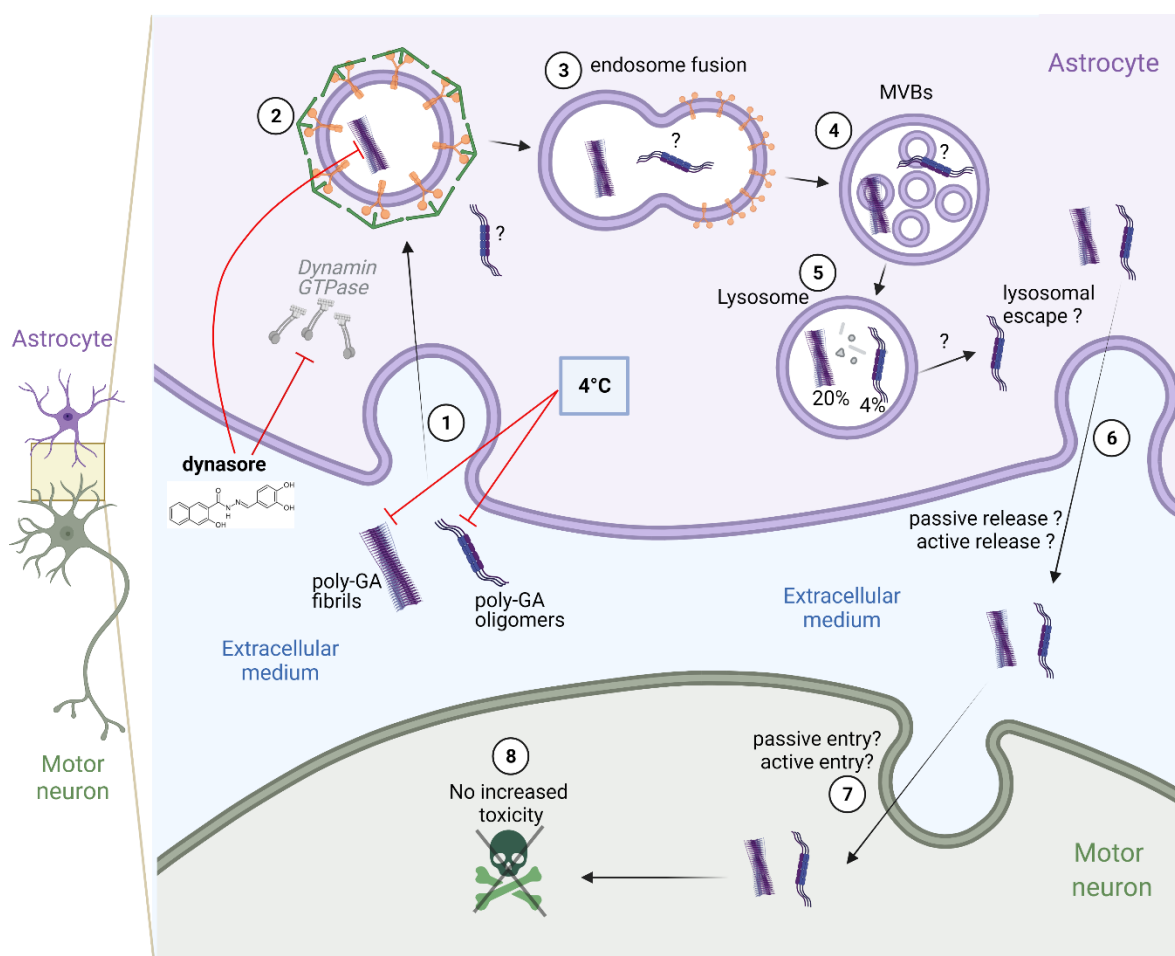


Figure 6.1 Project outcomes and highlights

Schematic illustration summarising the main outcomes of this project. We closely monitored the fate of poly-GA DPRs in either their oligomeric or fibrillized forms in iAstrocytes after administration in cell culture medium. In iAstrocytes, a general block of most endocytic pathways (via 4°C incubation) reduces the uptake of both poly-GA fibrils and poly-GA oligomers. However, the compound dynasore (a GTPase dynamin inhibitor) only reduces the uptake of poly-GA fibrils but not poly-GA oligomers, implying that the same DPR species but at different stages of amyloid formation can use different cell entry pathways. Both poly-GA DPRs eventually converge at the lysosomal compartment in iAstrocytes – and cause lysosomal swelling in neurons (not shown). Interestingly, when we used a co-culture system between astrocytes and motor neurons, we discovered astrocyte-to-motor neuron DPR propagation, indicating that astrocytes may act as hubs for the internalisation and release of aberrant peptides in disease pathogenesis; however, no apparent increase in toxicity was observed in our experiments.

6.2 Future directions and main challenges

The most exciting studies demonstrating the critical role of astrocytes in ALS-FTD neuropathology were carried out by looking at ALS-associated mutations. Numerous cell culture and *in vivo* studies have revealed that astrocytes from various ALS models contribute to motor neuron death^{294,295,453,562–566}. Non-cell autonomous effects of SOD1 mutations in astrocytes are required for motor neuron death in mice^{604,605}, as restricted expression of mutant SOD1 in neurons is insufficient⁶⁰⁶.

My thesis work highlights the importance of non-cell autonomous mechanisms in C9 ALS/FTD by demonstrating that astrocytes can spread poly-GA DPRs to motor neurons in cell culture. However, it is unclear how the astrocyte-to-neuron spread plays a role in disease because we found no evidence of toxicity in motor neurons where the poly-GA was transmitted. *In vivo* studies will be required to clarify the role of glial-specific DPR aggregation as a potential contributor to neurotoxicity, as cell culture studies are frequently limited by their relatively simple environment, which lacks other cell components or adaptive immune responses⁶⁰⁷ that could influence complex processes like cell-to-cell transmission. All of these processes may be influenced further by ageing and the disease penetrance of certain ALS/FTD mutations, such as the C9-HRE, which was extensively discussed in the Introduction chapters. An intriguing line of research would be to investigate whether recombinant DPRs injected in a localised area of the brain in a mouse (i.e., via intracranial stereotaxic injection) could further spread and extend in other neuroanatomical regions, and whether this would be influenced by DPR-repeat length, mouse age, and the presence or absence of C9-HRE in these mice. These studies were discussed during my PhD project but were not pursued due to time constraints, most of which were caused by the COVID-19 pandemic. It is significant to note that Virginia Lee's seminal research established that injecting recombinant human α -syn fibrils is completely sufficient to cause Lewy bodies and Lewy neurites far from the injection sites (striatum and cortex) and to start the disease *in vivo* in M83 transgenic mice (these mice express the mutant human A53T α -syn under the mouse prion protein promoter)⁶⁰⁸. What is perhaps even more remarkable is the evidence that intrastriatal injection of mouse recombinant α -syn fibrils in wild-type nontransgenic mice can seed the aggregation of endogenous mouse α -syn and cause Parkinson's-like Lewy pathology in interconnected brain areas, progressive loss of dopamine

neurons in the substantia nigra pars compacta, and reduced dopamine levels culminating in a few motor deficits⁹⁷. These two landmark investigations by Virginia Lee's team may serve as the impetus for further research into the potential prion-like propagation properties of poly-GA and other DPRs in mice or other mammals. However, it is important to note that these experiments would necessitate C9-HRE-expressing animals because the injected seeds (e.g., poly-GA recombinant fibrils) would require a substrate for the spread of aggregation and, possibly, the start of a neurodegenerative cascade. The extent to which the selection of a specific C9-HRE-expressing animal model would influence the outcome of these experiments is unknown. As previously stated, C9-500 BAC mice recapitulate the molecular hallmarks of C9 ALS/FTD, such as the presence of RNA foci and dipeptide repeat proteins, but fail to consistently show disease-associated behavioural phenotypes, neurodegeneration and decreased survival^{395,396,398}. Furthermore, these mice still carry the entire murine C9ORF72 gene, as well as the inserted "partial"³⁹⁶ or "full"^{395,397,398} human C9ORF72 gene, and it's unclear whether the C9-HRE can successfully drive C9 haploinsufficiency of both the murine and human genes, therefore all loss-of-function pathogenic mechanisms are unlikely to be replicated by these mouse models. The use of C9-HRE-expressing animal models developed by the Cleveland group could potentially better recapitulate both gain-of-function and loss-of-function pathogenicity mechanisms of the C9-HRE⁴⁴²; in fact, these mice were created by breeding (i) C9ORF72 knockout mice to (ii) BAC transgenic mice expressing a portion of the C9ORF72 gene (with 450 repeat expansions) that does not encode the 54 kD C9orf72 protein. Because a number of studies have recently proposed that C9ORF72 haploinsufficiency-driven autophagy dysregulation synergizes with DPR gain-of-function toxicity^{366,441,442}, it is likely that the Cleveland mouse model⁴⁴² would be more informative for addressing the aforementioned experiments looking at the potential prion-like propagation properties of poly-GA and other DPRs.

In conclusion, progress in defeating ALS/FTD is not helped by polarized yes–no debates, which have previously paralysed the field. Decades of research have revealed the complexities of these devastating diseases, as well as the wide range of disease manifestations and progression. This complexity, which appears insurmountable even with today's cutting-edge technologies, stems from the fact that the majority of ALS and FTD cases are reported as sporadic and linked to environmental risk factors that are still being investigated. Previous studies have also suggested an oligogenic and/or polygenic basis for ALS, where multiple ALS gene variants have been identified in both familial and sporadic cases and are thought to act together to cause ALS or influence clinical manifestations.

Although the frequency of oligogenic contributions appears to be low, we cannot rule out the presence of additional genetic risks or variants that have not yet been identified and might act in concert to cause disease or influence its progression. This complex genetic architecture of ALS, and potentially FTD, complicates therapeutic approaches, which would have to target multiple mutation-derived pathological mechanisms, each of which may act differently or have different penetrance from one individual to the next. Recruitment of patients into clinical trials is complicated by the strong heterogeneity of disease progression and manifestations, as well as the different disease penetrance of important mutations such as the C9-HRE; additionally, ageing, environmental, lifestyle, and geographically based risk factors complicate clinical trials and may confound drug efficacy results. ALS and FTD are complex disorders that frequently coexist, and akin to cancer, it is unlikely that a single simple hypothesis and a single silver bullet will explain and treat all.

Overall, our findings shed light on the uptake and release pathways of poly-GA DPRs in astrocytes and, to a lesser extent, neurons. We propose that astrocytes play a role in the transmission of DPRs to neighbouring motor neurons, which could be a non-cell autonomous contributor to the neuropathology of C9 ALS/FTD. We hope that this basic research into pathophysiological mechanisms will help to elucidate druggable molecular pathways for future therapies. The sole nature of cell culture observations was a significant limitation of our work; these are extremely useful for rapidly investigating potential molecular mechanisms driven by poly-GA DPRs but would need to be confirmed in animal studies, as previously discussed.

7. References

1. Waudby, C. A., Dobson, C. M. & Christodoulou, J. Nature and Regulation of Protein Folding on the Ribosome. *Trends Biochem. Sci.* **44**, 914–926 (2019).
2. Olzmann, J. A., Kopito, R. R. & Christianson, J. C. The Mammalian Endoplasmic Reticulum-Associated Degradation System. *Cold Spring Harb. Perspect. Biol.* **5**, a013185–a013185 (2013).
3. Hipp, M. S., Park, S.-H. & Hartl, F. U. Proteostasis impairment in protein-misfolding and -aggregation diseases. *Trends Cell Biol.* **24**, 506–514 (2014).
4. Hetz, C. & Papa, F. R. The Unfolded Protein Response and Cell Fate Control. *Mol. Cell* **69**, 169–181 (2018).
5. Jackson, M. P. & Hewitt, E. W. Cellular proteostasis: degradation of misfolded proteins by lysosomes. *Essays Biochem.* **60**, 173–180 (2016).
6. Hartl, F. U., Bracher, A. & Hayer-Hartl, M. Molecular chaperones in protein folding and proteostasis. *Nature* **475**, 324–332 (2011).
7. Hwang, J. & Qi, L. Quality Control in the Endoplasmic Reticulum: Crosstalk between ERAD and UPR pathways. *Trends Biochem. Sci.* **43**, 593–605 (2018).
8. Lu, M., Boschetti, C. & Tunnacliffe, A. Long Term Aggresome Accumulation Leads to DNA Damage, p53-dependent Cell Cycle Arrest, and Steric Interference in Mitosis. *J. Biol. Chem.* **290**, 27986–28000 (2015).
9. Shearman, M. S., Ragan, C. I. & Iversen, L. L. Inhibition of PC12 cell redox activity is a specific, early indicator of the mechanism of beta-amyloid-mediated cell death. *Proc. Natl. Acad. Sci.* **91**, 1470–1474 (1994).
10. Wang, W. *et al.* The ALS disease-associated mutant TDP-43 impairs mitochondrial dynamics and function in motor neurons. *Hum. Mol. Genet.* **22**, 4706–4719 (2013).
11. Jiang, L.-L., Guan, W.-L., Wang, J.-Y., Zhang, S.-X. & Hu, H.-Y. RNA-assisted sequestration of RNA-binding proteins by cytoplasmic inclusions of the C-terminal 35-kDa fragment of TDP-43. *J. Cell Sci.* (2022) doi:10.1242/jcs.259380.
12. Moller, A., Bauer, C. S., Cohen, R. N., Webster, C. P. & De Vos, K. J. Amyotrophic lateral sclerosis-associated mutant SOD1 inhibits anterograde axonal transport of mitochondria by reducing Miro1 levels. *Hum. Mol. Genet.* **26**, 4668–4679 (2017).
13. Wang, P. & Ye, Y. Filamentous recombinant human Tau activates primary astrocytes via an integrin receptor complex. *Nat. Commun.* **12**, 95 (2021).
14. Zhou, Q. *et al.* Active poly-GA vaccination prevents microglia activation and motor deficits in a C9orf72 mouse model. *EMBO Mol. Med.* **12**, 1–13 (2020).
15. Bourdenx, M. *et al.* Protein aggregation and neurodegeneration in prototypical neurodegenerative diseases: Examples of amyloidopathies, tauopathies and synucleinopathies. *Prog. Neurobiol.* **155**, 171–193 (2017).
16. Ross, C. A. & Poirier, M. A. What is the role of protein aggregation in neurodegeneration? *Nat. Rev. Mol. Cell Biol.* **6**, 891–898 (2005).
17. Dobson, C. M. The amyloid phenomenon and its links with human disease. *Cold Spring Harb. Perspect. Biol.* **9**, 1–14 (2017).
18. Sachse, C., Fandrich, M. & Grigorieff, N. Paired-sheet structure of an A β (1-40) amyloid fibril revealed by electron microscopy. *Proc. Natl. Acad. Sci.* **105**, 7462–7466 (2008).
19. Shodai, A. *et al.* Aberrant assembly of RNA recognition motif 1 links to pathogenic conversion of TAR DNA-binding protein of 43 kDa (TDP-43). *J. Biol. Chem.* **288**, 14886–14905 (2013).
20. Fitzpatrick, A. W. P. *et al.* Cryo-EM structures of tau filaments from Alzheimer’s disease. *Nature* **547**, 185–190 (2017).
21. Bresseur, L., Coens, A., Waeytens, J., Melki, R. & Bousset, L. Dipeptide repeat derived from C9orf72 hexanucleotide expansions forms amyloids or natively unfolded structures in vitro. *Biochem. Biophys. Res. Commun.* 0–6 (2020) doi:10.1016/j.bbrc.2020.03.108.
22. Sunde, M. & Blake, C. The Structure of Amyloid Fibrils by Electron Microscopy and X-Ray Diffraction. in *Advances in Protein Chemistry Volume 50* 123–159 (Elsevier, 1997). doi:10.1016/S0065-3233(08)60320-4.
23. Maji, S. K., Wang, L., Greenwald, J. & Riek, R. Structure-activity relationship of amyloid fibrils. *FEBS Lett.* **583**, 2610–2617 (2009).

24. Knowles, T. P. *et al.* Role of intermolecular forces in defining material properties of protein nanofibrils. *Science* (80-.). **318**, 1900–1903 (2007).
25. Cheng, P. N., Pham, J. D. & Nowick, J. S. The supramolecular chemistry of β -sheets. *J. Am. Chem. Soc.* **135**, 5477–5492 (2013).
26. Howie, A. J. Origins of a pervasive, erroneous idea: The “green birefringence” of Congo red-stained amyloid. *Int. J. Exp. Pathol.* **100**, 208–221 (2019).
27. Sipe, J. D. *et al.* Amyloid fibril proteins and amyloidosis: chemical identification and clinical classification International Society of Amyloidosis 2016 Nomenclature Guidelines. *Amyloid* **23**, 209–213 (2016).
28. Iadanza, M. G., Jackson, M. P., Hewitt, E. W., Ranson, N. A. & Radford, S. E. A new era for understanding amyloid structures and disease. *Nat. Rev. Mol. Cell Biol.* **19**, 755–773 (2018).
29. Karran, E., Mercken, M. & Strooper, B. De. The amyloid cascade hypothesis for Alzheimer’s disease: an appraisal for the development of therapeutics. *Nat. Rev. Drug Discov.* **10**, 698–712 (2011).
30. Goate, A. *et al.* Segregation of a missense mutation in the amyloid precursor protein gene with familial Alzheimer’s disease. *Nature* **349**, 704–706 (1991).
31. Sherrington, R. *et al.* Cloning of a gene bearing missense mutations in early-onset familial Alzheimer’s disease. *Nature* **375**, 754–760 (1995).
32. Rogaev, E. I. *et al.* Familial Alzheimer’s disease in kindreds with missense mutations in a gene on chromosome 1 related to the Alzheimer’s disease type 3 gene. *Nature* **376**, 775–778 (1995).
33. Jonsson, T. *et al.* A mutation in APP protects against Alzheimer’s disease and age-related cognitive decline. *Nature* **488**, 96–99 (2012).
34. Caughey, B. & Lansbury, P. T. Protofibrils, poires, fibrils, and neurodegeneration: separating the responsible protein aggregates from the innocent bystanders. *Annu. Rev. Neurosci.* **26**, 267–298 (2003).
35. Haass, C. & Selkoe, D. J. Soluble protein oligomers in neurodegeneration: lessons from the Alzheimer’s amyloid β -peptide. *Nat. Rev. Mol. Cell Biol.* **8**, 101–112 (2007).
36. Walsh, D. M. *et al.* Naturally secreted oligomers of amyloid β protein potently inhibit hippocampal long-term potentiation in vivo. *Nature* **416**, 535–539 (2002).
37. Cremades, N. *et al.* Direct Observation of the Interconversion of Normal and Toxic Forms of α -Synuclein. *Cell* **149**, 1048–1059 (2012).
38. Campioni, S. *et al.* A causative link between the structure of aberrant protein oligomers and their toxicity. *Nat. Chem. Biol.* **6**, 140–147 (2010).
39. Uhlmann, R. E. *et al.* Acute targeting of pre-amyloid seeds in transgenic mice reduces Alzheimer-like pathology later in life. *Nat. Neurosci.* **23**, 1580–1588 (2020).
40. McDade, E. *et al.* Longitudinal cognitive and biomarker changes in dominantly inherited Alzheimer disease. *Neurology* **91**, e1295–e1306 (2018).
41. Villemagne, V. L., Doré, V., Burnham, S. C., Masters, C. L. & Rowe, C. C. Imaging tau and amyloid- β proteinopathies in Alzheimer disease and other conditions. *Nat. Rev. Neurol.* **14**, 225–236 (2018).
42. Braak, H., Thal, D. R., Ghebremedhin, E. & Del Tredici, K. Stages of the Pathologic Process in Alzheimer Disease: Age Categories From 1 to 100 Years. *J. Neuropathol. Exp. Neurol.* **70**, 960–969 (2011).
43. Pletnikova, O. *et al.* Alzheimer Lesions in the Autopsied Brains of People 30 to 50 Years of Age. *Cogn. Behav. Neurol.* **28**, 144–152 (2015).
44. Doody, R. S. *et al.* Phase 3 Trials of Solanezumab for Mild-to-Moderate Alzheimer’s Disease. *N. Engl. J. Med.* **370**, 311–321 (2014).
45. Honig, L. S. *et al.* Trial of Solanezumab for Mild Dementia Due to Alzheimer’s Disease. *N. Engl. J. Med.* **378**, 321–330 (2018).
46. Hong, W. *et al.* Diffusible, highly bioactive oligomers represent a critical minority of soluble A β in Alzheimer’s disease brain. *Acta Neuropathol.* **136**, 19–40 (2018).
47. Benilova, I., Karran, E. & De Strooper, B. The toxic A β oligomer and Alzheimer’s disease: An emperor in need of clothes. *Nature Neuroscience* vol. 15 349–357 (2012).
48. Yang, T., Li, S., Xu, H., Walsh, D. M. & Selkoe, D. J. Large Soluble Oligomers of Amyloid β -Protein from Alzheimer Brain Are Far Less Neuroactive Than the Smaller Oligomers to Which They Dissociate. *J. Neurosci.* **37**, 152–163 (2017).
49. Amar, F. *et al.* The amyloid- β oligomer A β *56 induces specific alterations in neuronal signaling that lead to tau phosphorylation and aggregation. *Sci. Signal.* **10**, (2017).
50. Karran, E. & De Strooper, B. The amyloid hypothesis in Alzheimer disease: new insights from new

- therapeutics. *Nat. Rev. Drug Discov.* (2022) doi:10.1038/s41573-022-00391-w.
51. Alexander, G. C. *et al.* Revisiting FDA Approval of Aducanumab. *N. Engl. J. Med.* **385**, 769–771 (2021).
 52. Perlmutter, J. S. FDA’s green light, science’s red light. *Science* (80-.). **372**, 1371–1371 (2021).
 53. Mullard, A. Landmark Alzheimer’s drug approval confounds research community. *Nature* **594**, 309–310 (2021).
 54. Lalli, G., Schott, J. M., Hardy, J. & De Strooper, B. Aducanumab: a new phase in therapeutic development for Alzheimer’s disease? *EMBO Mol. Med.* **13**, 2–4 (2021).
 55. Rijal Upadhaya, A. *et al.* Biochemical stages of amyloid- β peptide aggregation and accumulation in the human brain and their association with symptomatic and pathologically preclinical Alzheimer’s disease. *Brain* **137**, 887–903 (2014).
 56. Nyström, S. *et al.* Evidence for Age-Dependent in Vivo Conformational Rearrangement within A β Amyloid Deposits. *ACS Chem. Biol.* **8**, 1128–1133 (2013).
 57. Braak, H. & Braak, E. Staging of alzheimer’s disease-related neurofibrillary changes. *Neurobiol. Aging* **16**, 271–278 (1995).
 58. Braak, H. *et al.* Amyotrophic lateral sclerosis—a model of corticofugal axonal spread. *Nat. Rev. Neurol.* **9**, 708–714 (2013).
 59. Braak, H. & Braak, E. Neuropathological staging of Alzheimer-related changes. *Acta Neuropathol.* **82**, 239–259 (1991).
 60. Stephenson, J. Nobel Prize to Stanley Prusiner for prion discovery. *JAMA* **278**, 1479 (1997).
 61. Prusiner, S. Novel proteinaceous infectious particles cause scrapie. *Science* (80-.). **216**, 136–144 (1982).
 62. Bolton, D. C., McKinley, M. P. & Prusiner, S. B. Identification of a Protein That Purifies with the Scrapie Prion. *Science* (80-.). **218**, 1309–1311 (1982).
 63. Büeler, H. *et al.* Mice devoid of PrP are resistant to scrapie. *Cell* **73**, 1339–1347 (1993).
 64. Scheckel, C. & Aguzzi, A. Prions, prionoids and protein misfolding disorders. *Nat. Rev. Genet.* **19**, 405–418 (2018).
 65. Brown, P., Cathala, F., Castaigne, P. & Gajdusek, D. C. Creutzfeldt-Jakob disease: Clinical analysis of a consecutive series of 230 neuropathologically verified cases. *Ann. Neurol.* **20**, 597–602 (1986).
 66. Puoti, G. *et al.* Sporadic human prion diseases: molecular insights and diagnosis. *Lancet Neurol.* **11**, 618–628 (2012).
 67. Beekes, M., Thomzig, A., Schulz-Schaeffer, W. J. & Burger, R. Is there a risk of prion-like disease transmission by Alzheimer- or Parkinson-associated protein particles? *Acta Neuropathol.* **128**, 463–476 (2014).
 68. Colby, D. W. & Prusiner, S. B. Prions. *Cold Spring Harb. Perspect. Biol.* **3**, a006833 (2011).
 69. Frost, B. & Diamond, M. I. Prion-like mechanisms in neurodegenerative diseases. *Nat. Rev. Neurosci.* **11**, 155–159 (2010).
 70. Brandner, S. *et al.* Normal host prion protein necessary for scrapie-induced neurotoxicity. *Nature* **379**, 339–343 (1996).
 71. Sailer, A. No propagation of prions in mice devoid of PrP. *Cell* **77**, 967–968 (1994).
 72. Frost, B. & Diamond, M. I. Prion-like mechanisms in neurodegenerative diseases. *Nature Reviews Neuroscience* vol. 11 155–159 (2010).
 73. Brundin, P., Melki, R. & Kopito, R. Prion-like transmission of protein aggregates in neurodegenerative diseases. *Nat. Rev. Mol. Cell Biol.* **11**, 301–307 (2010).
 74. Lauwers, E. *et al.* Potential human transmission of amyloid β pathology: surveillance and risks. *Lancet Neurol.* **19**, 872–878 (2020).
 75. Purro, S. A. *et al.* Transmission of amyloid- β protein pathology from cadaveric pituitary growth hormone. *Nature* **564**, 415–419 (2018).
 76. Renner, M. *et al.* Deleterious Effects of Amyloid β Oligomers Acting as an Extracellular Scaffold for mGluR5. *Neuron* **66**, 739–754 (2010).
 77. Zhao, Y. *et al.* Amyloid Beta Peptides Block New Synapse Assembly by Nogo Receptor-Mediated Inhibition of T-Type Calcium Channels. *Neuron* **96**, 355–372.e6 (2017).
 78. Cascella, R. *et al.* Soluble Oligomers Require a Ganglioside to Trigger Neuronal Calcium Overload. *J. Alzheimer’s Dis.* **60**, 923–938 (2017).
 79. Eisele, Y. S. *et al.* Induction of cerebral β -amyloidosis: Intracerebral versus systemic A β inoculation.

- Proc. Natl. Acad. Sci.* **106**, 12926–12931 (2009).
80. Eisele, Y. S. *et al.* Peripherally Applied A β -Containing Inoculates Induce Cerebral β -Amyloidosis. *Science* (80-.). **330**, 980–982 (2010).
 81. Nath, S. *et al.* Spreading of Neurodegenerative Pathology via Neuron-to-Neuron Transmission of β -Amyloid. *J. Neurosci.* **32**, 8767–8777 (2012).
 82. Domert, J. *et al.* Spreading of amyloid- β peptides via neuritic cell-to-cell transfer is dependent on insufficient cellular clearance. *Neurobiol. Dis.* **65**, 82–92 (2014).
 83. Song, H.-L. *et al.* β -Amyloid is transmitted via neuronal connections along axonal membranes. *Ann. Neurol.* **75**, 88–97 (2014).
 84. Roos, T. T. *et al.* Neuronal spreading and plaque induction of intracellular A β and its disruption of A β homeostasis. *Acta Neuropathol.* **142**, 669–687 (2021).
 85. Olsson, T. T., Klementieva, O. & Gouras, G. K. Prion-like seeding and nucleation of intracellular amyloid- β . *Neurobiol. Dis.* **113**, 1–10 (2018).
 86. Aoyagi, A. *et al.* A β and tau prion-like activities decline with longevity in the Alzheimer’s disease human brain. *Sci. Transl. Med.* **11**, (2019).
 87. Kane, M. D. *et al.* Evidence for Seeding of β -Amyloid by Intracerebral Infusion of Alzheimer Brain Extracts in β -Amyloid Precursor Protein-Transgenic Mice. *J. Neurosci.* **20**, 3606–3611 (2000).
 88. Meyer-Luehmann, M. *et al.* Exogenous Induction of Cerebral β -Amyloidogenesis Is Governed by Agent and Host. *Science* (80-.). **313**, 1781–1784 (2006).
 89. Nonaka, T., Watanabe, S. T., Iwatsubo, T. & Hasegawa, M. Seeded aggregation and toxicity of α -synuclein and tau: Cellular models of neurodegenerative diseases. *J. Biol. Chem.* **285**, 34885–34898 (2010).
 90. Clavaguera, F. *et al.* Brain homogenates from human tauopathies induce tau inclusions in mouse brain. *Proc. Natl. Acad. Sci. U. S. A.* **110**, 9535–9540 (2013).
 91. Holmes, B. B. *et al.* Heparan sulfate proteoglycans mediate internalization and propagation of specific proteopathic seeds. *Proc. Natl. Acad. Sci. U. S. A.* **110**, (2013).
 92. Guo, J. L. & Lee, V. M.-Y. Seeding of Normal Tau by Pathological Tau Conformers Drives Pathogenesis of Alzheimer-like Tangles. *J. Biol. Chem.* **286**, 15317–15331 (2011).
 93. Sanders, D. W. *et al.* Distinct tau prion strains propagate in cells and mice and define different tauopathies. *Neuron* **82**, 1271–1288 (2014).
 94. Boluda, S. *et al.* Differential induction and spread of tau pathology in young PS19 tau transgenic mice following intracerebral injections of pathological tau from Alzheimer’s disease or corticobasal degeneration brains. *Acta Neuropathol.* **129**, 221–237 (2015).
 95. Desplats, P. *et al.* Inclusion formation and neuronal cell death through neuron-to-neuron transmission of α -synuclein. *Proc. Natl. Acad. Sci.* **106**, 13010–13015 (2009).
 96. Volpicelli-Daley, L. A. *et al.* Exogenous α -synuclein fibrils induce Lewy body pathology leading to synaptic dysfunction and neuron death. *Neuron* **72**, 57–71 (2011).
 97. Luk, K. C. *et al.* Pathological α -Synuclein Transmission Initiates Parkinson-like Neurodegeneration in Nontransgenic Mice. *Science* (80-.). **338**, 949–953 (2012).
 98. Danzer, K. M., Krebs, S. K., Wolff, M., Birk, G. & Hengerer, B. Seeding induced by α -synuclein oligomers provides evidence for spreading of α -synuclein pathology. *J. Neurochem.* **111**, 192–203 (2009).
 99. Loria, F. *et al.* α -Synuclein transfer between neurons and astrocytes indicates that astrocytes play a role in degradation rather than in spreading. *Acta Neuropathol.* **134**, 789–808 (2017).
 100. Luk, K. C. *et al.* Exogenous α -synuclein fibrils seed the formation of Lewy body-like intracellular inclusions in cultured cells. *Proc. Natl. Acad. Sci.* **106**, 20051–20056 (2009).
 101. Hansen, C. *et al.* α -Synuclein propagates from mouse brain to grafted dopaminergic neurons and seeds aggregation in cultured human cells. *J. Clin. Invest.* **121**, 715–25 (2011).
 102. Kordower, J. H., Chu, Y., Hauser, R. A., Freeman, T. B. & Olanow, C. W. Lewy body-like pathology in long-term embryonic nigral transplants in Parkinson’s disease. *Nat. Med.* **14**, 504–506 (2008).
 103. Li, J.-Y. *et al.* Lewy bodies in grafted neurons in subjects with Parkinson’s disease suggest host-to-graft disease propagation. *Nat. Med.* **14**, 501–503 (2008).
 104. Rey, N. L. *et al.* Widespread transneuronal propagation of α -synucleinopathy triggered in olfactory bulb mimics prodromal Parkinson’s disease. *J. Exp. Med.* **213**, 1759–1778 (2016).
 105. Herrera, F., Tenreiro, S., Miller-Fleming, L. & Outeiro, T. F. Visualization of cell-to-cell transmission of mutant huntingtin oligomers. *PLoS Curr.* **3**, RRN1210 (2011).

106. Babcock, D. T. & Ganetzky, B. Transcellular spreading of huntingtin aggregates in the *Drosophila* brain. *Proc. Natl. Acad. Sci.* **112**, E5427–E5433 (2015).
107. Pecho-Vrieseling, E. *et al.* Transneuronal propagation of mutant huntingtin contributes to non-cell autonomous pathology in neurons. *Nat. Neurosci.* **17**, 1064–72 (2014).
108. Ren, P.-H. *et al.* Cytoplasmic penetration and persistent infection of mammalian cells by polyglutamine aggregates. *Nat. Cell Biol.* **11**, 219–225 (2009).
109. Pearce, M. M. P., Spartz, E. J., Hong, W., Luo, L. & Kopito, R. R. Prion-like transmission of neuronal huntingtin aggregates to phagocytic glia in the *Drosophila* brain. *Nat. Commun.* **6**, 6768 (2015).
110. Benkler, C. *et al.* Aggregated SOD1 causes selective death of cultured human motor neurons. *Sci. Rep.* **8**, 1–14 (2018).
111. Prudencio, M., Durazo, A., Whitelegge, J. P. & Borchelt, D. R. An examination of wild-type SOD1 in modulating the toxicity and aggregation of ALS-associated mutant SOD1. *Hum. Mol. Genet.* **19**, 4774–4789 (2010).
112. Münch, C., O’Brien, J. & Bertolotti, A. Prion-like propagation of mutant superoxide dismutase-1 misfolding in neuronal cells. *Proc. Natl. Acad. Sci. U. S. A.* **108**, 3548–53 (2011).
113. Grad, L. I. *et al.* Intercellular propagated misfolding of wild-type Cu/Zn superoxide dismutase occurs via exosome-dependent and -independent mechanisms. *Proc. Natl. Acad. Sci. U. S. A.* **111**, 3620–5 (2014).
114. Ayers, J. I., Fromholt, S. E., O’neal, V. M., Diamond, J. H. & Borchelt, D. R. Prion-like propagation of mutant SOD1 misfolding and motor neuron disease spread along neuroanatomical pathways. *Acta Neuropathol* **3**, 103–114 (2016).
115. Grad, L. I. *et al.* Intermolecular transmission of superoxide dismutase 1 misfolding in living cells. *Proc. Natl. Acad. Sci.* **108**, 16398–16403 (2011).
116. Thomas, E. V., Fenton, W. A., McGrath, J. & Horwich, A. L. Transfer of pathogenic and nonpathogenic cytosolic proteins between spinal cord motor neurons in vivo in chimeric mice. *Proc. Natl. Acad. Sci.* **114**, E3139–E3148 (2017).
117. Yamashita, M. *et al.* Distinct pathways leading to TDP-43-induced cellular dysfunctions. *Hum. Mol. Genet.* **23**, 4345–4356 (2014).
118. Wils, H. *et al.* TDP-43 transgenic mice develop spastic paralysis and neuronal inclusions characteristic of ALS and frontotemporal lobar degeneration. *Proc. Natl. Acad. Sci.* **107**, 3858–3863 (2010).
119. Nonaka, T. *et al.* Prion-like Properties of Pathological TDP-43 Aggregates from Diseased Brains. *Cell Rep.* **4**, 124–134 (2013).
120. Feiler, M. S. *et al.* TDP-43 is intercellularly transmitted across axon terminals. *J. Cell Biol.* **211**, 897–911 (2015).
121. Smethurst, P. *et al.* Distinct responses of neurons and astrocytes to TDP-43 proteinopathy in amyotrophic lateral sclerosis. *Brain* **143**, 430–440 (2020).
122. Ding, X. *et al.* Spreading of TDP-43 pathology via pyramidal tract induces ALS-like phenotypes in TDP-43 transgenic mice. *Acta Neuropathol. Commun.* **9**, 15 (2021).
123. Shimonaka, S., Nonaka, T., Suzuki, G., Hisanaga, S. & Hasegawa, M. Templated Aggregation of TAR DNA-binding Protein of 43 kDa (TDP-43) by Seeding with TDP-43 Peptide Fibrils. *J. Biol. Chem.* **291**, 8896–8907 (2016).
124. Porta, S. *et al.* Patient-derived frontotemporal lobar degeneration brain extracts induce formation and spreading of TDP-43 pathology in vivo. *Nat. Commun.* **9**, 4220 (2018).
125. Chang, Y.-J., Jeng, U.-S., Chiang, Y.-L., Hwang, I.-S. & Chen, Y.-R. The Glycine-Alanine Dipeptide Repeat from C9orf72 Hexanucleotide Expansions Forms Toxic Amyloids Possessing Cell-to-Cell Transmission Properties. *J. Biol. Chem.* **291**, 4903–11 (2016).
126. Zhou, Q. *et al.* Antibodies inhibit transmission and aggregation of C9orf72 poly- GA dipeptide repeat proteins. *EMBO Mol. Med.* **9**, 687–702 (2017).
127. Nihei, Y. *et al.* Poly-glycine–alanine exacerbates C9orf72 repeat expansion-mediated DNA damage via sequestration of phosphorylated ATM and loss of nuclear hnRNPA3. *Acta Neuropathol.* **139**, 99–118 (2020).
128. LaClair, K. D. *et al.* Congenic expression of poly-GA but not poly-PR in mice triggers selective neuron loss and interferon responses found in C9orf72 ALS. *Acta Neuropathol.* 1–22 (2020) doi:10.1007/s00401-020-02176-0.
129. Nguyen, L. *et al.* Antibody Therapy Targeting RAN Proteins Rescues C9 ALS/FTD Phenotypes in C9orf72 Mouse Model. *Neuron* **105**, 645-662.e11 (2020).

130. Westergard, T. *et al.* Cell-to-Cell Transmission of Dipeptide Repeat Proteins Linked to C9orf72-ALS/FTD. *Cell Rep.* **17**, 645–652 (2016).
131. Morón-Oset, J. *et al.* Glycine-alanine dipeptide repeats spread rapidly in a repeat length- and age-dependent manner in the fly brain. *Acta Neuropathol. Commun.* **7**, 209 (2019).
132. Khosravi, B. *et al.* Cell-to-cell transmission of C9orf72 poly-(Gly-Ala) triggers key features of ALS / FTD. *EMBO J.* 1–19 (2020) doi:10.15252/embj.2019102811.
133. Guo, J. L. *et al.* Unique pathological tau conformers from Alzheimer’s brains transmit tau pathology in nontransgenic mice. *J. Exp. Med.* **213**, 2635–2654 (2016).
134. Luk, K. C. *et al.* Intracerebral inoculation of pathological α -synuclein initiates a rapidly progressive neurodegenerative α -synucleinopathy in mice. *J. Exp. Med.* **209**, 975–86 (2012).
135. Higuchi-Sanabria, R., Frankino, P. A., Paul, J. W., Tronnes, S. U. & Dillin, A. A Futile Battle? Protein Quality Control and the Stress of Aging. *Dev. Cell* **44**, 139–163 (2018).
136. Lin, M. & Beal, M. F. Mitochondrial dysfunction and oxidative stress in neurodegenerative diseases. *Nature* **443**, 787–795 (2006).
137. De Groot, N. S. & Burgas, M. T. Is membrane homeostasis the missing link between inflammation and neurodegenerative diseases? *Cell. Mol. Life Sci.* **72**, 4795–4805 (2015).
138. Patel, A. *et al.* A Liquid-to-Solid Phase Transition of the ALS Protein FUS Accelerated by Disease Mutation. *Cell* **162**, 1066–1077 (2015).
139. Fujikake, N., Shin, M. & Shimizu, S. Association between autophagy and neurodegenerative diseases. *Frontiers in Neuroscience* vol. 12 (2018).
140. Baradaran-Heravi, Y., Van Broeckhoven, C. & van der Zee, J. Stress granule mediated protein aggregation and underlying gene defects in the FTD-ALS spectrum. *Neurobiol. Dis.* **134**, 104639 (2020).
141. Currais, A., Fischer, W., Maher, P. & Schubert, D. Intraneuronal protein aggregation as a trigger for inflammation and neurodegeneration in the aging brain. *FASEB J.* **31**, 5–10 (2017).
142. Guerreiro, R. *et al.* TREM2 variants in Alzheimer’s disease. *N. Engl. J. Med.* **368**, 117–127 (2013).
143. Maday, S. & Holzbaur, E. L. F. Autophagosome assembly and cargo capture in the distal axon. *Autophagy* **8**, 858–860 (2012).
144. Feng, Y., He, D., Yao, Z. & Klionsky, D. J. The machinery of macroautophagy. *Cell Res.* **24**, 24–41 (2014).
145. Deter, R. L. & de Duve, C. Influence of glucagon, an inducer of cellular autophagy, on some physical properties of rat liver lysosomes. *J. Cell Biol.* **33**, 437–449 (1967).
146. Tsukada, M. & Ohsumi, Y. Isolation and characterization of autophagy-defective mutants of *Saccharomyces cerevisiae*. *FEBS Lett.* **333**, 169–174 (1993).
147. Harding, T. M., Morano, K. A., Scott, S. V & Klionsky, D. J. Isolation and characterization of yeast mutants in the cytoplasm to vacuole protein targeting pathway. *J. Cell Biol.* **131**, 591–602 (1995).
148. Schlumpberger, M. *et al.* AUT1, a gene essential for autophagocytosis in the yeast *Saccharomyces cerevisiae*. *J. Bacteriol.* **179**, 1068–1076 (1997).
149. Straub, M., Bredschneider, M. & Thumm, M. AUT3, a serine/threonine kinase gene, is essential for autophagocytosis in *Saccharomyces cerevisiae*. *J. Bacteriol.* **179**, 3875–3883 (1997).
150. Walker, S. A. & Ktistakis, N. T. Autophagosome Biogenesis Machinery. *J. Mol. Biol.* (2019) doi:10.1016/j.jmb.2019.10.027.
151. Mijaljica, D., Prescott, M. & Devenish, R. J. Microautophagy in mammalian cells: Revisiting a 40-year-old conundrum. *Autophagy* **7**, 673–682 (2011).
152. Kaushik, S. & Cuervo, A. M. The coming of age of chaperone-mediated autophagy. *Nat. Rev. Mol. Cell Biol.* **19**, 365–381 (2018).
153. Saftig, P. & Klumperman, J. Lysosome biogenesis and lysosomal membrane proteins: trafficking meets function. *Nat. Rev. Mol. Cell Biol.* **10**, 623–635 (2009).
154. Xu, H. & Ren, D. Lysosomal physiology. *Annu. Rev. Physiol.* **77**, 57–80 (2015).
155. Stoka, V., Turk, V. & Turk, B. Lysosomal cathepsins and their regulation in aging and neurodegeneration. *Ageing Res. Rev.* **32**, 22–37 (2016).
156. Suire, C. N. *et al.* Cathepsin D regulates cerebral A β 42/40 ratios via differential degradation of A β 42 and A β 40. *Alzheimers. Res. Ther.* **12**, 80 (2020).
157. McGlinchey, R. P. & Lee, J. C. Cysteine cathepsins are essential in lysosomal degradation of α -synuclein. *Proc. Natl. Acad. Sci.* **112**, 9322–9327 (2015).
158. Bhutani, N., Piccirillo, R., Hourez, R., Venkatraman, P. & Goldberg, A. L. Cathepsins L and Z Are

- Critical in Degrading Polyglutamine-containing Proteins within Lysosomes. *J. Biol. Chem.* **287**, 17471–17482 (2012).
159. Yadati, T., Houben, T., Bitorina, A. & Shiri-Sverdlov, R. The Ins and Outs of Cathepsins: Physiological Function and Role in Disease Management. *Cells* **9**, 1679 (2020).
 160. Kikuchi, H. *et al.* Involvement of cathepsin B in the motor neuron degeneration of amyotrophic lateral sclerosis. *Acta Neuropathol.* **105**, 462–468 (2003).
 161. Offen, D. *et al.* Spinal Cord mRNA Profile in Patients with ALS: Comparison with Transgenic Mice Expressing the Human SOD-1 Mutant. *J. Mol. Neurosci.* **38**, 85–93 (2009).
 162. Li, L. *et al.* Parkinson's disease involves autophagy and abnormal distribution of cathepsin L. *Neurosci. Lett.* **489**, 62–67 (2011).
 163. Ravikumar, B. Aggregate-prone proteins with polyglutamine and polyalanine expansions are degraded by autophagy. *Hum. Mol. Genet.* **11**, 1107–1117 (2002).
 164. Hara, T. *et al.* Suppression of basal autophagy in neural cells causes neurodegenerative disease in mice. *Nature* **441**, 885–889 (2006).
 165. Komatsu, M. *et al.* Loss of autophagy in the central nervous system causes neurodegeneration in mice. *Nature* **441**, 880–4 (2006).
 166. Komatsu, M. *et al.* Essential role for autophagy protein Atg7 in the maintenance of axonal homeostasis and the prevention of axonal degeneration. *Proc. Natl. Acad. Sci. U. S. A.* **104**, 14489–94 (2007).
 167. Ravikumar, B. *et al.* Inhibition of mTOR induces autophagy and reduces toxicity of polyglutamine expansions in fly and mouse models of Huntington disease. *Nat. Genet.* **36**, 585–595 (2004).
 168. Sarkar, S. *et al.* Small molecules enhance autophagy and reduce toxicity in Huntington's disease models. *Nat. Chem. Biol.* **3**, 331–338 (2007).
 169. Pyo, J.-O. *et al.* Overexpression of Atg5 in mice activates autophagy and extends lifespan. *Nat. Commun.* **4**, 2300 (2013).
 170. Barmada, S. J. *et al.* Autophagy induction enhances TDP43 turnover and survival in neuronal ALS models. *Nat. Chem. Biol.* **10**, 677–685 (2014).
 171. Cleeter, M. W. J. *et al.* Glucocerebrosidase inhibition causes mitochondrial dysfunction and free radical damage. *Neurochem. Int.* **62**, 1–7 (2013).
 172. Freeman, D. *et al.* Alpha-Synuclein Induces Lysosomal Rupture and Cathepsin Dependent Reactive Oxygen Species Following Endocytosis. *PLoS One* **8**, e62143 (2013).
 173. Serrano-Puebla, A. & Boya, P. Lysosomal membrane permeabilization in cell death: new evidence and implications for health and disease. *Ann. N. Y. Acad. Sci.* **1371**, 30–44 (2016).
 174. Annunziata, I. *et al.* Lysosomal NEU1 deficiency affects amyloid precursor protein levels and amyloid- β secretion via deregulated lysosomal exocytosis. *Nat. Commun.* **4**, 2734 (2013).
 175. Alvarez-Erviti, L. *et al.* Lysosomal dysfunction increases exosome-mediated alpha-synuclein release and transmission. *Neurobiol. Dis.* **42**, 360–367 (2011).
 176. Bae, E.-J. *et al.* Haploinsufficiency of cathepsin D leads to lysosomal dysfunction and promotes cell-to-cell transmission of α -synuclein aggregates. *Cell Death Dis.* **6**, e1901–e1901 (2015).
 177. Jiang, P., Gan, M., Yen, S.-H., McLean, P. J. & Dickson, D. W. Impaired endo-lysosomal membrane integrity accelerates the seeding progression of α -synuclein aggregates. *Sci. Rep.* **7**, 7690 (2017).
 178. Bourdenx, M., Bezard, E. & Dehay, B. Lysosomes and α -synuclein form a dangerous duet leading to neuronal cell death. *Front. Neuroanat.* **8**, 83 (2014).
 179. Baker, M. *et al.* Mutations in progranulin cause tau-negative frontotemporal dementia linked to chromosome 17. *Nature* **442**, 916–919 (2006).
 180. Cruts, M. *et al.* Null mutations in progranulin cause ubiquitin-positive frontotemporal dementia linked to chromosome 17q21. *Nature* **442**, 920–924 (2006).
 181. Neumann, M. *et al.* Ubiquitinated TDP-43 in frontotemporal lobar degeneration and amyotrophic lateral sclerosis. *Science (80-.)*. **314**, 130–133 (2006).
 182. Stagi, M., Klein, Z. A., Gould, T. J., Bewersdorf, J. & Strittmatter, S. M. Lysosome size, motility and stress response regulated by fronto-temporal dementia modifier TMEM106B. *Mol. Cell. Neurosci.* **61**, 226–240 (2014).
 183. Freischmidt, A. *et al.* Haploinsufficiency of TBK1 causes familial ALS and fronto-temporal dementia. *Nat. Neurosci.* **18**, 631–636 (2015).
 184. Pottier, C. *et al.* Whole-genome sequencing reveals important role for TBK1 and OPTN mutations in frontotemporal lobar degeneration without motor neuron disease. *Acta Neuropathol.* **130**, 77–92 (2015).
 185. Hao, J., Wells, M.F., Niu, G., San Juan, I.G., Limone, F., Fukuda, A., Leyton-Jaimes, M.F., Joseph,

- B., Qian, M., Mordes, D.A. and Budnik, B. Loss of TBK1 activity leads to TDP-43 proteinopathy through lysosomal dysfunction in human motor neurons. *bioRxiv* (2021) doi:https://doi.org/10.1101/2021.10.11.464011.
186. Maruyama, H. *et al.* Mutations of optineurin in amyotrophic lateral sclerosis. *Nature* **465**, 223–226 (2010).
 187. Sundaramoorthy, V. *et al.* Defects in optineurin- and myosin VI-mediated cellular trafficking in amyotrophic lateral sclerosis. *Hum. Mol. Genet.* **24**, 3830–3846 (2015).
 188. Bansal, M. *et al.* Optineurin promotes autophagosome formation by recruiting the autophagy-related Atg12-5-16L1 complex to phagophores containing the Wipi2 protein. *J. Biol. Chem.* **293**, 132–147 (2018).
 189. Korac, J. *et al.* Ubiquitin-independent function of optineurin in autophagic clearance of protein aggregates. *J. Cell Sci.* **126**, 580–592 (2013).
 190. Moharir, S. C., Raghawan, A. K., Ramaswamy, R. & Swarup, G. Autophagy-independent cytoprotection by optineurin from toxicity of aggregates formed by mutant huntingtin and mutant ataxin-3. *J. Biochem.* **171**, 555–565 (2022).
 191. Charcot, J. M. Deux cas d'atrophie musculaire progressive avec lesions de la substance grise et des faisceaux anterolateraux de la moelle epiniere. *Arch. Pathol. Norm. Pathol.* **2** 744–760 (1869).
 192. Goetz, C. G. Amyotrophic lateral sclerosis: Early contributions of Jean-Martin Charcot. *Muscle Nerve* **23**, 336–343 (2000).
 193. Norton, N. S. & Willett, G. Amyotrophic Lateral Sclerosis. in *xPharm: The Comprehensive Pharmacology Reference* 1–5 (Elsevier, 2007). doi:10.1016/B978-008055232-3.60661-0.
 194. Robinson, R. Iron horse: Lou Gehrig in his time. *WW Nort. Co.* (2006).
 195. Rowland, L. P. & Shneider, N. A. Amyotrophic Lateral Sclerosis. *N. Engl. J. Med.* **344**, 1688–1700 (2001).
 196. Brown, R. H. & Al-Chalabi, A. Amyotrophic Lateral Sclerosis. *N. Engl. J. Med.* **377**, 162–172 (2017).
 197. Goldstein, L. H. & Abrahams, S. Changes in cognition and behaviour in amyotrophic lateral sclerosis: nature of impairment and implications for assessment. *Lancet Neurol.* **12**, 368–380 (2013).
 198. Phukan, J. *et al.* The syndrome of cognitive impairment in amyotrophic lateral sclerosis: a population-based study. *J. Neurol. Neurosurg. Psychiatry* **83**, 102–108 (2012).
 199. Christensen, P. B., Højer-Pedersen, E. & Jensen, MD, N. B. Survival of patients with amyotrophic lateral sclerosis in 2 Danish counties. *Neurology* **40**, 600–600 (1990).
 200. Moura, M. C. *et al.* Prognostic Factors in Amyotrophic Lateral Sclerosis: A Population-Based Study. *PLoS One* **10**, e0141500 (2015).
 201. Mateen, F. J., Carone, M. & Sorenson, E. J. Patients who survive 5 years or more with ALS in Olmsted County, 1925–2004. *J. Neurol. Neurosurg. Psychiatry* **81**, 1144–1146 (2010).
 202. M R Turner , M J Parton, C E Shaw, P N Leigh, A. A.-C. Prolonged survival in motor neuron disease: a descriptive study of the King's database 1990–2002. *J. Neurol. Neurosurg. Psychiatry* **74**, 995–997 (2003).
 203. Bensimon, G., Lacomblez, L. & Meininger, V. A Controlled Trial of Riluzole in Amyotrophic Lateral Sclerosis. *N. Engl. J. Med.* **330**, 585–591 (1994).
 204. Abe, K. *et al.* Safety and efficacy of edaravone in well defined patients with amyotrophic lateral sclerosis: a randomised, double-blind, placebo-controlled trial. *Lancet Neurol.* **16**, 505–512 (2017).
 205. Niccoli, T., Partridge, L. & Isaacs, A. M. Ageing as a risk factor for ALS/FTD. *Hum. Mol. Genet.* **26**, R105–R113 (2017).
 206. Logroscino, G. *et al.* Incidence of amyotrophic lateral sclerosis in Europe. *J. Neurol. Neurosurg. Psychiatry* **81**, 385–390 (2010).
 207. Longinetti, E. *et al.* The Swedish motor neuron disease quality registry. *Amyotroph. Lateral Scler. Front. Degener.* **19**, 528–537 (2018).
 208. Benjaminsen, E., Alstadhaug, K. B., Gulsvik, M., Baloch, F. K. & Odeh, F. Amyotrophic lateral sclerosis in Nordland county, Norway, 2000–2015: prevalence, incidence, and clinical features. *Amyotroph. Lateral Scler. Front. Degener.* **19**, 522–527 (2018).
 209. Jun, K. Y. *et al.* Epidemiology of ALS in Korea using nationwide big data. *J. Neurol. Neurosurg. Psychiatry* **90**, 395–403 (2019).
 210. Dorst, J. *et al.* Prognostic factors in ALS: a comparison between Germany and China. *J. Neurol.* **266**, 1516–1525 (2019).
 211. Longinetti, E. & Fang, F. Epidemiology of amyotrophic lateral sclerosis: an update of recent literature.

- Curr. Opin. Neurol.* **32**, 771–776 (2019).
212. Alonso, A., Logroscino, G., Jick, S. S. & Hernán, M. A. Incidence and lifetime risk of motor neuron disease in the United Kingdom: a population-based study. *Eur. J. Neurol.* **16**, 745–751 (2009).
 213. Johnston, C. A. *et al.* Amyotrophic lateral sclerosis in an urban setting: A population based study of inner city London [2]. *Journal of Neurology* vol. 253 1642–1643 (2006).
 214. Lehky, T. & Grunseich, C. Juvenile Amyotrophic Lateral Sclerosis: A Review. *Genes (Basel)*. **12**, 1935 (2021).
 215. Cronin, S., Hardiman, O. & Traynor, B. J. Ethnic variation in the incidence of ALS. *Neurology* **68**, 1002–1007 (2007).
 216. Rechtman, L., Jordan, H., Wagner, L., Horton, D. K. & Kaye, W. Racial and ethnic differences among amyotrophic lateral sclerosis cases in the United States. *Amyotroph. Lateral Scler. Front. Degener.* **16**, 65–71 (2015).
 217. Lasser, K. E., Himmelstein, D. U. & Woolhandler, S. Access to care, health status, and health disparities in the United States and Canada: results of a cross-national population-based survey. *Am. J. Public Health* **96**, 1300–7 (2006).
 218. Müller, K. *et al.* De novo mutations in SOD1 are a cause of ALS. *J. Neurol. Neurosurg. Psychiatry* **93**, 201–206 (2022).
 219. Morrice, J. R., Shaw, C. A. & Gregory-Evans, C. Y. Susceptibility Genes and Epigenetics in Sporadic ALS. in *Spectrums of Amyotrophic Lateral Sclerosis* 35–56 (Wiley, 2021). doi:10.1002/9781119745532.ch3.
 220. Wang, H. *et al.* Smoking and Risk of Amyotrophic Lateral Sclerosis. *Arch. Neurol.* **68**, (2011).
 221. Weisskopf, M. G. *et al.* Prospective study of military service and mortality from ALS. *Neurology* **64**, 32–37 (2005).
 222. Fang, F., Ingre, C., Roos, P., Kamel, F. & Piehl, F. Risk factors for amyotrophic lateral sclerosis. *Clin. Epidemiol.* 181 (2015) doi:10.2147/CLEP.S37505.
 223. Julian, T. H. *et al.* Physical exercise is a risk factor for amyotrophic lateral sclerosis: Convergent evidence from Mendelian randomisation, transcriptomics and risk genotypes. *EBioMedicine* **68**, 103397 (2021).
 224. Wang, M.-D., Little, J., Gomes, J., Cashman, N. R. & Krewski, D. Identification of risk factors associated with onset and progression of amyotrophic lateral sclerosis using systematic review and meta-analysis. *Neurotoxicology* **61**, 101–130 (2017).
 225. Seals, R. M., Hansen, J., Gredal, O. & Weisskopf, M. G. Physical Trauma and Amyotrophic Lateral Sclerosis: A Population-Based Study Using Danish National Registries. *Am. J. Epidemiol.* **183**, 294–301 (2016).
 226. Al-Chalabi, A. *et al.* The epidemiology of ALS: a conspiracy of genes, environment and time. *Nat. Rev. Neurol.* **9**, 617–628 (2013).
 227. Boylan, K. Familial Amyotrophic Lateral Sclerosis. *Neurol. Clin.* **33**, 807–830 (2015).
 228. Volk, A. E., Weishaupt, J. H., Andersen, P. M., Ludolph, A. C. & Kubisch, C. Current knowledge and recent insights into the genetic basis of amyotrophic lateral sclerosis. *Medizinische Genet.* **30**, 252–258 (2018).
 229. van Blitterswijk, M. *et al.* Evidence for an oligogenic basis of amyotrophic lateral sclerosis. *Hum. Mol. Genet.* **21**, 3776–3784 (2012).
 230. Abel, O., Powell, J. F., Andersen, P. M. & Al-Chalabi, A. ALSod: A user-friendly online bioinformatics tool for amyotrophic lateral sclerosis genetics. *Hum. Mutat.* **33**, 1345–1351 (2012).
 231. Renton, A. E., Chiò, A. & Traynor, B. J. State of play in amyotrophic lateral sclerosis genetics. *Nat. Neurosci.* **17**, 17–23 (2014).
 232. Rosen, D. R. *et al.* Mutations in Cu/Zn superoxide dismutase gene are associated with familial amyotrophic lateral sclerosis. *Nature* **362**, 59–62 (1993).
 233. Sreedharan, J. *et al.* TDP-43 mutations in familial and sporadic amyotrophic lateral sclerosis. *Science (80-.)*. **319**, 1668–1672 (2008).
 234. Kabashi, E. *et al.* TARDBP mutations in individuals with sporadic and familial amyotrophic lateral sclerosis. *Nat. Genet.* **40**, 572–574 (2008).
 235. Kwiatkowski, T. J. *et al.* Mutations in the FUS/TLS Gene on Chromosome 16 Cause Familial Amyotrophic Lateral Sclerosis. *Science (80-.)*. **323**, 1205–1208 (2009).
 236. Vance, C. *et al.* Mutations in FUS, an RNA Processing Protein, Cause Familial Amyotrophic Lateral Sclerosis Type 6. *Science (80-.)*. **323**, 1208–1211 (2009).

237. DeJesus-Hernandez, M. *et al.* Expanded GGGGCC hexanucleotide repeat in noncoding region of C9ORF72 causes chromosome 9p-linked FTD and ALS. *Neuron* **72**, 245–56 (2011).
238. Renton, A. E. *et al.* A Hexanucleotide Repeat Expansion in C9ORF72 Is the Cause of Chromosome 9p21-Linked ALS-FTD. *Neuron* **72**, 257–268 (2011).
239. Pick, A. Über die Beziehungen der senilen Hirnatrophie zur Aphasie. *Prag Med Wochenschr* 165–167 (1892).
240. Bott, N. T., Radke, A., Stephens, M. L. & Kramer, J. H. Frontotemporal dementia: diagnosis, deficits and management. *Neurodegener. Dis. Manag.* **4**, 439–454 (2014).
241. Seltman, R. E. & Matthews, B. R. Frontotemporal Lobar Degeneration. *CNS Drugs* **26**, 841–870 (2012).
242. Lomen-Hoerth, C., Anderson, T. & Miller, B. The overlap of amyotrophic lateral sclerosis and frontotemporal dementia. *Neurology* **59**, 1077–1079 (2002).
243. Lillo, P., Garcin, B., Hornberger, M., Bak, T. H. & Hodges, J. R. Neurobehavioral Features in Frontotemporal Dementia With Amyotrophic Lateral Sclerosis. *Arch. Neurol.* **67**, (2010).
244. Sieben, A. *et al.* The genetics and neuropathology of frontotemporal lobar degeneration. *Acta Neuropathol.* **124**, 353–372 (2012).
245. Young, J. J., Lavakumar, M., Tampi, D., Balachandran, S. & Tampi, R. R. Frontotemporal dementia: latest evidence and clinical implications. *Ther. Adv. Psychopharmacol.* **8**, 33–48 (2018).
246. Piguet, O., Hornberger, M., Mioshi, E. & Hodges, J. R. Behavioural-variant frontotemporal dementia: diagnosis, clinical staging, and management. *Lancet Neurol.* **10**, 162–172 (2011).
247. Agosta, F. *et al.* Disruption of structural connectivity along the dorsal and ventral language pathways in patients with nonfluent and semantic variant primary progressive aphasia: A DT MRI study and a literature review. *Brain Lang.* **127**, 157–166 (2013).
248. Kertesz, A., McMonagle, P., Blair, M., Davidson, W. & Munoz, D. G. The evolution and pathology of frontotemporal dementia. *Brain* **128**, 1996–2005 (2005).
249. Murley, A. G. *et al.* Redefining the multidimensional clinical phenotypes of frontotemporal lobar degeneration syndromes. *Brain* **143**, 1555–1571 (2020).
250. Olney, N. T., Spina, S. & Miller, B. L. Frontotemporal Dementia. *Neurol. Clin.* **35**, 339–374 (2017).
251. Bang, J., Spina, S. & Miller, B. L. Frontotemporal dementia. *Lancet* **386**, 1672–1682 (2015).
252. Rascovsky, K. *et al.* Rate of progression differs in frontotemporal dementia and Alzheimer disease. *Neurology* **65**, 397–403 (2005).
253. Hodges, J. R., Davies, R., Xuereb, J., Kril, J. & Halliday, G. Survival in frontotemporal dementia. *Neurology* **61**, 349–354 (2003).
254. Boxer, A. L. *et al.* New directions in clinical trials for frontotemporal lobar degeneration: Methods and outcome measures. *Alzheimer's Dement.* **16**, 131–143 (2020).
255. Boxer, A. L. & Boeve, B. F. Frontotemporal Dementia Treatment: Current Symptomatic Therapies and Implications of Recent Genetic, Biochemical, and Neuroimaging Studies. *Alzheimer Dis. Assoc. Disord.* **21**, S79–S87 (2007).
256. Tsai, R. M. & Boxer, A. L. Treatment of Frontotemporal Dementia. *Curr. Treat. Options Neurol.* **16**, 319 (2014).
257. Merrilees, J. A Model for Management of Behavioral Symptoms in Frontotemporal Lobar Degeneration. *Alzheimer Dis. Assoc. Disord.* **21**, S64–S69 (2007).
258. Peet, B. T., Spina, S., Mundada, N. & La Joie, R. Neuroimaging in Frontotemporal Dementia: Heterogeneity and Relationships with Underlying Neuropathology. *Neurotherapeutics* **18**, 728–752 (2021).
259. Niccoli, T., Partridge, L. & Isaacs, A. M. Ageing as a risk factor for ALS/FTD. *Hum. Mol. Genet.* **26**, R105–R113 (2017).
260. Nilsson, C., Landqvist Waldö, M., Nilsson, K., Santillo, A. & Vestberg, S. Age-Related Incidence and Family History in Frontotemporal Dementia: Data from the Swedish Dementia Registry. *PLoS One* **9**, e94901 (2014).
261. Snowden, J. S., Neary, D. & Mann, D. M. A. Frontotemporal dementia. *Br. J. Psychiatry* **180**, 140–143 (2002).
262. Moore, K. M. *et al.* Age at symptom onset and death and disease duration in genetic frontotemporal dementia: an international retrospective cohort study. *Lancet Neurol.* **19**, 145–156 (2020).
263. Coyle-Gilchrist, I. T. S. *et al.* Prevalence, characteristics, and survival of frontotemporal lobar degeneration syndromes. *Neurology* **86**, 1736–1743 (2016).
264. Knopman, D. S. & Roberts, R. O. Estimating the Number of Persons with Frontotemporal Lobar

- Degeneration in the US Population. *J. Mol. Neurosci.* **45**, 330–335 (2011).
265. Curtis, A. F. *et al.* Sex differences in the prevalence of genetic mutations in FTD and ALS. *Neurology* **89**, 1633–1642 (2017).
 266. Greaves, C. V. & Rohrer, J. D. An update on genetic frontotemporal dementia. *Journal of Neurology* vol. 266 2075–2086 (2019).
 267. Rosso, S. M. Medical and environmental risk factors for sporadic frontotemporal dementia: a retrospective case-control study. *J. Neurol. Neurosurg. Psychiatry* **74**, 1574–1576 (2003).
 268. Turner, M. R. *et al.* Genetic screening in sporadic ALS and FTD. *J. Neurol. Neurosurg. Psychiatry* **88**, 1042–1044 (2017).
 269. Olszewska, D. A., Lonergan, R., Fallon, E. M. & Lynch, T. Genetics of Frontotemporal Dementia. *Curr. Neurol. Neurosci. Rep.* **16**, 107 (2016).
 270. Montgomery, G. K. & Erickson, L. M. Neuropsychological perspectives in amyotrophic lateral sclerosis. *Neurol. Clin.* **5**, 61–81 (1987).
 271. Culler, A. Troubles mentales dans la sclérose latérale amyotrophique. *Arch. Neurol.* **21**, pp.433-450 (1906).
 272. Abe, K. *et al.* Cognitive function in amyotrophic lateral sclerosis. *J. Neurol. Sci.* **148**, 95–100 (1997).
 273. Abrahams, S. *et al.* Frontal lobe dysfunction in amyotrophic lateral sclerosis. *Brain* **119**, 2105–2120 (1996).
 274. Ludolph, A. C. *et al.* Frontal lobe function in amyotrophic lateral sclerosis: a neuropsychologic and positron emission tomography study. *Acta Neurol. Scand.* **85**, 81–89 (1992).
 275. Kew, J. J. M. *et al.* Cortical function in amyotrophic lateral sclerosis. *Brain* **116**, 655–680 (1993).
 276. Arai, T. *et al.* TDP-43 is a component of ubiquitin-positive tau-negative inclusions in frontotemporal lobar degeneration and amyotrophic lateral sclerosis. *Biochem. Biophys. Res. Commun.* **351**, 602–611 (2006).
 277. Majoor-Krakauer, D., Ottman, R., Johnson, W. G. & Rowland, L. P. Familial aggregation of amyotrophic lateral sclerosis, dementia, and Parkinson's disease: Evidence of shared genetic susceptibility. *Neurology* **44**, 1872–1872 (1994).
 278. Gunnarsson, L.-G., Dahlbom, K. & Strandman, E. Motor neuron disease and dementia reported among 13 members of a single family. *Acta Neurol. Scand.* **84**, 429–433 (1991).
 279. Kircher, M. & Kelso, J. High-throughput DNA sequencing - concepts and limitations. *BioEssays* **32**, 524–536 (2010).
 280. Gijssels, I. *et al.* Identification of 2 Loci at Chromosomes 9 and 14 in a Multiplex Family With Frontotemporal Lobar Degeneration and Amyotrophic Lateral Sclerosis. *Arch. Neurol.* **67**, (2010).
 281. Hosler, B. A. Linkage of Familial Amyotrophic Lateral Sclerosis With Frontotemporal Dementia to Chromosome 9q21-q22. *JAMA* **284**, 1664 (2000).
 282. Morita, M. *et al.* A locus on chromosome 9p confers susceptibility to ALS and frontotemporal dementia. *Neurology* **66**, 839–844 (2006).
 283. Vance, C. *et al.* Familial amyotrophic lateral sclerosis with frontotemporal dementia is linked to a locus on chromosome 9p13.2-21.3. *Brain* **129**, 868–876 (2006).
 284. Renton, A. E. *et al.* A hexanucleotide repeat expansion in C9ORF72 is the cause of chromosome 9p21-linked ALS-FTD. *Neuron* (2011) doi:10.1016/j.neuron.2011.09.010.
 285. Woollacott, I. O. C. & Mead, S. The C9ORF72 expansion mutation: gene structure, phenotypic and diagnostic issues. *Acta Neuropathol.* **127**, 319–332 (2014).
 286. Majounie, E. *et al.* Frequency of the C9orf72 hexanucleotide repeat expansion in patients with amyotrophic lateral sclerosis and frontotemporal dementia: a cross-sectional study. *Lancet. Neurol.* **11**, 323–30 (2012).
 287. Ratti, A. *et al.* C9ORF72 repeat expansion in a large Italian ALS cohort: evidence of a founder effect. *Neurobiol. Aging* **33**, 2528.e7-2528.e14 (2012).
 288. Balendra, R. & Isaacs, A. M. C9orf72-mediated ALS and FTD: multiple pathways to disease. *Nat. Rev. Neurol.* **14**, 544–558 (2018).
 289. Brenner, D. & Weishaupt, J. H. Update on amyotrophic lateral sclerosis genetics. *Curr. Opin. Neurol.* **32**, 735–739 (2019).
 290. Haydon, P. G. Glia: Listening and talking to the synapse. *Nat. Rev. Neurosci.* **2**, 185–193 (2001).
 291. Ilieva, H., Polymenidou, M. & Cleveland, D. W. Non-cell autonomous toxicity in neurodegenerative disorders: ALS and beyond. *Journal of Cell Biology* vol. 187 761–772 (2009).
 292. Allaman, I. *et al.* Amyloid- β aggregates cause alterations of astrocytic metabolic phenotype: Impact

- on neuronal viability. *J. Neurosci.* **30**, 3326–3338 (2010).
293. Lee, Y. *et al.* Oligodendroglia metabolically support axons and contribute to neurodegeneration. *Nature* **487**, 443–448 (2012).
294. Di Giorgio, F. P., Carrasco, M. A., Siao, M. C., Maniatis, T. & Eggan, K. Non-cell autonomous effect of glia on motor neurons in an embryonic stem cell-based ALS model. *Nat. Neurosci.* **10**, 608–614 (2007).
295. Nagai, M. *et al.* Astrocytes expressing ALS-linked mutated SOD1 release factors selectively toxic to motor neurons. *Nat. Neurosci.* **10**, 615–622 (2007).
296. Spiller, K. J. *et al.* Microglia-mediated recovery from ALS-relevant motor neuron degeneration in a mouse model of TDP-43 proteinopathy. *Nat. Neurosci.* **21**, 329–340 (2018).
297. Boillée, S. *et al.* Onset and Progression in Inherited ALS Determined by Motor Neurons and Microglia. *Science (80-.)*. **312**, 1389–1392 (2006).
298. Lewandowski, S. A. *et al.* Presymptomatic activation of the PDGF-CC pathway accelerates onset of ALS neurodegeneration. *Acta Neuropathol.* **131**, 453–464 (2016).
299. Månberg, A. *et al.* Altered perivascular fibroblast activity precedes ALS disease onset. *Nat. Med.* **27**, 640–646 (2021).
300. Richter, B. *et al.* Phosphorylation of OPTN by TBK1 enhances its binding to Ub chains and promotes selective autophagy of damaged mitochondria. *Proc. Natl. Acad. Sci.* **113**, 4039–4044 (2016).
301. Pomerantz, J. L. & Baltimore, D. *NF-κB activation by a signaling complex containing TRAF2, TANK and TBK1, a novel IKK-related kinase.* *The EMBO Journal* vol. 18 (1999).
302. Zhu, G., Wu, C. J., Zhao, Y. & Ashwell, J. D. Optineurin Negatively Regulates TNFα- Induced NF-κB Activation by Competing with NEMO for Ubiquitinated RIP. *Curr. Biol.* **17**, 1438–1443 (2007).
303. Duran, A. *et al.* The Signaling Adaptor p62 Is an Important NF-κB Mediator in Tumorigenesis. *Cancer Cell* **13**, 343–354 (2008).
304. Sanjuan, M. A. *et al.* Toll-like receptor signalling in macrophages links the autophagy pathway to phagocytosis. *Nature* **450**, 1253–1257 (2007).
305. Crişan, T. O. *et al.* Inflammasome-independent modulation of cytokine response by autophagy in human cells. *PLoS One* **6**, (2011).
306. Martinez, J. *et al.* Microtubule-associated protein 1 light chain 3 alpha (LC3)-associated phagocytosis is required for the efficient clearance of dead cells. *Proc. Natl. Acad. Sci. U. S. A.* **108**, 17396–17401 (2011).
307. Heckmann, B. L. *et al.* LC3-Associated Endocytosis Facilitates β-Amyloid Clearance and Mitigates Neurodegeneration in Murine Alzheimer’s Disease. *Cell* **178**, 536–551.e14 (2019).
308. Karunakaran, I. *et al.* Neural sphingosine 1-phosphate accumulation activates microglia and links impaired autophagy and inflammation. *Glia* **67**, 1859–1872 (2019).
309. Sullivan, P. M. *et al.* The ALS/FTLD associated protein C9orf72 associates with SMCR8 and WDR41 to regulate the autophagy-lysosome pathway. *Acta Neuropathol. Commun.* **4**, 51 (2016).
310. Yang, M. *et al.* A C9ORF72/SMCR8-containing complex regulates ULK1 and plays a dual role in autophagy. *Sci. Adv.* **2**, e1601167–e1601167 (2016).
311. Webster, C. P. *et al.* The C9orf72 protein interacts with Rab1a and the ULK1 complex to regulate initiation of autophagy. *EMBO J.* **35**, 1656–76 (2016).
312. Nassif, M., Woehlbier, U. & Manque, P. A. The enigmatic role of C9ORF72 in autophagy. *Frontiers in Neuroscience* vol. 11 (2017).
313. O’Rourke, J. G. *et al.* C9orf72 is required for proper macrophage and microglial function in mice. *Science* **351**, 1324–9 (2016).
314. Pickford, F. *et al.* Progranulin is a chemoattractant for microglia and stimulates their endocytic activity. *Am. J. Pathol.* **178**, 284–295 (2011).
315. Chang, M. C. *et al.* Progranulin deficiency causes impairment of autophagy and TDP-43 accumulation. *J. Exp. Med.* **214**, 2611–2628 (2017).
316. Massenzio, F. *et al.* Microglial overexpression of fALS-linked mutant SOD1 induces SOD1 processing impairment, activation and neurotoxicity and is counteracted by the autophagy inducer trehalose. *Biochim. Biophys. Acta - Mol. Basis Dis.* **1864**, 3771–3785 (2018).
317. Bussi, C. *et al.* Autophagy down regulates pro-inflammatory mediators in BV2 microglial cells and rescues both LPS and alpha-synuclein induced neuronal cell death. *Sci. Rep.* **7**, (2017).
318. Choi, S. S., Lee, H. J., Lim, I., Satoh, J. I. & Kim, S. U. Human astrocytes: Secretome profiles of cytokines and chemokines. *PLoS One* **9**, (2014).

319. Bruijn, L. I. *et al.* ALS-linked SOD1 mutant G85R mediates damage to astrocytes and promotes rapidly progressive disease with SOD1-containing inclusions. *Neuron* **18**, 327–338 (1997).
320. Rossi, D. *et al.* Focal degeneration of astrocytes in amyotrophic lateral sclerosis. *Cell Death Differ.* **15**, 1691–1700 (2008).
321. Ferguson, C. J., Lenk, G. M. & Meisler, M. H. Defective autophagy in neurons and astrocytes from mice deficient in PI(3,5)P2. *Hum. Mol. Genet.* **18**, 4868–4878 (2009).
322. Chow, C. Y. *et al.* Deleterious Variants of FIG4, a Phosphoinositide Phosphatase, in Patients with ALS. *Am. J. Hum. Genet.* **84**, 85–88 (2009).
323. Osmanovic, A. *et al.* FIG4 variants in central European patients with amyotrophic lateral sclerosis: A whole-exome and targeted sequencing study. *Eur. J. Hum. Genet.* **25**, 324–331 (2017).
324. Di Malta, C., Fryer, J. D., Settembre, C. & Ballabio, A. Astrocyte dysfunction triggers neurodegeneration in a lysosomal storage disorder. *Proc. Natl. Acad. Sci.* **109**, (2012).
325. Gossye, H., Engelborghs, S., Van Broeckhoven, C. & van der Zee, J. *C9orf72 Frontotemporal Dementia and/or Amyotrophic Lateral Sclerosis. GeneReviews®* (1993).
326. Murphy, N. A. *et al.* Age-related penetrance of the C9orf72 repeat expansion. *Sci. Rep.* **7**, 2116 (2017).
327. Yates, A. D. *et al.* Ensembl 2020. *Nucleic Acids Res.* (2019) doi:10.1093/nar/gkz966.
328. Zhang, D., Iyer, L. M., He, F. & Aravind, L. Discovery of Novel DENN Proteins: Implications for the Evolution of Eukaryotic Intracellular Membrane Structures and Human Disease. *Front. Genet.* **3**, (2012).
329. Marat, A. L., Dokainish, H. & McPherson, P. S. DENN Domain Proteins: Regulators of Rab GTPases. *J. Biol. Chem.* **286**, 13791–13800 (2011).
330. Farg, M. A. *et al.* C9ORF72, implicated in amyotrophic lateral sclerosis and frontotemporal dementia, regulates endosomal trafficking. *Hum. Mol. Genet.* **23**, 3579–3595 (2014).
331. Webster, C. P. *et al.* The C9orf72 protein interacts with Rab1a and the ULK1 complex to regulate initiation of autophagy. *EMBO J.* **35**, 1656–1676 (2016).
332. Yang, M. *et al.* A C9ORF72/SMCR8-containing complex regulates ULK1 and plays a dual role in autophagy. *Sci. Adv.* **2**, e1601167–e1601167 (2016).
333. Corbier, C. & Sellier, C. C9ORF72 is a GDP/GTP exchange factor for Rab8 and Rab39 and regulates autophagy. *Small GTPases* **8**, 181–186 (2017).
334. Tang, D. *et al.* Cryo-EM structure of C9ORF72–SMCR8–WDR41 reveals the role as a GAP for Rab8a and Rab11a. (2020) doi:10.1073/pnas.2002110117.
335. Su, M.-Y., Zoncu, R. & Hurley, J. Structure of the C9orf72 ARF GAP complex that is haploinsufficient in ALS and FTD. *Nature* (2020) doi:10.1101/2020.04.15.042515.
336. Tang, D., Sheng, J., Xu, L., Yan, C. & Qi, S. The C9orf72-SMCR8-WDR41 complex is a GAP for small GTPases. *Autophagy* **16**, 1542–1543 (2020).
337. Su, M.-Y., Fromm, S. A., Remis, J., Toso, D. B. & Hurley, J. H. Structural basis for the ARF GAP activity and specificity of the C9orf72 complex. *Nat. Commun.* **12**, 3786 (2021).
338. ORourke, J. G. *et al.* C9orf72 is required for proper macrophage and microglial function in mice. *Science (80-.).* **351**, 1324–1329 (2016).
339. Atanasio, A. *et al.* C9orf72 ablation causes immune dysregulation characterized by leukocyte expansion, autoantibody production and glomerulonephropathy in mice. *Sci. Rep.* **6**, 23204 (2016).
340. Burberry, A. *et al.* Loss-of-function mutations in the C9ORF72 mouse ortholog cause fatal autoimmune disease. *Sci. Transl. Med.* **8**, (2016).
341. Burberry, A. *et al.* C9orf72 suppresses systemic and neural inflammation induced by gut bacteria. *Nature* **582**, 89–94 (2020).
342. van Blitterswijk, M. *et al.* Association between repeat sizes and clinical and pathological characteristics in carriers of C9ORF72 repeat expansions (Xpansize-72): a cross-sectional cohort study. *Lancet Neurol.* **12**, 978–988 (2013).
343. Beck, J. *et al.* Large C9orf72 Hexanucleotide Repeat Expansions Are Seen in Multiple Neurodegenerative Syndromes and Are More Frequent Than Expected in the UK Population. *Am. J. Hum. Genet.* **92**, 345–353 (2013).
344. Iacoangeli, A. *et al.* C9orf72 intermediate expansions of 24–30 repeats are associated with ALS. *Acta Neuropathol. Commun.* **7**, (2019).
345. Nordin, A. *et al.* Extensive size variability of the GGGGCC expansion in C9orf72 in both neuronal and non-neuronal tissues in 18 patients with ALS or FTD. *Hum. Mol. Genet.* **24**, 3133–3142 (2015).
346. Reddy, K., Zamiri, B., Stanley, S. Y. R., Macgregor, R. B. & Pearson, C. E. The Disease-associated

- r(GGGGCC) Repeat from the C9orf72 Gene Forms Tract Length-dependent Uni- and Multimolecular RNA G-quadruplex Structures. *J. Biol. Chem.* **288**, 9860–9866 (2013).
347. Fratta, P. *et al.* C9orf72 hexanucleotide repeat associated with amyotrophic lateral sclerosis and frontotemporal dementia forms RNA G-quadruplexes. *Sci. Rep.* **2**, 1016 (2012).
348. Geng, Y. *et al.* Crystal structure of parallel G-quadruplex formed by the two-repeat ALS- and FTD-related GGGGCC sequence. *Nucleic Acids Res.* **49**, 5881–5890 (2021).
349. Sen, D. & Gilbert, W. Formation of parallel four-stranded complexes by guanine-rich motifs in DNA and its implications for meiosis. *Nature* **334**, 364–366 (1988).
350. Xi, Z. *et al.* The C9orf72 repeat expansion itself is methylated in ALS and FTLN patients. *Acta Neuropathol.* **129**, 715–727 (2015).
351. Esanov, R. *et al.* A C9ORF72 BAC mouse model recapitulates key epigenetic perturbations of ALS/FTD. *Mol. Neurodegener.* **12**, 46 (2017).
352. Edbauer, D. & Haass, C. An amyloid-like cascade hypothesis for C9orf72 ALS/FTD. *Curr. Opin. Neurobiol.* **36**, 99–106 (2016).
353. Belzil, V. V. *et al.* Reduced C9orf72 gene expression in c9FTD/ALS is caused by histone trimethylation, an epigenetic event detectable in blood. *Acta Neuropathol.* **126**, 895–905 (2013).
354. Ciura, S. *et al.* Loss of function of C9orf72 causes motor deficits in a zebrafish model of amyotrophic lateral sclerosis. *Ann. Neurol.* **74**, 180–187 (2013).
355. Donnelly, C. J. *et al.* RNA toxicity from the ALS/FTD C9ORF72 expansion is mitigated by antisense intervention. *Neuron* **80**, 415–428 (2014).
356. Mori, K. *et al.* The C9orf72 GGGGCC repeat is translated into aggregating dipeptide-repeat proteins in FTLN/ALS. *Science* **339**, 1335–8 (2013).
357. Cooper-Knock, J. *et al.* Clinico-pathological features in amyotrophic lateral sclerosis with expansions in C9ORF72. *Brain* **135**, 751–764 (2012).
358. Xi, Z. *et al.* Hypermethylation of the CpG Island Near the G4C2 Repeat in ALS with a C9orf72 Expansion. *Am. J. Hum. Genet.* **92**, 981–989 (2013).
359. Almeida, S. *et al.* Modeling key pathological features of frontotemporal dementia with C9ORF72 repeat expansion in iPSC-derived human neurons. *Acta Neuropathol.* **126**, 385–399 (2013).
360. Xiao, S. *et al.* Isoform-specific antibodies reveal distinct subcellular localizations of <scp>C</scp>9orf72 in amyotrophic lateral sclerosis. *Ann. Neurol.* **78**, 568–583 (2015).
361. Waite, A. J. *et al.* Reduced C9orf72 protein levels in frontal cortex of amyotrophic lateral sclerosis and frontotemporal degeneration brain with the C9ORF72 hexanucleotide repeat expansion. *Neurobiol. Aging* **35**, 1779.e5–1779.e13 (2014).
362. Dictionary of Genetics Terms. *Natl. Cancer Inst. NIH.*
363. Šviković, S. *et al.* R-loop formation during S phase is restricted by PrimPol-mediated repriming. *EMBO J.* **38**, (2019).
364. Therrien, M., Rouleau, G. A., Dion, P. A. & Parker, J. A. Deletion of C9ORF72 results in motor neuron degeneration and stress sensitivity in *C. elegans*. *PLoS One* **8**, 1–11 (2013).
365. Fratta, P. *et al.* Homozygosity for the C9orf72 GGGGCC repeat expansion in frontotemporal dementia. *Acta Neuropathol.* **126**, 401–409 (2013).
366. Shi, Y. *et al.* Haploinsufficiency leads to neurodegeneration in C9ORF72 ALS/FTD human induced motor neurons. *Nat. Med.* **24**, 313–325 (2018).
367. Koppers, M. *et al.* C9orf72 ablation in mice does not cause motor neuron degeneration or motor deficits. *Ann. Neurol.* **78**, 426–438 (2015).
368. Atanasio, A. *et al.* C9orf72 ablation causes immune dysregulation characterized by leukocyte expansion, autoantibody production and glomerulonephropathy in mice. *Sci. Rep.* **6**, 23204 (2016).
369. O'Rourke, J. G. *et al.* C9orf72 is required for proper macrophage and microglial function in mice. *Science* **351**, 1324–9 (2016).
370. Sudria-Lopez, E. *et al.* Full ablation of C9orf72 in mice causes immune system-related pathology and neoplastic events but no motor neuron defects. *Acta Neuropathol.* **132**, 145–147 (2016).
371. Shibutani, S. T., Saitoh, T., Nowag, H., Münz, C. & Yoshimori, T. Autophagy and autophagy-related proteins in the immune system. *Nat. Immunol.* **16**, 1014–1024 (2015).
372. Plaza-Zabala, A., Sierra-Torre, V. & Sierra, A. Autophagy and microglia: Novel partners in neurodegeneration and aging. *Int. J. Mol. Sci.* **18**, (2017).
373. Liang, C.-C., Wang, C., Peng, X., Gan, B. & Guan, J.-L. Neural-specific Deletion of FIP200 Leads to Cerebellar Degeneration Caused by Increased Neuronal Death and Axon Degeneration. *J. Biol. Chem.*

- 285**, 3499–3509 (2010).
374. Komatsu, M. *et al.* Essential role for autophagy protein Atg7 in the maintenance of axonal homeostasis and the prevention of axonal degeneration. *Proc Natl Acad Sci U S A* **104**, 14489–14494 (2007).
 375. Wong, P. C. *et al.* An adverse property of a familial ALS-linked SOD1 mutation causes motor neuron disease characterized by vacuolar degeneration of mitochondria. *Neuron* **14**, 1105–1116 (1995).
 376. Ripps, M. E., Huntley, G. W., Hof, P. R., Morrison, J. H. & Gordon, J. W. Transgenic mice expressing an altered murine superoxide dismutase gene provide an animal model of amyotrophic lateral sclerosis. *Proc. Natl. Acad. Sci.* **92**, 689–693 (1995).
 377. Koppers, M. *et al.* C9orf72 ablation in mice does not cause motor neuron degeneration or motor deficits. *Ann. Neurol.* **78**, 426–438 (2015).
 378. Mizielinska, S. *et al.* C9orf72 frontotemporal lobar degeneration is characterised by frequent neuronal sense and antisense RNA foci. *Acta Neuropathol.* **126**, 845–857 (2013).
 379. Cooper-Knock, J. *et al.* Antisense RNA foci in the motor neurons of C9ORF72-ALS patients are associated with TDP-43 proteinopathy. *Acta Neuropathol.* **130**, 63–75 (2015).
 380. DeJesus-Hernandez, M. *et al.* In-depth clinico-pathological examination of RNA foci in a large cohort of C9ORF72 expansion carriers. *Acta Neuropathol.* **134**, 255–269 (2017).
 381. Sareen, D. *et al.* Targeting RNA Foci in iPSC-Derived Motor Neurons from ALS Patients with a C9ORF72 Repeat Expansion. *Sci. Transl. Med.* **5**, 208ra149–208ra149 (2013).
 382. Dafinca, R. *et al.* C9orf72 Hexanucleotide Expansions Are Associated with Altered Endoplasmic Reticulum Calcium Homeostasis and Stress Granule Formation in Induced Pluripotent Stem Cell-Derived Neurons from Patients with Amyotrophic Lateral Sclerosis and Frontotemporal Dement. *Stem Cells* **34**, 2063–2078 (2016).
 383. Kumar, V., Hasan, G. M. & Hassan, M. I. Unraveling the Role of RNA Mediated Toxicity of C9orf72 Repeats in C9-FTD/ALS. *Front. Neurosci.* **11**, (2017).
 384. Taneja, K. L., McCurrach, M., Schalling, M., Housman, D. & Singer, R. H. Foci of trinucleotide repeat transcripts in nuclei of myotonic dystrophy cells and tissues. *J. Cell Biol.* **128**, 995–1002 (1995).
 385. Wojciechowska, M. & Krzyzosiak, W. J. Cellular toxicity of expanded RNA repeats: focus on RNA foci. *Hum. Mol. Genet.* **20**, 3811–3821 (2011).
 386. Cooper-Knock, J. *et al.* Sequestration of multiple RNA recognition motif-containing proteins by C9orf72 repeat expansions. *Brain* **137**, 2040–2051 (2014).
 387. Haeusler, A. R. *et al.* C9orf72 nucleotide repeat structures initiate molecular cascades of disease. *Nature* 1–20 (2014) doi:10.1038/nature13124.C9orf72.
 388. Mori, K. *et al.* hnRNP A3 binds to GGGGCC repeats and is a constituent of p62-positive/TDP43-negative inclusions in the hippocampus of patients with C9orf72 mutations. *Acta Neuropathol.* **125**, 413–423 (2013).
 389. Lee, Y.-B. *et al.* Hexanucleotide Repeats in ALS/FTD Form Length-Dependent RNA Foci, Sequester RNA Binding Proteins, and Are Neurotoxic. *Cell Rep.* **5**, 1178–1186 (2013).
 390. Conlon, E. G. *et al.* The C9ORF72 GGGGCC expansion forms RNA G-quadruplex inclusions and sequesters hnRNP H to disrupt splicing in ALS brains. *Elife* **5**, 1–28 (2016).
 391. Low, Y.-H., Asi, Y., Foti, S. C. & Lashley, T. Heterogeneous Nuclear Ribonucleoproteins: Implications in Neurological Diseases. *Mol. Neurobiol.* **58**, 631–646 (2021).
 392. Burguete, A. S. *et al.* GGGGCC microsatellite RNA is neuritically localized, induces branching defects, and perturbs transport granule function. *Elife* **4**, e08881 (2015).
 393. Mizielinska, S. *et al.* C9orf72 repeat expansions cause neurodegeneration in Drosophila through arginine-rich proteins. *Science (80-.).* **345**, 1192–1194 (2014).
 394. Tran, H. *et al.* Differential Toxicity of Nuclear RNA Foci versus Dipeptide Repeat Proteins in a Drosophila Model of C9ORF72 FTD/ALS. *Neuron* **87**, 1207–1214 (2015).
 395. O'Rourke, J. G. *et al.* C9orf72 BAC Transgenic Mice Display Typical Pathologic Features of ALS/FTD. *Neuron* **88**, 892–901 (2015).
 396. Peters, O. M. *et al.* Human C9ORF72 Hexanucleotide Expansion Reproduces RNA Foci and Dipeptide Repeat Proteins but Not Neurodegeneration in BAC Transgenic Mice. *Neuron* **88**, 902–909 (2015).
 397. Liu, Y. *et al.* C9orf72 BAC Mouse Model with Motor Deficits and Neurodegenerative Features of ALS/FTD. *Neuron* **90**, 521–534 (2016).
 398. Mordes, D. A. *et al.* Absence of Survival and Motor Deficits in 500 Repeat C9ORF72 BAC Mice. *Neuron* **108**, 775–783.e4 (2020).
 399. Blacher, E. *et al.* Potential roles of gut microbiome and metabolites in modulating ALS in mice. *Nature*

- 572, 474–480 (2019).
400. Goelz, M.F., Mahler, J., Harry, J., Myers, P., Clark, J., Thigpen, J.E. and Forsythe, D. B. Neuropathologic findings associated with seizures in FVB mice. *Comp. Med.* **48(1)**, 34–37 (1998).
 401. Silva-Fernandes, A., Oliveira, P., Sousa, N., Maciel, P. Motor and Behavioural Abnormalities Associated with Persistent Spontaneous Epilepsy in the fvb/n Mouse Strain. *Scand. J. Lab. Anim. Sci.* **37(3)**, 213–222 (2010).
 402. Diagnosis | ‘Space cadet’ syndrome of female FVB/n mice. *Lab Anim. (NY)*. **36(16)**, (2007).
 403. Ward, J.M., Mahler, J.F., Maronport, R.R., Sundberg, J.P. and Frederickson, R. M. *Pathology of genetically engineered mice*. Iowa State University Press (2000).
 404. Zu, T. *et al.* Non-ATG-initiated translation directed by microsatellite expansions. *Proc. Natl. Acad. Sci.* **108**, 260–265 (2011).
 405. Gendron, T. F. *et al.* Antisense transcripts of the expanded C9ORF72 hexanucleotide repeat form nuclear RNA foci and undergo repeat-associated non-ATG translation in c9FTD/ALS. *Acta Neuropathol.* (2013) doi:10.1007/s00401-013-1192-8.
 406. Mori, K. *et al.* Bidirectional transcripts of the expanded C9orf72 hexanucleotide repeat are translated into aggregating dipeptide repeat proteins. *Acta Neuropathol.* **126**, 881–893 (2013).
 407. Mann, D. M. *et al.* Dipeptide repeat proteins are present in the p62 positive inclusions in patients with frontotemporal lobar degeneration and motor neurone disease associated with expansions in C9ORF72. *Acta Neuropathol. Commun.* **1**, 68 (2013).
 408. Zu, T. *et al.* RAN proteins and RNA foci from antisense transcripts in C9ORF72 ALS and frontotemporal dementia. *Proc. Natl. Acad. Sci. U. S. A.* (2013) doi:10.1073/pnas.1315438110.
 409. Freibaum, B. D. & Taylor, J. P. The Role of Dipeptide Repeats in C9ORF72-Related ALS-FTD. *Front. Mol. Neurosci.* **10**, 35 (2017).
 410. Al-Sarraj, S. *et al.* p62 positive, TDP-43 negative, neuronal cytoplasmic and intranuclear inclusions in the cerebellum and hippocampus define the pathology of C9orf72-linked FTL and MND/ALS. *Acta Neuropathol.* **122**, 691–702 (2011).
 411. Hsiung, G.-Y. R. *et al.* Clinical and pathological features of familial frontotemporal dementia caused by C9ORF72 mutation on chromosome 9p. *Brain* **135**, 709–722 (2012).
 412. Troakes, C. *et al.* An MND/ALS phenotype associated with C9orf72 repeat expansion: Abundant p62-positive, TDP-43-negative inclusions in cerebral cortex, hippocampus and cerebellum but without associated cognitive decline. *Neuropathology* **32**, 505–514 (2012).
 413. Schipper, L. J. *et al.* Prevalence of brain and spinal cord inclusions, including dipeptide repeat proteins, in patients with the C9ORF72 hexanucleotide repeat expansion: a systematic neuropathological review. *Neuropathol. Appl. Neurobiol.* **42**, 547–560 (2016).
 414. Ash, P. E. A. *et al.* Unconventional Translation of C9ORF72 GGGGCC Expansion Generates Insoluble Polypeptides Specific to c9FTD/ALS. *Neuron* **77**, 639–646 (2013).
 415. Gomez-Deza, J. *et al.* Dipeptide repeat protein inclusions are rare in the spinal cord and almost absent from motor neurons in C9ORF72 mutant amyotrophic lateral sclerosis and are unlikely to cause their degeneration. *Acta Neuropathol. Commun.* **3**, 38 (2015).
 416. Schludi, M. H. *et al.* Distribution of dipeptide repeat proteins in cellular models and C9orf72 mutation cases suggests link to transcriptional silencing. *Acta Neuropathol.* **130**, 537–555 (2015).
 417. Saberi, S. *et al.* Sense-encoded poly-GR dipeptide repeat proteins correlate to neurodegeneration and uniquely co-localize with TDP-43 in dendrites of repeat-expanded C9orf72 amyotrophic lateral sclerosis. *Acta Neuropathol.* **135**, 459–474 (2018).
 418. Ohki, Y. *et al.* Glycine-alanine dipeptide repeat protein contributes to toxicity in a zebrafish model of C9orf72 associated neurodegeneration. *Mol. Neurodegener.* **12**, 1–11 (2017).
 419. Swaminathan, A. *et al.* Expression of C9orf72-related dipeptides impairs motor function in a vertebrate model. *Hum. Mol. Genet.* **27**, 1754–1762 (2018).
 420. Jovičić, A. *et al.* Modifiers of C9orf72 dipeptide repeat toxicity connect nucleocytoplasmic transport defects to FTD/ALS. *Nat. Neurosci.* **18**, 1226–1229 (2015).
 421. Freibaum, B. D. *et al.* GGGGCC repeat expansion in C9ORF72 compromises nucleocytoplasmic transport. *Nature* **525**, 129–133 (2015).
 422. Xu, W. & Xu, J. C9orf72 dipeptide repeats cause selective neurodegeneration and cell-autonomous excitotoxicity in Drosophila glutamatergic neurons. *J. Neurosci.* **38**, 7741–7752 (2018).
 423. Choi, S. Y. *et al.* C9ORF72-ALS/FTD-associated poly(GR) binds Atp5a1 and compromises mitochondrial function in vivo. *Nat. Neurosci.* **22**, 851–862 (2019).

424. Schludi, M. H. *et al.* Spinal poly-GA inclusions in a C9orf72 mouse model trigger motor deficits and inflammation without neuron loss. *Acta Neuropathol* **3**, 241–254 (2017).
425. Zhang, Y. J. *et al.* Poly(GR) impairs protein translation and stress granule dynamics in C9orf72-associated frontotemporal dementia and amyotrophic lateral sclerosis. *Nature Medicine* vol. 24 1136–1142 (2018).
426. Walker, C. *et al.* C9orf72 expansion disrupts ATM-mediated chromosomal break repair. *Nat. Neurosci.* **20**, 1225–1235 (2017).
427. Lee, K. H. *et al.* C9orf72 Dipeptide Repeats Impair the Assembly, Dynamics, and Function of Membrane-Less Organelles. *Cell* **167**, 774–788.e17 (2016).
428. Tao, Z. *et al.* Nucleolar stress and impaired stress granule formation contribute to C9orf72 RAN translation-induced cytotoxicity. *Hum. Mol. Genet.* **24**, 2426–41 (2015).
429. May, S. *et al.* C9orf72 FTL/ALS-associated Gly-Ala dipeptide repeat proteins cause neuronal toxicity and Unc119 sequestration. *Acta Neuropathol.* **128**, 485–503 (2014).
430. Zhang, Y. J. *et al.* C9ORF72 poly(GA) aggregates sequester and impair HR23 and nucleocytoplasmic transport proteins. *Nat. Neurosci.* **19**, 668–677 (2016).
431. Chew, J. *et al.* C9ORF72 repeat expansions in mice cause TDP-43 pathology, neuronal loss, and behavioral deficits. *Science (80-.)*. **348**, 1151–1154 (2015).
432. Lin, Y. *et al.* Toxic PR Poly-Dipeptides Encoded by the C9orf72 Repeat Expansion Target LC Domain Polymers. *Cell* **167**, 789–802.e12 (2016).
433. Zhao, Y. G. & Zhang, H. Phase Separation in Membrane Biology: The Interplay between Membrane-Bound Organelles and Membraneless Condensates. *Dev. Cell* **55**, 30–44 (2020).
434. Molliex, A. *et al.* Phase separation by low complexity domains promotes stress granule assembly and drives pathological fibrillization. *Cell* **163**, 123–33 (2015).
435. Boeynaems, S. *et al.* Drosophila screen connects nuclear transport genes to DPR pathology in c9ALS/FTD. *Sci. Rep.* **6**, 20877 (2016).
436. Lopez-Gonzalez, R. *et al.* Poly(GR) in C9ORF72-Related ALS/FTD Compromises Mitochondrial Function and Increases Oxidative Stress and DNA Damage in iPSC-Derived Motor Neurons. *Neuron* **92**, 383–391 (2016).
437. Wen, X. *et al.* Antisense Proline-Arginine RAN Dipeptides Linked to C9ORF72-ALS/FTD Form Toxic Nuclear Aggregates that Initiate In Vitro and In Vivo Neuronal Death. *Neuron* **84**, 1213–1225 (2014).
438. Yamakawa, M. *et al.* Characterization of the dipeptide repeat protein in the molecular pathogenesis of c9FTD/ALS. *Hum. Mol. Genet.* **24**, 1630–1645 (2015).
439. Mackenzie, I. R. *et al.* Dipeptide repeat protein pathology in C9ORF72 mutation cases: clinico-pathological correlations. *Acta Neuropathol.* **126**, 859–879 (2013).
440. Davidson, Y. S. *et al.* Brain distribution of dipeptide repeat proteins in frontotemporal lobar degeneration and motor neurone disease associated with expansions in C9ORF72. *Acta Neuropathol. Commun.* **2**, 70 (2014).
441. Boivin, M. *et al.* Reduced autophagy upon C9ORF72 loss synergizes with dipeptide repeat protein toxicity in G4C2 repeat expansion disorders. *EMBO J.* **39**, 1–15 (2020).
442. Zhu, Q. *et al.* Reduced C9ORF72 function exacerbates gain of toxicity from ALS/FTD-causing repeat expansion in C9orf72. *Nat. Neurosci.* **23**, 615–624 (2020).
443. Gitler, A. D. & Tsuiji, H. There has been an awakening: Emerging mechanisms of C9orf72 mutations in FTD/ALS. *Brain Res.* **1647**, 19–29 (2016).
444. Zhang, Y.-J. *et al.* Aggregation-prone c9FTD/ALS poly(GA) RAN-translated proteins cause neurotoxicity by inducing ER stress. *Acta Neuropathol.* **128**, 505–524 (2014).
445. Mackenzie, I. R. A. *et al.* Quantitative analysis and clinico-pathological correlations of different dipeptide repeat protein pathologies in C9ORF72 mutation carriers. *Acta Neuropathol.* **130**, 845–861 (2015).
446. Chang, Y. J., Jeng, U. S., Chiang, Y. L., Hwang, I. S. & Chen, Y. R. The glycine-alanine dipeptide repeat from C9 or f72 hexanucleotide expansions forms toxic amyloids possessing cell-to-cell transmission properties. *J. Biol. Chem.* **291**, 4903–4911 (2016).
447. Guo, Q. *et al.* In Situ Structure of Neuronal C9orf72 Poly-GA Aggregates Reveals Proteasome Recruitment. *Cell* **172**, 696–705.e12 (2018).
448. Chang, Y.-J., Jeng, U.-S., Chiang, Y.-L., Hwang, I.-S. & Chen, Y.-R. The Glycine-Alanine Dipeptide Repeat from C9orf72 Hexanucleotide Expansions Forms Toxic Amyloids Possessing Cell-to-Cell

- Transmission Properties. *J. Biol. Chem.* **291**, 4903–4911 (2016).
449. Brinster, R. L., Allen, J. M., Behringer, R. R., Gelinas, R. E. & Palmiter, R. D. Introns increase transcriptional efficiency in transgenic mice. *Proc. Natl. Acad. Sci.* **85**, 836–840 (1988).
450. Dirkmann, M., Nowack, J. & Schulz, F. An in Vitro Biosynthesis of Sesquiterpenes Starting from Acetic Acid. *ChemBioChem* **19**, 2146–2151 (2018).
451. Pontén, J. & Macintyre, E. H. Long term culture of normal and neoplastic human glia. *Acta Pathol. Microbiol. Scand.* **74**, 465–86 (1968).
452. Wichterle, H., Lieberam, I., Porter, J. A. & Jessell, T. M. Directed differentiation of embryonic stem cells into motor neurons. *Cell* **110**, 385–97 (2002).
453. Meyer, K. *et al.* Direct conversion of patient fibroblasts demonstrates non-cell autonomous toxicity of astrocytes to motor neurons in familial and sporadic ALS. *Proc. Natl. Acad. Sci. U. S. A.* **111**, 829–832 (2014).
454. Hautbergue, G. M. *et al.* SRSF1-dependent nuclear export inhibition of C9ORF72 repeat transcripts prevents neurodegeneration and associated motor deficits. *Nat. Commun.* **8**, 1–18 (2017).
455. Mcintyre, G. J., Groneman, J. L., Tran, A. & Applegate, T. L. An Infinitely Expandable Cloning Strategy plus Repeat-Proof PCR for Working with Multiple shRNA. *PLoS One* **3**, e3827 (2008).
456. James B. Pawley. *Handbook Of Biological Confocal Microscopy*. (Springer US, 2006). doi:10.1007/978-0-387-45524-2.
457. Schindelin, J. *et al.* Fiji: An open-source platform for biological-image analysis. *Nature Methods* vol. 9 676–682 (2012).
458. Arganda-Carreras, I. *et al.* Trainable Weka Segmentation: a machine learning tool for microscopy pixel classification. *Bioinformatics* **33**, 2424–2426 (2017).
459. Ehrlich, M. *et al.* Endocytosis by random initiation and stabilization of clathrin-coated pits. *Cell* **118**, 591–605 (2004).
460. Kirchhausen, T., Macia, E. & Pelish, H. E. Use of Dynasore, the Small Molecule Inhibitor of Dynamin, in the Regulation of Endocytosis. *Methods in Enzymology* vol. 438 77–93 (2008).
461. Richter, K. N. *et al.* Glyoxal as an alternative fixative to formaldehyde in immunostaining and super-resolution microscopy. *EMBO J.* **37**, 139–159 (2018).
462. Fonin, A. V., Sulatskaya, A. I., Kuznetsova, I. M. & Turoverov, K. K. Fluorescence of dyes in solutions with high absorbance. Inner filter effect correction. *PLoS One* **9**, (2014).
463. Tinevez, J. Y. *et al.* TrackMate: An open and extensible platform for single-particle tracking. *Methods* **115**, 80–90 (2017).
464. Van Den Heuvel, M. G. L., Bolhuis, S. & Dekker, C. Persistence length measurements from stochastic single-microtubule trajectories. *Nano Lett.* **7**, 3138–3144 (2007).
465. Dunderdale, G., Ebbens, S., Fairclough, P. & Howse, J. Importance of particle tracking and calculating the mean-squared displacement in distinguishing nanopropulsion from other processes. *Langmuir* **28**, 10997–11006 (2012).
466. Tarantino, N. *et al.* TNF and IL-1 exhibit distinct ubiquitin requirements for inducing NEMO–IKK supramolecular structures. *J. Cell Biol.* **204**, 231–245 (2014).
467. Miura, K. & Sladoje, N. *Bioimage Data Analysis Workflows*. (Springer International Publishing, 2020). doi:10.1007/978-3-030-22386-1.
468. Tanaka, K. A. K. *et al.* Membrane molecules mobile even after chemical fixation. *Nature Methods* vol. 7 865–866 (2010).
469. Hust, M. *et al.* Single chain Fab (scFab) fragment. *BMC Biotechnol.* **7**, (2007).
470. Culley, S. *et al.* Quantitative mapping and minimization of super-resolution optical imaging artifacts. *Nat. Methods* **15**, 263–266 (2018).
471. Leterrier, C. *et al.* Nanoscale Architecture of the Axon Initial Segment Reveals an Organized and Robust Scaffold. *Cell Rep.* **13**, 2781–2793 (2015).
472. Ovesný, M., Křížek, P., Borkovec, J., Švindrych, Z. & Hagen, G. M. ThunderSTORM: A comprehensive ImageJ plug-in for PALM and STORM data analysis and super-resolution imaging. *Bioinformatics* **30**, 2389–2390 (2014).
473. Thompson, R. E., Larson, D. R. & Webb, W. W. Precise nanometer localization analysis for individual fluorescent probes. *Biophys. J.* **82**, 2775–2783 (2002).
474. Pagoon, S. V., Nicovich, P. R., Mollazade, M., Tabarin, T. & Gaus, K. Clus-DoC: a combined cluster detection and colocalization analysis for single-molecule localization microscopy data. *Mol. Biol. Cell* **27**, 3627–3636 (2016).

475. Caetano, F. A. *et al.* MIiSR: Molecular Interactions in Super-Resolution Imaging Enables the Analysis of Protein Interactions, Dynamics and Formation of Multi-protein Structures. *PLOS Comput. Biol.* **11**, e1004634 (2015).
476. Rostalski, H. *et al.* Astrocytes and Microglia as Potential Contributors to the Pathogenesis of C9orf72 Repeat Expansion-Associated FTL and ALS. *Front. Neurosci.* **13**, 1–11 (2019).
477. Zhang, Y.-J. *et al.* Aggregation-prone c9FTD/ALS poly(GA) RAN-translated proteins cause neurotoxicity by inducing ER stress. *Acta Neuropathol.* **128**, 505–524 (2014).
478. Lee, Y. B. *et al.* C9orf72 poly GA RAN-translated protein plays a key role in amyotrophic lateral sclerosis via aggregation and toxicity. *Hum. Mol. Genet.* **26**, 4765–4777 (2017).
479. Boeynaems, S. *et al.* Phase Separation of C9orf72 Dipeptide Repeats Perturbs Stress Granule Dynamics. *Mol. Cell* **65**, 1044–1055.e5 (2017).
480. White, M. R. *et al.* C9orf72 Poly(PR) Dipeptide Repeats Disturb Biomolecular Phase Separation and Disrupt Nucleolar Function. *Mol. Cell* **74**, 713–728.e6 (2019).
481. Varciana, A. *et al.* Micro-RNAs secreted through astrocyte-derived extracellular vesicles cause neuronal network degeneration in C9orf72 ALS. *EBioMedicine* **40**, 626–635 (2019).
482. Shrivastava, A. N., Aperia, A., Melki, R. & Triller, A. Physico-Pathologic Mechanisms Involved in Neurodegeneration: Misfolded Protein-Plasma Membrane Interactions. *Neuron* **95**, 33–50 (2017).
483. Rust, M. J., Bates, M. & Zhuang, X. Sub-diffraction-limit imaging by stochastic optical reconstruction microscopy (STORM). *Nat. Methods* **3**, 793–5 (2006).
484. Ambrose, E. J. A surface contact microscope for the study of cell movements [32]. *Nature* vol. 178 1194 (1956).
485. Axelrod, D. Cell-substrate contacts illuminated by total internal reflection fluorescence. *J. Cell Biol.* **89**, 141–145 (1981).
486. Dempsey, G. T., Vaughan, J. C., Chen, K. H., Bates, M. & Zhuang, X. Evaluation of fluorophores for optimal performance in localization-based super-resolution imaging. *Nat. Methods* **8**, 1027–1040 (2011).
487. Rosano, G. L. & Ceccarelli, E. A. Recombinant protein expression in Escherichia coli: advances and challenges. *Front. Microbiol.* **5**, (2014).
488. De Strooper, B. & Karran, E. The Cellular Phase of Alzheimer’s Disease. *Cell* **164**, 603–615 (2016).
489. Yerbury, J. J. *et al.* The metastability of the proteome of spinal motor neurons underlies their selective vulnerability in ALS. *Neurosci. Lett.* **704**, 89–94 (2019).
490. Bucciantini, M. *et al.* Inherent toxicity of aggregates implies a common mechanism for protein misfolding diseases. *Nature* **416**, 507–511 (2002).
491. Kaye, R. *et al.* Common structure of soluble amyloid oligomers implies common mechanism of pathogenesis. *Science (80-.)*. **300**, 486–489 (2003).
492. Tomic, J. L., Pensalfini, A., Head, E. & Glabe, C. G. Soluble fibrillar oligomer levels are elevated in Alzheimer’s disease brain and correlate with cognitive dysfunction. *Neurobiol. Dis.* **35**, 352–358 (2009).
493. Vanneste, J. *et al.* C9orf72-generated poly-GR and poly-PR do not directly interfere with nucleocytoplasmic transport. *Sci. Rep.* **9**, 15728 (2019).
494. Peskett, T. R. *et al.* A Liquid to Solid Phase Transition Underlying Pathological Huntingtin Exon1 Aggregation. *Mol. Cell* **70**, 588–601.e6 (2018).
495. Ray, S. *et al.* Liquid-liquid phase separation and liquid-to-solid transition mediate α -synuclein amyloid fibril containing hydrogel formation. *bioRxiv* 619858 (2019) doi:10.1101/619858.
496. McSwiggen, D. T., Mir, M., Darzacq, X. & Tjian, R. Evaluating phase separation in live cells: diagnosis, caveats, and functional consequences. *Genes Dev.* **33**, 1619–1634 (2019).
497. Alberti, S., Gladfelter, A. & Mittag, T. Considerations and Challenges in Studying Liquid-Liquid Phase Separation and Biomolecular Condensates. *Cell* **176**, 419–434 (2019).
498. Taylor, N. O., Wei, M.-T., Stone, H. A. & Brangwynne, C. P. Quantifying Dynamics in Phase-Separated Condensates Using Fluorescence Recovery after Photobleaching. *Biophys. J.* **117**, 1285–1300 (2019).
499. Brangwynne, C. P. *et al.* Germline P granules are liquid droplets that localize by controlled dissolution/condensation. *Science (80-.)*. **324**, 1729–1732 (2009).
500. Hyman, A. A., Weber, C. A. & Jülicher, F. Liquid-Liquid Phase Separation in Biology. *Annu. Rev. Cell Dev. Biol.* **30**, 39–58 (2014).
501. Ganser, L. R. & Myong, S. Methods to Study Phase-Separated Condensates and the Underlying

- Molecular Interactions. *Trends Biochem. Sci.* **45**, 1004–1005 (2020).
502. Landreh, M. *et al.* The formation, function and regulation of amyloids: insights from structural biology. *J. Intern. Med.* **280**, 164–176 (2016).
 503. Flores, B. N. *et al.* Distinct c9orf72-associated dipeptide repeat structures correlate with neuronal toxicity. *PLoS One* **11**, 1–18 (2016).
 504. Meeter, L. H. H. *et al.* Poly(GP), neurofilament and grey matter deficits in C9orf72 expansion carriers. *Ann. Clin. Transl. Neurol.* **5**, 583–597 (2018).
 505. Möckl, L., Lamb, D. C. & Bräuchle, C. Super-resolved Fluorescence Microscopy: Nobel Prize in Chemistry 2014 for Eric Betzig, Stefan Hell, and William E. Moerner. *Angew. Chemie Int. Ed.* **53**, 13972–13977 (2014).
 506. Shrivastava, A. N. *et al.* Clustering of Tau fibrils impairs the synaptic composition of $\alpha 3$ -Na⁺/K⁺-ATPase and AMPA receptors. *EMBO J.* **38**, e99871 (2019).
 507. Shrivastava, A. N. *et al.* α -synuclein assemblies sequester neuronal $\alpha 3$ -Na⁺/K⁺-ATPase and impair Na⁺ gradient. *EMBO J.* **34**, 2408–2423 (2015).
 508. Jin, S. *et al.* Amyloid- β (1–42) Aggregation Initiates Its Cellular Uptake and Cytotoxicity. *J. Biol. Chem.* **291**, 19590–19606 (2016).
 509. Lobsiger, C. S. & Cleveland, D. W. Glial cells as intrinsic components of non-cell-autonomous neurodegenerative disease. *Nat. Neurosci.* **10**, 1355–60 (2007).
 510. Lee, J. *et al.* Astrocytes and Microglia as Non-cell Autonomous Players in the Pathogenesis of ALS. *Exp. Neurol.* **25**, 233 (2016).
 511. Chai, M. & Kohyama, J. Non-Cell-Autonomous Neurotoxicity in Parkinson’s Disease Mediated by Astroglial α -Synuclein. *Stem Cell Reports* **12**, 183–185 (2019).
 512. di Domenico, A. *et al.* Patient-Specific iPSC-Derived Astrocytes Contribute to Non-Cell-Autonomous Neurodegeneration in Parkinson’s Disease. *Stem Cell Reports* **12**, 213–229 (2019).
 513. Verkhratsky, A. & Butt, A. The History of the Decline and Fall of the Glial Numbers Legend. *Neuroglia* **1**, 188–192 (2018).
 514. Sofroniew, M. V. & Vinters, H. V. Astrocytes: biology and pathology. *Acta Neuropathol.* **119**, 7–35 (2010).
 515. Mahmoud, S., Gharagozloo, M., Simard, C. & Gris, D. Astrocytes Maintain Glutamate Homeostasis in the CNS by Controlling the Balance between Glutamate Uptake and Release. *Cells* **8**, 184 (2019).
 516. Ogata, K. & Kosaka, T. Structural and quantitative analysis of astrocytes in the mouse hippocampus. *Neuroscience* **113**, 221–233 (2002).
 517. Halassa, M. M., Fellin, T., Takano, H., Dong, J. H. & Haydon, P. G. Synaptic islands defined by the territory of a single astrocyte. *J. Neurosci.* **27**, 6473–6477 (2007).
 518. Rossi, D. *et al.* Focal degeneration of astrocytes in amyotrophic lateral sclerosis. *Cell Death Differ.* **15**, 1691–1700 (2008).
 519. Tripathi, P. *et al.* Reactive Astrocytes Promote ALS-like Degeneration and Intracellular Protein Aggregation in Human Motor Neurons by Disrupting Autophagy through TGF- β 1. *Stem Cell Reports* **9**, 667–680 (2017).
 520. Mackenzie, I. R. *et al.* Dipeptide repeat protein pathology in C9ORF72 mutation cases: clinico-pathological correlations. *Acta Neuropathol.* **126**, 859–879 (2013).
 521. Jiménez, A. J., Domínguez-Pinos, M. D., Guerra, M. M., Fernández-Llebrez, P. & Pérez-Fígares, J. M. Structure and function of the ependymal barrier and diseases associated with ependyma disruption. *Tissue Barriers* vol. 2 1–14 (2014).
 522. Lehmer, C. *et al.* Poly-GP in cerebrospinal fluid links C9orf72 -associated dipeptide repeat expression to the asymptomatic phase of ALS / FTD. *EMBO Mol. Med.* **9**, 859–868 (2017).
 523. Knobloch, M., Konietzko, U., Krebs, D. C. & Nitsch, R. M. Intracellular A β and cognitive deficits precede β -amyloid deposition in transgenic arcA β mice. *Neurobiol. Aging* **28**, 1297–1306 (2007).
 524. Gouras, G. K. *et al.* Intraneuronal A β 42 Accumulation in Human Brain. *Am. J. Pathol.* **156**, 15–20 (2000).
 525. Wesén, E., Jeffries, G. D. M., Dzebo, M. M. & Esbjörner, E. K. Endocytic uptake of monomeric amyloid- β peptides is clathrin- and dynamin-independent and results in selective accumulation of A β (1–42) compared to A β (1–40). *Sci. Rep.* **7**, (2017).
 526. Evans, L. D. *et al.* Extracellular Monomeric and Aggregated Tau Efficiently Enter Human Neurons through Overlapping but Distinct Pathways. *Cell Rep.* **22**, 3612–3624 (2018).
 527. Wu, J. W. *et al.* Small Misfolded Tau Species Are Internalized via Bulk Endocytosis and Anterogradely

- and Retrogradely Transported in Neurons. *J. Biol. Chem.* **288**, 1856–1870 (2013).
528. Zhang, Q. *et al.* A myosin-7B–dependent endocytosis pathway mediates cellular entry of α -synuclein fibrils and polycation-bearing cargos. *Proc. Natl. Acad. Sci.* **117**, 10865–10875 (2020).
529. Zeineddine, R. *et al.* SOD1 protein aggregates stimulate macropinocytosis in neurons to facilitate their propagation. *Mol. Neurodegener.* **10**, (2015).
530. Chen, J. J. *et al.* Compromised function of the ESCRT pathway promotes endolysosomal escape of tau seeds and propagation of tau aggregation. *J. Biol. Chem.* **294**, 18952–18966 (2019).
531. Lata, S. *et al.* Structure and function of ESCRT-III. *Biochem. Soc. Trans.* **37**, 156–160 (2009).
532. Liu, G. *et al.* Endocytosis regulates TDP-43 toxicity and turnover. *Nat. Commun.* **8**, 2092 (2017).
533. Liu, G. *et al.* Cdc48/VCP and Endocytosis Regulate TDP-43 and FUS Toxicity and Turnover. *Mol. Cell. Biol.* **40**, (2020).
534. McLaurin, J. & Lai, A. Y. Mechanisms of amyloid-beta peptide uptake by neurons: The role of lipid rafts and lipid raft-associated proteins. *Int. J. Alzheimers. Dis.* **2011**, (2011).
535. Mori, K. *et al.* The C9orf72 GGGGCC repeat is translated into aggregating dipeptide-repeat proteins in FTL/ALS. *Science (80-.)*. (2013) doi:10.1126/science.1232927.
536. Wang, R. *et al.* Poly-PR in C9ORF72-Related Amyotrophic Lateral Sclerosis/Frontotemporal Dementia Causes Neurotoxicity by Clathrin-Dependent Endocytosis. *Neurosci. Bull.* **35**, 889–900 (2019).
537. Thiele, L., Merkle, H. P. & Walter, E. Phagocytosis and phagosomal fate of surface-modified microparticles in dendritic cells and macrophages. *Pharm. Res.* **20**, 221–8 (2003).
538. Rejman, J., Oberle, V., Zuhorn, I. S. & Hoekstra, D. Size-dependent internalization of particles via the pathways of clathrin- and caveolae-mediated endocytosis. *Biochem. J.* **377**, 159–69 (2004).
539. Harding, C., Heuser, J. & Stahl, P. Receptor-mediated endocytosis of transferrin and recycling of the transferrin receptor in rat reticulocytes. *J. Cell Biol.* **97**, 329–339 (1983).
540. Hanover, J. A., Willingham, M. C. & Pastan, I. Kinetics of transit of transferrin and epidermal growth factor through clathrin-coated membranes. *Cell* **39**, 283–293 (1984).
541. Macia, E. *et al.* Dynasore, a Cell-Permeable Inhibitor of Dynamin. *Dev. Cell* **10**, 839–850 (2006).
542. Fumagalli, L. *et al.* C9orf72 -derived arginine-containing dipeptide repeats associate with axonal transport machinery and impede microtubule-based motility. *Sci. Adv.* **7**, (2021).
543. Mason, R. P. *et al.* Distribution and fluidizing action of soluble and aggregated amyloid β - peptide in rat synaptic plasma membranes. *J. Biol. Chem.* **274**, 18801–18807 (1999).
544. Kandimalla, K. K., Scott, O. G., Fulzele, S., Davidson, M. W. & Poduslo, J. F. Mechanism of Neuronal versus endothelial cell uptake of Alzheimer’s disease amyloid β protein. *PLoS One* **4**, (2009).
545. Lee, H. J. *et al.* Assembly-dependent endocytosis and clearance of extracellular α -synuclein. *Int. J. Biochem. Cell Biol.* **40**, 1835–1849 (2008).
546. Ahn, K. J., Paik, S. R., Chung, K. C. & Kim, J. Amino acid sequence motifs and mechanistic features of the membrane translocation of α -synuclein. *J. Neurochem.* **97**, 265–279 (2006).
547. Boya, P. & Kroemer, G. Lysosomal membrane permeabilization in cell death. *Oncogene* **27**, 6434–6451 (2008).
548. Kavčič, N. *et al.* Intracellular cathepsin C levels determine sensitivity of cells to leucyl-leucine methyl ester-triggered apoptosis. *FEBS J.* **287**, 5148–5166 (2020).
549. Aits, S. *et al.* Sensitive detection of lysosomal membrane permeabilization by lysosomal galectin puncta assay. *Autophagy* **11**, 1408–1424 (2015).
550. Flavin, W. P. *et al.* Endocytic vesicle rupture is a conserved mechanism of cellular invasion by amyloid proteins. *Acta Neuropathol.* **134**, 629–653 (2017).
551. Jia, J. *et al.* MERIT, a cellular system coordinating lysosomal repair, removal and replacement. *Autophagy* **16**, 1539–1541 (2020).
552. Jia, J. *et al.* Galectin-3 Coordinates a Cellular System for Lysosomal Repair and Removal. *Dev. Cell* **52**, 69-87.e8 (2020).
553. Cullen, V. *et al.* Cathepsin D expression level affects alpha-synuclein processing, aggregation, and toxicity in vivo. *Mol. Brain* **2**, 5 (2009).
554. Mazzulli, J. R. *et al.* Gaucher Disease Glucocerebrosidase and α -Synuclein Form a Bidirectional Pathogenic Loop in Synucleinopathies. *Cell* **146**, 37–52 (2011).
555. Wang, H. *et al.* Cathepsin L Mediates the Degradation of Novel APP C-Terminal Fragments. *Biochemistry* **54**, 2806–2816 (2015).

556. Humphries, W. H. & Payne, C. K. Imaging lysosomal enzyme activity in live cells using self-quenched substrates. *Anal. Biochem.* **424**, 178–183 (2012).
557. Crowley, L. C. & Waterhouse, N. J. Detecting Cleaved Caspase-3 in Apoptotic Cells by Flow Cytometry. *Cold Spring Harb. Protoc.* **2016**, pdb.prot087312 (2016).
558. Radulovic, M. *et al.* ESCRT -mediated lysosome repair precedes lysophagy and promotes cell survival. *EMBO J.* **37**, 1–15 (2018).
559. Eriksson, I., Wäster, P. & Öllinger, K. Restoration of lysosomal function after damage is accompanied by recycling of lysosomal membrane proteins. *Cell Death Dis.* **11**, 370 (2020).
560. Chia, R. *et al.* Superoxide dismutase 1 and tgSOD1 mouse spinal cord seed fibrils, suggesting a propagative cell death mechanism in amyotrophic lateral sclerosis. *PLoS One* **5**, e10627 (2010).
561. Nonaka, T. *et al.* Prion-like Properties of Pathological TDP-43 Aggregates from Diseased Brains. *Cell Rep.* **4**, 124–134 (2013).
562. Di Giorgio, F. P., Boulting, G. L., Bobrowicz, S. & Eggan, K. C. Human Embryonic Stem Cell-Derived Motor Neurons Are Sensitive to the Toxic Effect of Glial Cells Carrying an ALS-Causing Mutation. *Cell Stem Cell* **3**, 637–648 (2008).
563. Marchetto, M. C. N. *et al.* Non-Cell-Autonomous Effect of Human SOD1G37R Astrocytes on Motor Neurons Derived from Human Embryonic Stem Cells. *Cell Stem Cell* **3**, 649–657 (2008).
564. Haidet-Phillips, A. M. *et al.* Altered astrocytic expression of TDP-43 does not influence motor neuron survival. *Exp. Neurol.* **250**, 250–259 (2013).
565. Ferraiuolo, L. *et al.* Dysregulation of astrocyte-motoneuron cross-talk in mutant superoxide dismutase 1-related amyotrophic lateral sclerosis. *Brain* **134**, 2627–2641 (2011).
566. Papadeas, S., Kraig, S., ... C. O.-P. of the & 2011, undefined. Astrocytes carrying the superoxide dismutase 1 (SOD1G93A) mutation induce wild-type motor neuron degeneration in vivo. *Natl. Acad. Sci.*
567. Yamanaka, K. & Komine, O. The multi-dimensional roles of astrocytes in ALS. *Neurosci. Res.* **126**, 31–38 (2018).
568. Victoria, G. S., Arkhipenko, A., Zhu, S., Syan, S. & Zurzolo, C. Astrocyte-to-neuron intercellular prion transfer is mediated by cell-cell contact. *Sci. Rep.* **6**, 25–28 (2016).
569. Wang, W. *et al.* Toxic amyloid- β oligomers induced self-replication in astrocytes triggering neuronal injury. *EBioMedicine* **42**, 174–187 (2019).
570. Guttenplan, K. A. *et al.* Neurotoxic reactive astrocytes induce cell death via saturated lipids. *Nature* **599**, 102–107 (2021).
571. Abounit, S. *et al.* Tunneling nanotubes spread fibrillar α -synuclein by intercellular trafficking of lysosomes. *EMBO J.* **35**, 2120–2138 (2016).
572. Lee, H. J. *et al.* Autophagic failure promotes the exocytosis and intercellular transfer of α -synuclein. *Exp. Mol. Med.* **45**, e22–e22 (2013).
573. Eisele, Y. S. *et al.* Targeting protein aggregation for the treatment of degenerative diseases. *Nat. Rev. Drug Discov.* **14**, 759–780 (2015).
574. Pu, J., Guardia, C. M., Keren-Kaplan, T. & Bonifacino, J. S. Mechanisms and functions of lysosome positioning. *J. Cell Sci.* jcs.196287 (2016).
575. Araujo, M. E. G., Liebscher, G., Hess, M. W. & Huber, L. A. Lysosomal size matters. *Traffic* **21**, 60–75 (2020).
576. Rey, N. L. *et al.* α -Synuclein conformational strains spread, seed and target neuronal cells differentially after injection into the olfactory bulb. *Acta Neuropathol. Commun.* **7**, 1–18 (2019).
577. Volles, M. J. & Lansbury, P. T. Vesicle permeabilization by protofibrillar α -synuclein is sensitive to Parkinson's disease-linked mutations and occurs by a pore-like mechanism. *Biochemistry* **41**, 4595–4602 (2002).
578. Chaudhary, H., Stefanovic, A. N. D., Subramaniam, V. & Claessens, M. M. A. E. Membrane interactions and fibrillization of α -synuclein play an essential role in membrane disruption. *FEBS Lett.* **588**, 4457–4463 (2014).
579. Katsinelos, T. *et al.* Unconventional Secretion Mediates the Trans-cellular Spreading of Tau. *Cell Rep.* **23**, 2039–2055 (2018).
580. Brettschneider, J. *et al.* Microglial activation correlates with disease progression and upper motor neuron clinical symptoms in amyotrophic lateral sclerosis. *PLoS One* **7**, (2012).
581. Shaw, P. J. Molecular and cellular pathways of neurodegeneration in motor neurone disease. *J. Neurol. Neurosurg. Psychiatry* **76**, 1046–1057 (2005).

582. World Health Organization (WHO). Global action plan on the public health response to dementia 2017 - 2025.
583. Chen JJ. Overview of current and emerging therapies for amyotrophic lateral sclerosis. *Am. J. Manag. Care* **26**, S191–S197 (2020).
584. Mullard, A. ALS antisense drug falters in phase III. *Nat. Rev. Drug Discov.* **20**, 883–885 (2021).
585. Gladman, M. & Zinman, L. The economic impact of amyotrophic lateral sclerosis: a systematic review. *Expert Rev. Pharmacoecon. Outcomes Res.* **15**, 439–450 (2015).
586. Achtert, K. & Kerkemeyer, L. The economic burden of amyotrophic lateral sclerosis: a systematic review. *Eur. J. Heal. Econ.* **22**, 1151–1166 (2021).
587. Galvin, J. E., Howard, D. H., Denny, S. S., Dickinson, S. & Tatton, N. The social and economic burden of frontotemporal degeneration. *Neurology* **89**, 2049–2056 (2017).
588. Grabler, M. R., Weyen, U., Juckel, G., Tegenthoff, M. & Mavrogiorgou-Juckel, P. Death Anxiety and Depression in Amyotrophic Lateral Sclerosis Patients and Their Primary Caregivers. *Front. Neurol.* **9**, (2018).
589. Calvo, V. *et al.* Impact on children of a parent with ALS: a case-control study. *Front. Psychol.* **6**, (2015).
590. de Wit, J. *et al.* Psychological distress and coping styles of caregivers of patients with amyotrophic lateral sclerosis: a longitudinal study. *Amyotroph. Lateral Scler. Front. Degener.* **20**, 235–241 (2019).
591. Pagnini, F. *et al.* Burden, depression, and anxiety in caregivers of people with amyotrophic lateral sclerosis. *Psychol. Health Med.* **15**, 685–693 (2010).
592. Krivickas, L. S., Shockley, L. & Mitumoto, H. Home care of patients with amyotrophic lateral sclerosis (ALS). *J. Neurol. Sci.* **152**, s82–s89 (1997).
593. Mourik, J. C. *et al.* Frontotemporal Dementia: Behavioral Symptoms and Caregiver Distress. *Dement. Geriatr. Cogn. Disord.* **18**, 299–306 (2004).
594. Hvidsten, L. *et al.* Quality of life of family carers of persons with young-onset dementia: A Nordic two-year observational multicenter study. *PLoS One* **14**, e0219859 (2019).
595. Lin, Y. *et al.* Toxic PR Poly-Dipeptides Encoded by the C9orf72 Repeat Expansion Target LC Domain Polymers. *Cell* **167**, 789–802.e12 (2016).
596. de Oliveira, G. A. P., Cordeiro, Y., Silva, J. L. & Vieira, T. C. R. G. *Liquid-liquid phase transitions and amyloid aggregation in proteins related to cancer and neurodegenerative diseases. Advances in Protein Chemistry and Structural Biology* vol. 118 (Elsevier Ltd, 2019).
597. Arseni, D. *et al.* Structure of pathological TDP-43 filaments from ALS with FTLD. *Nature* **601**, 139–143 (2022).
598. Zhang, W. *et al.* Novel tau filament fold in corticobasal degeneration. *Nature* **580**, 283–287 (2020).
599. Schweighauser, M. *et al.* Structures of α -synuclein filaments from multiple system atrophy. *Nature* **585**, 464–469 (2020).
600. Evans, L. D. *et al.* Extracellular Monomeric and Aggregated Tau Efficiently Enter Human Neurons through Overlapping but Distinct Pathways. *Cell Rep.* **22**, 3612–3624 (2018).
601. Ren, P.-H. *et al.* Cytoplasmic penetration and persistent infection of mammalian cells by polyglutamine aggregates. *Nat. Cell Biol.* **11**, 219–225 (2009).
602. Bonifacino, J. S. & Traub, L. M. Signals for Sorting of Transmembrane Proteins to Endosomes and Lysosomes. *Annu. Rev. Biochem.* **72**, 395–447 (2003).
603. Zhou, Q. *et al.* Antibodies inhibit transmission and aggregation of C9orf72 poly-GA dipeptide repeat proteins. *EMBO Mol. Med.* **9**, 687–702 (2017).
604. Clement, A. M. *et al.* Wild-type nonneuronal cells extend survival of SOD1 mutant motor neurons in ALS mice. *Science (80-.)*. **302**, 113–117 (2003).
605. Yamanaka, K. *et al.* Mutant SOD1 in cell types other than motor neurons and oligodendrocytes accelerates onset of disease in ALS mice. *Proc. Natl. Acad. Sci. U. S. A.* **105**, 7594–7599 (2008).
606. Pramatarova, A., Laganière, J., Roussel, J., Brisebois, K. & Rouleau, G. A. Neuron-specific expression of mutant superoxide dismutase 1 in transgenic mice does not lead to motor impairment. *J. Neurosci.* **21**, 3369–3374 (2001).
607. Hirsch, C. & Schildknecht, S. In Vitro Research Reproducibility: Keeping Up High Standards. *Front. Pharmacol.* **10**, (2019).
608. Luk, K. C. *et al.* Intracerebral inoculation of pathological α -synuclein initiates a rapidly progressive neurodegenerative α -synucleinopathy in mice. *J. Exp. Med.* **209**, 975–986 (2012).

8. Appendix

STORM-TIRF control images No poly-GA DPRs added - iAstrocyte

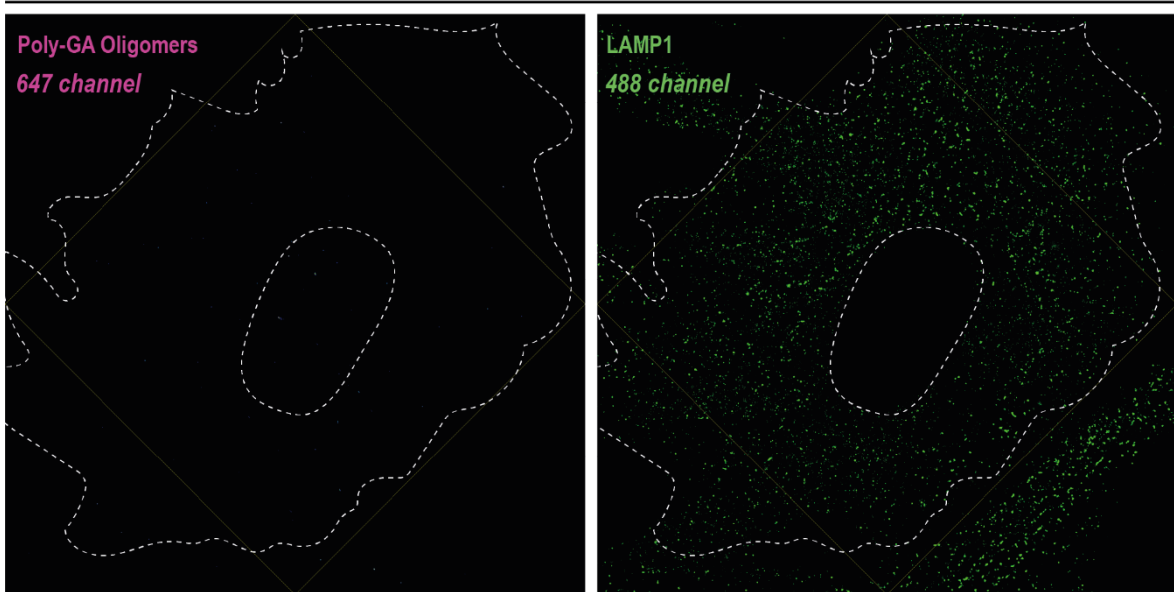


Figure 8.1 STORM-TIRF control images

To rule out potential imaging artefacts caused by autofluorescent molecules illuminated by the 647nm laser source, we imaged an iAstrocyte cell that had previously not been exposed to poly GA DPRs and was later stained with anti-LAMP1 antibody (and AlexaFluor 488 nm secondary antibody). As illustrated in the figure, we detect no signal in the 647 channel, indicating that our imaging settings did not result in the production of any artificial autofluorescence signal for the 647 channel.

Legends for supplementary Movies

Supplementary Movie S1. 3D-volume and -surface rendering of poly-GA phase-separated oligomers at 20 μ M and 24h in low salt solution in the test tube. After deconvolution, 3D-surface rendering algorithms were applied to better visualize the massive and compact structure of the assemblies, along with concavity features. Deconvolution and 3D-rendering criteria are explained in the Method's section 2.2.7.

Supplementary Movie S2. 3D-volume and –surface rendering of poly-PA phase-separated oligomers at 20 μ M and 24h in low salt solution in the test tube. The application of 3D-rendering algorithms on deconvolved data enables to better appreciate the presence of extremely circular poly-PA liquid-like droplets (average circularity = 0.95) coalescing in the test tube. The 3D-reconstructions exhibit a bulk loss of sphericity of the assemblies in the three-dimensional space concomitant with elongation along the z-axis; this is due to poor Z-axis resolution. Deconvolution and 3D-rendering criteria are explained in the Method's section 2.2.7.

Supplementary Movie S3. 3D-volume and –surface rendering of iAstrocyte-mediated uptake of poly-GA fibrils. The movie illustrates the presence of the aggregates in the perinuclear region of the cell, by showing the lateral view of the cell along the XZ axes. Red = ATTO550 poly-GA fibrils; Green = Vimentin-stained cell.

Supplementary Movie S4. The iAstrocyte-mediated uptake of poly-GA fibrils (same of *Movie S3*) is further presented as dynamic orthogonal views (XZ, YZ) moving along the Z-stack planes.

Supplementary Movie S5. Poly-GA fibrils undergo a mixture of Brownian motion, directed motion and constrained motion after 24h uptake in a healthy iAstrocyte cell. Poly-GA fibrils are colour-coded by the signal intensity (blue=min; red=max). 60 frames were imaged at 1Hz at ~190 nm lateral resolution in Airyscan mode. Deconvolution was applied to each frame, and the movie was generated as reported in the Method's section 2.2.13. Fibrils were, by approximation, treated as single particles and their trajectories were analysed by Mean Square Displacement ($MSD(\Delta t)$ analysis; Method's section 2.2.13).

Supplementary Movie S6. Accumulation of poly-GA DPRs (magenta) in large spherical structures (arrow heads) along the axons of primary mouse cortical neurons. By zooming into few of these structures with higher resolution (airyscan mode), during live-imaging, we report the presence of small poly-GA proteins (by ATTO550 fluorescence) erratically moving within each structure overtime.

Supplementary Movie S7. Poly-GA DPRs (magenta) and LysoTracker Green (green) in large spherical structures (arrow heads) along the axons of primary mouse cortical neurons. The time-lapse shows that these spherical axonal structures contain poly-GA DPRs that colocalize with lysosomal organelles (merged in white colour).

Supplementary Movie S8. The movie shows a three-dimensional view of co-localization between all the DPRs (magenta) and the lysosomes (green) contained in the proximal axons of mouse cortical neurons. Each region-of-interest (ROI) is delimited by a white square. On the right panel of the movie, each ROI is presented in a zoomed view moving through the Z-planes of the Z-stack dataset. This shows that co-localization between DPRs and lysosomes is consistent throughout the three-dimensional space.

Supplementary Movie S9. The movie compares widefield imaging to dSTORM imaging. Both imaging modalities were used on the same iAstrocyte cell that had been previously exposed to ATTO647N-polyGA fibrils. The comparison is explained in terms of a few technical aspects, such as xy resolution achieved, laser power used, and imaging principles used.

Research outputs from PhD

Communications in conferences

Oral platform communications:

- **Oral Presentation at the European Network to Cure ALS (ENCALS 2019)**
Marchi P.M., Bousset L., Ferraiuolo L., Hautbergue G., Melki R., & Azzouz M..
Role of potential cell-to-cell transmission of dipeptide repeat proteins in C9ORF72 ALS/FTD pathology.
Presented in Tours, France, at The European Network for the Cure of ALS (ENCALS) conference in May 2019.

Conferences/Seminars attended:

- **Quantitative BioImaging (QBI) 2020 Conference**, Oxford, England, UK
I had the pleasure of participating at the Quantitative BioImaging Conference in Oxford in early January 2020, with renowned experts of optical imaging.
- **The American Society of Gene & Cell Therapy 2020 Annual meeting**, Virtual
I followed virtually the annual meeting of The American Society of Gene & Cell Therapy 2020, regarding the latest achievements in the field.
- **Vesicle Trafficking & Pathways to Neurodegeneration 2021**
UK Wellcome Genome Campus, Virtual
- **Mechanistic insights into the pathophysiology of ALS 2021**
UK Dementia Research Institute, Virtual

Courses attended:

- **ESRIC 2019 Super-resolution Summer-school**, Edinburgh, Scotland, UK

I had the pleasure of participating at the 5-day course at the Edinburgh Super-Resolution Imaging Consortium and learn more about Super-resolution techniques for optical microscopy.

- **CamBioScience Cerebral organoids**

Online Course (October 2020)

Scientific publications

Research papers

- **Marchi P.M.**, Marrone L., Brasseur L., Bousset L., Webster C.P., Destro M., Walther C.G., Alfred V., Marroccella R., Robinson D.,... Melki R., Azzouz M., 2021.

C9orf72-derived poly-GA DPRs undergo endocytic uptake in iNPC-derived astrocytes and spread to motor neurons.

Life Science Alliance. Status: under revisions. First author.

- Marrone L., **Marchi P.M.**, Webster C.P., Marroccella R., Coldicott I., Reynolds S., Cruzeiro J.A., Yang Z.H, Higginbottom A., Khundadze M., Shaw P.J., Hübner C.A., Livesey M.R., Azzouz M., 2022.

SPG15 protein deficits are at the crossroads between lysosomal abnormalities, altered lipid metabolism and synaptic dysfunction.

Human Molecular Genetics. Status: **accepted**. Second author.

ACCEPTED MANUSCRIPT

SPG15 protein deficits are at the crossroads between lysosomal abnormalities, altered lipid metabolism and synaptic dysfunction

Lara Marrone, Paolo M Marchi, Christopher P Webster, Raffaele Marroccella, Ian Coldicott, Steven Reynolds, João Alves-Cruzeiro, Zih-Liang Yang, Adrian Higginbottom, Mukhran Khundadze ... Show more

Human Molecular Genetics, ddac063, <https://doi.org/10.1093/hmg/ddac063>

Published: 21 March 2022 **Article history** ▼

- Karyka E., Ramirez N.B., Webster C.P., **Marchi P.M.**, Graves E., Godena V., Marrone L., Bhargava A., Ray S., Ning K., Hautbergue G., El-khamisy S., and Azzouz M., 2022.

SMN-deficient cells exhibit increased ribosomal DNA damage.

Life Science Alliance. Status: under second revisions. Fourth author.

- Scarrott J.M., Cruzeiro J.A., **Marchi P.M.**, Coldicott I., Karyka E., Azzouz M., 2022.

CRISPR-mediated Ap4b1-knockout mouse model of SPG47 displays motor dysfunction, aberrant brain morphology and ATG9A mislocalisation.

Disease Models & Mechanisms. Status: in preparation. Third author.

Review articles

- **Marchi P.M.**, Marrone L. and Azzouz M., 2021.

Delivery of therapeutic AAV9 vectors via cisterna magna to treat neurological disorders.

Trends in molecular medicine. Status: **published**. First author.

Trends in Molecular Medicine | Strategy of the month

Delivery of therapeutic AAV9 vectors via cisterna magna to treat neurological disorders

Paolo M. Marchi,^{1,2} Lara Marrone,^{1,2} and Mimoun Azzouz ^{1,*}

¹Sheffield Institute for Translational Neuroscience (SITraN), Department of Neuroscience, University of Sheffield, 385A Glossop Road, Sheffield, S10 2HQ, UK

²These authors contributed equally to this work

- Marrone L., **Marchi P.M.** and Azzouz M., 2022.

Circumventing the packaging limit of AAV-mediated gene replacement therapy for neurological disorders.

Expert opinion on biological therapy. Status: **published**. Co-first author.



Expert Opinion on Biological Therapy



ISSN: (Print) (Online) Journal homepage: <https://www.tandfonline.com/loi/iebt20>

Circumventing the packaging limit of AAV-mediated gene replacement therapy for neurological disorders

Lara Marrone, Paolo M. Marchi & Mimoun Azzouz